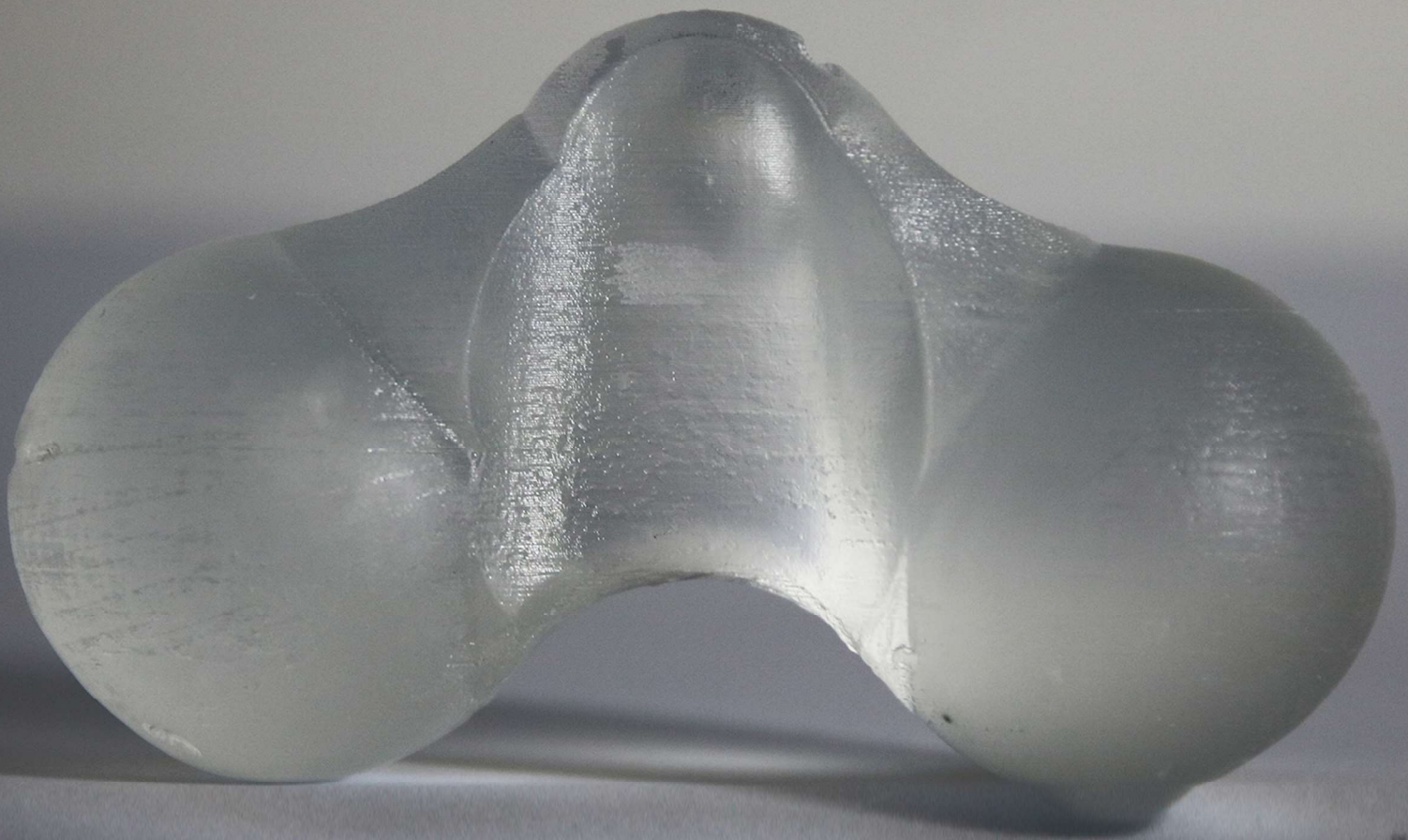
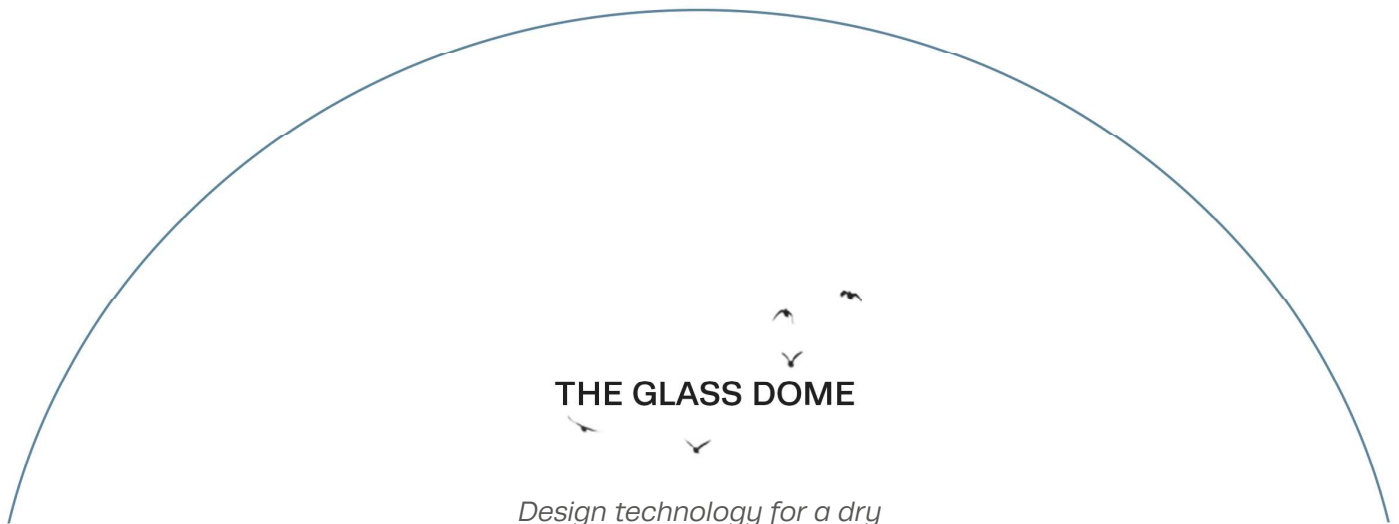


THE GLASS DOME

Design technology for a dry assembled and cast glass dome



Elke Janine Janssens



THE GLASS DOME

*Design technology for a dry
assembled and cast glass dome*

Master thesis TU Delft (24-01-2018)

Mentors:

Student:

- - - - - -
- | | |
|--------------------------|-----------------------|
| • Faidra Oikonomopoulou | • Elke Janssens |
| • Regina Bokel | • 4522036 |
| • Telesilla Bristogianni | • Building Technology |

Msc Architecture, Urbanism and Building Sciences

Preface

Short description of this research:

Glass is a versatile material applied in a large number of industries. It can for example be found in everyday household items, inside high tech machines or it can be used as part of mechanical structures in buildings. This research focuses on using structural cast glass components for a dome design forming a sustainable living habitat for Lori parrots in a moderate climate while being minimum invasive for the local environment.

Acknowledgements

The last nine months have been a very exciting learning process, working very hard on my research and as I told to my friends and family: 'I was living in my crazy glass dome bubble'. I could not stop talking about interlocking dome components in order to find out the complexity of a glass dome design. Although, I am very proud of my final glass dome design and it would not become like this without the good feedback and support of so many people.

First of all I would like to thank my supervisors for guiding me through my entire project. Foremost I would like to express my thanks to my main mentor Faidra Oikonomopoulou. I would like to thank Faidra Oikonomopoulou for her enthusiasm and inspirational ideas on interlocking cast glass components. Moreover, I would like to thank both Faidra Oikonomopoulou and Telesilla Bristogianni on sharing all their knowledge about glass, for believing in my design ideas and criticism that took my dome design to the next level. In addition, Telesilla Bristogianni, my third mentor, helped me with my mold design and she explained me all the principles about casting glass where I am very grateful for.

Secondly, I would like to express my gratitude to my second mentor Regina Bokel who ensured that both of my feet were kept on the ground, as well for explaining the fundamental physics involved for designing the dome.

During my design process I was very pleased by the help of Paul de Ruiter, Serdar Asut, Geert Coumans and Aidan Wyber that all helped me with providing 3D prints and gave me insight about my component geometry in order to optimize its transparency and sharp edges. Subsequently Lida Barou gave me good advice on how to create my mold design that was obtained, among other things, from the 3D print. Moreover, Lida Barou has giving me a supportive feeling where I would like to sincerely thank her for.

Regarding the structural performance of my glass dome design, I could not preform my structural assessments without the knowledge obtained from Peter Eigenraam. Thank you Peter Eigenraam for sharing your knowledge on the theory of domes and explaining me the principles of the Diana-software. I also would like to acknowledge Fred Veer for his guidance during my physical arch-test. And I also would like to express my gratitude to the meetings with James O'callaghan that were also very useful because James O'callaghan told me all about glass limitations and gave me insight in how I could solve my structural calculations.

During the week and long working nights I really was cheered up by my (BT) fellow students. Especially through Layla van Ellen, who was always there for me and gave me moral support.

Finally I would like to thank my colleagues from TAK architecten who encouraged me during my design process and who I always could approach for questions.

But most of all I would like to thank Frank Janssens, Nicole Janssens, Yves Janssens, Charlotte Bos and Lex Hagenbeek, who kept on listening to my design ideas and dragged me through my entire research. In addition, my friends from Eindhoven, where I did my bachelor studies, as well as my friends from Delft who have given me good advice on my report and made me realize that: '*pausing is learning too*' (Amy van Rietschoten).

Domes

According to Prenis (1973) dome structures were built for centuries and constructed with natural materials such as mud, thatch, skins, leaves, stones and snow as shown in figure 1 and 2. These natural materials were designed in an intuitively way because additional manufacturing methods were primitive and only natural shapes were present. Already by then double curved surfaces were preferred above plane surfaces because forming surfaces in a curve adds strength, the so called pre-stressing. Resulting in domes with large spans and the usage of less material. Moreover, residential domes with a large span result in spacious environments, increasing the quality of life.

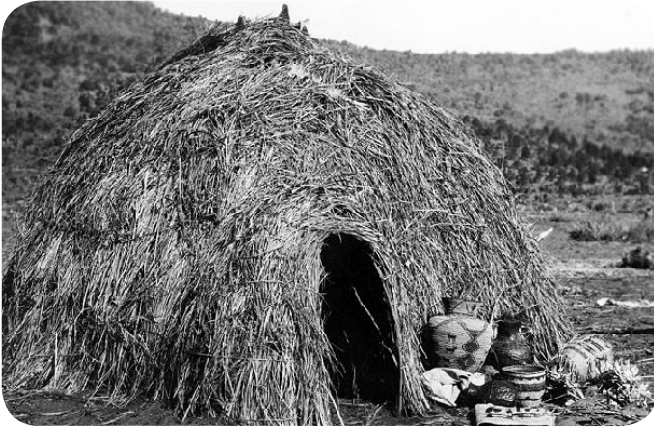


Figure 1. Wigwam in the Southwest US (Curtis, 1903)



Figure 2. Native American hogan
(source: www.arizonaforvisitors.com)

To create domes with even larger spans, in comparison with the old yurts and wigwams, a modification of the natural materials was needed. This modification led to uniform dimensions and geometric shapes of the components. Subsequently new dome structures with larger spans were built for ceremonial and mystical functions as shown in figure 3.

It was time for change, the Industrial Revolution in the 19th century led to new technologies and production techniques. The new technologies and production techniques allowed for fast production of cast, wrought iron and the usage of glass in the building industry. From this era metal framed, glass domes have been realized and functioned as hothouses, winter gardens and shopping arcades as shown in figure 4.



Figure 3. Pantheon Rome (source: www.stilus.ni)



Figure 4. Winter garden (source: www.balmori.com)

Future perspective

In the 21st century many architects and engineers still aim for large glass dome structures to create spacious environments while minimizing the visual connections to increase transparency. Figure 5 presents a brief evolution of the glass dome from 1998–2003, with metal framed main structures and substructures or cladding built up from glass. To maximize glass and minimize the steel visual connections in dome structures a transition towards structural glass is needed.

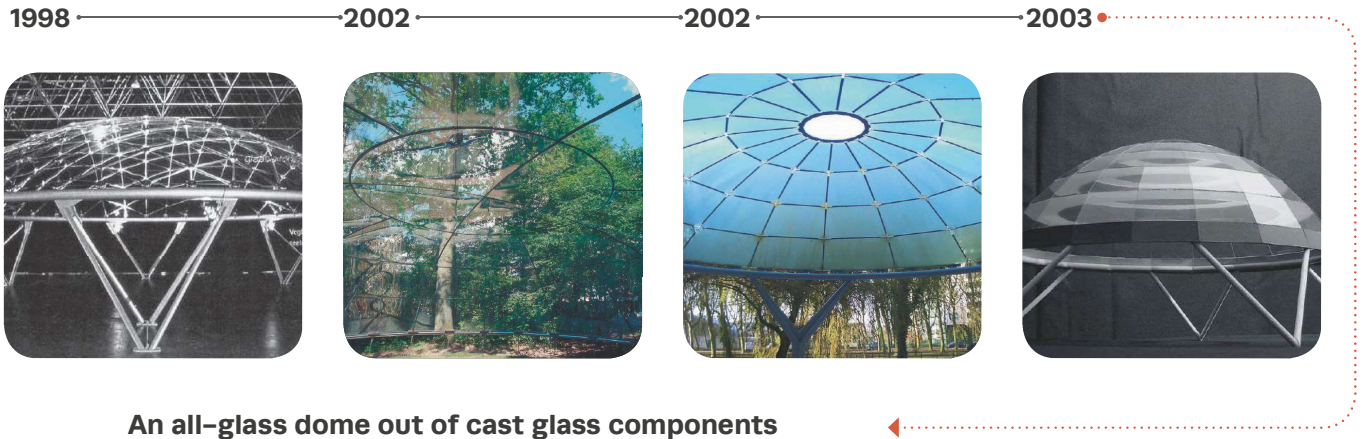


Figure 5. Brief evolution of the glass dome based on (Wurm, 2007)

Designing a solely glass dome with a dry assembled system asks for understanding of the material properties of glass and internal dome forces. Glass is known for its inability to yield, high compressive strength, high thermal conductivity, low tensile and bending strength. The dome is a suitable shape for constructing glass structures because most of the internal dome forces are in compression. The ideal design for a glass dome therefore would be a fully compressive shallow dome design which avoids tensile and bending stresses.

Using glass as a structural component in domes is a new challenge because an increased thickness is needed to prevent the glass planes from buckling failure. Two options can be used to increase the strength and thickness of the glass planes: lamination of float glass or by using monolithic cast glass. Other options, e.g. curved glass, are not very suitable because the thickness of float glass is limited due to its production process. This research focuses on cast glass because strong monolithic, high formed and transparent structures can be established.

A steel precision mold is needed to produce the cast glass components with the dry assembled system of the glass dome. Constructing a dry assembled system from cast glass components brings

the advantage of reassembly while optimizing transparency. The cast glass component is a durable product because, according to Nijssse (2003), glass consist of components abundant in earth, is corrosion-resistant and can be easily cleaned. Note that the production and recycling process of the cast glass components is not durable. Glass has a high embodied energy and this is even higher for the included steel molds, as shown in figure 6. Minimization of the amount of different cast glass components is needed to reduce the required production energy and cost. for steel molds.

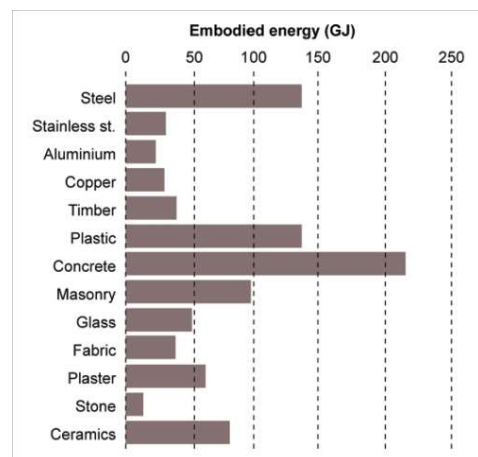


Figure 6. Embodied energy of some common materials (CSIRO, 2013)



Figure 7. Map of the zoological garden 'Parc des Oiseaux' (source: www.parcdesoiseaux.com)

This research proposes to design a **dry assembled cast glass dome** that creates a spacious environment and functions as an **aviary**. The proposed building location is in **Southern France**: 'Parc des Oiseaux' and this location is characterized as a moderate maritime climate. The moderate climate provides the opportunity to realize a large glass dome structure that requires minimal consumption of energy while maintaining an acceptable thermal comfort in the interior of the glass dome. In addition, this research replaces the current aviary for **Lori parrots** in 'Parc des Oiseaux' for the glass dome aviary.

Current aviaries are most often constructed from a steel or wooden structure that is covered a bird-net. This type of aviary design prevents interaction with the surrounding park and leaves both visitor and parrot with a locked up experience. In order to form a more creation of a natural habitat for Lori parrots this research proposes to construct a glass dome out of cast glass **spherical components** that have a **slight matt surface**. Hence, the cast glass blocks will form a **noticeable structure** to the Lori parrots while colours of the environment are transmitted, reflected and distorted in a **nice colour pattern** onto the glass dome surface. In addition, the only bird-net present is located at the dome top and will not create a locked up experience. The colour pattern on the glass dome surface shows a mix of colours of the environment such as the colours of different trees, flowers and the sky.

The location of the glass dome aviary within 'Parc des Oiseaux' is shown in figure 7. The dome has a dry assembled construction in order to make it possible to reassemble the glass dome in other locations with, if applicable, other functions. Possible functions have to cover the design requirements which relate to thermal, structural and aesthetic requirements. Examples of suitable other functions for this glass dome could be an exhibition place or a green house.

This research is divided into 5 phases:

- **Research framework** to explain the challenges of this research.
- **Literature review** of domes, thermal performance, glass and interlocking systems.
- **Dome design**, including the general design, component design, interlayer design and fabrication.
- **Validation**, distinguished into structural performance and thermal comfort performance.
- **Conclusions** and recommendations are given for further development of the presented technology.

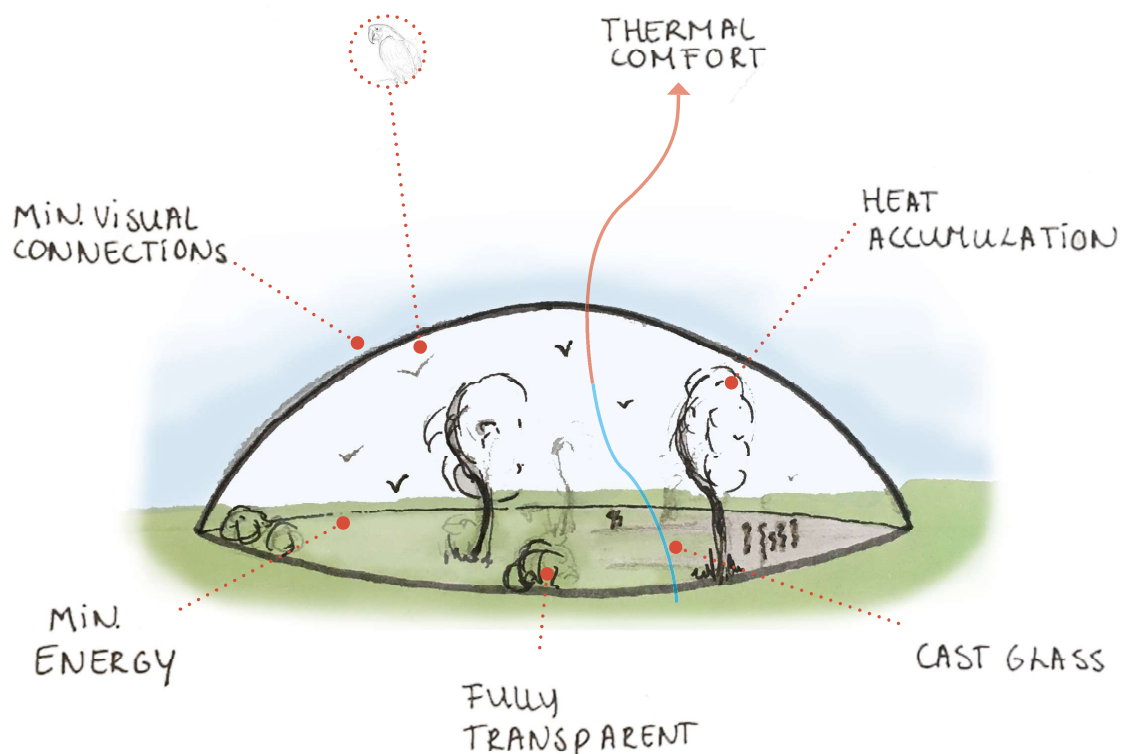


Figure 8. Concept scheme of the glass dome

1. Research framework	11	3. Design	87
1.1 Location	12	3.1 Introduction	88
1.2 Problem statement	13	3.2 General dome design	88
1.3 Objectives.....	14	3.2.1 <i>Design principles</i>	88
1.4 Research questions	14	3.2.2 <i>Building elements</i>	88
1.5 Methodology	15	3.3 Component design	92
1.6 Relevance	15	3.3.1 <i>Design principles</i>	92
1.7 Time-planning	15	3.3.2 <i>Sphere based design</i>	94
2. Literature review	19	3.3.3 <i>Previous attempts</i>	95
2.1 Domes.....	20	3.3.4 <i>Final component</i>	96
2.1.1 <i>Introduction</i>	20	3.3.5 <i>Fabrication</i>	100
2.1.2 <i>Why domes</i>	20	3.4 Interlayer design	102
2.1.3 <i>Building approaches</i>	20	3.4.1 <i>Optimization and principles</i>	102
2.1.4 <i>Shapes</i>	26	3.4.2 <i>Dimensions</i>	104
2.1.5 <i>Membrane forces</i>	29	3.4.3 <i>Geometry</i>	105
2.1.6 <i>Conclusion</i>	32	3.5 Feasibility	106
2.2 Thermal performance	33	3.5.1 <i>Construction</i>	106
2.2.1 <i>Introduction</i>	33	3.5.2 <i>Maintenance & Pre-stressing</i>	107
2.2.2 <i>Thermal comfort models</i>	33	3.6 Prototype	111
2.2.3 <i>Thermal comfort steps</i>	35	3.7 Transparency	122
2.2.4 <i>Passive strategies</i>	41	4. Validation	125
2.3 Glass	48	4.1 Structural validation.....	126
2.3.1 <i>Introduction</i>	48	4.1.1 <i>Introduction</i>	126
2.3.2 <i>The definition of glass</i>	48	4.1.2 <i>Analytical analysis</i>	126
2.3.3 <i>Types of glass</i>	49	4.1.3 <i>Numerical analysis</i>	136
2.3.4 <i>Material properties glass</i>	50	4.1.4 <i>Experimental analysis</i>	142
2.3.5 <i>Designing with glass</i>	56	4.1.5 <i>Conclusion</i>	147
2.3.6 <i>Safe design methods</i>	57	4.2 Thermal validation	148
2.3.7 <i>Production methods</i>	60	4.2.1 <i>Introduction</i>	148
2.3.8 <i>Existing cast glass structures</i>	68	4.2.2 <i>Natural ventilation rate</i>	148
2.3.9 <i>Structural configurations</i>	74	4.2.3 <i>Input data Design Builder</i>	152
2.3.10 <i>Glass dome structures</i>	76	4.2.4 <i>Thermal simulation; passive design</i>	155
2.4 Interlocking systems.....	80	4.2.5 <i>Heating/cooling unit</i>	159
2.4.1 <i>Types of interlock</i>	80	4.2.6 <i>Conclusion</i>	161
2.4.2 <i>Interlayer</i>	82	5. Conclusion	163
2.5 Conclusion	85	5.1 Conclusion	164
		5.2 Recommendations.....	168
		6. References	171
		7. Appendices	175
		7.1 Amount of components	176
		7.2 Physical arch test	177
		7.3 Lab data	178



1. Research framework

1.1 Location



Figure 9. Location: Villars Les Dombes
(source: www.freecountrymaps.com).



Figure 10. Current aviary of the Lori parrots
in 'Parc des Oiseaux' (Leca, 2012).

The proposed building location of the glass dome aviary for Lori parrots has a moderate climate and is located in **Southern France: 'Parc des Oiseaux'**. Parc des Oiseaux is situated in the municipality **Villars Les Dombes**, as shown in figure 9.

Parc des Oiseaux is chosen as a building location because it is one of the biggest natural bird parks in Europe and maintains 3000 birds and a landscape of 35 hectares. Most of the birds live outside in an imitation of their natural environment and some of them live in an aviary, such as the Lori parrots. Within these aviaries, a tropical imitation of the environment is required as well. The indoor temperatures and interior landscape need to be set to ensure the required conditions for the Lori parrots^[1].

Fundamental knowledge is required about the weather data of Villars Les Dombes to control the interior temperatures. General information about the climate in Villars Les Dombes is given below and is explained in more detail within this research in the chapter 'thermal performance' of the glass dome.

Villars Les Dombes is classified as c.f.b.: temperate oceanic climate. During the entire year, the average temperature and rainfall are 10.9°C and 831mm respectively. July is stated as the warmest month, with an average temperature of 20°C and January is the coldest month with an average temperature of 1.7°C. In between the driest and wettest month the precipitation varies 28 mm^[2].

[1] <http://www.parcdesoiseaux.com>

[2] <http://www.en.climate-data.org>

1.2 Problem statement

The **main challenge** of this research is to develop a **dry assembled cast glass dome** which provides **thermal comfort** to the Lori parrots and is **minimum invasive for the local environment**. Under this context a glass dome with an aviary function in Southern France in 'Parc des Oiseaux' is proposed.

The corresponding challenges for this research are divided into **two sub challenges**: a technical challenge and a durability challenge.

The **technical challenge** is to create a structural design based on compression **(1)**, while preventing buckling failure **(2)** and optimizing transparency **(3)**.

The **durability challenge** is to create a durable design by minimizing the amount of different steel molds **(4)**, using a dry assembled construction **(5)** and by performing passive climate strategies **(6)**.

The relation between the technical and durability corresponding challenges are presented in a scheme in figure 11. This scheme shows that the challenges are all related to each other and determine the entire dome design. For example, the transparency can be influenced by passive strategies and is further determined by the geometry of the component, dry assembled system and entire dome design.

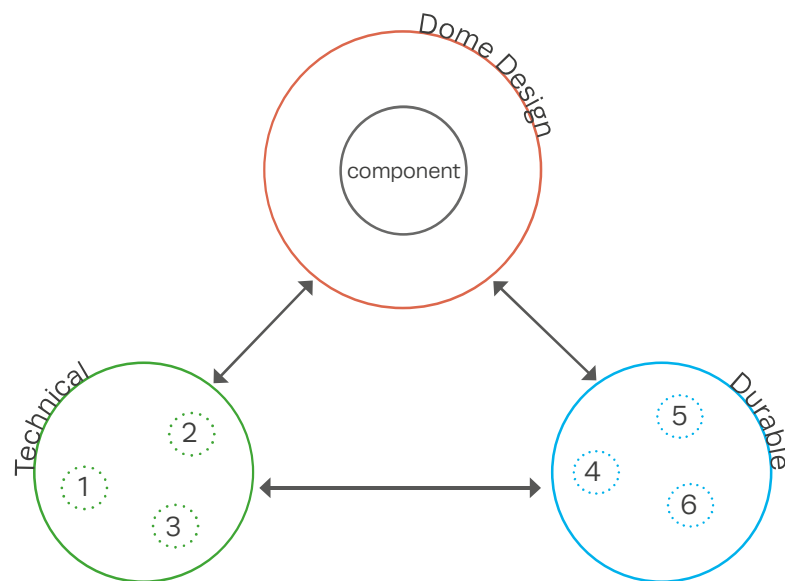


Figure 11. Illustrative scheme of the relations between the involved challenges

1.3 Objectives

The main goal of this research is to design a solely glass dome consisting of dry assembled cast glass components that ensure the desired durability and structural performance. Sub goals are formulated to achieve this main goal and are divided in structural and durability sub goals.

Concerning the **structural performance**, the sub goals are:

- Create a structural scheme based on compression.
- Design an optimal shape for one type of component.
- Minimize the visible steel connections.

Regarding the **durability performance**, the sub goals are:

- Minimize the number of different required molds.
- Design a dry assembled construction method.
- Perform passive climate strategies for thermal comfort

1.4 Research questions

Based on the aforementioned objectives and problem statement the main research question is:

“How can a solely glass dome be developed and assembled from structural cast glass components while providing thermal comfort and being minimum invasive for the local environment? ”.

This research question is divided into sub research questions:

- What is the **optimal shape** of the cast glass components?
- What techniques can be used to **minimize** the **number** of different molds?
- What techniques can be used to connect the components and create a **demountable structure**?
- What strategies can optimize the dome **transparency**?
- What strategies can be used to create **thermal comfort** while being **minimum invasive** for the local environment?

1.5 Methodology

This research is structured into four phases: literature review, analyses, design, and conclusion. An overview is given in figure 12.

The main subjects of the literature studies are: dome structures, thermal comfort, glass technology and interlocking systems. The first design limits and criteria of the glass dome are obtained from dome structures, thermal comfort, glass technology and interlocking systems literature. These first design limits and criteria will result in a conceptual design of the glass dome. This concept design includes general dimensions (sagitta and span) and thermal comfort criteria for the interior of the glass dome.

From additional literature focused on passive strategies, dry assembled systems and interlayers improved design limits and criteria are formulated. The dry assembled systems and interlayer literature will result in design studies of the component, interlayer and mold. These last mentioned design studies contributed to a fundamental understanding of the structural and durable performance of the glass dome, such as

critical buckling stress and amount of different components, interlayers and steel molds. Research in passive strategies will result in passive systems that require minimal energy while maintaining the desired thermal comfort in the interior of the glass dome. The performed literature study will develop a multi-disciplinary approach where glass, dome construction and thermal comfort are combined into one integral design.

Structural validation is derived from analytical, numerical and experimental analyses. Experimental qualitative analyses are performed at arch- and component level. These analyses gave fundamental insights about the structural behaviour of the dry assembled system of the glass dome. Apart from these structural validations analytical and numerical thermal simulations are performed to validate the thermal performance in the interior of the glass dome.

Finally, based on the results, recommendations are provided for further development of the presented technology.

1.6 Relevance

Since cast glass applications become more popular in the (building) industry, e.g. in real applications such as the Crystal Houses and Giant Telescope Mirrors research on cast glass has taken a big improvement. However, new glass structures are continuously developed in the building industry (such as the Glass Bridge) and require further investigation. This to investigate if cast glass can be utilized as structural component for more complex building configurations such as a double curved structure.

The current research can function as a basis on how cast glass can be used in structural double curved configurations, which in this research equals a dome structure. Hence, this research provides a scientific relevance and could be useful for structural engineers and architects to see the possibilities of cast glass in structural configurations. The current research provides fundamental insight in the optimal interlock for structures with changing curvatures. And secondly the research provides insight in an energy efficient glass dome structure.

1.7 Time-planning

Figure 13 presents the general time framework of this research. The time framework shows the actions that need to be taken for each week.

Figure 12. Research methodology

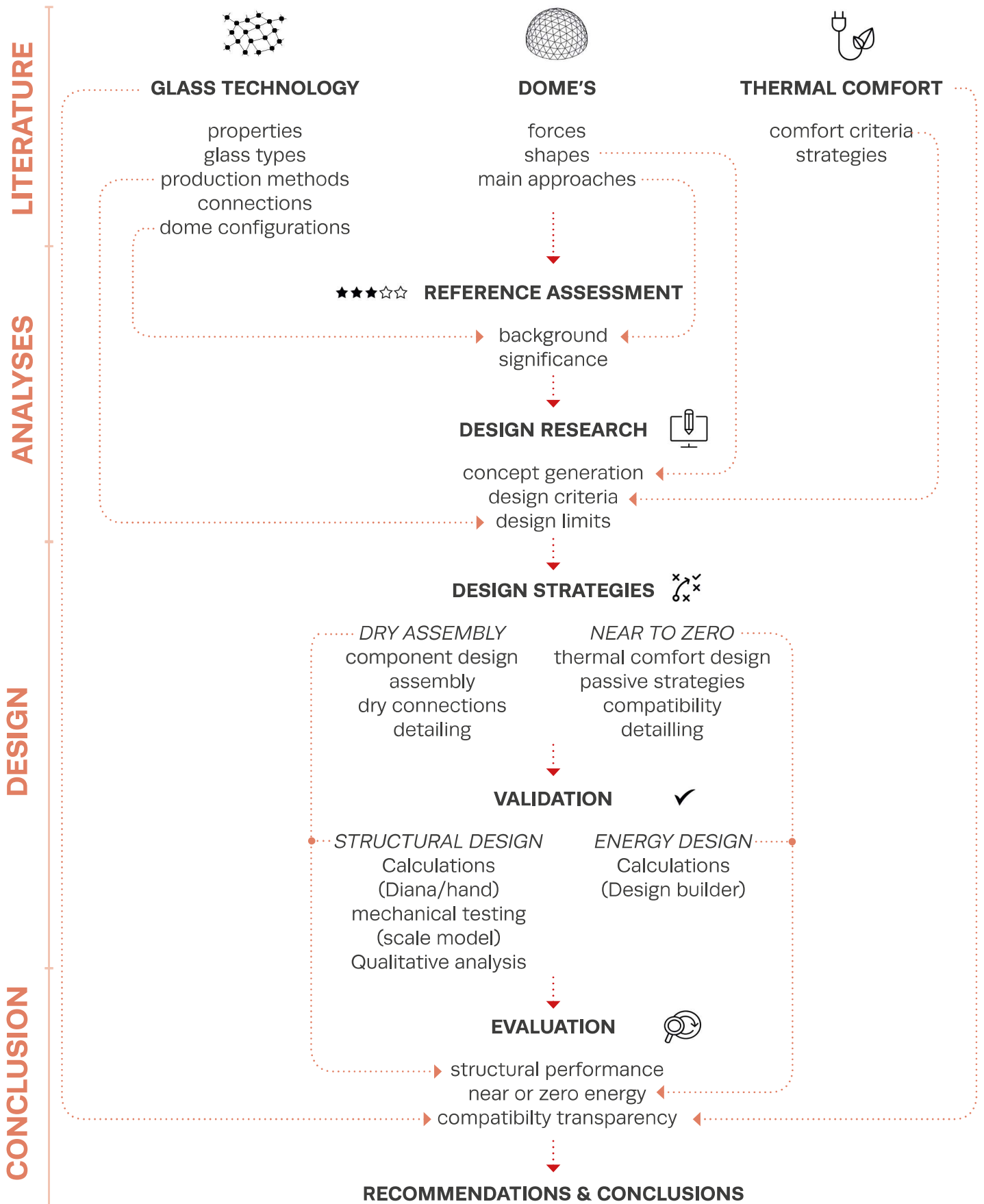
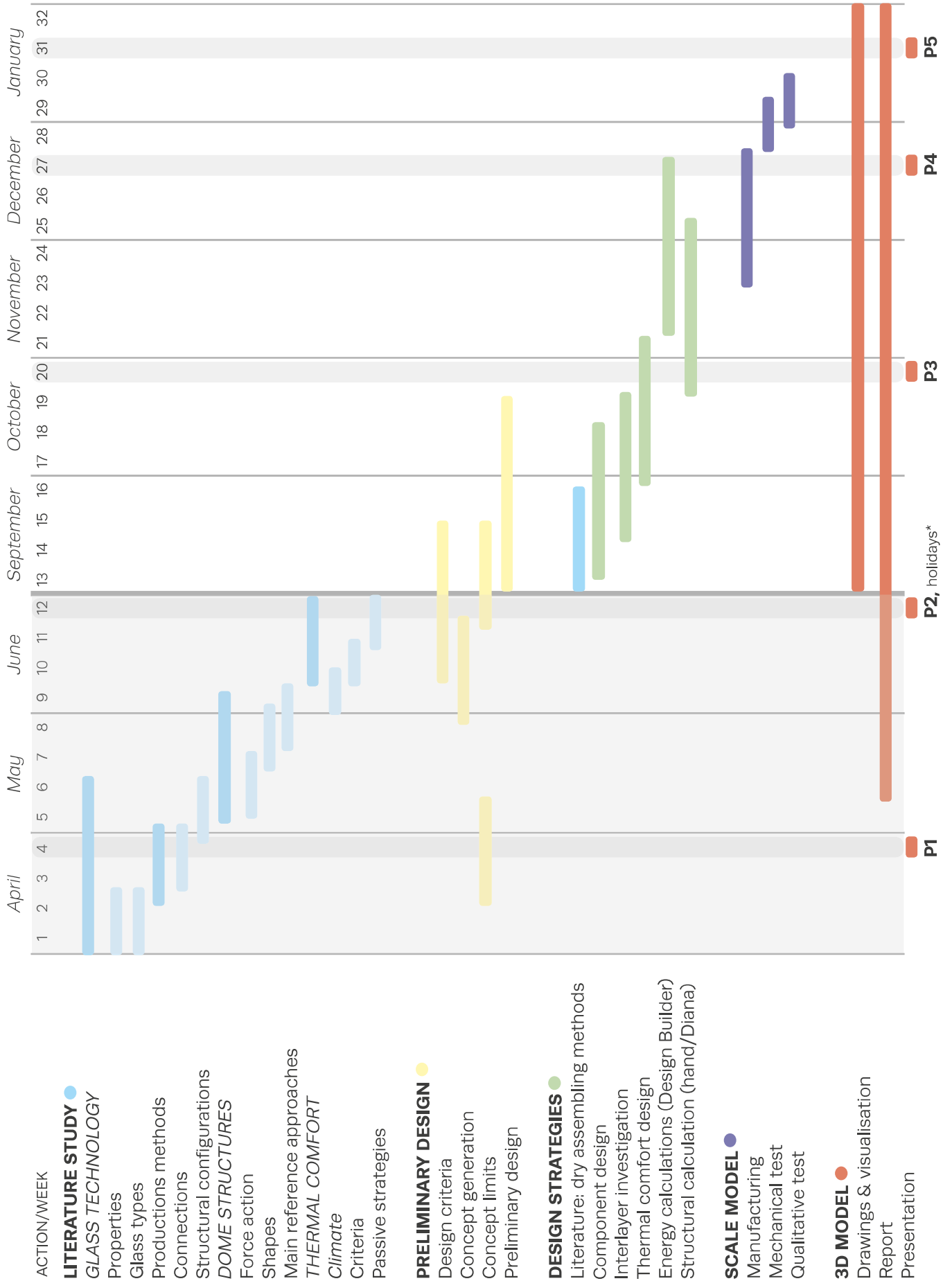


Figure 13. Global time-planning





2. Literature review

2.1 Domes

2.1.1 Introduction

This chapter explains the following aspects: advantages of a dome design, building approaches, the most popular dome shapes and force system within domes or rather said membrane forces.

Each sub-chapter is provided with a conclusion and finally a conclusion of the entire chapter which will define the general dimensions of the glass dome and specific function description is given.

2.1.2 Why domes

According to Prenis (1973) dome designs become more and more popular due to technical and psychological reasons. The psychological reason is that a dome design creates a 'centric feeling', humans are in the centre of things.

Some technical advantages are listed below:

- Domes conserve heat and the shape of the dome allows for natural air circulation, due to an accelerated airflow. Because of this reason an 'easy' heating and cooling system can be applied.
- Mass production is possible when using identical building parts.
- Easy constructed by its basic simplicity.

2.1.3 Building approaches

Introduction

Several dry assembled building techniques of dome structures are analysed and compared to develop a building method for a transparent dry assembled cast glass dome. A multi criteria analysis is performed to analyse and compare the chosen building techniques. The multi criteria analysis is presented in table 1.

The chosen projects are selected on their dry assembled connection capability, associated geometry and are assessed on seven assessment points. Each project is explained and a conclusion is given which approach or combination of approaches suits best for making a dry assembled cast glass dome for this research.

Existing assembly approaches					
criteria		Igloo	Geodesic	Armadillo Vault	Brunelleschi
COST	1. Number components	high	high	very high	very high
	2. Shell thickness (m)	0,15–0,40	≈ 0,20	0,05–0,12	0,5
STRUCTURAL	3. Compressive structure*	No > $\phi=51^\circ$	No > $\phi=51^\circ$	fully	No > $\phi=51^\circ$
	4. (C)Strength/thickness	intermediate	intermediate	high	low
	5. Base material	snow	glass & steel	limestone	bricks
	6. Stresses in components	blocks	icosa triangle	curved vaults	<i>all shapes;</i> triangular–angular
TRANSP.	7. Connection type	stacked	structul skin	interlocked	stacked & mortar
* under dead load best intermediate worst					

Table 1. Multi criteria analysis of the building approaches

Criteria

The **input criteria** for the assessment of the different building approaches are explained below and are divided into three aspects.

The first aspect is reducing the cost influenced by:

- **Number of different components:** reducing the number of different components result in a reduction of the production costs due to the utilization of less different steel molds.
- **Shell thickness,** reducing the shell thickness results in a decreased annealing time and reduction in the production costs.

The second aspect is creating a high structural performance influenced by:

- **Compressive zone** created by the components. Compressive structures are required due to the mechanical material properties of glass: weak in tension and strong in compression.
- **Compressive strength/thickness ratio:** high compressive strength/thickness ratios are required because, as shown above, low thicknesses reduce the annealing time and high compression lines result in low bending stresses.
- **Base material,** which categorizes each project.
- **Shape of component,** round edges and organic shapes are required to prevent peak stresses around the edges of the glass components.

The third and last aspect is creating a high transparency influenced by:

- **Connection type.** For example: stacking adhesives or steel reinforcements. Note that the type of connection has strong influence on the structural performance of the entire design. However, for this criteria it is assessed on its transparency for creating a solely glass structure.

Chosen reference projects

1. Igloo

One of the oldest and most famous dome techniques is the igloo. Igloos in Canada are used by Eskimos as a temporary home during the winter. According to Houben and Janssen (2013) igloos have many advantages. Some of the

advantages are strong form structure (prevent them from blizzard) and the high insulating properties (approximately a temperature of 2°C can be reached).

The biggest igloo ever made by the Eskimos had a span of 6m and was constructed by following these building steps:

- Choosing the right location. The requirement for building an igloo is the usage of hard field snow to ensure strong solid snow components. The snow needs to be compressed by high winds leading to a located snow depth of 1m.
- The snow components are prepared by utilizing a big knife or saw and a spade. Next, the snow can be placed into a mold to adjust the shape but this is not necessary. The snow blocks should not fail under its dead load and need to carry the horizontal loads. Hence, large components are placed at the bottom and smaller components are located at the top.
- The igloo is built in a hemispherical arrangement, as shown in figure 14. The edges are smoothed by hand resulting in a strong bond between the snow block components.
- Occurred cracks are filled with snow and maintained by hand. Eskimos use fire for creating light in the interior of their igloo. In addition the Eskimos make an opening at the top (zenith) when the interior begins to melt or soften. Subsequently, stack effect occurs due to the opened zenith and the softened interior causes an airtight skin of ice.

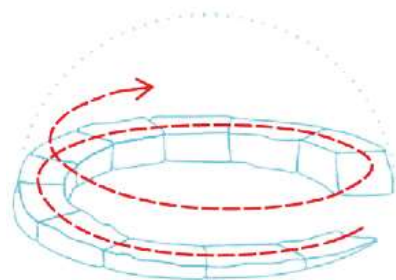


Figure 14. Igloo approach, where the snow blocks require a hemispherical arrangement (Houben et. al, 2013).

2. Geodesic dome

According to Prenis (1973) a big change in 1951 led to new dome designs. Buckminster Fuller provided in 1951 a method for building a spherical surface by dividing it into triangles. The triangle is the only rigid structural composition. Fuller developed the Geodesic Dome that was made from these components, where the dome acts as a climate shield reducing the heat and insulation costs. The Geodesic Dome was the most strongest, lightest and competent building structure ever designed.

A framework for geodesic domes include triangles which form a sphere or close to a sphere. An icosahedron is the largest solid with equal triangles and can be used as a starting point for creating a geodesic dome frame. The five regular solids are presented in figure 16. The icosahedron is not very spherical and asks for big structural members and internal bracing.

Subsequently subdivision into smaller triangles led to a more spherical shape: at this point the icosahedron triangle was introduced. The largest spherical dome structure with identical triangles consists of 6 smaller triangles where 20x60 triangles are covering the entire dome. This is the largest number of identical parts because subdividing causes an increment of different triangles.

The two most often used subdividing methods, or rather said breakdown schemes, are the triacon and alternate breakdown. The number of parts in which one icosahedron triangle is divided is called the frequency (f) and defines the complexity of a geodesic dome structure. The triacon method draws perpendicular lines to the sides of the icosahedron triangle, while the alternate method draws parallel lines, this principle is shown in figure 17. The differences between those two methods are defined in their frequencies. A triacon breakdown results in even frequencies while an alternate breakdown results in even and odd frequencies. Moreover the even alternate breakdowns (2V, 4V and 6V) create a form which is very close to a hemisphere. Unlike odd alternate frequencies that result in a dome shape that is half or less than a sphere, which is caused by the bands of the triangles. A triacon breakdown cannot form a hemisphere from triangles, however an approximation can be made as the triangles are cut in half, this principle is shown in figure 18.



Figure 15. Geodesic dome from Buckminster Fuller (Good, 1976)

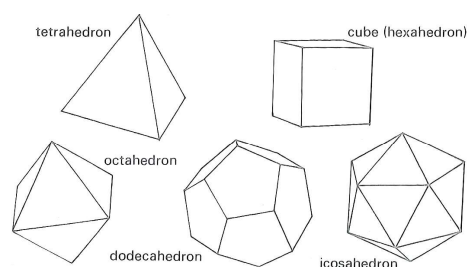


Figure 16. The five regular solids (Prenis, 1973)

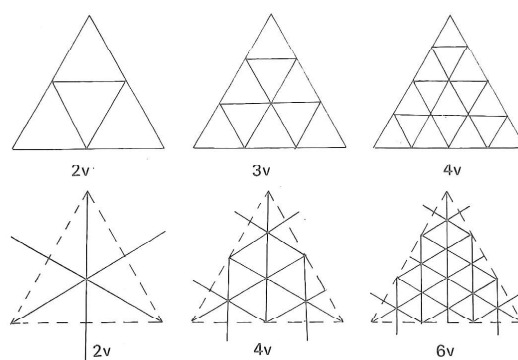


Figure 17. Triacon and alternate breakdown (Prenis, 1973)

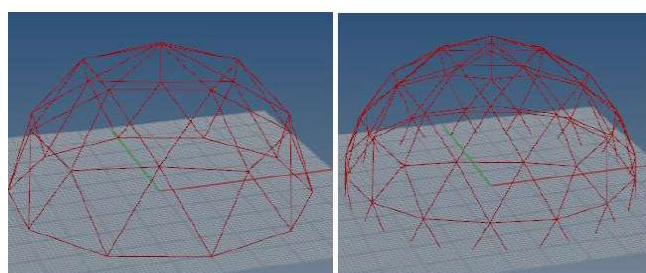


Figure 18. (left) $f = 2$: Horizontal struts at the equator (right) $f = 3$: Struts are cut into half at the equator (Ottenhaus, 2015)

3. The Armadillo Vault

According to Augustunowicz et al., (n.d.) the Armadillo Vault was created for the international architecture exhibition: 'Architecture Biennale' in Venice, Italy. This structure is a double curved free-form vault which contains of a force system that is in pure compression. Moreover, it is a shell structure built up from 399 dry assembled lime stone blocks and the geometry is further defined by a thickness range of 0,05–0,12m, span of 15m and total surface area of 75m².

The shape and components are generated by using a complex form-finding process with a thrust network analyses. Sketches were drawn in RhinoVault in the preliminary design phase. From this point a mesh was created and further refined to obtain the pure compressive structure using the 'best fit' procedure, in addition with other architectural requirements. Subsequently, a pure **compressive structure** was created which is caused by its double curved shape and **shallow geometry**. In addition, the components have a staggered arrangement where the load transfer surfaces are aligned with the force flow causing an adequate interlocking system and prevent the structure from sliding. Finally the interlocking system is created by using male and female notches that are attached to the load transferring surfaces, this principle is shown in figure 20.

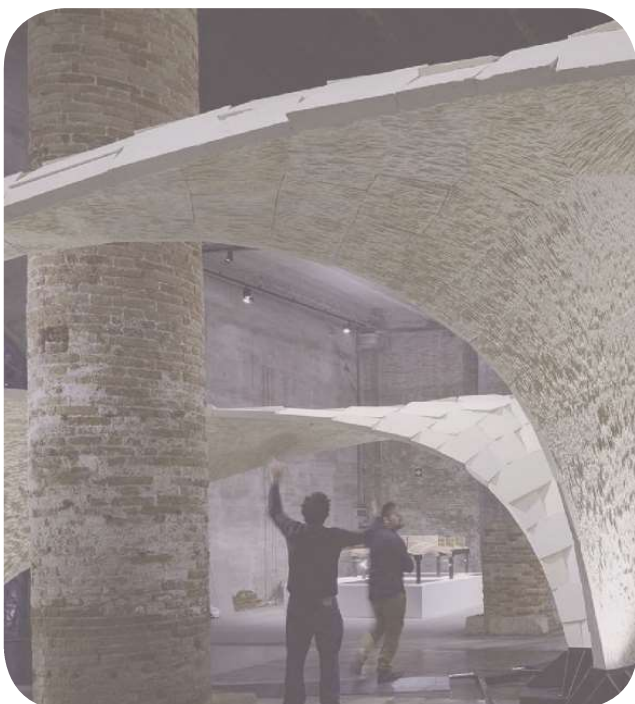


Figure 19. The Armadillo Vault (Augustunowicz et al., n.d.)

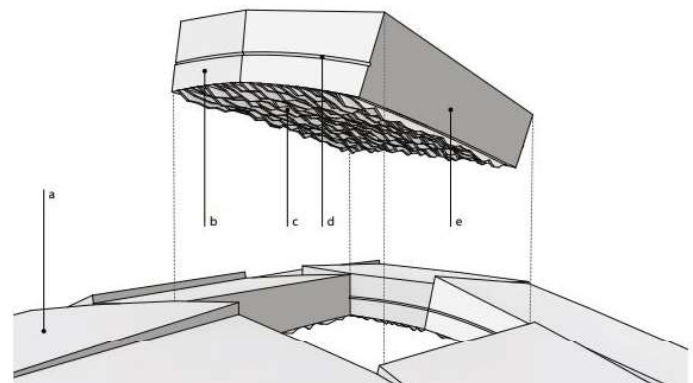


Figure 20. One voisoir lifted from the stone surface where side b and d refer to the load transferring surfaces with registration notch (Augustunowicz et al., n.d.)

4. Brunelleschi's dome

The dome of Brunelleschi is situated in Florence and exist of two adjacent shells, as shown in figure 21. Several assumptions in literature are made on how Brunelleschi constructed the dome because their are no existing blueprints. According to Museum Florence (2017) the dome is built without any scaffolding due to its double shell. The inner shell has a thickness of almost 2m and is constructed by light bricks with a herring bone arrangement. The inner shell is a self-supported structure. The outer shell serves as a weather skin where top is finished with a conical roof, designed by himself and unfortunately built after he died.

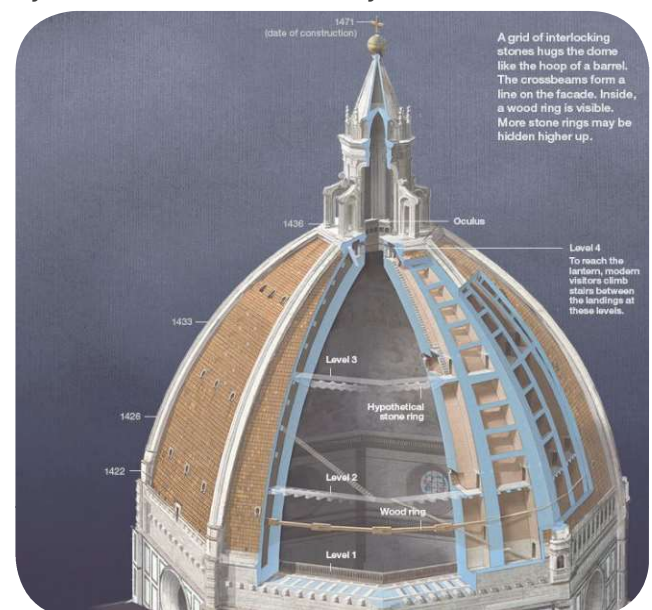


Figure 21. The two shell structure of Brunelleschi's dome (source: www.metalocus.es)

Brunelleschi used a herring/fish bone technique for constructing the inner shell. This technique creates stacked layers of bricks in a horizontal way although they are vertical oriented and have a regular interval, this technique is shown in figure 23. According to Vereyken (2007) this interval is wide at the bottom and narrows at the top resulting in large spirals. The bricks are constructed using radial sliders with an imaginary central focus point and guiding cord. The bricks in between these spirals needed to be cut (since the distance between the spirals narrows down) resulting in a high number of different components. Moreover the inner shell is constructed in phases and is raised in rings, this principle is shown in figure 22. The radial sliding method made it possible to utilize scaffolding for labours. The geometry of the fifth ring has an angle of 60 degrees, an increase in angle was not allowed, this would cause structural problem.

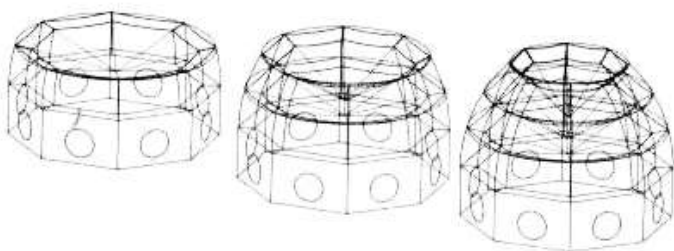


Figure 22. Radial sliding method
(source: www.solidariteetprogres.org).

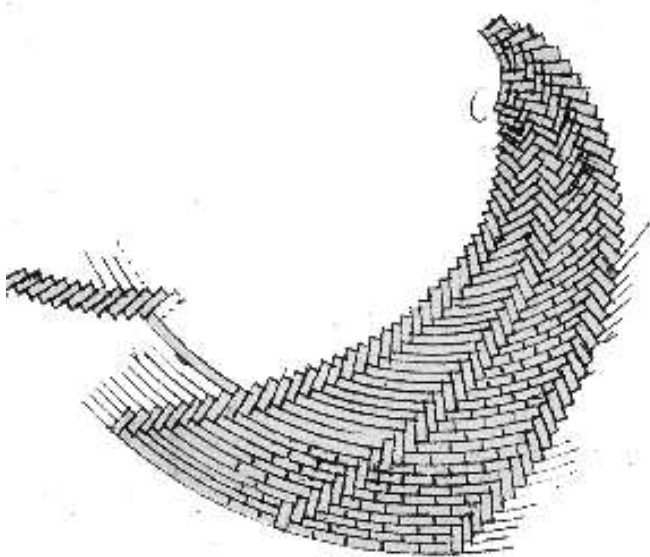


Figure 23. Herring/fish bone pattern of the inner shell
(source: www.solidariteetprogres.org).

Conclusion

A high number of different components is not preferred in this research since it will increase the number of molds and the related production costs. All the projects have a high to very high number of different components and therefore have a ranking of worst or intermediate.

The components of an igloo are created by hand and are large at the bottom and small at the zenith. Increasing the frequency of geodesic domes result in a high number of different components, this principle is shown in figure 24.

The form finding process of the Armadillo Vault was leading and the fish bone technique of the dome of Brunelleschi caused a high number of different components.

Geodesic structures can be made with an equal, in comparison with the other projects, small thickness which is preferred because it reduces the annealing time and therefore production costs. The Armadillo Vault is a shallow shell structure and is in pure compression. The Armadillo vault scores best on the compressive strength and thickness ratio, resulting in a high ratio. Although a thickness variance is not required because this will also lead to a high number of different components.

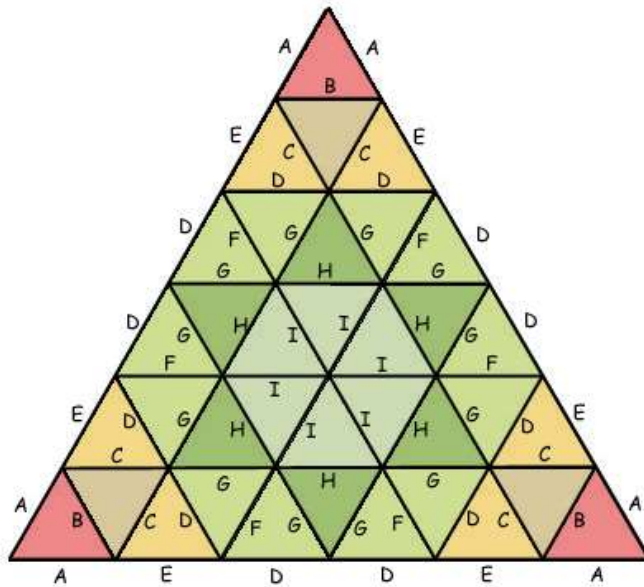
Curved components are preferred, like the Armadillo Vault components, because they will guide forces due to its round shape.

Stacked and interlocked connection are required to ensure high transparency because these type of connections will not require additional connections, such as steel reinforcements.

The criteria: 'the number of different components' and 'connection type' are dominant in the analysis because this research aims for a transparent structure with a minimum number of different components.

The building approach for constructing igloos is used as a starting point for designing the glass dome components. This decision is based on the dominant criteria within the multi criteria analysis.

The assessment of the building approaches of the different projects have led to design requirements for the glass dome. These design requirements are shown in table 2.



Example of an alternate dome structure with a radius of 12,5m and the following struts length:

- A=2,032m
- B=2,380m
- C=2,273m
- D=2,535m
- E=2,342m
- F=2,475m
- G=2,573m
- H=2,691m
- I=2,707m

Figure 24. Alternate dome structure (source: www.desertdomes.com)

Design requirements new components			
<i>criteria</i>		WHAT	WHY
COST	1. Number components	minimum	costs of molds
	2. Mass (kg)	< 10	annealing time
	3. Type of mold	permanent	precise result
STRUCTURAL	4. (C)Strength/thickness	high	reduce bending stresses
	5. Base material	cast glass	flexibility, one structure & transparent
	6. Form component	organic configuration of a block	avoid stress concentration at the edges
TRANSP.	7. Connection type	stacked with a transparent interlayer	deals with the tolerances

Table 2. Design requirements for the glass dome components based on the assessment of different building approaches.

2.1.4 Shapes

Introduction

The geometry of a dome depends among others on the structural requirements and constraints. The structural design requirement for this research is creating a **complete compressive force system** for the glass dome when subjected to symmetrical uniform loads, which is its self-weight. This design requirement aims for a reduction of the tension zone within the force system of the glass dome and gains advantage of the mechanical properties of glass, weak in tension and strong in compression.

A multi criteria table is provided in this chapter, in which various characteristics of the most common dome structures are rated. Based on this rating, it is concluded which dome shape is utilized and meets the defined requirement stated above: a force system based on compression which is subjected under its self-weight. Further analyses about the shape requires fundamental knowledge about the unsymmetrical non-uniform loads, which could be wind and is defined after the literature review.

Dome shapes

According to Borgart (2017) domes are also called surfaces of revolution, synclastic forms and are a variant of shell structures. A synclastic form is defined as a geometry that has a curvature (K) that is equal to $K > 0$. Other geometries can also be defined by its curvature, this is shown in figure 25.

Assessed dome shapes

A few shapes are assessed and all have synclastic curvatures and are obtained from Byzantine and Islamic architecture. According to Schueller (1996) most common dome shapes were obtained from Byzantine and Islamic architecture. Hence, most common dome shapes were assessed, which are: spherical, elliptical, melon, union, bulbous, parabolic and conical shapes.

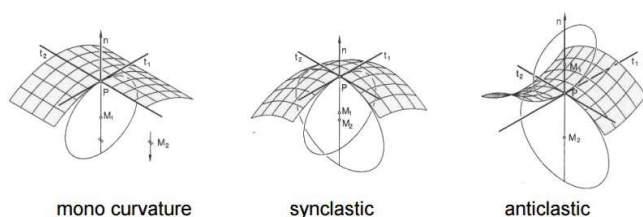


Figure 25. Different curvatures and definition (Borgart, 2017)

Multi criteria analysis

The multi criteria table is presented in table 3 and is assessed by four criteria. The 4 points are: capacity of compression **(1)**, volume-floor area ratio (2), possibility of openings **(3)** and usable floor area (4). The first and third criteria are both multiplied with a factor 2 since these criteria cover the main goal of the structural requirements. Criteria 2 is multiplied with a factor 1,5 since this criteria defines the important aim of being minimum invasive for the local environment.

The first criteria is the capacity of the compressive membrane forces in a dome. The meridian or arch forces (circumferential or hoop forces) need to be in compression to fulfil the requirement of creating a fully compressive structure. According to Schueller (1996) the membrane forces of a dome are in compression when the angle ϕ lies in between **45–51,83°**, this defines the boundaries for a compressive shell structure and depend on the height-span ratio. The latter mentioned aspect is explained in more detail in the chapter 'forces in domes'. Hence **shallow domes** are preferred above high rise domes because shallow domes can reach an angle ϕ which is close to 51,83° resulting in a fully compressive structure.

Secondly, the volume-floor area ratio aims for large floor areas and small volumes to reduce the energy demand for heating and cooling.

The third criteria, possibility of openings, is needed to allow for natural ventilation in the glass dome. Parabolic shapes have the advantage

of the presence of zero bending stress (when subjected to symmetrical loading), however when peak stresses do occur, bending stresses become infinite.

The last criteria is the usable floor area. The function of the dome is an aviary and is used by visitors as a passage or walk through. According to this, a height limit is set: height $\geq 3\text{m}$. This results in different usable floor areas, where high rise domes are preferred above shallow domes, this principle is seen in figure 26.

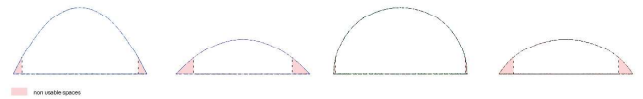


Figure 26. Unusable floor area (red) of the (shallow) parabolic dome and (shallow) hemisphere dome.

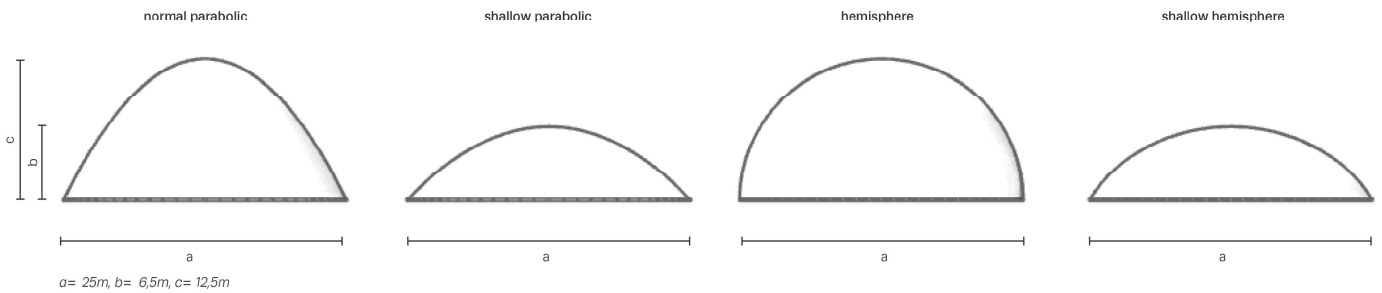


Figure 27. Overview (2D) dome shapes: (shallow) parabolic dome shape and (shallow) hemisphere dome shape.

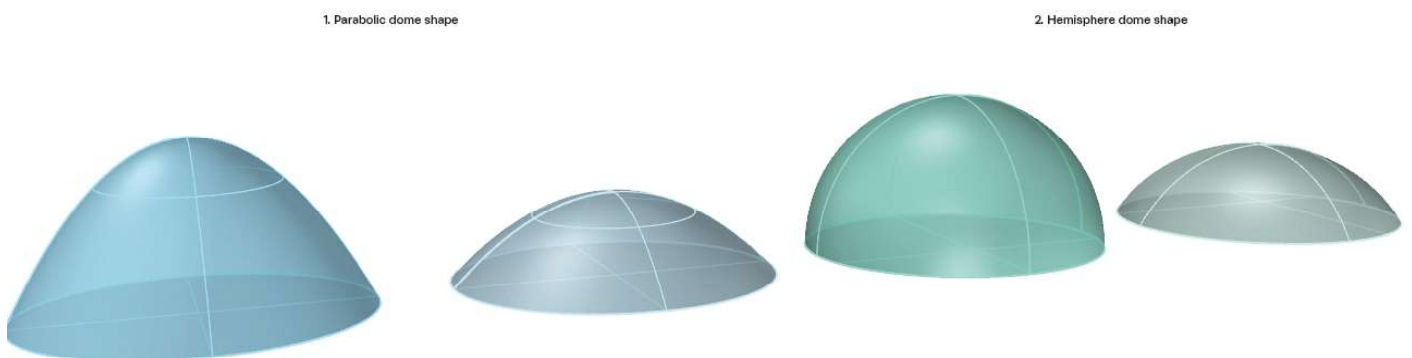


Figure 28. Overview (3D) dome shapes: (shallow) parabolic dome shape and (shallow) hemisphere dome shape.

Conclusion

It is concluded from the multi criteria analysis that spherical **shallow domes** are the most suitable shapes for this research because of the following reasons:

- A fully compressive force system, when subjected to its self-weight, can be created.
- The shallow dome allows for a respectively large usable floor area and small volume, resulting in a reduced energy demand for heating and cooling
- Openings within the shallow spherical dome structure are possible and are preferred above parabolic shaped domes. As mentioned before, parabolic shapes cannot resist peak stresses because this will result in an infinite bending stress. Parabolic shapes are not preferred because tensile stresses will occur and these tensile stresses cannot be fully absorbed by the glass components due to the material property of glass: weak in tension.

Dome shapes						
1. spherical	2. elliptical	3. melon	4. union	5. bulbous	6. parabolic	7. conical
a. shallow b. hemisphere	elliptical		cycloidal		a. shallow parabolic b. normal parabolic	
<i>Flat upper part of the dome leads to bending and buckling</i>						

Multi criteria table				
	spherical		parabolic	
	shallow	normal	shallow	normal
1. Capacity compression (1) <i>(height to span ratio, with span = constant: 25m)</i>	**	*	**	*
2. m ³ /m ² (2) <i>(floor area vs. Energy)</i>	***	*	****	**
3. Allows for openings	**		*	
4. Usable floor area <i>(h ≥ 3m)</i>	**	****	*	***
Total ranking (*)	14,5	11,5	13	10

* = x2
 * = x1,5
 (1) capacity compression under dead load, shell boundaries: $\Phi=45^\circ - 51,83^\circ$
 (2) m³ is constant, greatest value's of m³/m² are preferred to reduce the energy demand for heating and cooling

Table 3. Multi criteria analysis of the most common dome shapes

2.1.5 Membrane forces

The membrane theory of masonry domes is used to define the analytical stress analysis of the glass dome, the reason is two folded. The first reason is the equal main characteristics of glass and masonry: low tensile strength and high compressive strength. Secondly, a cast glass dome is never been built before. This chapter addresses the membrane theory, stresses and cracking pattern of masonry domes.

Hooke's hanging chain

According to Heyman (1995) a dome shape can be described as a rounded vault or arch and can take different forms. The structural performance of domes may be assessed by using the Hooke's hanging chain. The principle of Hooke's hanging chain is shown in figure 29, it shows a hanging flexible chain and when inverted presents the rigid arch.

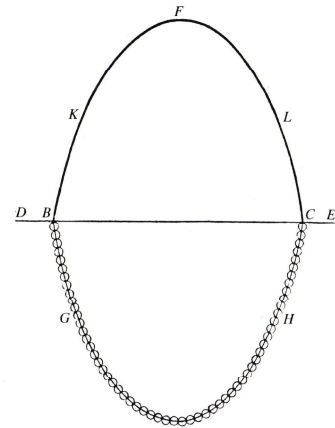


Figure 29. Hooke's hanging chain (Heyman, 1995).

The dome as a membrane

According to Heyman (1995) a shell can be designed and mathematically optimized as a curved surface. The membrane theory assumes that the thickness of a shell is small in comparison with the rise and span of the entire dome. The dome must resist its self-weight and other external loads by its internal forces, the so called membrane forces. The membrane forces of the dome are presented in figure 30. Another assumption of the membrane theory is: there is no stiffness against bending which will result in pure compressive internal forces.

The shape of the dome may be described as a rotated arch, however the force action within an arch and dome is different. The force actions within an arch and dome are explained by Hooke's hanging chain. The force action within a hanging membrane, e.g. made out of cloth, is different than the chain because the hanging membrane can take a wider range of loads without altering its shape. This principle is similar to a thin dome shell made from of a rigid material, where the dome can take a wide range of loads resisted by its membrane forces. Thin dome structures can be created because of the latter mentioned reason, however a certain thickness is needed to prevent local compressive buckling.

The inverted chain or membrane represents the line of thrust. The master of safe theorem states that a structure is stable when the line of thrust lies within the masonry. In addition, tensile

stresses will not occur when the line of thrust stays within the middle third of the cross section. This principle is shown in figure 31, where the line of thrust is located in red, which is the middle third of the cross section.

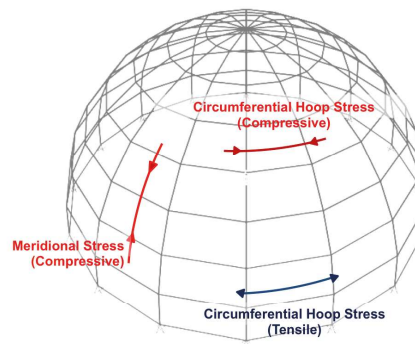


Figure 30. Hoop and meridional stresses in a dome (source: www.shells.princeton.edu)

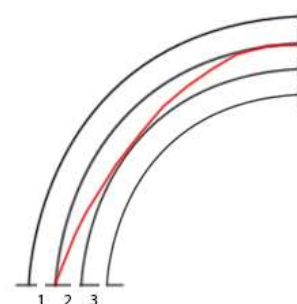


Figure 31. Principle of the line of thrust in an arch, where 2 represent the middle third of the cross section and the red line represents the line of thrust, based on (source: www.earth-auroville.com).

Stresses in domes

According to Heyman (1995) stresses in dome structures are generally low. This is explained by figure 32, where the dome is subjected to its self-weight and has a uniform thickness (t). The dome in figure 32 is supported by a horizontal diametric plane at its base where the support forces produce an equally distributed compressive stress (σ) to the dome. The compressive stress can be calculated using equation (1) and the dimensions given in the figure.

$$\sigma(2\pi at) = \rho(2\pi a^2 t) \quad (1)$$

Where,

$2\pi a^2 t$ = the volume of the dome

$2\pi at$ = the area of the diametrical ring

ρ = the unit weight

σ = the supporting stress

The necessary compressive stress is independent of the thickness of the dome because a doubling in thickness will result in a doubled weight and involved area. Thus, stresses in domes are assumed to be low because of the latter mentioned reason.

Buckling stress

Buckling analyses for domes are not easy to obtain however literature from Hoogenboom (2017) and Heyman (1995), agree and use equation (2) to determine the critical buckling stress.

$$\sigma_{cr} = kE(t/R) \quad (2)$$

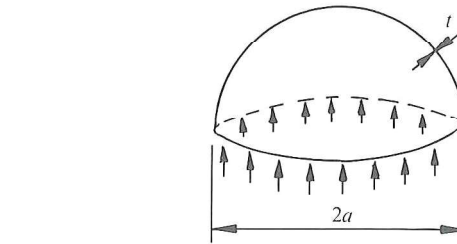
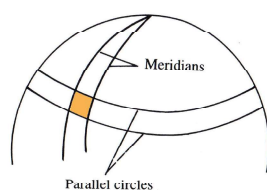
Where,

K represents the knockdown factor for including imperfections and varies from author to author but according to Heyman (1995) is equal to 0,25.

E represents the Young's modulus of the material

R represents the radius of curvature of the sphere

t represents the thickness



$$\sigma(2\pi at) = \rho(2\pi a^2 t),$$

$$\text{or } \sigma = \rho a.$$

Figure 32. Hemispherical shell subjected to its self-weight (Heyman, 1995).

Stress resultants (symmetrical loading)

Stress resultants are used in the membrane theory of domes instead of stresses (σ), where $N = \sigma t$. Self-weight (w) loads are defined per unit area, where $w = \rho t$. Substitution leads to the new equation 3:

$$N = wa \quad (3)$$

Figure 33 is used to explain the stress resultants acting within domes. The orange part in the left side of the figure is cut out and defined by two neighbouring meridians and parallel circles. This small element is shown at the right side of the figure and is located by the co-latitude ϕ (Φ) and co-longitude θ (Θ). There are stress resultants present in this small element, the meridional stress resultant (N_ϕ) and Hoop stress resultant (N_θ). Four stress resultants work on the cut edge of the element. These four resultants are needed to obtain equilibrium of the small element which is subjected to its self-weight. Note that asymmetrical loading results in an extra resultant, which is the shear stress resultant, however this resultant is neglected due to the symmetrical loading case.

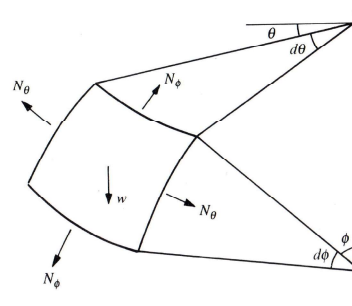


Figure 33. left side: meridians and parallels defining an element of the shell, right side: equilibrium of a small element of the shell, modified by author based on (Heyman, 1995).

The meridional stress can be calculated by using equation 4 and the hoop stress can be calculated by using equation 5. The results of these two equations are presented in figure 36. The meridional stress resultant ($N\Phi$) is compressive from base till dome top, $1/2wa$ at the top and wa at the support. The hoop stress ($N\Theta$) resultant is compressive from the dome top till a co-latitude of $51,82^\circ$, wa at the dome top, zero when the co-latitude equals $51,82^\circ$ and after this value it becomes a tensile stress which increases rapidly.

$$N\Theta = - (wa)/(1+\cos(\Phi)) \quad (4)$$

$$N\Phi = - (wa)*\cos(\Phi) - N\Theta \quad (5)$$

The equations for the hoop and meridional stresses are determined for small thick domes. However the actual thickness of the dome is never vanishingly small. It is assumed that domes will act the same as an arch, where the line of thrust creates an implied thrust against its supports which will result in slight yielding. This principle is shown in figure 34, where b and c represent the minimum thickness with a five hinge collapse mechanism. The slight yielding of the supports can be resisted by using an encircled tie.

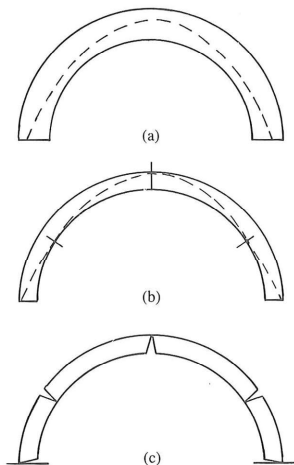


Figure 34. The semicircular arch (a) stable and (b),(c) of minimum thickness (Heyman, 1995).

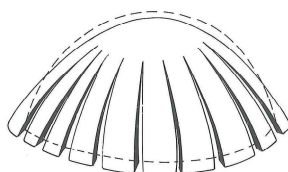


Figure 35. Greatly exaggerated scheme of a cracked dome due to the yielding effect of its supports (Heyman, 1995).

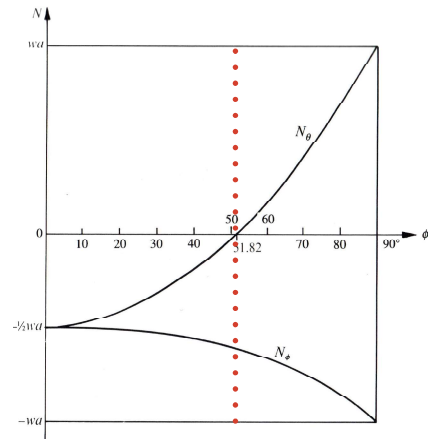


Figure 36. Values of the stress resultants in a hemisphere from crown ($\Phi=0$) to the base ($\Phi=90^\circ$), modified by author based on (Heyman, 1995)

Cracking pattern of domes

The literature states that supports of a purely compressive force system within a hemispherical dome with reasonable thickness gives a way slightly. This yielding effect of its supports, when not encircled by a tie to resist tension, will result in a cracked dome. The principle of a cracked dome, which is greatly exaggerated, is shown in figure 35. The dome will stay intact from the dome top till a co-latitude of approximately 25° , after this the dome is divided into meridional cracks.

It was found in the literature that Poleni illustrated this cracking effect for the St Peter's dome. Poleni found out that a dome is stable in cracked state when the thrust line of two lunes, which represents a quasi-two-dimensional arch, lies within the entire cross section of the material. The arch represents a slice of the entire dome, this shows that the arch is stable and therefore the dome is stable as well, in cracked state or not.

Conclusion

The overall conclusion from this sub-chapter is that the membrane stresses in domes are generally low and do not depend on the thickness. The membrane stresses are in full compression when the co-latitude equals $51,82^\circ$. And based on this literature review it is assumed that the analytical stress analysis will show that the glass dome need to be buttressed at its base supports with a tie to resist tension. The supports will start to yield when the glass dome is not supported at its base.

2.1.6 Conclusion

Literature review about dome structures have result in the general dimensions of the glass dome and related specific function description. These two results are explained below.

The general dimensions of the glass dome are a result of the shell boundaries for creating a compressive force system. A fully compressive shell structure, subjected to its self-weight, requires a co-latitude of $\leq 51,82^\circ$. This research proposes a **co-latitude of 45°** . The co-latitude of 45° is chosen to guarantee for maximum compressive membrane stresses when subjected to load, for example when subjected to asymmetrical loading such as wind. It should be noted that the structural behaviour of the glass dome should be investigated when subjected to asymmetrical loading, this to gain fundamental knowledge about occurring tensile stresses.

The general dimensions of the glass dome are shown in figure 37 and an overview is given in table 4. The simple formula: $\varphi = 17988,4 / (\sin(45))$ is used for determination of the general dimensions.

The general dimensions result in a shallow dome structure with a compressive force system when subjected to its self-weight. The glass dome aviary, with a shallow structure, does not allow for large tropical birds because these birds require high flying spaces.

This research proposes to design a **shallow glass dome aviary for Lori parrots**, this because of two reasons. First, Lori parrots do not require high flying spaces and secondly to perform a **fully compressive** force system.

DIMENSIONS				
index	discription	value	unit	used formula
Angle				
α	Angle of compression	45	°	
		0,79	radian	
Dome				
l	Span	35,98	m	
r	Radius foot dome	17,99	m	
s	Sagitta/rise	7,45	m	a-h
Sphere				
a	Radius	25,44	m	$r/\sin(\alpha)$
h	Height till dome	17,99	m	$\sqrt{a^2-r^2}$

Table 4. Overview of the general dimensions of the glass dome

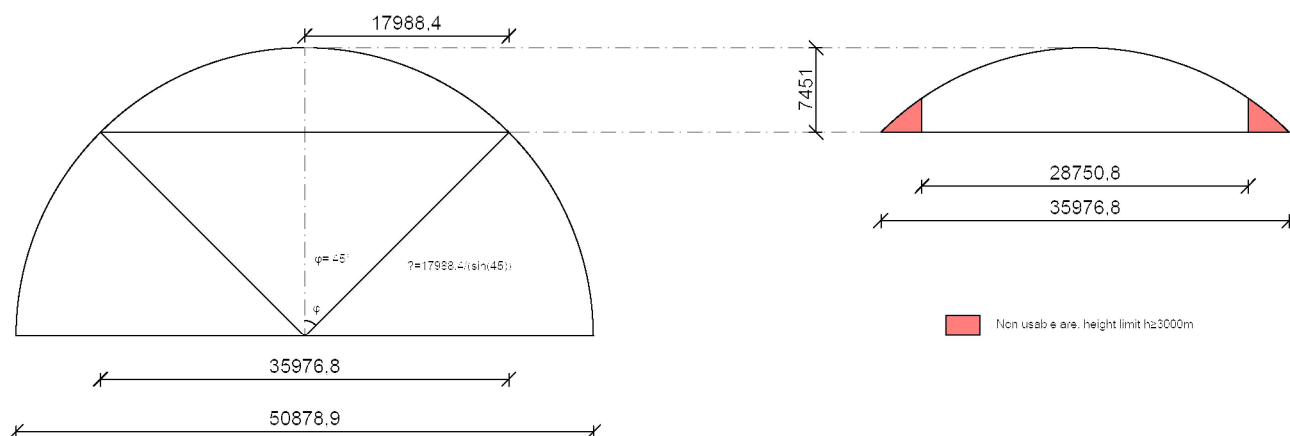


Figure 37. Overview of the determination of the general dimensions of the glass dome

2.2.1 Introduction

This chapter provides literature for describing the thermal performance of the glass dome with an aviary function. The overall aim is to obtain thermal comfort in the interior of the glass dome for Lori parrots, while being minimum invasive for the local environment by utilization of passive strategies. Passive strategies need to provide an ideal combination of material properties and passive systems such as natural ventilation, earth ducts and coloured glass.

Three main steps are taken to obtain the required thermal performance: addressing, assessing and optimizing the thermal performance. The first two steps are provided in this chapter and the last step is addressed in the chapter ‘thermal calculations’. The first step, addressing the thermal performance, defines and explains the different thermal comfort models and steps to create thermal comfort. Secondly, assessing the thermal performance, passive strategies are explained and assessed on suitability for the entire design of the glass dome, i.e. based on structural, thermal and aesthetic performance.

2.2.2 Thermal comfort models

Introduction

Some common thermal comfort models are explained in this sub-chapter: Fangers thermal comfort model, the Standard New Effective Temperature thermal comfort model, Thermoregulation two node-model and the adaptive thermal comfort model. One of the latter mentioned thermal comfort models is chosen for determination of the acceptable temperature range for the interior of the glass dome.

Thermal comfort models

The definition of thermal comfort is hard to define but in literature is stated as:

“that condition of mind which expresses satisfaction with the thermal environment and is assessed by subjective evaluation” (ASHRAE Standard 55, 2004, p.3).

According to ASHRAE Standard 55 (2004), the primary factors that define thermal comfort are: air temperature, mean radiant temperature, air velocity, humidity, clothing and metabolic rate. These aforementioned factors are not important, according to the definition of thermal comfort by ASHREA Standard 55, the perception of these combined factors is important.

According to Lee and K. Strand (2001) the **Fanger Comfort Model** was developed by P.O. Fanger in 1967 at the Technical University of Denmark and Kansas State University, established in 1972.

According to Nakano (2003), Fanger (1970) announced a heat balance equation to determine thermal neutrality where the generated energy within the body, i.e. metabolic rate, is equal to the heat loss to the environment in a steady state condition, i.e. equal physiological conditions due to mechanical equipments. Thermal sensation beyond the thermal neutrality is formulated in the sensation index, the so called **Predicted Mean Value (PMV)**. According to Lee et al.(2001), this value can be calculated with the formula shown in equation 1:

$$PMV = (0.303e - 0.036M + 0.028) * (H - L) \tag{1}$$

Where,

H = the internal heat production rate of an occupant per unit area (= M – W), W/m²

L = all the modes of energy loss from body, W/m²

M = the metabolic rate per unit area, W/m²

The calculated Predicted Mean Value is classified on a seven point scale shown in table 5, where the 0 represents thermal neutrality, positive values represent warm till hot conditions and negative values represent slightly cool till cold conditions.

Value	Sensation
3	Hot
2	Warm
1	Slightly warm
0	Neutral
-1	Slightly cool
-2	Cool
-3	Cold

Table 5. seven point sensational scale based on (Fanger, 1970)

According to Nakano (2003) it is not possible to predict the extent of satisfaction for occupants for a certain thermal environment by using the PMV model. Hence, to predict the satisfactions for occupants within a thermal environment related to the PMV model the **Predicted Percentage of Dissatisfied (PPD) model** was introduced. The PDD model predicts the percentage of dissatisfaction for occupants within a thermal environment where dissatisfaction occurs when the PMV-value reaches +/- 2 or greater.

According to Lee et al. (2001), **The Pierce Two-Node Model (2NM)** was developed by the John B. Pierce Foundation at the Yale University and began with development in 1970. The 2NM model divides the human body into two parts, the first part is the internal core and the second part defines the skin. Several factors should be taken into account when defining the thermal sensations of the human body with the 2NM. These factors are: passive heat conduction from core to skin, differences in core and skin temperature and the effects of shivering. The thermal sensation, termed as TSENS, can be calculated by using the formula's 2,3 and 4. The resulting sensation index established from these formula's given below are classified with a similar scale used for the PMV calculation of the Fanger model.

$$\text{TSENS} = 0.4685 * (\text{T}_b - \text{T}_{b,c})$$

$\text{T}_b < \text{T}_{b,c}$ in a cold environment (2)

$$\text{TSENS} = 4.7 \eta_{ev} * (\text{T}_b - \text{T}_{b,c}) / (\text{T}_{b,h} - \text{T}_{b,c})$$

$\text{T}_{b,c} \leq \text{T}_b \leq \text{T}_{b,h}$ in a warm environment (3)

$$\text{TSENS} = 4.7 \eta_{ev} + 0.4685 * (\text{T}_b - \text{T}_{b,h})$$

$\text{T}_{b,h} < \text{T}_b$ in a hot environment (4)

Where,

T_b = the mean body temperature in °C
 $\text{T}_{b,c}$ = the mean body temperature, lower limit for evaporative regulation zone in °C
 $\text{T}_{b,h}$ = the mean body temperature, upper limit for evaporative regulation zone in °C
 η_{ev} = the evaporative efficiency

According to Ye, Yang, Chen and Li (2003) **The Standard New Effective Temperature (SET)** thermal comfort model is based on the dynamic 2NM. The SET model was introduced in 1986 by ASHRAE and defined as the equivalent temperature of an isothermal environment* with a 50% relative humidity in which a subject, with standardized clothing according their activity, has equal skin temperature and skin wetness as the tested thermal environment.

To define comfort indexes of the SET's and 2NM models asks for complex calculations, in comparison with the steady state PMV calculation from Fanger, due to the thermal physiological factors that need to be determined within the 2NM.

The Fanger model (PMV & PDD model), SET and 2NM are all based on equal physiological, steady state conditions. It is very odd to use methods based on equal physiological, steady state conditions because temperatures are anything but steady.

According to Nicol, Humphreys and Roaf (2012) the **adaptive model** was proposed to interpreted thermal comfort for, inter alia, free running buildings. The principle of this adaptive model is stated in the following sentence: *'if a change occurs such as to produce discomfort, people react in ways which tend to restore their comfort'* (Nicol et al., 2012, p.29). Subsequently, there are many adaptive actions, taken by people, that define thermal comfort and are described by a combination of adaptive actions. The five basic adaptive actions taken by people are:

- Adjusting the rate of internal heat generation
- Adjusting the rate of body heat loss
- Adjusting the thermal environment
- Choosing a different thermal environment
- Adapting the body's physiological comfort conditions.

The result of the adaptive model is the comfort temperature. The adaptive standards are used to determine the comfort temperature and are given in the ASHRAE 55 and EN15251. The difference between these standards are the derived databases. The ASHRAE 55 standard obtained

* "Isothermal environment refers to the environment at sea level, in which the air temperature is equal to the mean radiant temperature, and the air velocity is zero" (Ye et al., 2003, p.36).

data from different countries, 30 different buildings taken and by different research teams and instruments. Unlike the EN15251 standard, ASHRAE 55 standard obtained data from five European countries using a uniform experimental measurements and instruments.

Conclusion

Within this research the **adaptive thermal comfort model** is proposed using the standards stated in **ASHRAE 55** for naturally conditioned buildings. The proposed glass dome is located in Southern France and is assumed to be a free running building where passive strategies are used to obtain the desired thermal comfort. Using the adaptive model to determine the thermal comfort temperature in a free running building is more accurate because the Fanger model (PMV & PDD model), SET and 2NM are all based on equal physiological, steady state conditions. Standards stated in the ASHRAE 55 are used because as shown in equation 5 the monthly/prevaling mean outdoor temperature is used and gives the advantages that it is widely available, i.e. as a historical mean over 20–30 years and monthly mean outdoor temperature.

$$T_{\text{comf}} = 0,31T_o + 17,8 \quad (5)$$

Where,

T_{comf} represents the optimal temperature for comfort within naturally conditioned buildings and T_o represents the prevailing mean outdoor temperature.

2.2.3 Thermal comfort steps

According to Regnier (2012) there are seven main thermal comfort steps to create thermal comfort, these steps are explained in relation with the glass dome design below.

1. Defining the thermal environment

According to Nakano (2003) the thermal environment indicates the applied environmental control and is divided into three layers: outdoor, semi-outdoor and indoor environment as shown in figure 38. The outer layer represents the outdoor environment with no environmental control, i.e. no artificial adjustments, where people take adaptive actions to obtain thermal comfort. The inner layer represents the indoor environment where HVAC (Heating, Ventilating and Cooling) systems provide the desired thermal comfort and is subdivided into two other layers: occupied zone and personal/task zone. The subdivision of the indoor environment is realized to create higher quality and efficiency of the environmental control. The layer in-between the outdoor environment and indoor environment represents the semi-outdoor environment and is stated in the literature as: *'an architectural environment where natural outdoor elements are designedly introduced with the aid of environmental control'* (Nakano, 2003, p.14). The level of control within a semi-outdoor environment range from passive to active strategies, such as simple shading in an open terrace or a mechanical heating, cooling and ventilation systems in a closed glazed atrium.

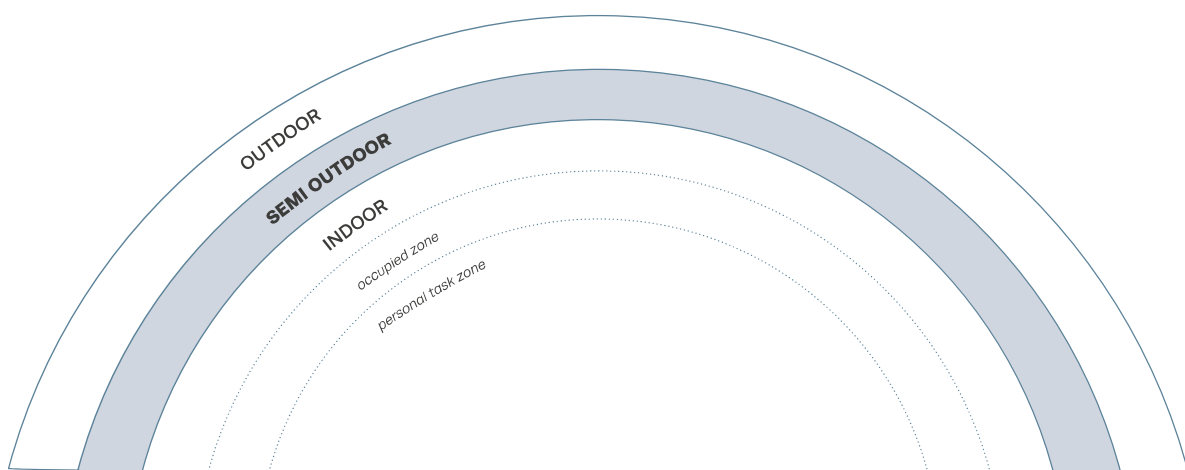


Figure 38. Layers of thermal environment surrounding a man, modified by author based on (Nakano, 2003)

The main use of a semi-outdoor environment is a passage or an agora where people can leave or can stay at their will. The thermal comfort criteria of a semi-outdoor environment should be investigated in relation to the actual usage of a semi-outdoor environment during the transition phase from outdoor to an indoor environment. In the literature the transition phase is divided into two phases: walking through and short term occupancy phase for a period less than an hour. Semi-outdoor environments act as thermal buffer spaces during the transition from indoor to outdoor environments. People experience a step change of the thermal environment when changing to another thermal environment, this step change is reduced by a thermal buffer space. Figure 39 represents a conceptual scheme of the consequence of the thermal buffer space.

Conclusion

In this research the glass dome functions as a **protection shield** for Lori parrots located in the zoological garden which is 'Parc des Oiseaux' in France. At the same time the glass dome functions as a **passage** or a **short term occupancy** place for humans to observe the Lori parrots. Hence, the thermal environment of the glass dome in this research is described as a **semi-outdoor environment** because of these reasons mentioned above.

2. Select weather and wind data

The location Villars Les Dombes in France is the proposed building location for this research, the exact location is the Zoological garden: 'Parc des Oiseaux' and will replace the current aviary: 'volière les loris'. Weather and wind data are given in this sub-chapter and are based on different climate sources.

The average temperatures and precipitation are shown in figure 40 with the minimum (blue) and maximum (red) daily average temperatures and precipitation for each month. The dashed lines present the daily average for the coldest night (blue) and hottest day (orange). The figure clearly shows that the warmest months are July and August resulting in minimum precipitation. The coldest months are January and December resulting in the greatest precipitation.

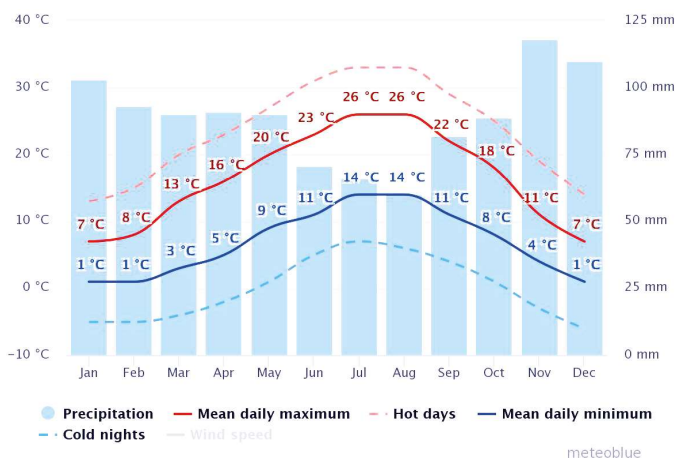


Figure 40. Average temperatures and precipitation (Source:www.meteoblue.com)

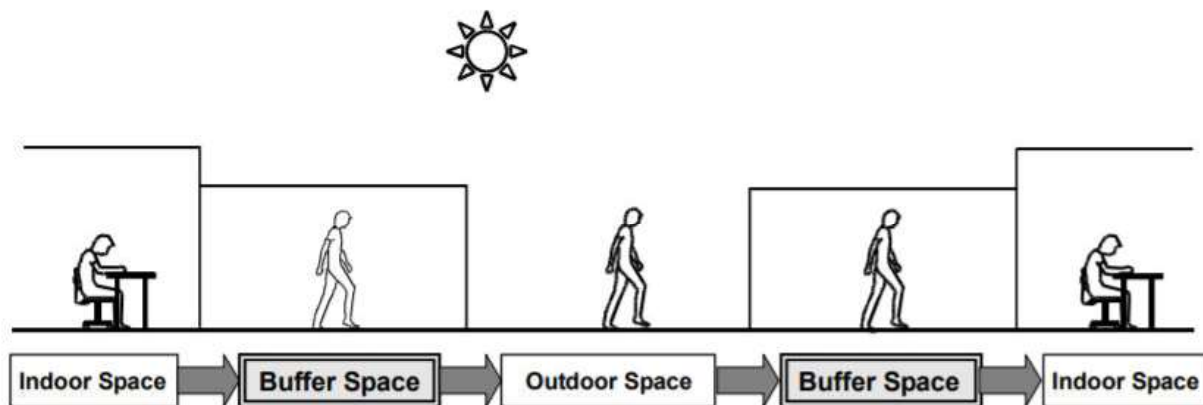


Figure 39. Conceptual scheme of the consequence of the thermal buffer space (Nakano, 2003)

Figure 41 presents the amount of sunny, overcast and precipitation days for each month. When the sky consists of < 20% clouds it is defined as sunny, between 20–80% defined as partly cloudy and above the 80% it is stated as overcast. The blue line presents the precipitation days for each month.

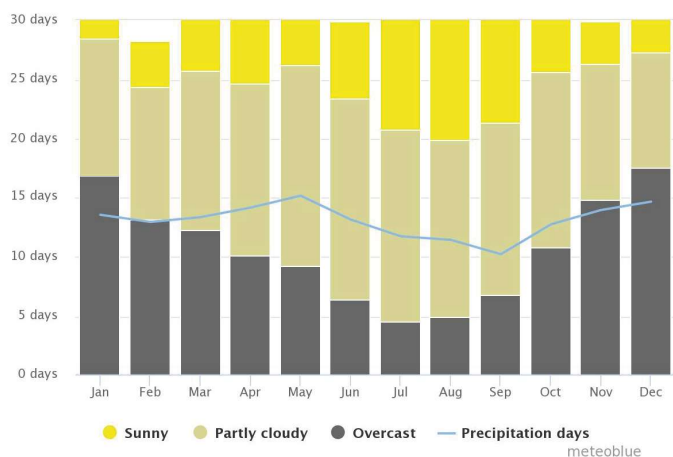


Figure 41. Cloudy, sunny and precipitation days (Source:www.meteoblue.com)

The number of days and correlated wind speeds vary for each month and are shown in figure 42. From December to April strong winds may occur (duration of approximately 0.5 day), with a related wind speed of ≥ 50 km/h, while from June to October calm winds are present. The dominant wind speed range equals: 5–28 km/h.

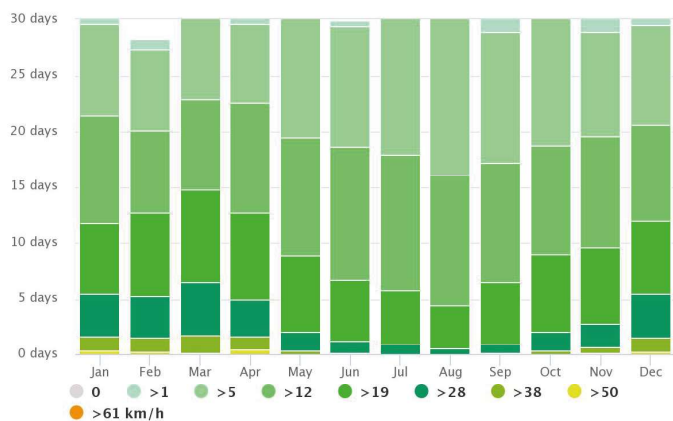


Figure 42. Wind speed (Source:www.meteoblue.com)

The hourly wind direction varies through the year, as shown in figure 43. The main dominant wind-direction, from the 28th of January to the 1st of October, is the North direction. The main dominant wind-direction, from the 1st of October to the 28th of January, is the South direction^[3].

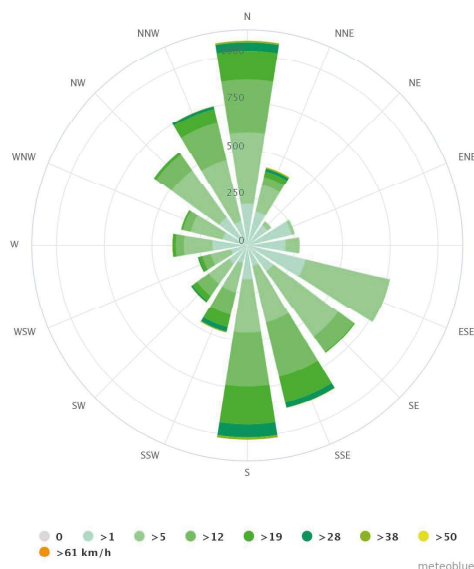


Figure 43. Wind rose (Source:www.meteoblue.com)

The relative humidity data from 2012 to 2017 are presented in figure 44. The relative humidity data varies from 90–62%, from 2012–2017, which represents a very humid climate. The relative humidity is related to the outdoor temperature: the lowest relative humidity occurs in summer when high temperatures are present and the highest relative humidity occurs in winter when lower temperatures are present^[4].

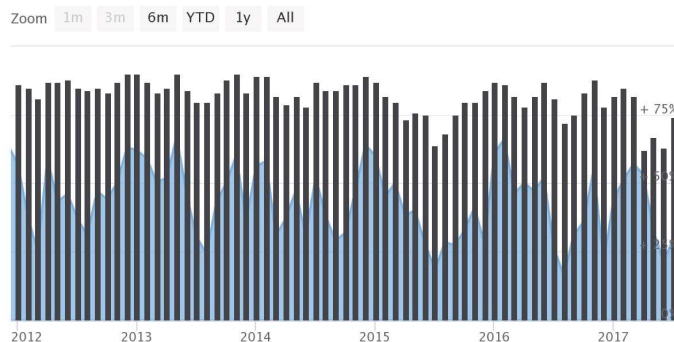


Figure 44. Relative humidity data from 2012–2017 for each month (source: https://www.worldweatheronline.com)

[3] <http://www.weatherspark.com>, [4] <http://www.worldweatheronline.com>

Conclusion

Based on the weather data presented in the climate diagrams some conclusions can be made. The warmest months are July and August with minimum precipitation and the coldest months are January and December with the highest precipitation. During the year the relative humidity varies from 90–62%. The mean daily maximum temperature in July and August is 26°C and the mean daily minimum temperature in January and December is 1°C. There are two main wind directions which are classified for two ranges: these are from the 28th of January to the 1st of October with a North dominant wind direction and from 1st of October to the 28th of January with a South dominant wind direction. Moreover Villars Les Dombes is classified as a cfb climate which is defined as a **temperate maritime climate** and used in this research.

3. Select thermal comfort standard

As a forementioned, The ASHRAE 55 standard and the adaptive thermal comfort model are used for this research, a recap of the mean thermal comfort temperature is given in the equation 6.

$$T_{\text{comf}} = 0,31T_o + 17,8 \quad (6)$$

4. Define conditioning systems

The overall aim is to obtain thermal comfort in the interior of the glass dome for Lori parrots while being minimum invasive for the local environment by the utilization of passive strategies. The assumption is made that the entire thermal comfort design cannot be obtained from using an all passive strategy design, because some passive systems need active systems, e.g. heat recovery systems and ground air heat exchange. Because of this aforementioned reason a **current mixed mode** is proposed.

5. Determine environmental comfort conditions

According to Nakano (2003) a semi-outdoor environment often appears in architecture in the form of an Atrium. The concept design of an atrium depends on the climate, location and required comfort level of the building. The comfort level is divided into four

main categories: 1) canopy, 2) buffer, 3) tempered buffer and 4) full comfort. Little literature is present about the target values of these aforementioned comfort levels but two empirical atrium designs are obtained from the literature. The empirical atrium designs provide thermal design criteria, for winter and summer situations in the UK and Japan, as shown in table 6 and 7. The difference between these latter two is that Japan has a hot, humid summer and UK has a moderate summer.

An assumption for determination of the environmental criteria of this research is made and is based on the environmental criteria for UK atrium's because the proposed location, which is Villars Les Dombes, has a similar summer climate which is a moderate climate. The glass dome is defined as **tempered buffer/partial comfort environment** based on several reasons concerning the Lori parrots, visitors and caregivers of the Lori parrots. The expected stay of visitors and caregivers of the Lori parrots would be less than an hour, therefore the environment cannot be defined as an entire tempered buffer or full comfort place. It was found that the comfort temperature range of **Lori parrots** is equal to the temperature range within residences^[5], which is **18–25°C** during winter and **18–30°C** during summer^[6]. In this research it is assumed that Lori parrots are comfortable in tempered buffer/partial comfort environments. The target winter and summer **comfort occupancy temperature** is obtained from table 6 and defines a tempered buffer/partial comfort environment with a minimum comfort temperature of **19°C** during winter and maximum comfort temperature of **30°C** during summer, with peak air temperatures to 35°C.

To resume, the occupancy temperature range for a buffer/partial comfort environment is 19–30°C. During the non-occupancy hours which is outside 09.30–18.00 o'clock, when the Zoological garden 'Parc des Oiseaux' closes, another temperature range is set because the Lori parrots tolerate lower temperatures. This results in a non-occupancy temperature range of 18°C–30°C. The temperature margins for the interior of the glass dome of the (non)occupancy hours are given in table 8.

[5] <http://www.vrolijkpepegaai.nl>

[6] <http://www.gemiddeldgezien.nl>

Atrium Type	Performance Level	Applications	Comfort Criteria	
			Heating (Winter)	Cooling (Summer)
Canopy	Shelter, shade, No air containment.	Shopping precincts, Links between buildings, or alongside buildings.	Ambient air temperature. No heating.	Ambient air temperature. No cooling.
Buffer	Winter air containment. Shelter, shade, summer natural ventilation	Conservatory link, Covered courtyard, Covered shopping center.	No heating. Air temperature above ambient due to internal solar gains by 5°C-	No cooling. Natural ventilation used to remove excess heat. Peak air temperature around 30 to 35 °C
Tempered Buffer	Winter air containment. Shelter, shade, background heating. Summer natural ventilation	Office entrance halls, Enclosed shopping centers.	Air temperature heated to 10 °C in occupancy zone.	As above.
Partial Comfort	Winter air containment. Shelter, shade, heating. Summer natural and or mechanical ventilation.	Office entrances and meeting halls, Enclosed shopping centers, Hotels, Restaurants, hospital, Glazed links.	Air temperature heated to 19 °C in occupancy zone. Radiant heating to offset cold glazing.	As above.
Full Comfort	Winter air containment. Shelter, shade, heating ventilation and mechanical cooling	Office space, banking halls, Enclosed shopping centers, Prestige hotels, restaurants.	Winter design 19 °C minimum.	Summer design 25 °C maximum. Mechanical cooling.
Passive Solar	Can be between buffer and full comfort according to design approach.	Any. Design approach seeks to optimize solar gains during winter and maximize natural ventilation effects in summer.	Winter design up to 19 °C as designed. Heating to supplement solar gains.	No mechanical cooling. Thermal stack effects optimized to achieve high air changes Peak temperatures around 27 to 30 °C.

Table 6. Environmental criteria for UK atrium (Mills, 1990)

Atrium Type	Performance Level	Applications	Comfort Criteria	
			Heating (Winter)	Cooling (Summer)
Canopy	Shelter, shade, No air containment.	Shopping precincts, Links between buildings, or alongside buildings.	Ambient air temperature. No heating.	Ambient air temperature. No cooling.
Buffer	Winter air containment. Shelter, shade, summer natural ventilation	Conservatory link, Covered courtyard, Covered shopping center.	No heating. Air temperature above ambient due to internal solar gains by 5°C+	No cooling. Natural ventilation used to remove excess heat. Peak air temperature around 30 to 35 °C
Tempered Buffer	Winter air containment. Shelter, shade, background heating. Summer natural ventilation	Office entrance halls, Enclosed shopping centers.	Air temperature heated to 10 °C in occupancy zone.	As above.
Partial Comfort	Winter air containment. Shelter, shade, heating. Summer natural and or mechanical ventilation.	Office entrances and meeting halls, Enclosed shopping centers, Hotels, Restaurants, hospital, Glazed links.	Air temperature heated to 19 °C in occupancy zone. Radiant heating to offset cold glazing.	As above.
Full Comfort	Winter air containment. Shelter, shade, heating ventilation and mechanical cooling	Office space, banking halls, Enclosed shopping centers, Prestige hotels, restaurants.	Winter design 19 °C minimum.	Summer design 25 °C maximum. Mechanical cooling.
Passive Solar	Can be between buffer and full comfort according to design approach.	Any. Design approach seeks to optimize solar gains during winter and maximize natural ventilation effects in summer.	Winter design up to 19 °C as designed. Heating to supplement solar gains.	No mechanical cooling. Thermal stack effects optimized to achieve high air changes Peak temperatures around 27 to 30 °C.

Table 7. Environmental criteria for Japanese atrium based on SHASE, 2002 (Nakano,2002)

Occupancy schedule	Time interval	Summer(Tc)	Winter(Tc)
Occupancy hours	09.30-18.00 o'clock	Max:30°C	Min: 19°C
Non-occupancy hours	18.00-09.30 o'clock	Max:30°C	Min: 18°C

Table 8. The target temperature margins of the interior of the glass dome based on (Nakano, 2003 and source: www.gemiddeldgezien.nl).

According to Nicol et al. (2010), a 2,5°C thermal comfort offset zone results in less than 10% discomfort. An thermal comfort offset zone of 3,5°C results in less than 20% discomfort. The comfort equation and related offset zones are based on indoor naturally conditioned environments. According to Gatsiou (2015), a semi-outdoor environment results in a thermal comfort offset zone of 5°C with less than 30% discomfort, this because people tolerate higher temperature differences in semi-outdoor environments. Table 9 presents the target temperature margins with a thermal comfort offset range of 5°C.

The temperature margins shown in table 9 and 8 do not take in account other weather conditions throughout the year. As aforementioned, the interior comfort temperature depends on the actual outdoor temperature and can be predicted for naturally conditioned buildings by using the adaptive model which is shown in equation 7 and based on the ASHRAE 55 standard.

$$T_{\text{comf}} = 0,31T_o + 17,8 \quad (7)$$

Table 10 presents the new proposed temperatures range during occupancy hours and non-occupancy hours to perform thermal comfort in the interior of the glass dome throughout the entire year. It should be noted that the following assumption is made: the determination of the comfort temperature for Lori parrots is equal to the determination of the comfort temperature for visitors and caregivers.

6. Determine occupant control standard

The caregivers of the Lori parrots and other staff from the zoological garden 'Parc des Oiseaux' can control the thermal comfort for the interior of the glass dome. Education of the caregivers and staff is required to to operate the climate control systems while creating thermal comfort.

7. Determine number of exceeding hours

According to Regnier (2012) the number of exceeding hours incorporates the performance of the conditioning systems. This criteria is defined after the simulation in the Design Builder software.

Occupancy schedule	Time	Summer(Tc)		Winter(Tc)	
<i>Occupancy hours</i>	09.30–18.00 o'clock	Max:30°C	Tc-5°C to Tc to Tc+5°C	Min: 19°C	Tc-5°C to Tc to Tc+5°C
<i>Non-occupancy hours</i>	18.00–09.30 o'clock	Max:30°C	Tc-5°C to Tc to Tc+5°C	Min: 18°C	Tc-5°C to Tc to Tc+5°C

Table 9. The target temperature margins associated with the thermal comfort offset range of 5°C.

occupancy hours			
To (°C)	Tc (°C)	Temperature range (°C)	correction (°C)
-10	14,7	9,7–19,7	19–19,7
-5	16,3	11,3–21,3	19–21,3
0	17,8	12,8–22,8	19–22,8
5	19,4	14,4–24,4	19–24,4
10	20,9	15,9–25,9	19–25,9
15	22,5	17,5–27,5	19–27,5
20	24	19–29	19–29
25	25,6	20,6–30,6	20,6–30
30	27,8	22,8–32,8	22,8–30
35	28,7	23,7–33,7	23,7–30
40	30,2	25,2–35,2	25,2–30

non-occupancy hours			
To (°C)	Tc (°C)	Temperature range (°C)	correction (°C)
-10	14,7	9,7–19,7	18–19,7
-5	16,3	11,3–21,3	18–21,3
0	17,8	12,8–22,8	18–22,8
5	19,4	14,4–24,4	18–24,4
10	20,9	15,9–25,9	18–25,9
15	22,5	17,5–27,5	18–27,5
20	24	19–29	19–29
25	25,6	20,6–30,6	20,6–30
30	27,8	22,8–32,8	22,8–30
35	28,7	23,7–33,7	23,7–30
40	30,2	25,2–35,2	25,2–30

Table 10. New proposed temperature margins during (non)occupancy hours for the interior of the glass dome based on the prevailing outdoor temperature (To).

2.2.4 Passive strategies

In this chapter the following definitions are explained in this chapter: (near to) zero energy building and passive strategies. The parameters, that can be used to optimize the thermal comfort for the interior of the glass dome by utilization of passive strategies, are addressed and analysed after the latter mentioned explanation.

Definitions

According to Rodriguez-Ubinas et al. (2014) the Energy Performance of Buildings Directive (EPBD) presented, in 2002, a directive which maintains energy supply and covers the needs of climate change and is based on the Kyoto protocol. The EPBD (2002) include directives to reduce the energy consumption while improving energy efficiency in buildings. This directive was changed in 2010 and new requirements were created for constructing (Near to) Zero Energy Buildings ((Near to)ZEB). The definition of a (near to) zero energy building is that these buildings have a high energy performance and an energy demand that is close to zero or very low. The directive aims for renewable sources, preferable available on site. The definition of a ZEB is very broad, and definitions include words as: low, very, high and nearly. It is not defined how close to zero is enough to be a near to zero building. The definition is not precise although the changed EPBD gives important conditions of zero energy buildings. The first condition states that it is important to decrease the energy consumption while improving the systems efficiency in buildings. Mechanical systems (active systems) maintain a comfortable indoor environment and cause high energy consumptions. Hence, passive design strategies are required to reduce the energy consumptions.

Figure 46 gives an overview of the ZEB approach, where passive design strategies are the goal to achieve ZEB and minimize the cooling and heat

load instead of using an innovative solution. This figure also presents the area's that can be optimized, these area's are: envelope, orientation, geometric and ratios, other passive strategies and hybrid solutions. The envelope, orientation, geometric and ratios require external energy to improve the thermal performance in buildings while other passive strategies and hybrid solutions do not require external energy. The latter mentioned strategies are defined as strategies that take advantage of their local climate conditions such as wind, solar radiation, daylight, ground temperature, clear skies and thermal variance. Examples of these other passive strategies and hybrid solutions are given in figure 45.

According to Santamouris (2007) the mean indoor temperature, within passively cooled or heated buildings, depends on the physics of the building form, the amount and location of its mass, size of the windows, the extent of their shading in summer, insulation, other material properties and the effect of passive systems.

Optimization of the thermal performance in buildings starts with explaining the needs for thermal comfort and a study of the available natural resources. Next, passive strategies and related natural resources can be sought. Passive strategies focus on air quality, natural daylight and hygrothermal comfort, these aspects can be optimized within the area's shown in figure 47.

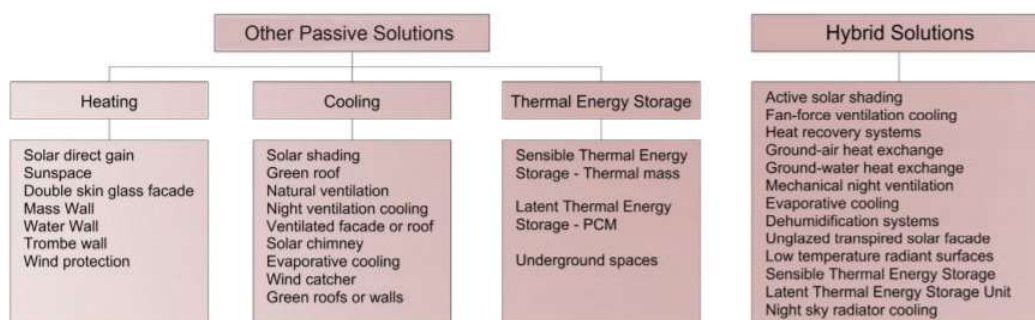


Figure 45. Other passive solutions and Hybrid solutions (Rodriguez-Ubinas et al., 2014)

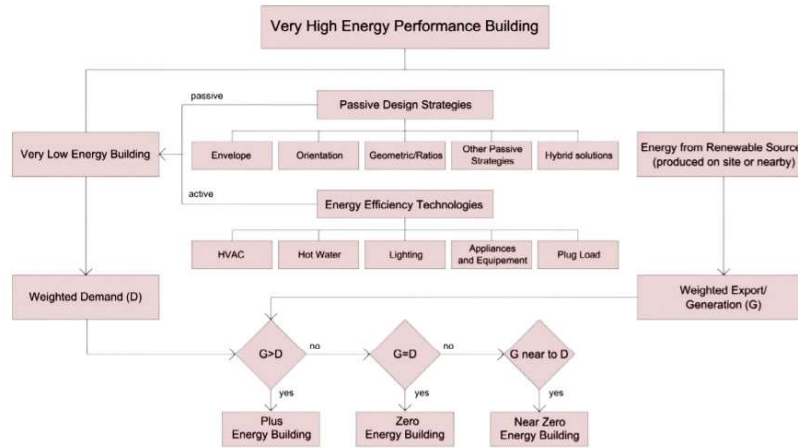


Figure 46. Diagram of the ZEB approach (Rodriguez-Ubinas et al., 2014)

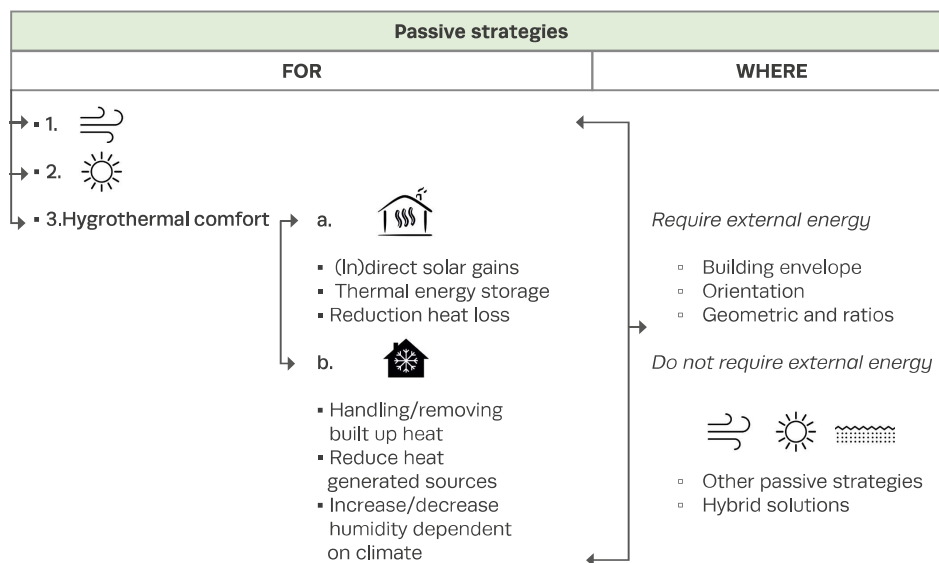


Figure 47. Overview passive strategies and related area's based on (Rodriguez-Ubinas et al., 2014)

Passive strategies for the glass dome

The passive strategies focus on **overheating risk** because high temperatures are most prevailing in the climate of 'Villars Les Dombes', as shown in figure 48. The effectiveness of the passive strategies is proved in the Design Builder software and explained in the chapter 'thermal calculation'. The results obtained from Design Builder present the amount of additional heat and cooling energy covered by mechanical systems. As aforementioned, an all passive strategy design is not possible because some passive systems require active systems. Although this research aims to use as many passive strategies as possible to reduce the energy demand and related cost. Three general parameters can be optimized, these are: 1) Thermal mass 2) Natural ventilation and 3) Glazing performance. These three parameters are analysed and explained in this sub-chapter.

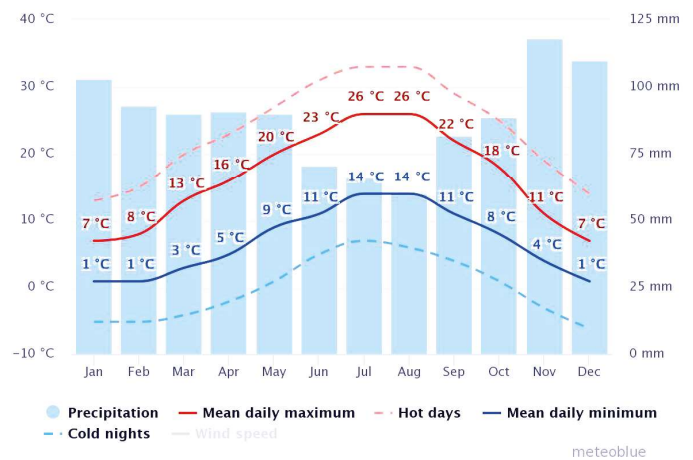


Figure 48. Average temperatures and precipitation (Source:www.meteoblue.com)

1. Thermal mass

The definition of thermal mass is the ability of a material to absorb and store heat energy. The advantage of thermal mass is that materials can store solar energy during day-time and release solar energy during night-time through natural ventilation. This results, if used in a correct way, in energy and cost savings and an increased indoor thermal comfort. Large differences between day and night outdoor temperatures are required for a beneficial thermal mass design and therefore will not work in every climate. It is concluded that beneficial thermal mass designs can be achieved in warm climates that have a large variance in mean daily maximum and minimum temperatures. Resulting in a reduced variance between interior and exterior temperatures^[7].

Thermal mass of the glass dome

A lowered ground floor is proposed for the glass dome design to create a higher rise which provides a higher flying space for the Lori parrots.

The lowered ground floor and walls are constructed from concrete, above the concrete floor there is soil layer present for vegetation to grow and there are some water basins which function as drinking basins for the Lori parrots. In this research it is assumed that the concrete ground floor and walls, water basins, soil, and glass all can be used as thermal mass because of the high amount of surfaces and specific heat as shown in figure 49 and table 11. The latter mentioned thermal masses are validated in the chapter 'thermal calculation'. The specific heat of water is very high which could lead to reduced indoor temperatures during summer by even using small drinking basins. The location of the glass dome is Villars Les Dombes, in France, which is a moderate climate with warm summers and has large differences between day and night outdoor temperatures. Hence, the use of thermal mass could be effective and can reduce the energy demand, costs and high indoor temperatures during summer. The principle of thermal mass during summer at day-time is shown in figure 50 and during night time in figure 51.

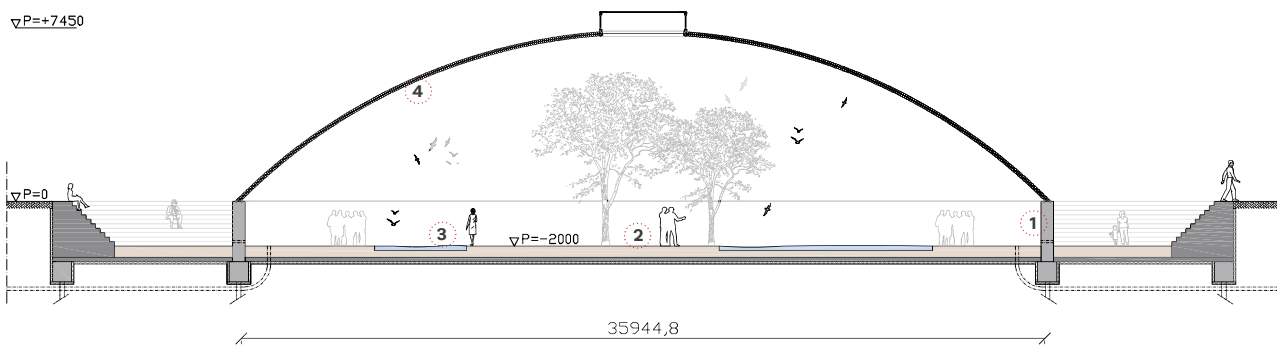


Figure 49. Schematic section of the glass dome and its related thermal mass

Material	SH (KJ/kgJ)
1. Concrete	0,75
2. Soil (dry)	0,8
3. Water (25°C)	4,18
4. Glass	0,84

SH= specific heat

Table 11. Specific heat of concrete, soil, water and glass, values obtained from (source: <https://www.engineeringtoolbox.com>)

[7] <http://www.yourhome.gov.au/passive-design/thermal-mass>

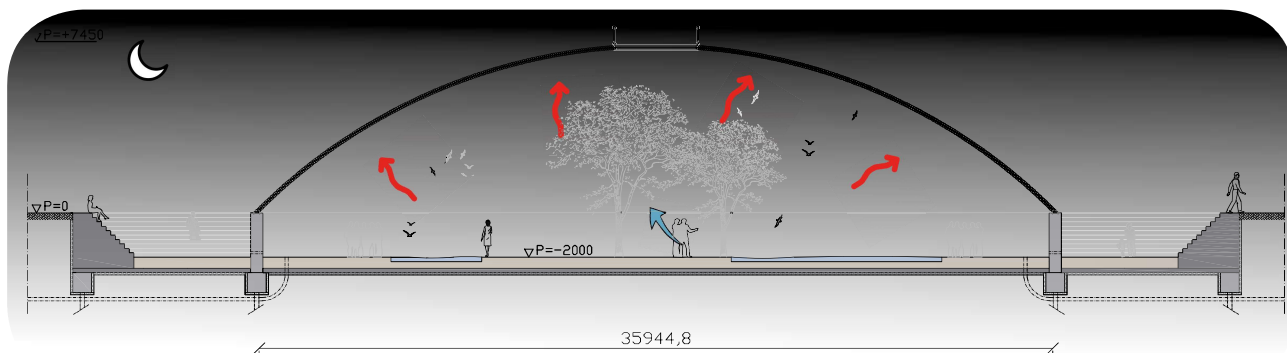


Figure 51. Thermal mass principal during summer at night-time, where the solar heat energy is released by the thermal mass

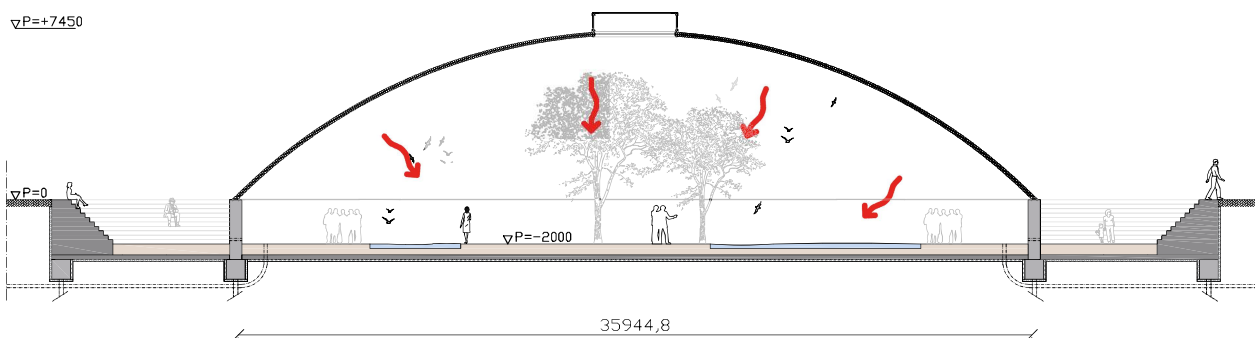


Figure 50. Thermal mass principal during summer at day-time, where the solar heat energy is absorbed by the thermal mass

2. Natural ventilation

According to Bokel (2017) ventilation in general is needed to remove bad particles, heat and moisture and to add oxygen. A driving force and an opening are necessary to provide this ventilation, where the force is the product of pressure difference and associated area.

Pressure difference can be created by ventilators, wind or temperature differences. Pressure difference caused by temperature differences create stack affect which will result in stack ventilation. In simple words the stack effect creates convective streams driven by temperature differences. An opening and large difference in height between air inlets and outlets is required to create stack ventilation, this principle is shown in figure 52 and 53. These figures show that equal heights result in a neutral plane of pressure with no stack ventilation, while increasing the height will ensure a greater pressure difference between in and outside thus creates stack ventilation.

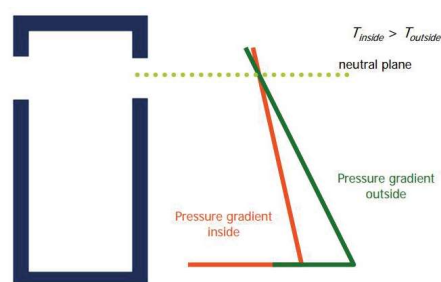


Figure 52. Inlet and outlet height are equal and result in a neutral plane of pressure with no stack ventilation (Bokel, 2017).

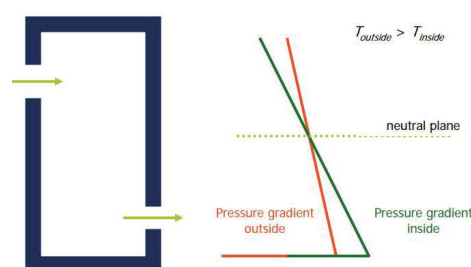


Figure 53. Large difference in height between inlet and outlet opening which result in stack ventilation (Bokel, 2017).

Natural ventilation of the glass dome

Stack ventilation and earth ducts are proposed to provide the glass dome of natural ventilation. Hot daytime air in the glass dome is released through openings in the oculus and is driven by convective streams. A large difference between inlet and outlet temperature will result in an improved convective stream/stack effect. Stack effect is further improved by means of a large difference in height between inlet and outlet, as explained above.

Cool air is drawn in through **six earth** ducts and openings encircled around the base. Next, hot air inside the dome is collected and removed at the oculus of the glass dome. The earth ducts are located underneath concrete support structure. Moreover, the earth ducts temper the outdoor air further through heat exchange with soil, which

result in preheated winter or pre-cooled summer inlet air. The utilization of earth ducts will enhance the stack effect because a larger inlet and outlet temperature difference will occur. The glass dome shape prevents hot air from being trapped in corners and accelerates the air flow. The accelerated air flow is caused by the reduction in radius from base till the dome top. The principle of stack ventilation in the glass dome is shown in figure 54.

To resume, the stack effect in the glass dome is caused by the following aspects.

- Difference between outdoor and indoor temperature
- Heat exchange between outdoor air and soil
- Height difference between inlet and outlet openings of 9,45m

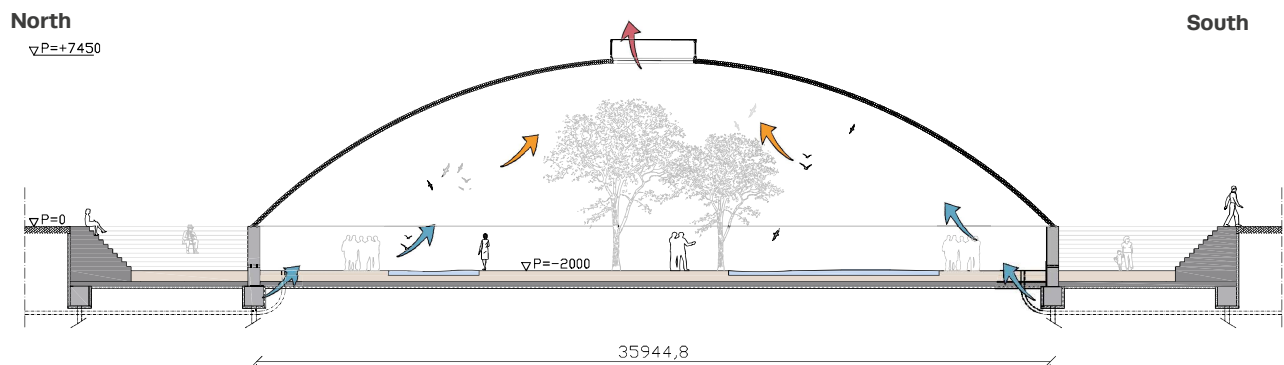


Figure 54. Principle of stack ventilation: cool air is drawn in from underneath façade, propagating through six earth ducts and hot air is released through openings at the oculus of the glass dome

3. Glazing performance

Glass has a high thermal conductivity so an increase in thermal resistance is needed to provide thermal comfort and reduce energy towards overheating in the interior of the glass dome. The main key to reduce heat load in the glass dome is achieved by an increased U-value of the glass component. The U-value depends on the internal and external surface conductance and the solar and light transmittance. As read in other chapters, an increased U-value is not the only parameter which influences the internal heat load in the glass dome. Other parameters such as the thermal mass and natural ventilation all collaborate and together will define the reduced heat load in the glass dome. The glazing performance needs to be assessed because this research proposes a solely glass dome structure. The glazing performance of the glass components is explained below.

Goal of the glass components

In this research cast glass serves as structural components with just one mold being used to cast the glass components of the entire dome. The glass dome has an aviary function with a two folded goal. The cast glass blocks need to form a **noticeable structure** to the Lori parrots while transmitting, reflecting and distorting colours of the environment in a **nice colour pattern** onto the glass dome surface in order to mimic a natural environment. Secondly, the glass components need to control the interior temperature in order to reduce the **overheating risk** during summer and creating acceptable temperatures during the **colder fall days**. Hence the twofold goal is: create a noticeable structure while transmitting, reflecting and distorting colours of the environment and create thermal comfort during summer and during the colder fall days.

To achieve this goal white wash paint is proposed to apply onto the glass components. Low e-coatings, fritting and coloured glass cannot be used, a brief explanation is given below.

Coatings

Glass coatings can improve the radiation properties of glass by reducing the emissivity, as explained in the chapter 'material properties of glass'. The emissivity presents the amount of emitted energy as thermal radiation. Low e-coatings are coatings that can reduce the emissivity of glass.

Coatings reduce this emissivity by absorbing or reflecting the radiation transmission. According to Burgess (n.d.) two general low e-coating are distinguished: pyrolytic and sputter coatings. Pyrolytic coatings are applied during the manufacturing process of float glass where a metallic coating is bonded with the chemical structure of glass in a semi-molten state. Whereas

sputter coating is applied after manufacturing and may be suitable for the cast glass components. The disadvantage of the sputter coating is that these coatings are not fused with the glass bonds and are not resistant against oxidation and scratching, thus are not fully weather resistant. Finally, low e-coatings are not proposed because pyrolytic coatings cannot be applied during manufacturing and sputter coatings are not oxidation and weather resistant.

Coloured glass

Enamelled and coloured glass can resist the interior of the glass dome from heat and glare. According to Wurm (2007) enamelled glass include ceramic pigments. These ceramic pigments are rolled, poured or screen-printed before heat treatment and change the chemical bond of glass which will result in a reduced bending strength. The reduction in bending strength is not preferred for the glass dome since this research proposes structural cast glass components with low bending strength. The bending strength of the glass components should not be reduced because this will lead to larger tensile stresses. Coloured white glass can reduce UV levels and bright summer sunlight in the interior of the glass



Figure 55. Greenhouse in San Francisco's Golden Gate Park with white wash paint (source: <http://www.travelandleisure.com>).

dome. Because coloured white glass reflects short wavelengths, such as UV and visible light and does not absorb short and long wavelengths of the solar spectrum.

The advantages of coloured white glass are:

- Short wave lengths are not changed into long wave lengths in the interior of the glass dome because short wave lengths are reflected. The lower amount of long wavelengths result in a reduced greenhouse effect.
- Overheating of the surface of the glass components will not occur because wavelengths of the solar spectrum are not absorbed.

It seems that utilization of white glass components is the perfect passive strategy. Although a large disadvantage of white glass is that it is permanently present. This results in a lowered indoor comfort temperature for both summer and winter design. Hence applying a white wash paint has the advantages of white glass and can be removed after summer through precipitation resulting in a not lowered comfort temperature during the colder fall days.

Existing structures that use these white wash paints are green houses, e.g. the greenhouse in

San Fransico's Golden Gate Park^[8], as shown in figure 55.

Finally, this research proposes to use a white **wash paint** which **covers ~ 50%** of the glass dome surface from the oculus till the centre of the dome surface and is removed through precipitation when reaching the fall. This to achieve the main goals of the glass components which are: create a noticeable structure while transmitting, reflecting and distorting colours of the environment and create thermal comfort during summer and during the colder fall days. In addition, the white wash paint is applied every year through building workers using cranes and paint-sprayers. Moreover this research assumes that if 50% of the glass dome surface is covered through the paint the dome still transmits, reflects and distorts a major part of the colours of the environment. This because of the large dome dimensions: span of approximately 36m and dome rise of 7,5m (height without the support structure).

Note that, the effectiveness and utilization of the proposed passive strategies is presented in the chapter 'thermal validation'.

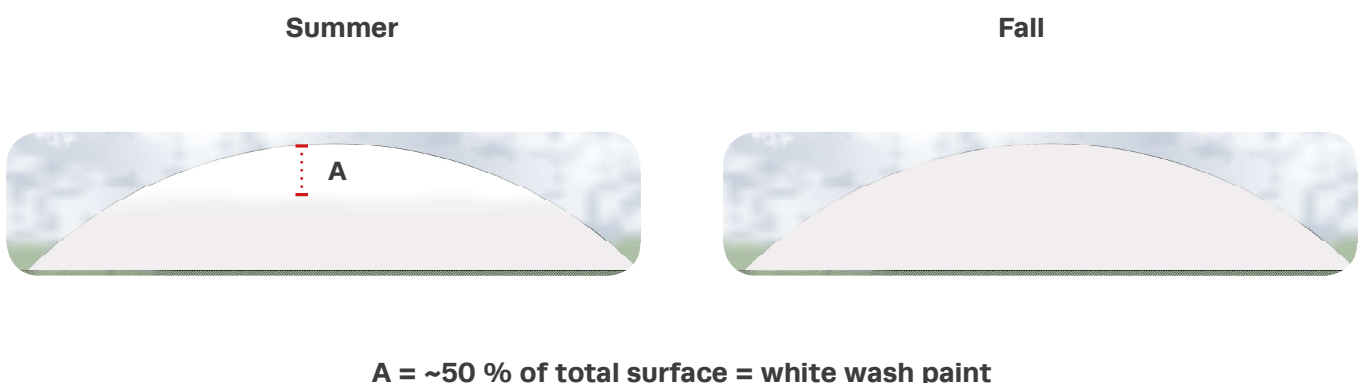


Figure 56. : (summer) ~ 50% is covered the white wash paint, (fall) the white wash paint is removed through precipitation

[8] <http://www.tanglewoodconservatories.com>

2.3 Glass

2.3.1 Introduction

An explanation of following subjects is given in this chapter: the definition of glass, types of glass, properties, production methods and existing cast glass connections. This chapter also addresses the requirements for designing with glass and finally presents the different structural glass configurations and glass dome references.

The chapters: Glass types, production methods and connections are provided with conclusions related to the glass dome design. Resulting in the glass type, production method and connection type of the glass dome. Other sub-chapters are used as fundamental background knowledge for designing the glass dome. In addition, the glass dome references at the end of this chapter are analysed and the outcome of this analysis could be used as design input for the glass dome.

2.3.2 The definition of glass

According to Schittich, Staib, Balkow, Schuler and Sobek (2007) and Weller, Härth, Tasche, an Unnewehr (2009), the term 'glass' has many definitions but in the scientific language it is assigned to a homogeneous and amorphous material. Glass is a rapid cooling liquid that can be solidified without crystallization and has a mixture of bonds. Glass has a random order of molecules, does not form a crystal lattice and because it is amorphous the properties are independent of direction. In addition, glass becomes viscous and liquid when heat is applied and glass does not have a melting point. Glass does have a melting temperature which depends on its composition. To resume the definition, 'glass' stands for a variety of substances resulting in different glass types: from natural glass, e.g. obsidian, till acrylic sheets and metallic glasses.

According to Weller (2009), 95% of the total glass production is covered the group of silicate glasses, where the produced silicate glass consist of 70% silicon-dioxide, i.e. quartz sand. Silicon-dioxide determines the elemental structure of glass during manufacturing. Other raw materials such as Alkali-oxide fluxes are added to lower the melting point of glass, this is required due to the high melting point of quartz sand (1700°C). Alkaline earth oxides are added to increase the chemical resistance and hardness of glass. All these latter mentioned raw materials are heated to a high temperature and become viscous before cooling down, resulting in a disordered molecular position of the ions and molecules.

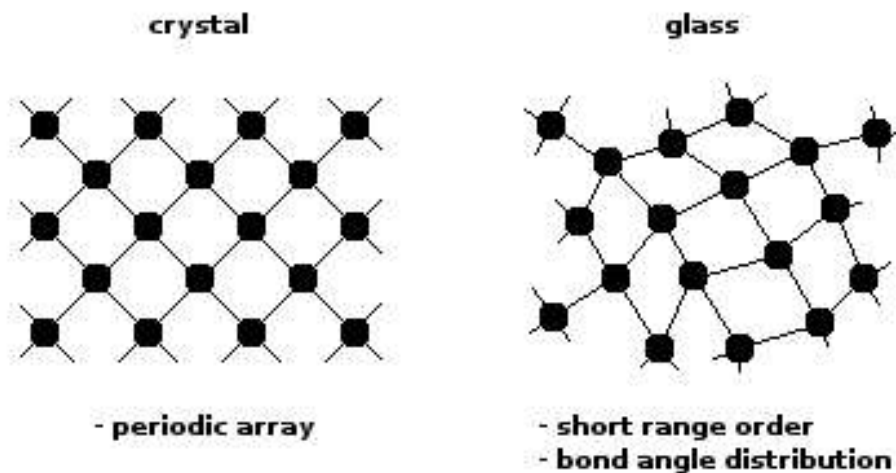


Figure 57. Differences between a crystalline structure and amorphous structure.
(Source: <http://www.users.aber.ac.uk>)

2.3.3 Types of glass

Glass in general is a three-dimensional structure of silicon (Si) and oxide (SiO_4) with cations in their apertures. The most common silicate glasses are listed and briefly explained below. The glass types with a bold font represent frequently used glasses for the building industry.

▪ Soda-lime

The main glasses that are used in the building industry are in the soda-lime category. The principal component is silicon dioxide, Sodium oxide (Na_2O) acts as a flux. Calcium oxide (CaO) is the dissolved stabilizer. Table 12 shows the composition of soda-lime glasses. The other small components, mentioned in the table, depend on the raw material and process conditions.

▪ Lead

Lead glass is not often used in the building industry. The calcium oxide (CaO) is replaced for lead oxide (PbO), and protects the glass against x-rays.

▪ Borosilicate

Borosilicate glass is often used in the building industry, especially for fire resistant glazing. Calcium oxide (CaO) is replaced for 7–15% boron oxide (B_2O_3). Table 13 presents the composition of borosilicate glass.

▪ Alkaline-earth

Alkaline earth glasses have again silicon dioxide as their main component and have some alkaline earth-oxides in their structure instead of calcium-oxides. The potassium oxide (K_2O) replaces the sodium-oxides. This type of glass has a higher density and higher Young's modulus than soda-lime glass.

▪ Alumino-silicate

Similar to the alkaline earth and lead glasses this type of glass is used for fire resistant glazing. Aside from the silicon dioxide the glass consists of 16–27 % aluminium trioxide (Al_2O_3) and approximately 15% alkaline earths. It does not consist of alkaline oxides (Schittich et al., 2007; Weller et al., 2009).

▪ Quartz

This type of glass is made from pure quartz, it is a pure material containing almost no other ingredients which are normally added in traditional glass for lowering the melting temperature. This means that quartz glass has a very high melting temperature. Quartz glass has superior thermal and optical properties caused by the purity of quartz^[9].

T1: Composition of soda-lime-silica glass to DIN EN 572-1

Silicon dioxide (SiO_2)	69–74 %
Calcium oxide (CaO)	5–14 %
Sodium oxide (Na_2O)	10–6 %
Magnesium oxide (MgO)	0–6 %
Aluminium oxide (Al_2O_3)	0–3 %
Others	0–5 %

Table 12. Composition of Soda-lime-silica glass (Weller et al., 2009)

Glass thickness	Tolerance
3 mm, 4 mm, 5 mm, 6.5 mm, 7.5 mm	- 0.4 / + 0.5 mm
9 mm, 11 mm, 13 mm, 15 mm	- 0.9 / + 1.0 mm
	2.1.11

Table 14. Glass thickness (Schittich et al., 2007)

Main constituents of borosilicate glass

Silicon dioxide	(SiO_2)	70–87%
Boron oxide	(CaO)	7–15%
Sodium oxide	(Na_2O)	1–8%
Potassium oxide	(MgO)	1–8%
Aluminium oxide	(Al_2O_3)	1–8%

Table 13. Main constituents of Borosilicate glass. (Schittich et al., 2007)

[9] <http://www.squallquartz.com/quartz-glass>

2.3.4 Material properties glass

According to Wurm (2007) and Weller et al. (2009), glass construction products e.g. flat glass and glass blocks are designed to meet all the project-specific requirements. These requirements include complex performance criteria for building physics, construction and design. Hence, it is important to understand the mechanical and physical properties of glass to categorize the different types of silicate glasses. Most common mechanical and physical properties are explained in this chapter.

Mechanical properties

The Young's modulus of glass equals 7000 N/mm^2 and expresses the relation between the stress (σ : N/mm^2) and strain (ε : proportional deformation). Glass deforms in a linear elastic way and has (practically) no yield point. Due to its brittle nature, upon overloading, glass breaks in a complete way without any visible warning, and without preserving any post-breakage carrying capacity. This above described effect is shown in figure 58. The maximum strain of glass is approximately 0.1%, exceeding this will lead to failure. The failure behaviour of glass is not possible to predict because plastic behaviour does not appear. This is caused by the high percentage of silicate, nonetheless silicate has a positive effect on the hardness and strength of glass.

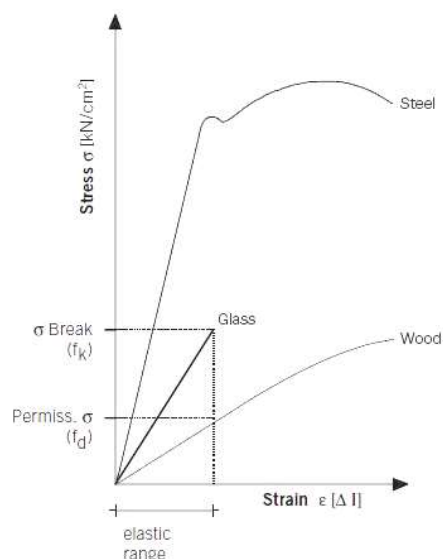


Figure 58. Qualitative comparison of the stress-strain graphs of steel and wood (Wurm, 2007)

Tensile strength

The tensile strength of glass is distinguished in theoretical (micro) and practical (macro) tensile strength. High theoretical tensile strength can be calculated from the atomic and ionic bonds in glass structures. These strong bonds come primarily from SiO_4 tetrahedron because it has a high binding energy, as shown in figure 59. The theoretical tensile strength equals 8000 N/mm^2 , which is thirty times the yield strength of steel. In practice, this value is not achieved due to the brittle nature of glass and the presence of micro-

flaws. Micro-flaws greatly affect its structural performance, reducing to a tensile strength value of 20 N/mm^2 for annealed glass.

Glass is not a compact solid because it has flaws in its micro-structure, the so called 'Griffith flaws'. Engineer Griffith explains the failure for brittle materials. This theory states that brittle materials have low fracture strength because of these flaws and that strength is size dependent: when the size of the loaded area increases, the cracks at the surface increase too^[10].

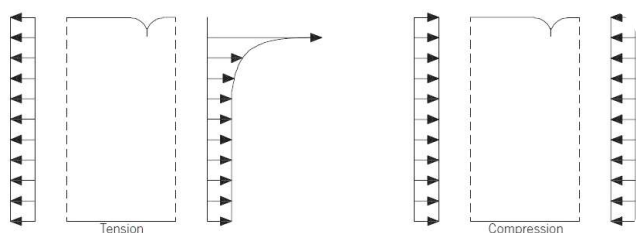


Figure 60. Stress distribution over the cross section of surface-damaged glass. (Wurm, 2007)

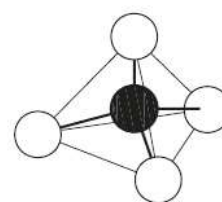


Figure 59. Bonds of the SiO_4 tetrahedron (Wurm 2007).

[10] <http://www.mindat.org>

According to Weller et al. (2009), these flaws are caused during manufacturing, treatments and handling. When glass is subjected to tensile stresses stress peaks around these 'Griffith flaws' occur. Peak stresses will result in a rapidly increasing tensile stress which will lead to failure because glass is known for its weak tensile strength. When glass is compressed this results in no peak stresses and will therefore not cause failure problems. Moreover, glass does not show plastic deformation so the cracks created from peak stresses start to propagate. Short peaks are preferred above long term loads because the load-bearing capacity of glass is reduced when the time is increased.

To summarize, the tensile strength of glass depends on the following aspects:

- The duration of load
- Size
- Properties of glass (Borosilicate or Soda-lime etc.)
- Glass type (Heat strengthened, annealed, fracture toughened, explained in more detail in the next chapter)
- Environment (humid environments increase crack propagation)
- Age

It is concluded that the tensile or bending strength follows the surface quality and is not a constant value but a characteristic value. This value lies in between 30–80 N/mm² according the literature of Wurm (2007) and Weller et al. (2009). According the CES EduPack software the tensile strength, of a frequently used glass type: Borosilicate, lies in between the 31,9–35,1 MPa and the compressive strength lies in between the 319–351 MPa.

Compressive strength

In comparison with the tensile strength of glass, the compressive strength is at least ten times greater. Because the surface of glass does not reduce in strength when the notches sites are in compression, as shown in figure 60. It is hard to find a consistent value of glass stated in literature, but all sources agree that it is at least 10 times greater than the tensile strength. For example the compressive strength according the literature of Weller et al. (2009) lies in between 400–900 N/mm².

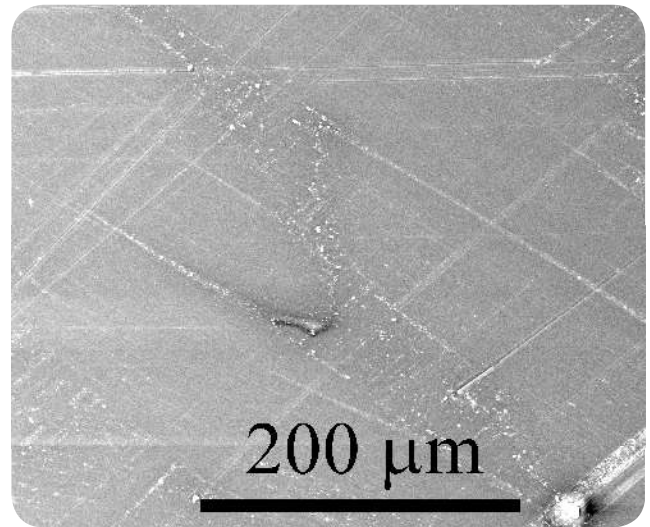


Figure 61. 'Griffith flaws', SEM micrographs showing the flaws (source:www.doitpoms.ac.uk).

Physical properties

According to Wurm (2007), glass is an amorphous material with no phase boundaries, light beams are scattered which makes glass a transparent material. Glass is a superior material for façades because of its transparency and chemical resistance to acids and salts. It only becomes opaque when silica-dissolving hydrofluoric acids attack the glass. This occurs, for example, by leachates of concrete or by the presence of standing water from condensation. Hence, the optical and thermal properties are explained below.

Solar radiation balance: transmission, reflection and absorption

The definition of transparency is very broad, but in literature the physics definition is: "a synonym for transmission and specifies the wavelengths for which a material is permeable, and to which extent"(Weller et al., 2009, p. 34). Hence, glass is not fully transparent because a part of the light, falling on the glass surface, is reflected and absorbed by the colour of glass, as shown in figure 62. According to Wurm (2007), the transmittance is the fraction of light that passes a glass surface without detectable scattering. While absorption characterizes the property of

glass to deform light into heat or other forms of energy and depends on the thickness of glass. The reflection of incident light can cause a disadvantage on transparency and disturb the optical properties for humans. Dielectric coatings solve this problem by eliminating the wavelength caused by the destructive interference. The relationship between transmission (t), reflection (r) and absorption (a) is stated in a radiation formula: $t+r+a=1$.

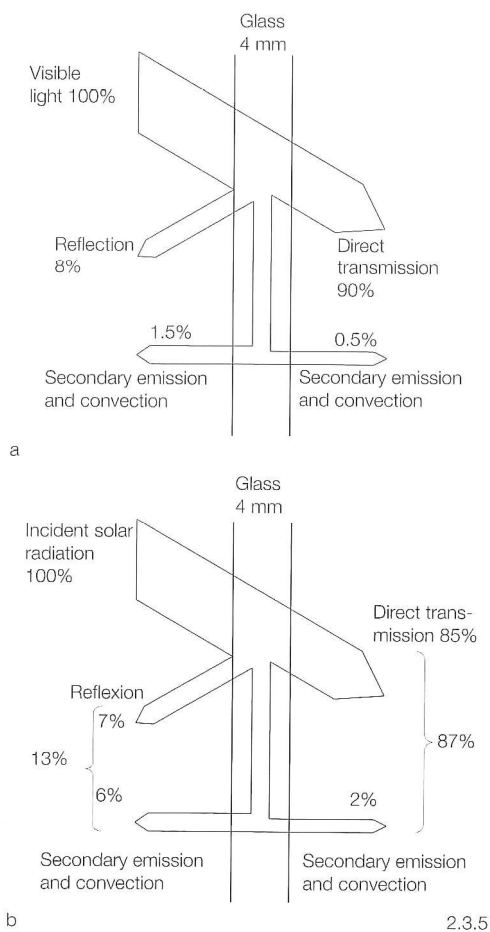


Figure 62. Radiation balance visible light vs. incident solar radiation (Schittich et al., 2007)

Glass is an excellent transmitter for the wavelengths in the visible light range (380–780 nm). The visible light range has a high intensity and takes in 50% of the total radiation of the solar spectrum. Below 320 nm (UV) and above 3000 nm (IR) wavelengths are almost fully absorbed by glass. The greenhouse effect depends on the fact that different transmission factors have different wavelengths.

The short wavelengths, visible light, is transmitted by the glass and is changed in the area into long wavelengths (heat wavelengths). These wavelengths are absorbed and transferred into the area by convection or radiation which causes a heat trap in the building as shown in figure 63. The radiation balance, for a wavelength of the solar spectrum, depends on the composition, thickness, surface qualities and angle of incidence of the glass. The input values t and r of the radiation balance are distinguished in the range of visible light: t_v, r_v, a_v (v stands for visible light) and the whole range of radiation: t_e, r_e, a_e (e stands for energy).

The total solar energy transmittance (g) is equal to the direct transmittance (t_v and t_e) and is added with the secondary heat transmittance through glass by radiation or convection. The ratio between the solar transmittance and transmission factor is called the selectivity index (S), where $S=2$, its physical limit, which is equals half of the total energy of the spectrum. Hence, it is important to reduce the amount of visible light as well because this will also reduce overheating.

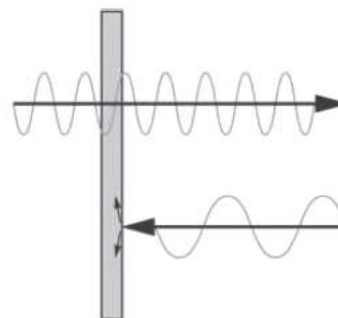


Figure 63. Greenhouse effect (Wurm, 2007)

Glass thickness and solar radiation balance

Iron oxide is the component of glass which causes absorption of light in glass. Approximately 0,1% Iron oxide causes absorption of red light and results in green coloured glass. Other metal-oxides are needed in order to change the colour of glass and may lead to an increase of the absorption factor.

Glass absorbs more heat when the thickness increases due to the increased absorption coefficient for solar radiation. Adding pure silicon dioxide to low-iron glass during manufacturing will cause a decrement of the absorption coefficient.

Reflectance, refractions and transmittance depend on the angle of incidence, it becomes greater when the angle is flattened. This is defined as a change in angle of the transmitted light with the surface area between two media: glass and air. Parallel surfaces do not show total reflection and non-parallel surfaces can cause a prism effect because the light is split into spectral colours.

The surface quality of glass, e.g. adding a texture, influences the direct, quasi-parallel, indirect, diffused and scattered light, this principle is shown in figure 64. Increasing the texture leads to a change from direct light to diffused transmission and a decrement in specular reflection. The term translucence glass means transmission of diffused light.

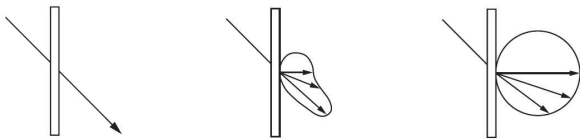


Figure 64. Transmission types in comparison with different surface types (Wurm, 2007)

Thermal insulation

According to Schittich et al. (2007), frost and condensation are examples of the low thermal resistance of single glazing. Thermal resistance of glass depends on the thermal resistance of the material and the resistance of the surface. Glass has a high thermal conductivity, thus an increase in thermal resistance is needed. An increase in thermal resistance is achieved by using multiple layers of glass with spaces (air or argon gas) in between or by using coatings.

To measure the heat loss through a component the thermal transmittance value (U-value) is introduced. It is stated in the literature as:

“the amount of heat that passes through 1m² of a component for a temperature difference of 1K between the inside and outside air” (Schittich et al., 2007, p. 123). A high U-value results in a better thermal insulation and is calculated by using this formula: $1/U = (1/h_e) + (1/ht) + (1/h_i)$. The U-value depends on the total thermal transmittance (ht), internal and external surface conductance (h_e & h_i). The internal conductance is derived from the summations of the thermal radiation and convection coefficients, $h_i = h_r + h_c$. The total thermal transmittance is equal to the summation of the reciprocal resistances of the surfaces of the cavities between the glass and the glass layers because $U = 1/R_{total}$. It is important to notice that the values include heat flows, i.e. conduction and radiation. There are different types of heat transfer which can cause heat loss, this is shown in figure 65. This figure shows the most important heat transports in an insulating unit.

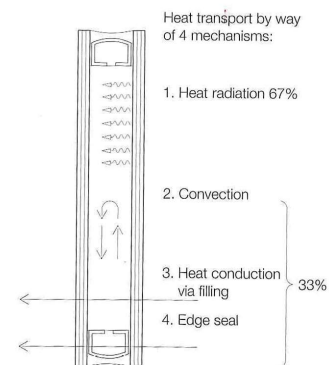


Figure 65. Heat transport by way of 4 mechanisms (Schittich et al., 2007)

Coatings can improve the radiation properties of glass by reducing the emissivity. The radiation transmission is absorbed or reflected. Low E coatings are an example of hard coatings and are also available on single glazing. The result of such coatings is an improved insulation with an U-value that is reduced with 50%. The insulating effect depends on the amount of radiation to the sky. To improve the insulation a lower temperature of the glass layer is required and therefore the condensation-risk is reduced. The result of placing Low-E coatings on the outer plane of the glass layers is a reduced condensation risk and a 10% long-wave radiation decrement.

The opposite, placing a Low-E coating on the inner-side of the glass layer, even leads to a greater U-value due to the low air velocity. Unfortunately the temperature of the glass layer is lower because it stays in contact with the outside and leads to a greater condensation-risk. Although this is a self-regulatory effect which only works during summer (moderate temperatures). In other climates, a winter optimization is required and therefore a coating on the outer layers works best, this principle is shown in figure 66.

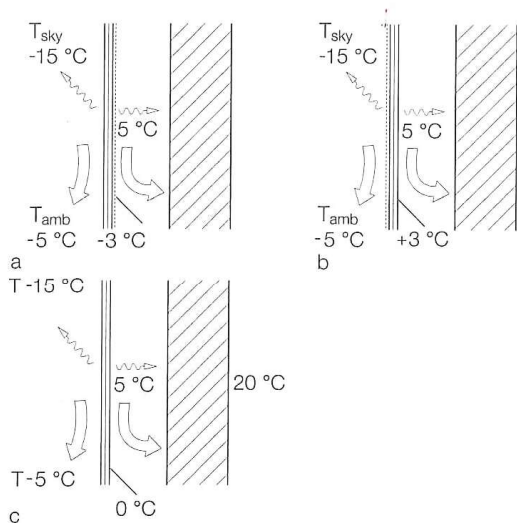


Figure 66. a) low E glass with coating inside b) low E glass with coating outside c) Float glass without coating (Schittich et al., 2007).

Material property charts (CES and Ashby)

Selecting a suitable glass type depends on the design requirements. Three important general requirements are given below. First, the **annealing** phase is a **time** consuming process and needs to be reduced in order to speed up the building period and to reduce the production costs. Secondly, concerning the **overall costs**, the costs of the material needs to be reduced as well. And finally, the design structure needs to avoid large **thermal stresses**, to prevent thermal shocks resulting in cracks, that depend on the building climate.

The annealing time of cast glass components is reduced by decreasing its mass. At the same time, the glass must be stiff enough to ensure a rigid structure. Regarding the Young's modulus-density ratio, Borosilicate glasses have a broad range and include glasses that are stiff with low weight. Lead glasses have the largest densities and Alumino silicate glasses have the largest Young's modulus. Concerning the feasibility of a design, low costs and high stiffness of a material are preferred. Alumino-silicate glasses have the best ratio between the Young's modulus and price, second best are the borosilicate glasses, third best the soda lime glasses and last the lead and silica glasses.

Another aspect that determines the annealing time is the thermal expansion coefficient. A lower thermal expansion results in a reduced annealing time and enhances the protections against thermal shocks. Hence, Borosilicate and Alumino-silicate glasses may result in acceptable annealing-times and enhance the protection against thermal shocks due to their low thermal expansion coefficient.

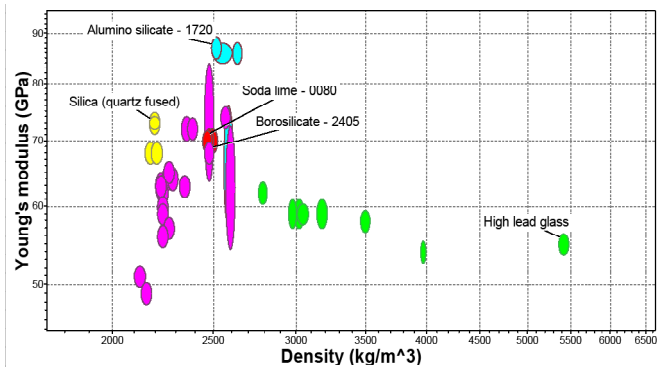


Figure 67. Young's modulus versus density (CES EduPack 2016)

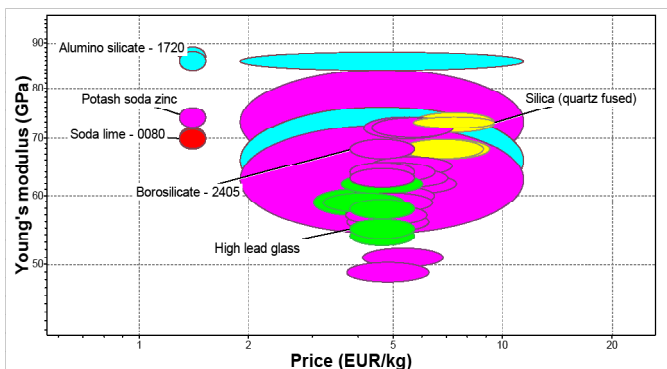


Figure 68. Young's modulus versus price. (CES EduPack 2016)

	GENERAL				MECHANICAL					THERMAL			
	density (kg/m ³)	price (€/kg)	young's mod. (Gpa)	poisson's ratio (-)	tensile str. (MPa)	compressive str. (MPa)	hardness (Hv=MPa/10)	expansion coeff. (μstrain/°C)		hermal conductivity (W/m. °C)	glass temperature. (°C)	max. service temperature (°C)	
QUARTZ (silica fused quartz)	2,17e ³	5,69	72	0,15	45,7	1,05e ³	952	QUARTZ (silica fused quartz)	0,48	1,4	1,56e ³	1,1e ³	
	-	-	-	-	-	-	-		-	-	-	-	-
	2,22e ³	9,5	74	0,16	50,4	1,16e ³	1,05e ³		0,52	1,5	1,96e ³	1,4e ³	
SODA LIME (0080)	2,44e ³	1,29	68,2	0,21	31	310	439	SODA LIME (0080)	9,16	0,7	442	110	
	-	-	-	-	-	-	-		-	-	-	-	-
	2,49e ³	1,52	71,7	0,22	34,2	342	484		9,53	1,3	592	460	
BOROSILICATE (2405)	2,45e ³	3,8	66,3	0,2	31,9	319	95,4	BOROSILICATE (2405)	4,21	1,1	463	200	
	-	-	-	-	-	-	-		-	-	-	-	-
	2,5e ³	5,7	69,7	0,21	35,1	351	105		4,38	1,2	618	480	
LEAD (high lead)	5,36e ³	3,8	53,6	0,27	23,6	236	69,1	LEAD (high lead)	8,23	0,82	305	100	
	-	-	-	-	-	-	-		-	-	-	-	-
	5,47e ³	5,7	56,3	0,28	24,9	249	76,4		8,56	0,86	426	300	
ALUMINOSILICATE (1720)	2,49e ³	1,29	84,8	0,23	39,9	399	476	ALUMINOSILICATE (1720)	4,11	1	622	200	
	-	-	-	-	-	-	-		-	-	-	-	-
	2,54e ³	1,52	89,1	0,24	43,9	439	525		4,28	1,5	810	650	

Table 15. General; mechanical and thermal properties of Quartz; Soda-lime; Borosilicate; lead and Alumino-silicate glass based on (CES EduPack 2016)

Conclusion

This research assumes that the glass dome components do not need a large protection against thermal stresses because the proposed building location is situated in Southern France. The climate in Southern France equals a **moderate maritime climate** and will not cause large temperature differences within the glass component during the day and season. Hence a large thermal expansion coefficient is not required in order to reduce the thermal stresses within the glass components. Although, a low thermal expansion coefficient does reduce the annealing time of the glass components and therefore makes Borosilicate glasses an excellent glass type, Borosilicate glass is not preferred due to its high price per kg.

Taking in account the two other requirements: low price per kg and low density, Soda lime glasses score best. It should be noted that Soda-lime glasses have a high thermal expansion coefficient, resulting in an increment of the annealing time. Although, the high thermal expansion coefficient causing an increment of the annealing time, this will not cause problems in case of the Glass dome design. This research will show that the glass **dome components are rather small**, leading to a low price per kg and acceptable annealing-time. Moreover, **a low price per kg is leading since the dimensions of the glass dome are large**. Because of the reasons mentioned above, **Soda-lime** cast glass components are preferred to construct the glass dome. Table 15 presents the characteristic values (red square) of Soda-lime glass according to Ces Edu Pack. The characteristic values according to the literature are given in table 16.

Soda-lime glass	
Refractive index η	1.5
Density ρ [kN/m ³]	25
Modulus of elasticity E [kN/cm ²]	7 000 (like aluminium)
Tensile strength $f_{t,k}$ [kN/cm ²]	4.5
Elongation at break ϵ in %	0.006–0.17
Compressive strength $f_{c,k}$ [kN/cm ²]	approx. 50
Limiting tensile stress σ_{Rd}	1.2/1.8
Safety factor γ	2.5
Breaking length σ/ρ [m]	480/720
Thermal conductivity [W/m x K]	1
Thermal shock resistance ΔT [1/K]	40
Coefficient of thermal expansion α_T [1/K]	9×10^{-6} 60 K = 0.5 mm/m

Table 16. Characteristic values of Soda-lime glass (Wurm, 2007)

2.3.5 Designing with glass

According to Schittisch et al. (2007) allowing daylight in buildings is one of the main tasks of glass, nowadays technical developments make it possible create solely glass structures. Mechanical and building properties are improved and therefore glass can be used for a lot of different functions, i.e. as a structural material.

Highlighted design considerations

Glass contradicts with other building materials because it is a brittle material, it breaks without warning. To use glass as a construction material designers need to take into account the load-bearing capacity (determined by local stress peaks, located at flaws etc.) and most important, the capability of carrying loads in fractured state, i.e. the residual load-bearing capacity. These have led to design considerations and principles which can be read in this chapter.

Duration & area distribution load

Mentioned in the material properties, short time loads are preferred above long term loads. Figure 69 shows the relation between strength and the duration of the load. A duration of 50 years will give a decrement of approximately 45 MPa in strength. The same aspect applies if the area of the distributed load increases, the crack starts to propagate in depth.

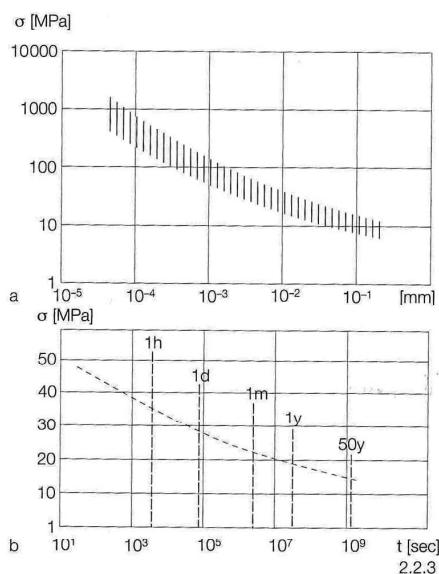


Figure 69. Relation between strength and flaw depth/duration load (Schittisch et al., 2007).

Surface structure

Damages at the glass surface can be caused by several aspects such as: weather caused damage or through chemical and mechanical treatments (cutting, grinding and sandblasting etc.). Serious damages occur at the edges of the drilled holes and cannot be improved by a polishing treatment and needs to be reinforced. Figure 70 shows the distribution of surface damages.

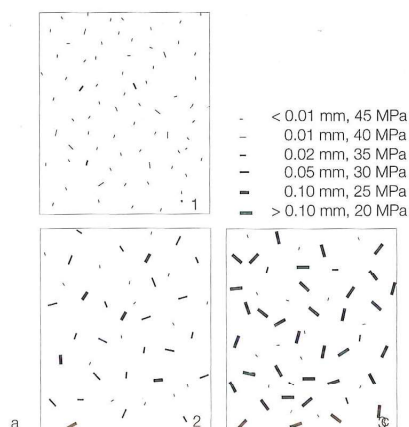


Figure 70. Distribution of surface damage for 1) new glass, 2) weathered glass, 3) glass with inherent damage (Schittisch et al., 2007).

Failure behaviour

Glass is brittle, above its elastic region it suddenly breaks and is dangerous to use in structural applications. Because of this it is important to design safe glass, which should be redundant: have a high residual load-bearing capacity and give a warning sign like other structures do, e.g. steel, stainless steel and aluminium, as shown in figure 71. These structures are ductile, this means the ability of withstanding tensile stress during plastic deformation.

	Glass soda- lime silica	Concr. C25/30	Steel S355	Stainl. steel 1.4301	Alumi- nium EN AW-6060
Mod. of elasticity [N/mm ²]	70000	26700	210000	200000	70000
Poisson's ratio	0.2	0.2	0.3	0.3	0.3
Strength [N/mm ²]	Yield point	-	360	190	160
	Tensile strength (comp.) (700)	45 (25)	2.6	510	500-700
Failure behaviour	brittle	brittle	ductile	ductile	ductile
Density [kN/m ³]	25	25	78	78	27
Coefficient of thermal expansion α [K ⁻¹]	0.9 × 10 ⁻⁵	1.0 × 10 ⁻⁵	1.2 × 10 ⁻⁵	1.6 × 10 ⁻⁵	23.5 × 10 ⁻⁶

2.2.32

Figure 71. Material parameters for some common building materials (Schittich et al., 2007).

Structural considerations

According to Weller et al. (2009) the two most important aims when designing a safe structural application with glass are: a great residual load-bearing capacity and redundancy. The safety limit for total failure of a partly fractured system is stated in the literature as the residual load-bearing capacity. This means that even when the construction is damaged, it needs to stay in position and carry other loads for an acceptable length of time. Splinters and other fragments need to be bonded to prevent the glass from falling down. This can be achieved by using ductile materials, e.g. polyvinylbutyral (PVB). Glass structures also need to be designed with redundancies, when one element fails, another element should carry the loads of the failed element. Hence, failure schemes to ensure the safety of the structural systems need to be included in the structural analysis.

2.3.6 Safe design methods

Risk is the probability of x consequences of failure. To reduce risk we can either reduce the probability of failure, e.g. by tempering the glass and making it stronger in tension, or reduce the consequences, e.g. by laminating glass so that even if one panel breaks the remaining panels can carry the load. According to Schittich et al. (2007), three methods define safe structural glass systems. These methods are not conflicting so they can be combined and are presented in the table below:

	Explanation	Advantages	Disadvantages
1. Permissible stress design	The design is based on the permissible stresses	* Simple * Similarity to existing methods	* Does not include materials behaviour * Incomplete and not real * High safety factors
2. Probability of failure	Fracture mechanics are used to assess influence of load duration and usable strength	* includes influence of stresses on large areas during long time periods * Probabilities of failure for every loading case * More accurate than permissible stress design	* Complicated compared with permissible stress design
3. Limit state design	Uses statistical distributions on the material and loading side i.e. strength and e.g. wind and it considers various limits.	* Include limit states for various loading cases and its duration * Consequences of failing components are also taken into account	* Time-consuming and complicated method which requires the examination of the unharmed structural system but also an assessment of the failure behaviour of the individual components.

Table 17. Safe design methods based on (Schittich et al., 2007)

Types of safe glass

To make glass safe, i.e. redundant and creating a great residual load-bearing capacity, reinforcements need to be created. A summation is given of the most important reinforced glasses.

Thermal treatment, tempering of glass

Thermal treated glass gives a greater resistance to thermal and mechanical loads. According to Wurm (2007) two different types of tempered glass are distinguished: fully tempered/toughened safety glass and partially tempered / heat strengthened glass. To create tempered glass, normal (annealed) glass is reheated to above 600°C (100°C above its transformation) and transported on a roller. Subsequently glass is cooled by cold air through nozzles, as shown in figure 72. Shrinkage occurs during the cooling process caused by its warmer core. This is easily explained since the surface of glass will cool down faster resulting in a warmer core. This result in internal stresses with a parabolic stress diagram over the section: a compressive zone at the surfaces and a tension zone in the core as shown in figure 73. The compressive forces provide the glass from losing its strength. Only when these pre-stresses disappear the strength will be reduced. A minimum glass thickness of 4 mm is required because stresses need to be carried by their cross section. In addition, the production size depends on the manufacturer's tempering ovens and the Young modulus of glass (ratio between elastic strain and stress) does not change through heat treatment.

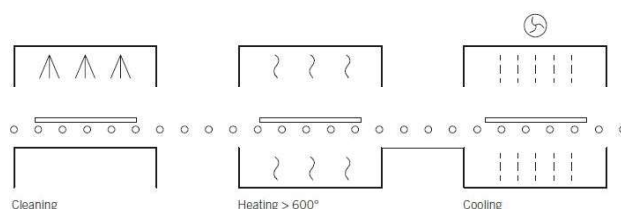


Figure 72. Production steps for tempered glass (Wurm, 2007)

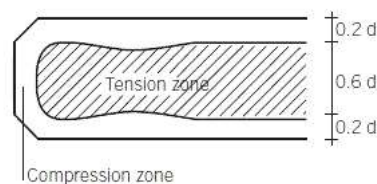


Figure 73. Cross section tempered glass with tension and compression zone (Wurm, 2007)

Heat strengthened glass

The two glass types mentioned above (FT & HS) differ in strength. Heat strengthened glass has a lower surface pre-compression and is approximately half the characteristic tensile strength of toughened glass but twice times greater than annealed glass. The thermal shock resistance is also improved, i.e. the resistance of glass against temperature fluctuations. The fracture pattern of heat strengthened glass breaks from the crack centre into larger pieces and islands, this principle is shown in figure 74.

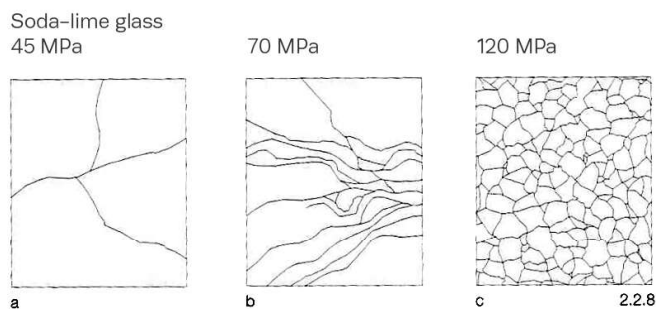


Figure 74. Fracture pattern: a) annealed glass, b) heat strengthened glass, c) fully tempered glass. (Schittich et al., 2007).

Fully tempered toughened glass

This type of glass has the highest tensile strength and thermal shock resistance. Unfortunately, its risk on spontaneous fracture is very high due to its fracture pattern. This type of glass breaks into small and large islands which could fall out. This is caused by the increase in volume of nickel sulphide (NiS) that depends on temperature. Although, nickel sulphides have no effect on heat strengthened glass

Chemically strengthened glass

Another form of pre-stressing is chemically strengthened glass. The glass goes through a hot potassium chloride bath where Sodium ion exchange take place. Resulting into a compact molecular structure. Utilization of chemically strengthened glass results in a large compressive surface strength, however this compressive strength is not very deep compared to toughened and heat strengthened glass, as shown in figure 75. It should be noted that this type of glass is not stated in literature as safety glass.

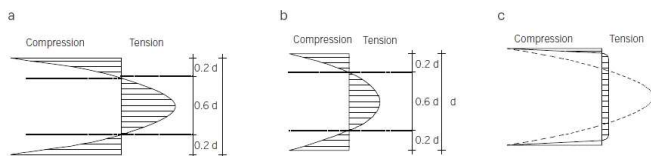


Figure 75. Stress cross sectional diagram for: a) fully tempered glass ,b) heat strengthened glass, c) chemically strengthened glass. (Wurm, 2007)

Laminated glass

Laminated glass includes at least two layers of glass that are bonded by inter-layers. The different inter-layers are: polyvinylbutyral (PVB), cast in place resin (CIP), ethylene vinyl acetate (EVA) and SentryGlas Plus (SGP). The different interlayers and thickness determine the mechanical and optical properties. Laminated safety glass has a great load-bearing capacity: if one sheet breaks the other sheet will carry the loads. Imagine a three laminated glass panel, the outer sheets can break while the inner sheet remains.

PVB, SGP and resin laminated glass

The lamination of PVB is suited in two stages, as shown in figure 76. The first step is washing the individuals sheets, then the pre-lamination process follows. This includes layering of the film and assembling by heating and pressing. This is achieved by using the roller process or vacuum bagging process. The last step is placing the component in an autoclave with high temperatures of approximately 140°C

The same approach for the PVB layer is used. It is different from a PVB layer because it is stiffer and it is delivered in standard sheets instead of using the roller process.

Examples of resins in laminated glass are EVA and CIP. It is not a complete automated process because the resin is poured in a wide gap of 1 to 2 mm. The edges are closed with a transparent tape. Due to these methods, different sheet thickness's are allowed.

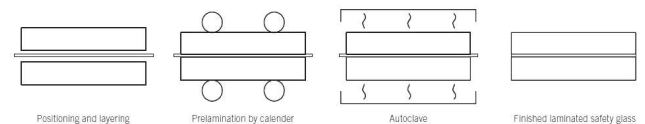


Figure 76. Scheme of the two-stage production of laminated glass (Wurm, 2007)

Mechanical pre-stressing & steel reinforcements

According to Schittich et al. (2007) pre-stressing means pre-compressing the surface and bringing an over compression of the surface cracks. Tensile stresses occur when pre-compression is neutralized, due to the appearance of tension in the component. Pre-stress can be accomplished by using dead load or spring systems. According to Louter (2017) steel reinforcements can improve the mechanical behaviour of a glass system. Moreover, choosing sufficient connections can lead to ductile behaviour of glass, which is a preference for a safe design with glass.

2.3.7 Production methods

The manufacturing process of glass leads to different types of glass with different batch sizes and properties. Different types of glass and related manufacturing processes are explained in this chapter. According to Wurm (2007) the manufacture process of glass is distinguished into two processes: a primary and a secondary process, as shown in figure 77.

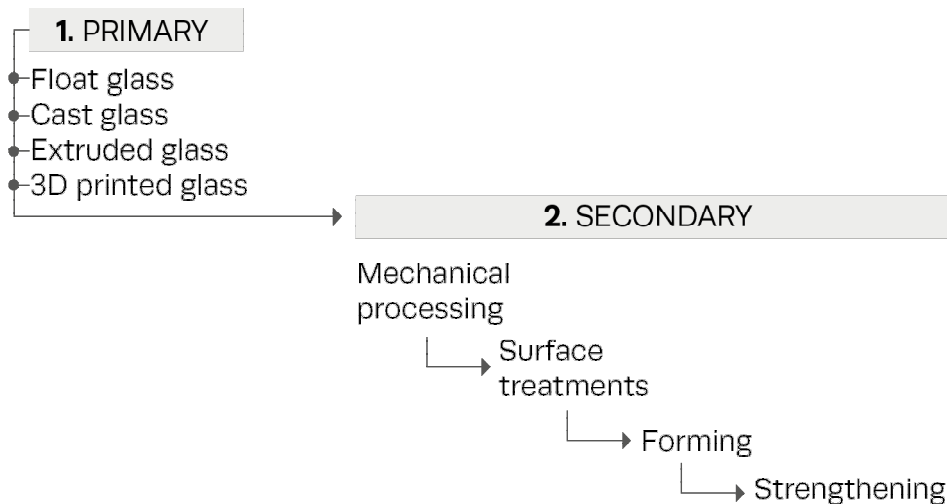


Figure 77. Manufacture process of glass based on (Wurm, 2007; Doulkari 2015)

1. Float glass

Approximately 90% of the glass production equals the production of Float glass. Alastiar Pilkington is the developer of the float glass production technique. The production of float glass forms a worldwide network where companies produce 750 tons (50000m²) glass per day.

The production technique has 6 'main' stages and are presented in figure 78. Melting and refining is the first stage. In this stage the raw materials are controlled, mixed and finally added to the melter and heated to a temperature of 1550°C.

According to Wurm (2007) and Weller (2009) refining is required to ensure bubble free and inclusion free glass. The second stage is the float bath: the 1000–1200°C glass flows onto a molten bath of tin with a length of approximately 50m. The solidified glass leaves the bath with a temperature of 600°C and goes to the third stage: the annealing lehr. Subsequently, the internal stresses are released and the temperature is slowly dropped to 100°C. The last stages represent cooling to room temperature, inspection and cutting to size.

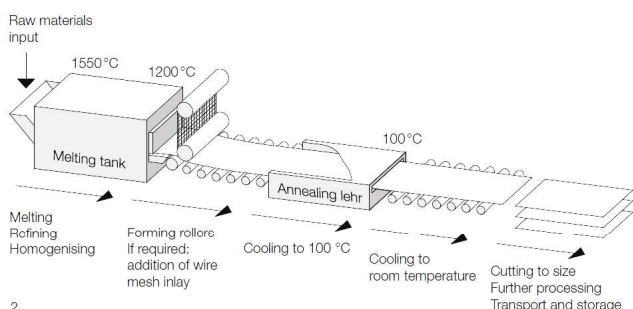


Figure 78. Float glass production technique (Weller, 2009)



Figure 79. Float tank interior (source: www.cmog.org)

2. Cast glass

The casting process differs from the production of float glass because the shape is created by casting glass into a mold. This is the biggest advantage of cast glass causing high form flexibility and a strong monolithic structure. A real example of a cast glass application in the building industry is the Crystal house in Amsterdam. Currently, the largest monolithic cast glass components are the mirrors of giant telescopes.

This chapter addresses three methods for casting glass: sand casting, kiln casting and spin casting. In addition, this chapter explains the different types of molds and finally defines the limitations of the casting process.

Sand casting

Sand casting is also called hot pour casting and is a very old technique. Molten glass from the furnace of approximately 1150°C is directly poured into a pre-formed mold. The mold is made from silica sand, clean sand, a little bit of bentonite and supported by a support material e.g. wood or steel. It is a disposable mold and cannot be used twice^[12].

Next, when the glass reaches a temperature of approximately 620°C the mold is released and the glass component is added to the annealing oven^[11].

Nowadays, these sand molds are replaced for steel molds, for example the molds used for constructing the Crystal House. These steel molds need a release coating to prevent the glass from sticking and micro-cracks.



Figure 81. Cast glass Semi-reclining dress impression
(source: www.ifitshipitshere.com)



Figure 80. Principle of sand casting
(source: www.washingtonglassschool.com)

[11] <http://www.glass-fusing-made-easy.com>, [12] <http://www.oshdopp.com>

Kiln casting

The difference between sand casting and kiln casting is the presence of the kiln. During this method the kiln is involved in the whole process, i.e. during the melting, annealing and cooling phase. Crushed glass pieces are placed in a kiln where the glass is melted (approximately 816°C), annealed. When it is cooled down, the mold is removed [13].



Figure 82. Kiln casting
(source:www.saltglasstudios.co.uk)

Spin casting

The biggest (mono-material) cast glass component realised is the giant Magellan telescope mirror, as shown in figure 83. It consists of 7 segments, with 6 asymmetrical outer segments (similar to potato chips). The diameter of the entire mirror equals 24.5m, and the diameter of each segment is 8.4m. The low-expansion glass is placed in chunks upon a honeycomb mold made out of ceramic cores and is melted. After this process, the segments are polished to the desired dimensions and coated with aluminium for maximum reflection.

The honeycomb structure is created by melting glass into an opposite honeycomb mold and the mirror itself is made with a new technique of casting, i.e. spin casting. In this process the kiln is rotated during the liquefaction of glass, resulting in a parabolic mirror shape. The advantage of this new technique is that the annealing and grinding times are shorter because it is already in a parabolic shape. The duration of this melting procedure took 4h (melting and pouring the glass) and the annealing time was 4 months [14].



Figure 83. Giant Telescope Mirror
(source:www.gmto.orgs.co.uk)



Figure 84. Preparation before casting: the honey comb mold (source:www.gmto.orgs.co.uk).

[13] <http://www.polytek.com>, [14] <http://www.gmto.org>

Molds

Any material that can withstand the high temperatures to melt glass and prevents the glass from sticking can be used as a mold. However, some materials can be used by adding a coating to prevent the glass from sticking. The following materials can be used without coating: ceramic fiber paper, ceramic fiber blanket, plaster and plaster/silica investment mix. Unlike the following materials that require a coating: ceramic and steel. Brass, steel and graphite are often used because of their tolerance on high temperatures. However Brass is preferred above steel and graphite due to the lower costs^[15]. Brass, steel and graphite are non-disposable molds. Unlike plaster molds that are often disposable molds because they have a lower working temperature and are cheaper .

According to Oikonomopoulou; Bristogianni; Nijssse; Veer (2017) two different types of molds are distinguished: a high precision press mold and open precision molds. Whereby high precision press molds press the molten glass to the dimensions during the rapid cooling phase.

Limitations

According to Nijssse (2015) the production of cast glass components looks very simple: the glass is melted, changed into a liquid and is casted into a mold. Next, when the glass is solidified the shape cannot change. Resulting in a very complicated process due to the different cooling parts of the glass components.

Explained in more detail, according to Oikonomopoulou et al. (2017) the first step is the rapidly cooling of the glass to a temperature of 700°C to prevent the molecular arrangement from crystallization, which leads to cloudy glass. In this phase the glass is still viscous and thermal stresses can be released. After this process the temperature is equal to approximately 720°C, i.e. its softening point. The component cannot deform under its dead load and is applied to the annealing oven. The surface is cooled down while the core of the glass element is still hot. As mentioned before this creates a surface compressive zone and a tension zone in the core which causes shrinkage with high stresses.

The annealing process is very important because it prevents the component from residual stresses during the cooling phase. There are two important temperatures during the annealing phase: the annealing point (approximately 545°C) and strain point (approximately 505°C). In literature the definitions are stated as: " The annealing point is defined as the temperature at which the viscosity of glass will allow any induced stress to relax out substantially in just a few minutes (Shelby 2005). The strain point is the temperature where the same stress is reduced to acceptable values in 4h (Shand and Armistead 1958; Shand 1968)" (Oikonomopoulou et al., 2017, p. 7). When the temperature decreases, after the strain point, the components can cool with a faster cooling rate. However it still needs to be controlled due to thermal shock and to prevent them from breaking.

In summary, the amount of internal stresses during the annealing phase depends on: temperature difference (surface-core), thermal expansion coefficient and thickness of the section. Heat transfer causes temperature difference and is influenced by different parameters; shape of the element, mass distribution, sides exposed to cooling (if you use an open mold), amount of thermal masses in the kiln, geometry and other features of the kiln. Figure 86 gives an overview of the factors that determine the annealing phase.



Figure 85. The high precision steel molds used for construction of the Crystal Houses facade (Oikonomopoulou, 2017)

[15] <http://www.glasscampus.com>

ADVANTAGES CAST GLASS

1. High form flexibility

2. One strong monolithic structure

3. Transparent

LIMIT: ANNEALING PHASE

a. Dependent factors

- Temperature difference
- Thermal expansion
- Thickness
- Type of glass

← Heat transfer →

b. parameters

- Shape
- Mass distribution
- Sides exposed to cooling
- Thermal mass & features kiln

Figure 86. Advantages cast glass versus limitations of cast glass

3. Extruded glass

According to Roeder (n.d.) most of the rods and tubes in the metal and plastic industry are made by the extrusion production process. Two forms are distinguished: direct and indirect extrusion. During direct process the glass is pressed by a punch through a small opening, shown in figure 87 (a). Before the glass is punched it is heated and it is shaped by changing the diameter of the opening. Tubes can be created by adding a mandrel in the opening, figure 87 (b). The difference with indirect extrusion is that a hollow punch is used, fixed to the die. The glass is compressed and flows in the other direction of the movement of the punch, figure 87 (c). The indirect process is very complex and therefore only used in special cases.

Glass extrusion components are not often used however various shapes in cross section are possible and therefore sometimes the only suitable production technique. Short glasses are characterized as glasses with big difference in viscosity when temperature changes occur.

Hence, short glasses have a narrow working range and are very suitable for the extrusion process. In addition, the shaping temperature zone is almost constant during the entire process.

Best known extrusion process is the Danner process, developed by Edward Denner in 1912. Glass falls onto a rotating mandrel where air is blown in the centre of the mandrel resulting in a hollow opening in the glass and drawn to the end by a tractor mechanism. The shape depends on the strength of the airflow and drawing speed^[16].

A mixture of various glass types can be used to increase the mechanical and physical properties of glass. An example of an interior design with glass tubes is given in figure 88 (the high thermal shock resistance allows for illuminating elements in the wall). In this example vertical glass tubes are used and laminated to each other. The advantage of laminating extrusion profiles is that different glass types can be used^[17].

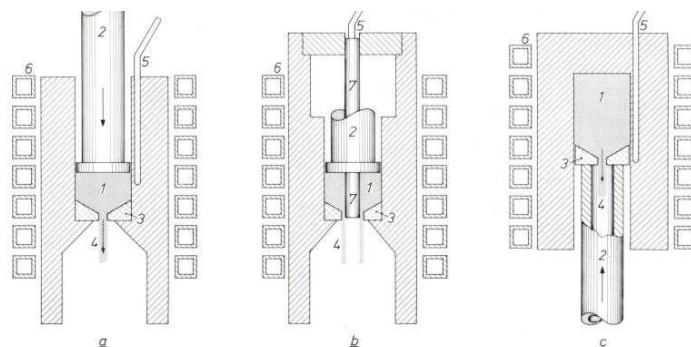


Figure 87. The three types of extrusion equipment (schematic): a) for direct extrusion of rods, b) for direct extrusion of tubes and c) for indirect extrusion of rods (source:www.extra.research.philips.com).



Figure 88. Example of extruded profiles in architecture (source: www.us.schott.com).



Figure 89. 3D Printed Glass object (Ryan, n.d.).

4. 3D printed glass

The Mediated Matter group created a new platform called G3DP: Additive manufacturing of optically transparent glass. G3DP is the first platform that prints 3D precise, optically transparent glass in association with the Glass lab at MIT. The platform has a double heating chamber where the kiln cartridge is present at the upper chamber and where lower chambers act as annealing kilns. The molten glass is poured through a alumina-silica nozzle. Note that this platform is still very experimental and not used in building industry. Up to now only small decorative objects are created^[18], as shown in figure 89.

Production method for the Glass dome

Table 18 provides a multi criteria analysis of the production methods explained in this chapter. The outcome of the analysis presents most suitable construction method for constructing the glass dome. The criteria in bold font, form freedom and structural capacity, are most important criteria for this research. Because an increase in thickness is

needed to prevent the glass dome from buckling failure. Secondly, a high form freedom is required for constructing omnidirectional components. It should be noted that an increase in thickness causes an increase in the annealing time. Hence, high values of strength/thickness ratio are required, increasing the strength while reducing the thickness.

The utilization of **cast glass components** is proposed to construct the glass dome, this because of 2 reasons. First cast glass ensures monolithic components and allows for a high form flexibility which is required due to the omnidirectional shapes. Secondly, cast glass reduces buckling failure and will not cause manufacturing problems, since an increase in thickness is possible. Using other production methods, e.g. float glass production technique, this thickness could be achieved by lamination however this will not ensure one rigid structure

Multi criteria analyses production methods				
Criteria	Float	Cast	Extruded	3D printed
Thickness (mm)	2,3,4,5,6 8,10,12 15 19,(25)	theoretically infinite	tube: 1,6–66,5 rods: 2–20	nozzle size dependent
Optical characteristics	smooth, transparent & textured	smooth, transparent & textured	smooth, transparent	transparent
Stock size (mm)	3210x6000	not in stock	600–10000	not in stock
Form freedom	*	***	**	***
Structural capacity	**	***	**	*
<div style="display: flex; align-items: center;"> <div style="width: 20px; height: 10px; background-color: #d9ead3; border: 1px solid black; margin-right: 5px;"></div> best <div style="width: 20px; height: 10px; background-color: #fff2cc; border: 1px solid black; margin-right: 5px; margin-left: 5px;"></div> intermediate <div style="width: 20px; height: 10px; background-color: #f4cccc; border: 1px solid black; margin-right: 5px; margin-left: 5px;"></div> worst </div>				

Table 18. Multi criteria analysis of the production methods

[16] <http://www.eurotherm.co.uk>, [17] <http://www.us.schott.com>, [18] <http://www.matter.media.mit.edu>

Secondary processes

After the primary process glass can be treated by different secondary processes. These processes are chronically arranged in figure 90.

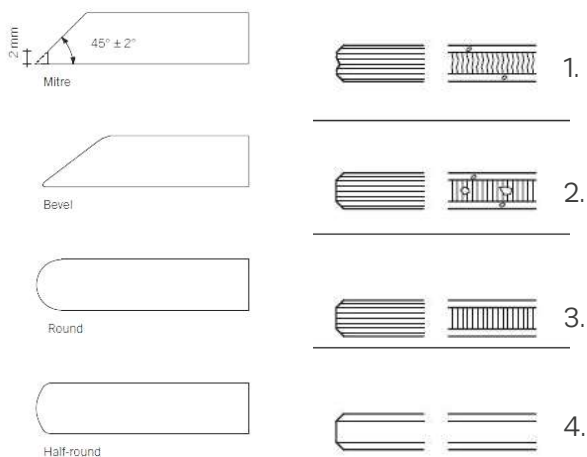
1. MECHANICAL

A. CUTTING

- Automatically diamond-tipped cutting arm (all types of glass)
- Abrasive water jet cutting, seen below (work-pieces from 120mm).



B. GRINDING & POLISHING



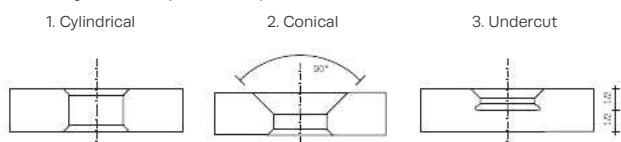
(Left) from top-bottom:

Edge work: mitre, bevel, round and half-round
(Right)

Edge type: 1. Arrised, 2. Ground, 3. Fine ground and 4. Polished

C. DRILLING HOLES

- Local grinding
- Water jet (complex shapes)



2. SURFACE

A. MATT FROSTED FINISH

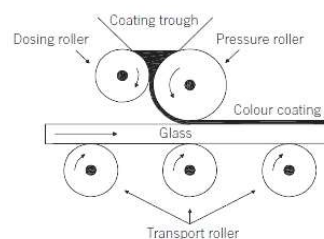
- Using:
- Sandblaster
 - Frosting machine



B. TRANSLUCENT (etched in acid bath)



C. PRINTING & ENAMELLING



Principle of roller-applied colour coating

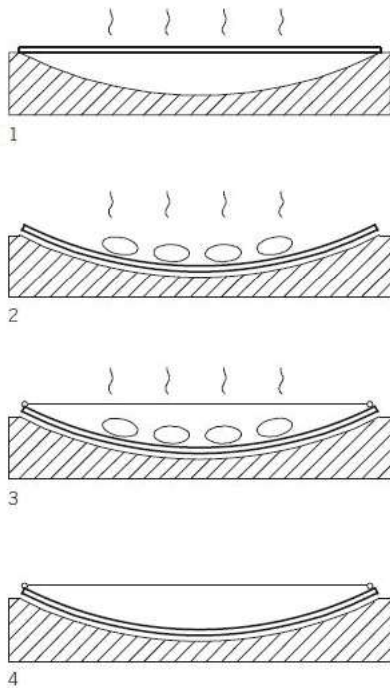
D. COATINGS



- Hard (self cleaning)
 - Soft
 - Online
 - Offline
- < Example with and without pyrolytic coating

3. FORMING

A. COLD & HOT BENDING



Cold

1. Heated to 70°C
2. Apply load
3. Fix shape
4. Cool to room temp.

Hot

1. Heated to 580–600°C
2. Apply load
3. Fix shape
4. Cool to room temp.

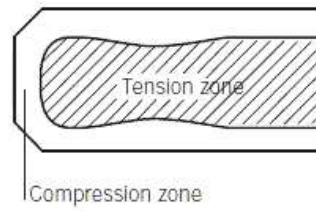
B. FUSING > "TEXTURING"



Example of textured float glass where an additional layer is added by heating the float glass and melting a fire resistant substrate.

4. STRENGTHENING

A. TEMPERING



Pre-stressed zone's due to heat treatment

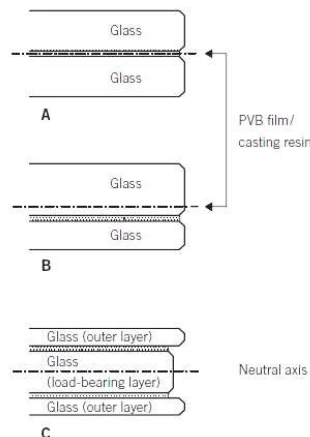
- Fully tempered (TH)
- Partially tempered (HS)

B. CHEMICAL



The glass dome at ILEK is an example of chemically strengthened glass.

C. LAMINATION



Forms:

- A. Symmetrical
- B. Asymmetrical
- C. Symmetrical with more than 2 layers

Figure 90.

Overview of the secondary processes and related phases, based on (Wurm, 2007).

2.3.8 Existing cast glass structures

Introduction

It was concluded in the chapter 'production methods' that the cast glass production technique is the most promising method to construct the glass dome. Hence an analysis of three existing cast glass structures is given in this chapter to gain fundamental insight of the connection of the cast glass components and the supporting system. The pros and cons of their connection type and support system are given, assessed on transparency, stability and reversibility. The following existing cast glass structures are analysed:

- Atocha Memorial (A)
- Crystal House (B)
- Optical House (C)
- Crwon fountain (D)

Finally a conclusion is given why an interlock system is preferred based on transparency, stability, reversibility and no necessity for sub-structure.

A. Atocha Memorial

The Atocha Memorial is a glass monument in remembrance of the terrorist attacks in Madrid of March 11, 2004. According to Göppert, Paech, Arbós and Teixidor (2007), the design includes a translucent upper structure located on top of an underground meditation place. During the day, the translucent upper structure allows for daylight in the underground meditation place. The opposite happens during the night resulting in an enlighten upper structure.

1. Glass blocks

The shape of the horizontal section of the glass outer shell resembles an elliptical form and is eleven metres high. The outer shell is constructed from 15100 cast glass components that are connected through transparent glue. The cast glass blocks are produced through a special pressure mold to its final dimensions of 200 mm x 300 mm x 70 mm, resulting in 8,4 kg blocks. A tolerance requirement of +/- 1 mm was set in order to apply the transparent glue with an uniform thickness. Moreover, borosilicate glass was chosen as raw material for producing the glass blocks. Borosilicate glass was preferred since the glass blocks are subjected to high temperature differences, e.g. rain on a hot summer day. The interlock of the glass blocks have a spherical configuration: concave and convex interlock. The concave and convex interlock allows for form freedom and will form the close to elliptical shape.



Figure 92. Monument at night (Göppert et al., 2007)



Figure 91. Glass block of the Atocha memorial (Halbe, n.d.)

2. Structure

The rigid structure is created through the structural cast glass components and curvature of the close to elliptical shape. In addition, the roof structure is connected with the free upper edge to create one rigid structure and prevents ovalisation. Finally, the glass components were placed onto 200 elastomer pads. The function of the elastomer pads is two folded. First, to reduce the shear forces in the lower glue joints caused through the post-tensioned floor. Secondly, the elastomer pads will compensate the temperature strains differences between the glass blocks and substructure.

3. Connection

The glass blocks were constructed on site, where the acrylic glue was UV-cured. In more detail, the mean thickness of the glue equals 2 mm, this to allow for an acceptable structural performance and to absorb the manufactures tolerances. Finally, eight transparent polyurethane spacers were placed to create a precise spacing of the adhesive between the blocks

B. Crystal House

The Crystal House is an innovative glass brick facade which is produced for the Chanel store. According to Oikonomopoulou et al. (2017), the glass brick facade replaces the initial brickwork of a old town-house located in Amsterdam. The glass bricks are constructed from cast glass components that are arranged in the traditional brick pattern. Finally, the facade is constructed out of 6500 cast glass bricks and cast glass elements that form the frames of windows and doors.

1. Glass blocks

According to Oikonomopoulou et al. (2014), the glass blocks differ in length size, where three different length were used: 105, 157.5 and 210 ± 0.25 mm. Unlike the width and height that have the same size: $w=210 \pm 0.25$ mm and $h=65 \pm 0.25$ mm. The tolerance of ± 0.25 mm relates to the flatness and dimensions of the glass blocks in order to apply a homogeneous adhesive layer. The glass bricks were produced through a precision mold that was coated with nickel, where



Figure 93. Spacers used for the glue (Göppert et al., 2007)



Figure 94. All glass brick façade: the Chanel shop in Amsterdam (Nijssse, 2015).

nickel ensures smooth surfaces and easy release of the glass brick from the mold.

2. Structure

The structural performance of the entire glass facade is obtained from the structural glass components and four buttresses located at the inner-side of the facade. It should be noted that the buttresses are essential to avoid buckling

of the glass facade caused by wind eccentricity. Explained in more detail, the buttresses consist of glass blocks forming that are interlocked with the facade glass blocks and have a total height of 5,5m.

3. Connections

The glass bricks are connected through a transparent acrylate, resulting in a high transparent structure. The adhesive was cured by using a photo-catalytically method and became after curing a weather-resistant adhesive. The optimum strength of the adhesive is reached in between a layer thickness of 0.1–0.3 mm respectively.

C. Optical House

The optical House is designed by Hiroshi Nakamura and his studio NAP. The Optical House functions as a private oasis while residents still can observe people and traffic along the busy road.

1. Glass blocks

The facade of the Optical House was constructed from 6000 cast glass components that have the following dimensions: 50mm x 235mm x 50mm. Resulting in a glass structure with a large mass per unit area that shuts out the sounds from the busy road. The raw material of the glass components is Borosilicate glass^[19].

2. Structure

The structural performance of the Optical House is obtained from a metal support structure. The seventy-five threaded metal dowels hang on a pre-tensioned beam and are perfectly aligned. The pre-tensioned beam is located at the top of the 8,6m² facade. Subsequently, flat horizontal metal bars of 40 mm x 4 mm were placed at every 10 cm, this to ensure the precise alignment of the glass bricks and to resist lateral forces and displacements^[20].

3. Connection

The horizontal metal plates are embedded within glass blocks thickness of 50 mm. Hence, the embedded connection results in an invisible horizontal metal structure and an equal seam

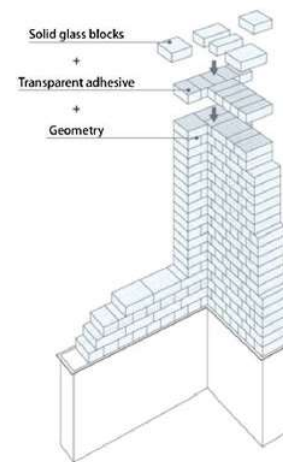


Figure 95. Principle of the structural system of the Crystal House (Oikonomopoulou et al., 2017)



Figure 96. Optical House (Fujii, nacasa & partners, 2013)

thickness of 6 mm between the cast glass blocks. Unlike the vertical threaded metal dowels which are visible. In addition, the glass blocks were punctured with holes during the post-processing in order to place them onto stainless steel bolts^[19].

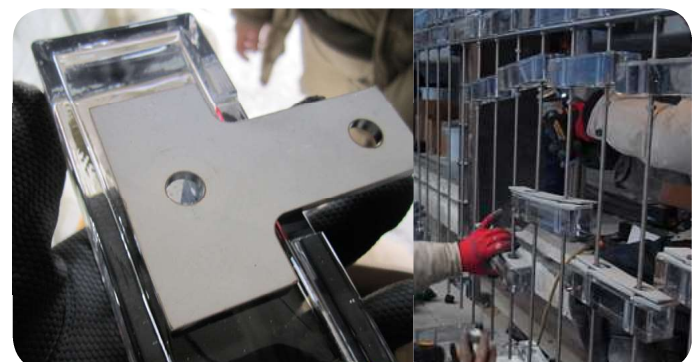


Figure 97. (left) embedded connection (right) placement of the glass blocks (Nakamura & NAP, 2013)

D. Crown Fountain

The Crown Fountain is 15,24m tall and consists of a translucent tower which was built by the Crown family as a present for the citizens of Chicago. The Crown fountain forms an interactive piece with its environment due to the internal lights and water flow over the glass surfaces. In addition, internal LED videos are placed behind the towers facades presenting different faces of the citizens of Chicago onto the glass surfaces. It should be noted that there exist little literature about the glass blocks, structure and connection^[21]. Hence, the latter mentioned subjects are explained together and are based on the interpretation of pictures retrieved from the literature

Glass blocks, structure and connection

The structural performance of the Crown Fountain is obtained from a stainless steel support structure located behind the glass facade. In addition, the glass facade is constructed out of cast glass components and it is assumed that the cast glass components do not function as structural components. Because the cast glass components are fixed onto a steel frame, as shown in figure 99. Subsequently this steel frame is fixed with the inner structure. To resume, the inner-structure will form the main structure out of stainless steel. Secondly the glass bricks with metal frame will form the sub-structure for lateral rigidity. If we take a closer look to the glass facade, the glass blocks are sealed by a coating to avoid water penetration.

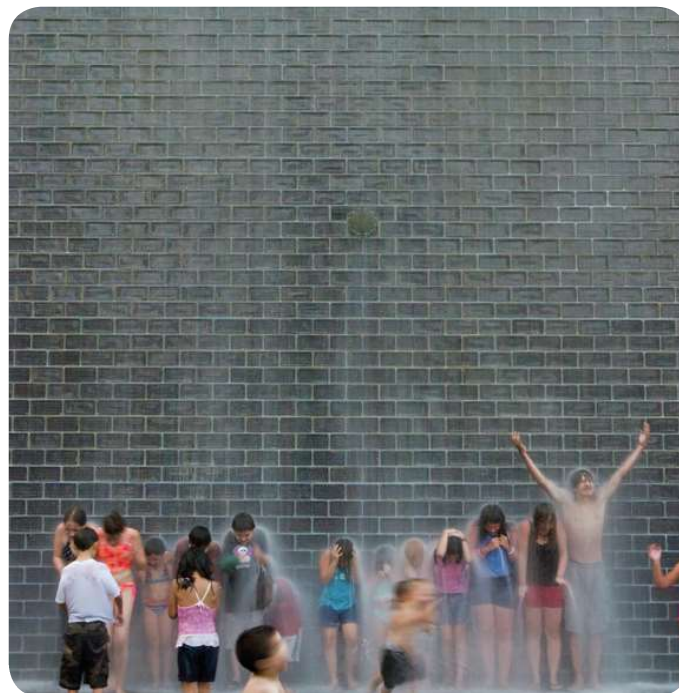


Figure 98. The Crown Fountain (Zbaren, 2011)



Figure 99. Construction of the Crown Fountain
(Courtesy of Krueck + Sexton Architects, 2011)

Pros en cons

The pros and the cons of each connection method of the existing cast glass structures are presented below and the effect on its transparency, stability and reversibility is taken in account.

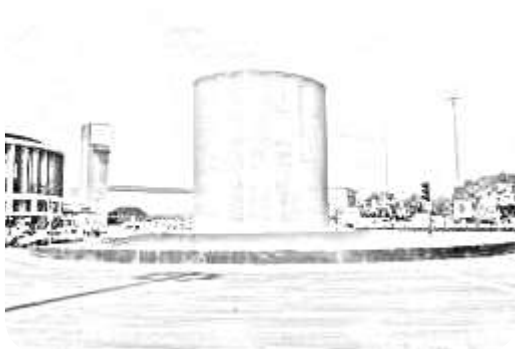


Figure 100. Line drawing: Atocha memorial based on (Sanders, 2013)



Figure 101. Line drawing: Crystal House based on (Nijssse, 2015)

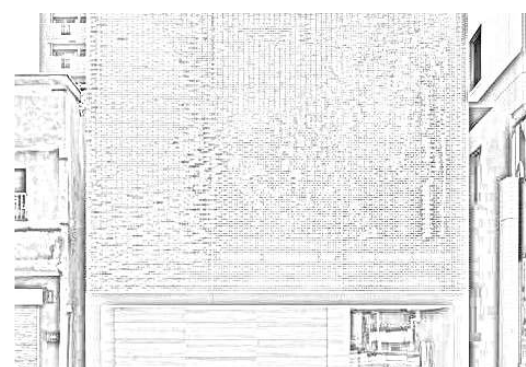


Figure 102. Line drawing: Optical House based on (Fujii, nacasa & partners, 2013)

Atocha Memorial



- The cast glass components do not differ, resulting in **one steel mold** and thus reduced production costs.
- The borosilicate glass can withstand the large temperature differences during the season and days in Madrid caused by the low thermal expansion coefficient of Borosilicate glass ($4,21-4,38 \times 10^{-6} \text{ K}^{-1}$).



- The cast glass blocks are permanent connected through adhesives. This results in a **non reversible** structure.

Crystal House



- Very transparent glass structure caused by the **high visible transmittance** through the glass blocks and thin adhesive layer.



- The adhesive connection makes the structure a **permanent structure**, hence it cannot be reassembled. According to Oikonomopoulou et al. (2014) the production and construction process are complex because the flatness of the glass blocks and dimensions cannot exceed the strict tolerances of $\pm 0.25 \text{ mm}$.

Optical House



- The connection of cast glass components is obtained from a steel interlock system which gives the possibility of **reassembly**.
- The horizontal metal substructure is very thin and embedded in the thickness of the glass component. Hence, the horizontal steel structure will not (or slightly) reduce the transparency.



- The vertical threaded metal dowels do obstruct the visual view and **reduce the transparency**.

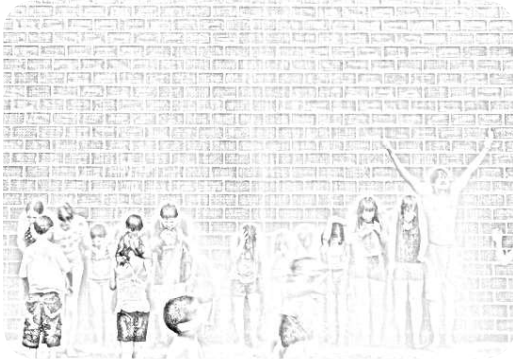


Figure 103. Line drawing: Crown Fountain based on (Zbaren, 2011)

Crown Fountain

⊕

- The glass blocks are fixed on metal frames which allow for **easy and fast construction** on site

⊖

- The glass blocks are **permanently fixed** onto the metal frames resulting in a **non reversible** structure

Conclusion

It is concluded from this chapter that cast glass blocks with an interlocking systems are preferred from the above discussed existing connection methods, this reason is two folded. First, connections from adhesives do create a fully transparent structure however it does not give the possibility of reassembly. The opposite using steel substructures do give the possibility of reassembly however it does not create a fully transparent structure. Thus, to create a fully transparent structure that allows reassembly, cast glass blocks need to be connected through an **interlocking system**.

2.3.9 Structural configurations

*Glass is constructed using a specific production method, mentioned in the previous chapter. After this process the glass components can be arranged in the required structural shape. Three external shapes are distinguished: planar, curved and double curved. A **dome** structure is a **double curved** structure. Hence, this chapter explains if cast glass, extruded glass and float glass products can create double curved structures.*

Cast glass

Double curved structures in building industry are still not constructed from cast glass components. Although, singular curved cast glass structures are under researched, e.g. the glass bridge, a project from the TU Delft is still experimental, as shown in figure 107.

Other forms, such as walls or columns, out of cast glass components in the building industry are the glass bricks used in the Crystal house and the mono cast glass column by Roni Harn, as shown in figure 108.

Extruded glass

An example of extruded glass components are hollow or solid glass rods. A structural configuration can be generated by an array of laminated components. Hence, a double curved structure cannot be formed. However planar or singular curved arrangements can be created, such as: a wall (vertical arrangement) or vault (horizontal arrangement).

Float glass

Finally a dome structure may be created from glass panels obtained from the float glass production technique. Subsequently, the dome is formed through how the glass panels are connected together. According to Wurm (2007) the following connection can be used (and combined):

- Adhesives: fully adhesive or hybrid adhesives, i.e. embedded connections.
- Bolted and clamped

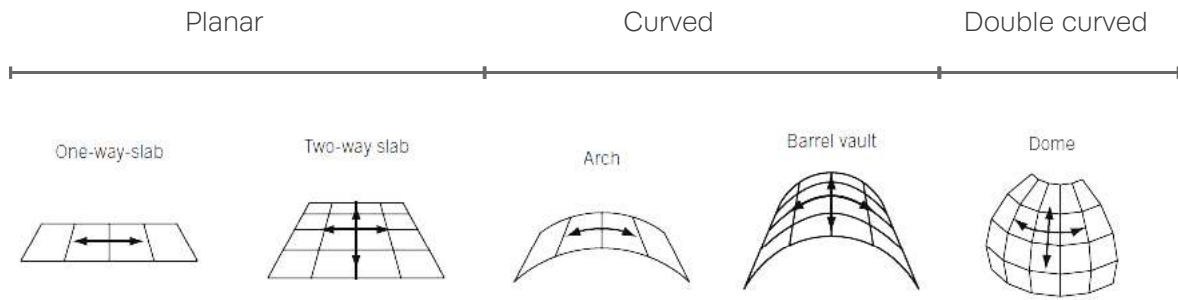


Figure 104. Load-bearing structural forms (Wurm, 2007)



Figure 105. Extruded glass used as a wall application (source: www.evstudio.com)



Figure 106. Extruded glass used as a vault (Borum, n.d.)



Figure 107. The Glass Bridge (Smits, 2015)



Figure 108. Glass column from Roni Harn (Maier, 2008)

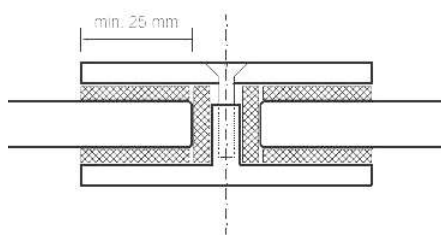


Figure 109. Clamp plate fixing (Wurm, 2007)

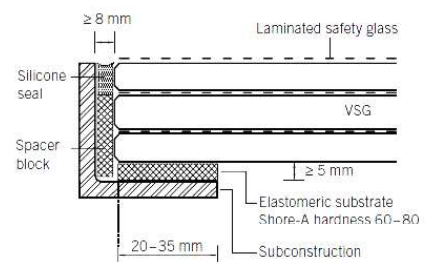


Figure 110. Hybrid connection (Wurm, 2007)

2.3.10 Glass dome structures

According to Wurm (2007) the most common glass dome references are defined by the first four summations given in the brief time line below. These common glass dome references are explained together with a new glass dome proposal from the Tu Delft within this chapter.

- 1998: Spherical homogeneous shell structure "glasstec " **(1)**
- 2002–2004: Delft glass dome **(2)**
- 2002: Stuttgart glass shell **(3)**
- 2003: "glasstex" dome **(4)**
- 2017: Cast glass dome proposal TU Delft **(5)**

Glass dome references

1. The spherical homogeneous shell structure "glasstec" is a dome structure and is supported by steel columns and a steel circumferential ring as shown in figure 111. The span of the dome is 12,3m and the height equals 2,5m. This glass dome is constructed by a steel skeleton built up from 27 different triangle components, with a total amount of 282 faces. Laminated safety glass is used with a layer thickness of 2x10mm. The steel columns are under an angle to create triangular panels. The corners of these panels are connected with steel shoes. Beneath the panel there are steel cables present causing a permanent compression strength. Moreover, the dome is less transparent due to the steel skeleton structure.

2. The Delft glass dome was developed at the Technical University of Delft in the year 2002, as shown in figure 112. A span of 25m was assumed however a span of 5m was handled for the prototype. The geometry equals a ring grid dome with an open apex: 4 rings, 16 meridians and flat plate elements with a variance of 4 different elements. The dome is a fully compressive structure (forces appear in the rings and meridians) subjected to its dead load due to the shallow dome structure ($h=0.9\text{m}$ thus lies above the zero force ring line).

The plates are connected through two connections: mechanical and bonded connections, as shown in figure 113. Point fixers were not allowed because a linear connection was preferred to ensure evenly distributed forces (compression, tension and shear) to the edges of the joints.

Hence, hinged connections were used and located in the ring direction. In addition, a PUR resin was used that bonded the connections and ensured the stress equalization to handle tolerances in the meridian direction. Moreover, the PUR resin has a compressive strength (4 N/mm^2).

The entire construction is fixed at a steel cold-bent tube where the lower panels are attached to steel flat elements. The structure is extremely transparent caused by the integrated connections. Although this structure seems completely perfect the long term effect of the adhesives requires further investigation.

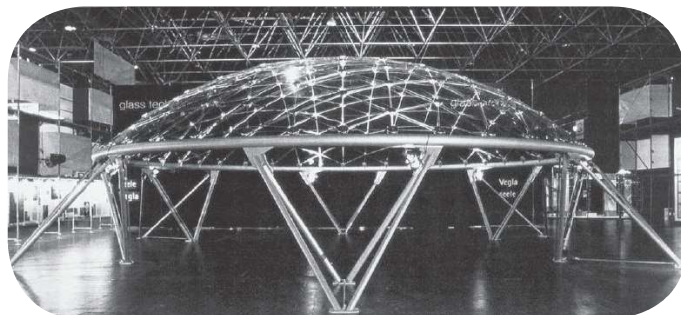


Figure 111. Multi-faceted steel and glass shell (Wurm, 2007)

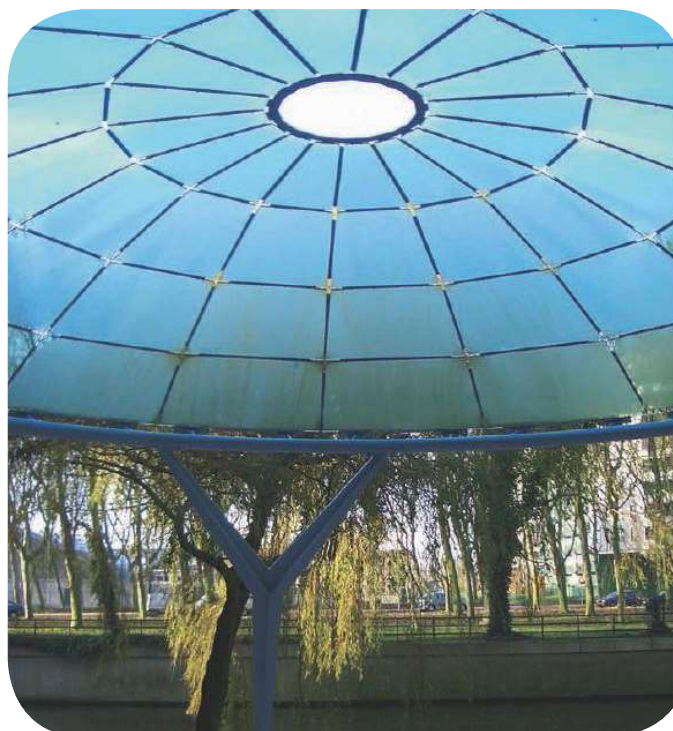


Figure 112. Delft Glass dome (Wurm, 2007)

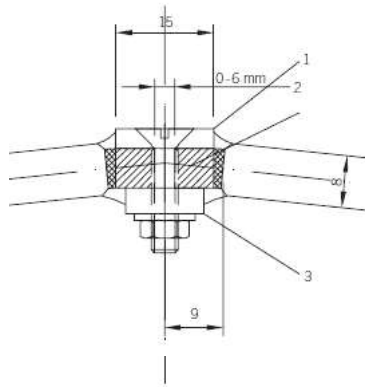


Figure 113. Connection with stainless steel (Wurm, 2007)

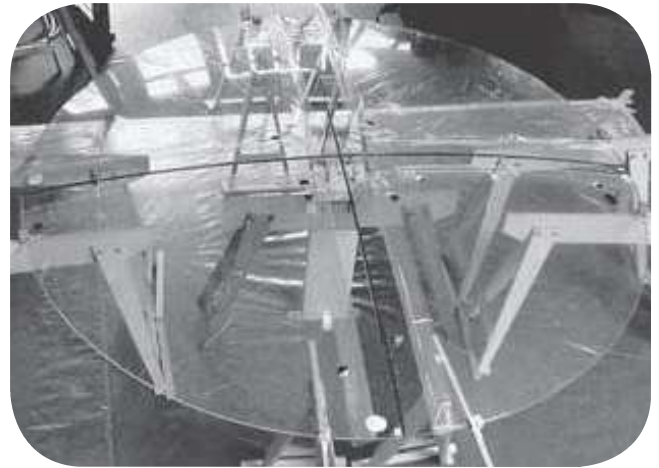


Figure 114. Prototype: Glasstec 2002 (Wurm, 2007)

3. In the year 2002 a prototype was built for a shallow spherical dome, that consists of 4 identical curved glass panels, as shown in figure 114. In the year 2003 the prototype was built on a bigger scale on site with a span of 8,5m and a height of 1,76m, as shown in figure 115. This prototype, built in 2003, is built from curved glass panels with also a variance of 4 different panels. The glass panels include a layer of 8mm float glass and a 2mm layer of chemically strengthened glass. The construction is minimal because epoxy butt joints of approximately 10mm were used, resulting in a high transparency. Note that this adhesive can only be applied under controlled environments, the replacements of broken panels is still unanswered by the literature.



Figure 115. Fully glaze dome on the experimental site at ILEK (Wurm, 2007)

4. The GlassTex dome design is created in the year 2003, that functions as an exhibition place. The glass dome has a spherical shell with a span of 8m, 20 meridians, open apex, 5 rings and therefore a variance of 5 different trapezoidal panels, as shown in figure 116. Moreover, the structure is a fully compressive structure and is built up from laminated glass composed out of 2 layers of 6mm annealed floats glass. The ring elements are attached by an extruded continuous profile located along the meridian with dry gaskets. The bended edges of the plates are bolted against the aluminium profiles and ensure the right position of the glass, load bearing capacity and prevent damage.

The horizontal fabric bands are pre-stressed with steel cables and attached to the inner side by a keder track resulting in a stable structure. In addition, the horizontal fabric bands provide glare and sun protection in the dome. The openings in the dome, located at the apex and bottom create natural convection to release warm air, as shown in figure 117.

During the night the fabrics are illuminated that

results in a clear view. Another feature of the fabric bands is that the reverberation time is reduced. To summarize the bands improve the thermal comfort of the interior of the dome.

5. In 2017 the Technical University of Delft proposed a design for a structural cast glass element that constructs a transparent dome, as shown in figure 118. According to Bristogianni, Nijse, Oikonomopoulou and Veer (2017) the glass dome consists of a hemisphere geometry with 20m span that is constructed with a minimum amount of hexagonal and pentagonal components. These components have stiffening ribs and a smooth surface. The structure is not fully in compression under its dead load, due to the hemispherical shape. The production process of the cast glass elements requires a mass limit, which is: $m < 10$ kg in order to reduce the annealing time. The results of the prototypes showed components with sharp edges that needs to be avoid next time. Because sharp edges result in peak stress concentrations with tensile stresses that can cause damage.

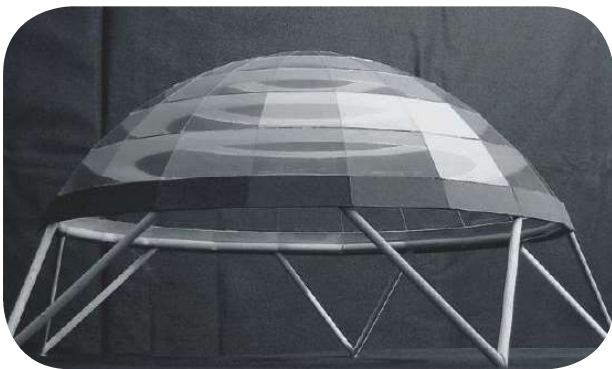


Figure 116. Model of the GlassTex dome (Wurm, 2007)

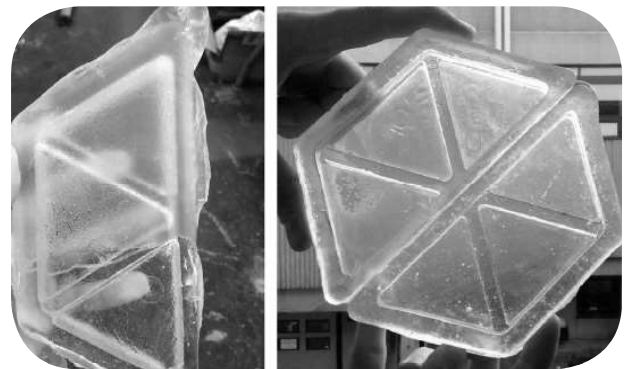


Figure 118. Cast glass element for a transparent dome (TU Delft, 2017)

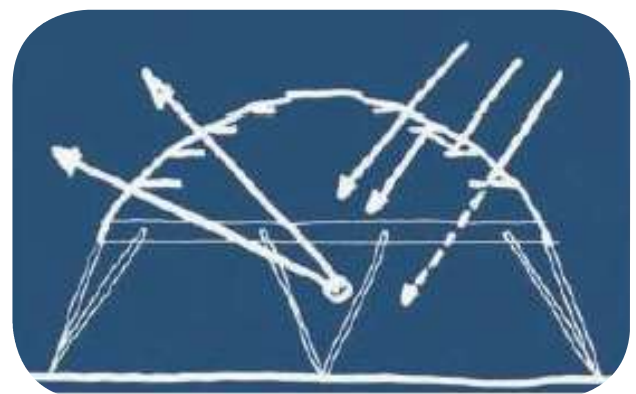
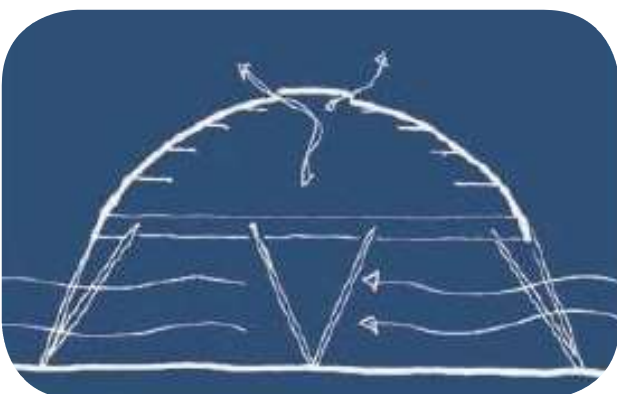


Figure 117. GlassTex dome: (left) the ventilation openings at dome top and bottom, (right) fabric bands reducing the overheating risk in the interior of the glass dome (Wurm, 2007)

Conclusion

Table 19 presents an overview of the examples explained in this chapter and addresses their advantages and disadvantages. The glass dome references are assessed on the proposed design criteria and ranked by: best, intermediate and worst. Fully compressive structures are **shallow dome** structures with a small height, as shown in the table. Bolted connections result in the possibility to create a demountable structure, however do not lead to a fully transparent structure. A **high span to thickness ratio** is required to reduce the annealing time of the cast glass components. An **open apex** is preferred because this leads to natural convection ventilation which results to an improved thermal environment. Because limiting the variance of the cast glass components reduces the production costs for steel molds, a minimum number of different components is set. The transparency is distinguished into two

aspects: the surface transparency, i.e. the amount of glass (1) and the transmission of light caused by the thickness of the element (2). Aspect 1 explains that structures with adhesives connections lead to transparent structures because the amount of glass is larger and number 2 explains that structures with a high span/thickness ratio lead to high transparency due to a higher percentage of transmitted light. Note that both adhesives and steel connections are not preferred for this research. Adhesives create a transparent structure and do not allow for reassembly. Steel connections do allow for reassembly and minimize transparency. Hence, the connections should be created through an **interlocking system** with **transparent interlayers**. The advantages of the glass dome references were blended together and formed the additional design requirements of this research as shown in table 20.

criteria		spherical				hemisphere
		1. GlassTec (1998)	2. Delft dome (2002)	4. Stuttgart shell (2003)	5. GlassTex (2003)	6. Cast element (2017)
structural	Compressive structure*	fully	fully	fully	fully	No
	connection & replacement	steel skeleton	hinges & adhesives	epoxy butt joints	bolted & dry gaskets	adhesive
	Type of glass	annealed safety glass	tempered glass	Float & chemically st.	laminated float glass	cast glass
geometry	Span (m)	12,3	5	8,5	8	20
	Span/thickness ratio	1/615	1/700	1/850	1/667	1/1111
	Type of dome	shallow	shallow	shallow	shallow	hemisphere
	Height (m)	2,5	0,9	1,76	unknown	10
	Apex	closed	open	closed	open	closed
element	Variance	27 flat triangles	4 flat trapezoid panels	4 curved glass panels	5 flat trapezoid panels	depend on deviation
comfort	Transparency (structure)	poor	good	excellent	good	extraordinary
	Transparency (transm.)					
	Thermal comfort	very poor	poor	very poor	good	very poor

* under dead load

best
intermediate
worst

Table 19. Multi criteria analysis of the glass dome references

Design requirements based on references of glass domes		
criteria	WHAT	WHY
1. Shape	shallow	fully compressive structures
2. Apex	open	stack effect & better thermal comfort
3. Span/thickness	high	reduce annealing time & costs
		increase transparency
4. Connection	interlocking system	replacement possible
		high transparency

Table 20. Design requirements based on the glass dome references.

2.4 Interlocking systems

1.1 Introduction

To resume, an interlocking system is required to create a structure that is fully transparent and allows for reassembly. More over an interlocking system creates one rigid structure for the glass dome where all elements work as a whole. The word 'elements' represents the interlayer and glass components. In addition, the shape of the component forms the interlock and determines the geometry of the interlayer. This chapter addresses different interlocking systems and defines the design criteria of the interlayer design. This chapter ends with an interlock system proposal which may be suitable for the glass dome design and gives a summation of the most important design criteria of the interlayer.

2.4.1 Types of interlock

According to Kintingu (2009) four typical interlocking systems are distinguished into four groups, which are:

- Protrusions and depressions
- Tongue and groove
- Topological non-planar contact
- Recursive puzzle interlocking

Some examples of these interlocking systems are given in figure 119-122.



Figure 119. Puzzle interlocking (source: www.fantv.nl)

Topological non-planar contact is defined as:

'a design principle by which elements (blocks) of special shape are arranged in such a way that the whole structure can be held together by a global peripheral constraint, while locally the elements are kept in place by kinematic constraints imposed through the shape and mutual arrangement of the elements' (Y. Estrin et al., 2010, p.1).



Figure 121. Topological non-planar (Macleaod, 2014)

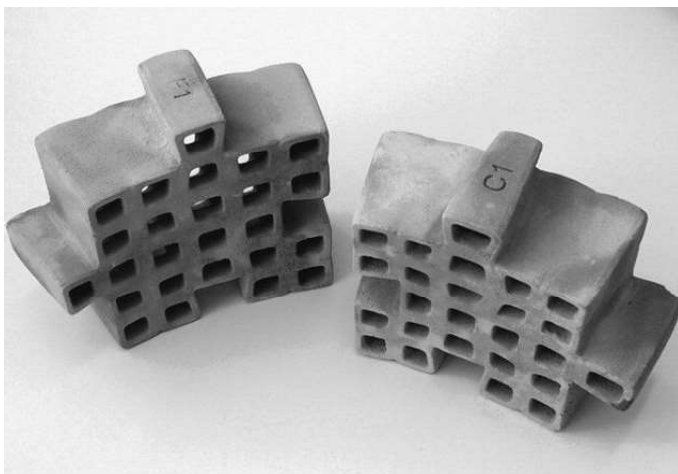


Figure 120. Protrusions and depressions (Archiweb, 2014)



Figure 122. Bottle holders (Roblin, 2011)

Conclusion

The figures on the previous page are nice examples of divers interlocking systems, however the question is if these interlocking systems are suitable for a dome design. The challenge of a dome design is its changing curvature in horizontal section. Latter mentioned principle makes it seem that it is possible to create divers interlocks in arch direction while spherical shapes are required in ring direction. Divers arch interlocks may be possible due to the fact that it has a non-changing curvature. This principle is shown in figure 123.

From above mentioned reasons it seems that every interlock in arch direction is possible when using a spherical ring interlock. This assumption is invalidated by explaining the interlock system of the atocha memorial The Atocha memorial is constructed by utilization of glass bricks with a spherical ring interlock (convex and concave). The spherical ring interlock allows for rotation which results in architectural 'freedom' because multiple shapes are possible. Utilization of the Atocha component for a dome design solves the ring interlock since every curvature can be made. However, if the Atocha component is used in a dome design this will not enable the arch interlock caused through wrong overlapping components, this principle is shown in figure 125.

Moreover, it can be said that the glass dome design requires an interlock system in ring and arch direction which is constructed out of **spherical shapes** because these shapes do not depend on direction. Spherical and independent of direction-shapes are defined as **omnidirectional shapes** and can be used to construct the entire dome design. Another option for constructing a sufficient interlock includes utilization of adjustable molds which take in account the curvature changes. Last mentioned option is not preferred because it adds complexity to the mold design and increases the productions costs for steel molds.

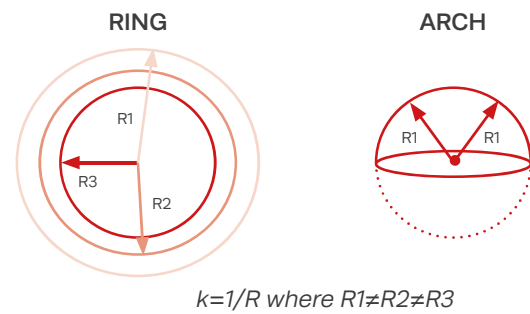


Figure 123. Changing and non-changing curvature

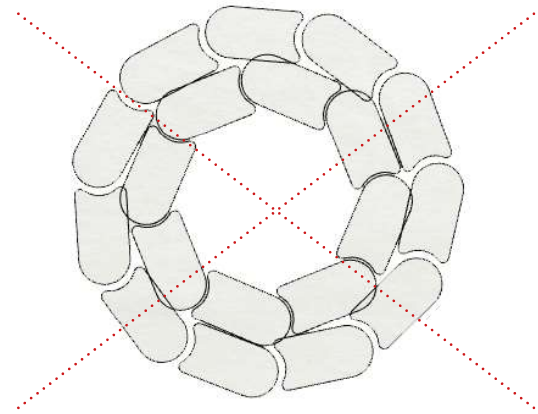


Figure 125. Atocha component applied in dome design

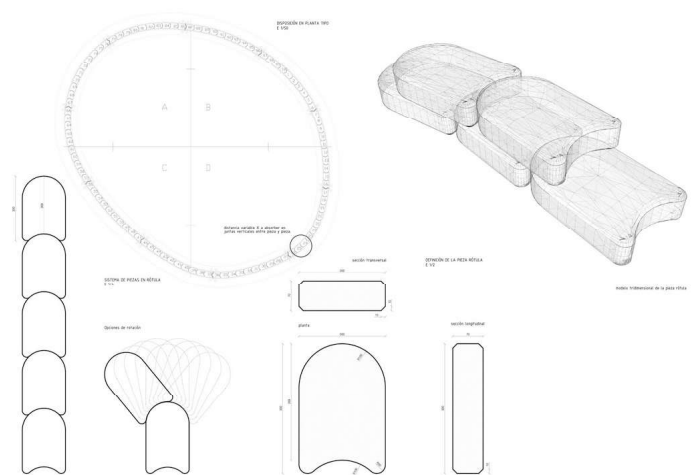


Figure 124. Glass bricks Atocha memorial (source www.folio.brighton.ac.uk)

2.4.2 Interlayer

Introduction

The glass dome components will fail without the use of an interlayer due to local protrusions. These local protrusions result in hard-to-hard material contact with local (tensile) peak stresses and cause failure, as shown in figure 126a. The imperfect surface area of glass is a result of the cast glass production technique. A full contact area would ensure a homogeneous loading. This is the reason why an interlayer is necessary, as shown in figure 126b. The interlayer requires a reasonable thickness and stiffness to absorb the occurred tensile stresses.

This chapter explains the procedure of the material selection and interlayer stiffness/thickness ratio. Chapter structural validation provides a selection of materials that can be used as resilient interlayer.

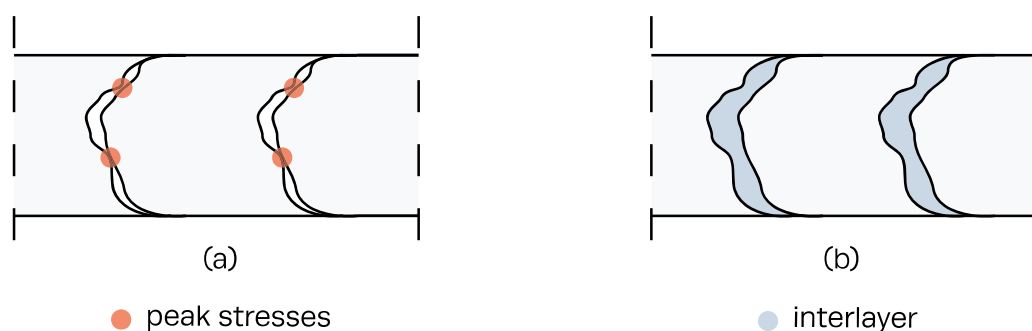


Figure 126. (a) Imperfect glass surface with peak stresses, (b) Resilient interlayer which accommodates the peak stresses based on (Aurik, 2017).

Suitable interlayer materials

The CES EduPack 2017 software was used to obtain suitable interlayer materials. Requirements were addressed, determined and used as data input for the CES EduPack 2017 software. Heat shrink plastics were investigated during this process because heat shrink plastics ensure a large contact area. The plastic will shrink after heating which results in a tight cover and great contact area with the glass component. This has a big advantage for the glass dome components because it allows complex geometries. However the process of thermoforming allows for a section thickness of 0,25–6 mm and as explained later on in chapter 'design' not acceptable for the glass dome.

Material selection

The first interlayer material selection is based on mechanical, optical and durability requirements. The most important requirement is the interlayer stiffness/thickness ratio, explained in the next sub-chapter.

Secondly, the stiffness of the component-interlayer system is the product of the interlayer deformation which will determine the elasticity of the interlayer. The formula of the elasticity, Young's modulus equals: $E = \sigma/\epsilon$, where ϵ stands for the change in length $\Delta L/l$. The change in length increases through high temperatures and during the lifetime of the interlayer material (creep). This concludes that the elasticity (E) depends on time and temperature $E(t,T)$. In addition, the thickness and volume of the interlayer also influence the elasticity. Friction occurs between the component and interlayer which is a result of the contact area of the interlayer with the component. The contact area of the interlayer is defined by its geometry.

It is concluded that the interlayer material selection requires investigation in the following aspects:

- Temperature dependent behaviour
- Time dependent behaviour
- Effect of the interlayer thickness on elasticity

Interlayer stiffness/thickness ratio

Results of glass-to-glass testing indicate that

failure occurs without using an interlayer. This failure occurred already around the tensile value of glass which indicates that an intermediate material is necessary to ensure the homogeneous load distribution and account for local protrusions. It should be noted that a full contact area is the optimum for homogeneous loading. However it is not always necessary but highly recommended. For example, a glass block with a uniformly distributed load supported around its edges, it is expected to have a high failure load as it starts to bend.

Conclusion

It is concluded from this chapter that the glass dome needs an interlocking with suitable interlayer to construct one rigid glass dome structure. The interlocking system should lie both in the ring and arch direction. It requires a omnidirectional interlock which deals with the changing curvature in horizontal section. Figure 127 presents a

scheme of divers interlocks, as explained above, only spherical interlocks are suitable for the glass dome design.

Suitable interlayers are necessary to deal with local protrusions caused by the casting process. The interlayers ensure a full contact area and homogeneous loading. Moreover, it is concluded that the interlayer requires a reasonable thickness and stiffness to absorb the occurred tensile stresses.

The suitable interlayer is defined in the chapter 'structural validation' where the material selection is based on mechanical, optical and durability requirements. Note that experiments should be performed to determine the elastic behaviour of the different interlayer materials within the glass dome system. However, this is beyond the scope of this research and therefore it is assumed that the selected materials, provided in the chapter 'structural validation', can be used as suitable interlayer materials.

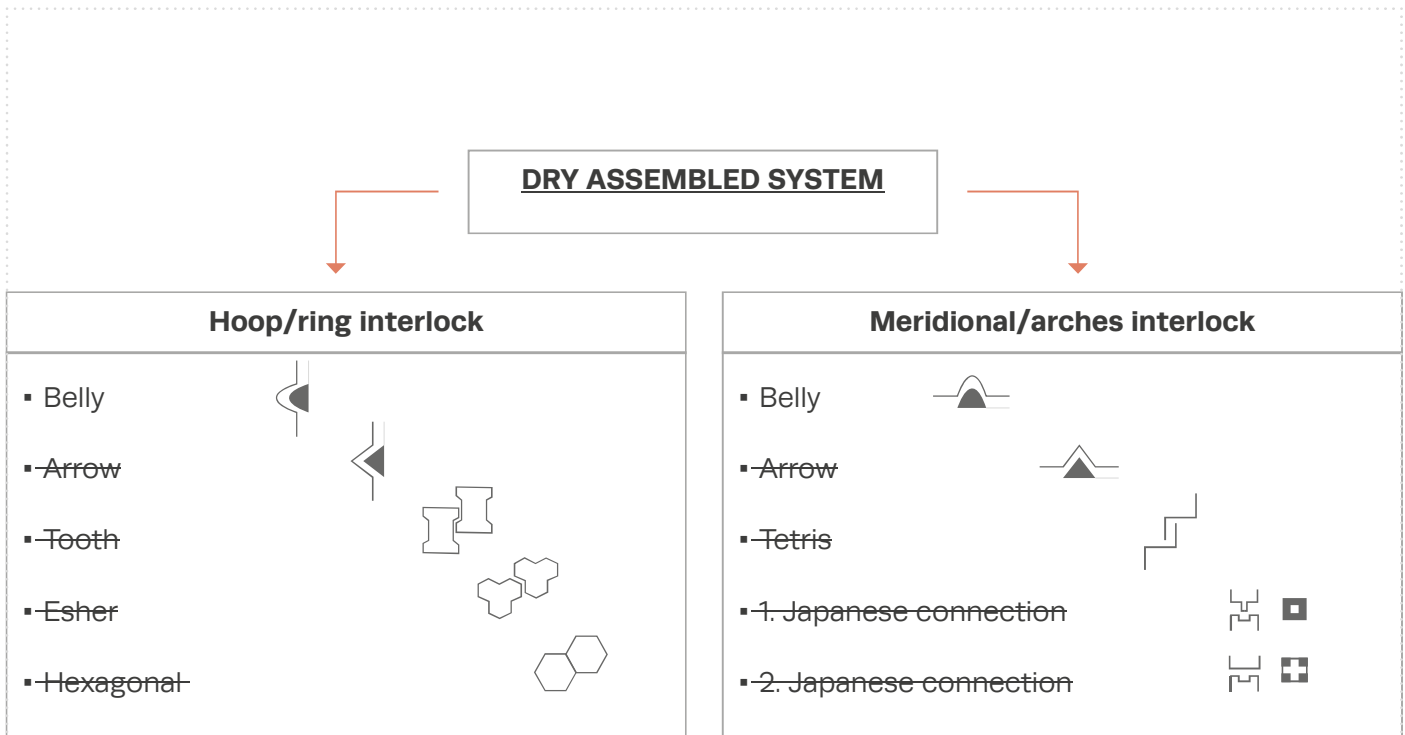
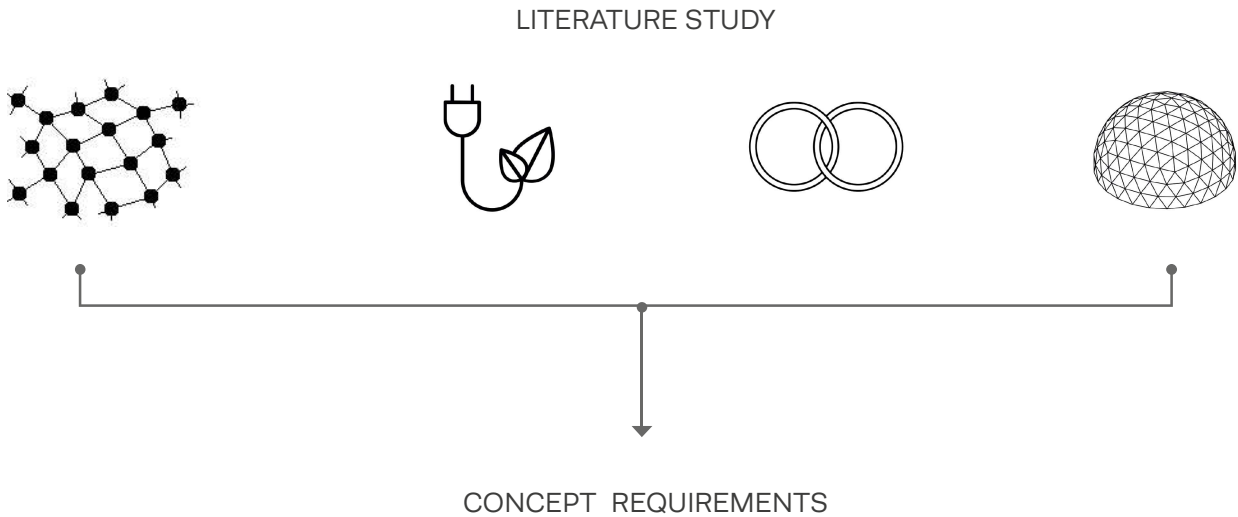


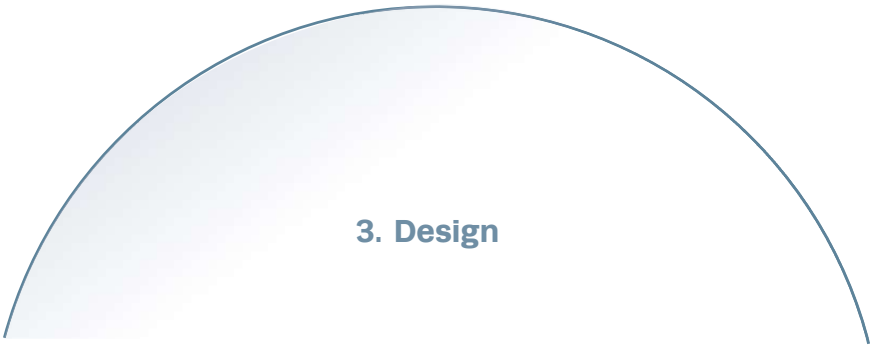
Figure 127. Scheme of different interlocks where the crossed out interlocks are not suitable for the glass dome design.

Finally, it is concluded that the literature reviews result in concept requirements. These concept requirements are shown in table 21 and are used during the entire design process.



		WHAT	WHY
Dome	Shape	Shallow ($0^\circ \leq \varphi \leq 51,82^\circ$)	<i>Compressive structure</i>
	Spann/thickness	High	<i>Increase transparency</i>
	Mass (kg)	<10	<i>Reduction in annealing time</i>
	Different components	Minimum	<i>Reduction costs for molds</i>
	Height	$\geq 9\text{m}$	<i>Fly height of the Lori parrots</i>
Thermal	Temperature	Min: 18/19°C	<i>Comfort of Lori parrots and visitors</i>
		Max: 30°C	<i>Comfort of Lori parrots and visitors</i>
	Energy	Passive strategies (Thermal mass, Natural ventilation and Glazing performance)	<i>Near to zero energy building</i>
Glass	Type	Soda-Lime	<i>Low price per kg</i>
	Production	Cast glass	<i>High form freedom</i>
			<i>One monolithic structure</i>
	Connection	dry & disassembled	<i>Increase transparency</i>
<i>Demountable & re-assemble structure</i>			
Interlock	Shape	Omnidirectional	<i>deal with the curvature changes</i>
	Interlayer	Resilient	<i>homogenous loading</i>

Table 21. Design requirements based on literature reviews



3.1 Introduction

The concept design was obtained from the performed literature study. The performed literature study showed that the dimensions of the glass dome design are based on a shallow dome structure. Because a shallow dome structure will ensure a fully compressive force system when subjected to load. The general dimensions of a shallow compressive dome structure are presented in figure 128. The concept design was developed into a final design which is based on several design principles.

This chapter provides the final drawings of glass dome design and gives insight in the train of thought and decision making during the entire design process. Most important, this chapter explains the necessity of omnidirectional components which will construct the entire cast glass dome. Other related designs that are explained include the general and interlayer design. Finally, the chapter ends with the feasibility of the glass dome design.

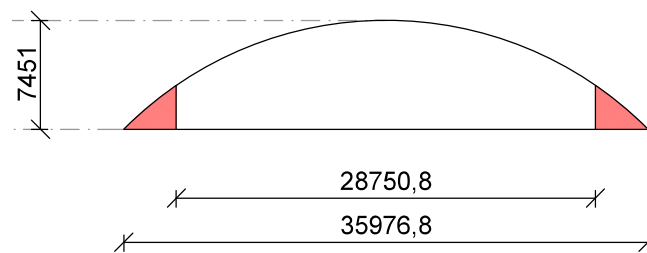


Figure 128. General dimensions of the glass dome

3.2 General dome design

3.2.1 Design principles

The main design principles of the general dome design are divided into three aims which are:

- Increase the flying height for the Lori parrots
- Create a gradual transition between existing and new routes
- Create a passage with a clear route

The first aim is accomplished through a lowered concrete support structure, which has a cylindrical shape. The concrete support structure will increase the rise of the dome with 2m, leading to a new dome rise of 9,5m and increased flying height for the Lori parrots. This principle is shown in the vertical section A-A', presented in figure 130.

Concerning the second aim, create a gradual transition between existing and new routes, this is accomplished by a continuous route and staircase, as shown in the plan in figure 130. The continuous route (represented in the figure with red arrows) merges the existing route through the encircled staircase. The staircase is encircled around the glass dome and has a two folded function: it creates a high accessibility to the entrance of the glass dome and secondly it can be used as a seating. The staircase with seating

function has the advantage of observing the glass dome while enjoying the environment of 'Parc des Oiseaux'.

The glass dome will mainly function as a passage because the interior of the glass dome is defined as a short-term occupancy space. Visitors will have a short term stay within the interior of the glass dome and will walk through the glass dome while observing the Lori parrots. This reason as mentioned above presents the importance of creating a clear route and well positioned entrances. The clear route and main passage is presented in figure 129 with a blue arrow and the light blue arrow shows the transition space. Both entrances are designed with an enclosed porch: the first door opens when the second door closes. The enclosed porch with two doors prevents the birds from leaving the glass dome .

3.2.2 Building elements

The main building elements of the glass dome are divided into interior and exterior elements.

The **exterior** elements are:

- Concrete cylindrical support structure

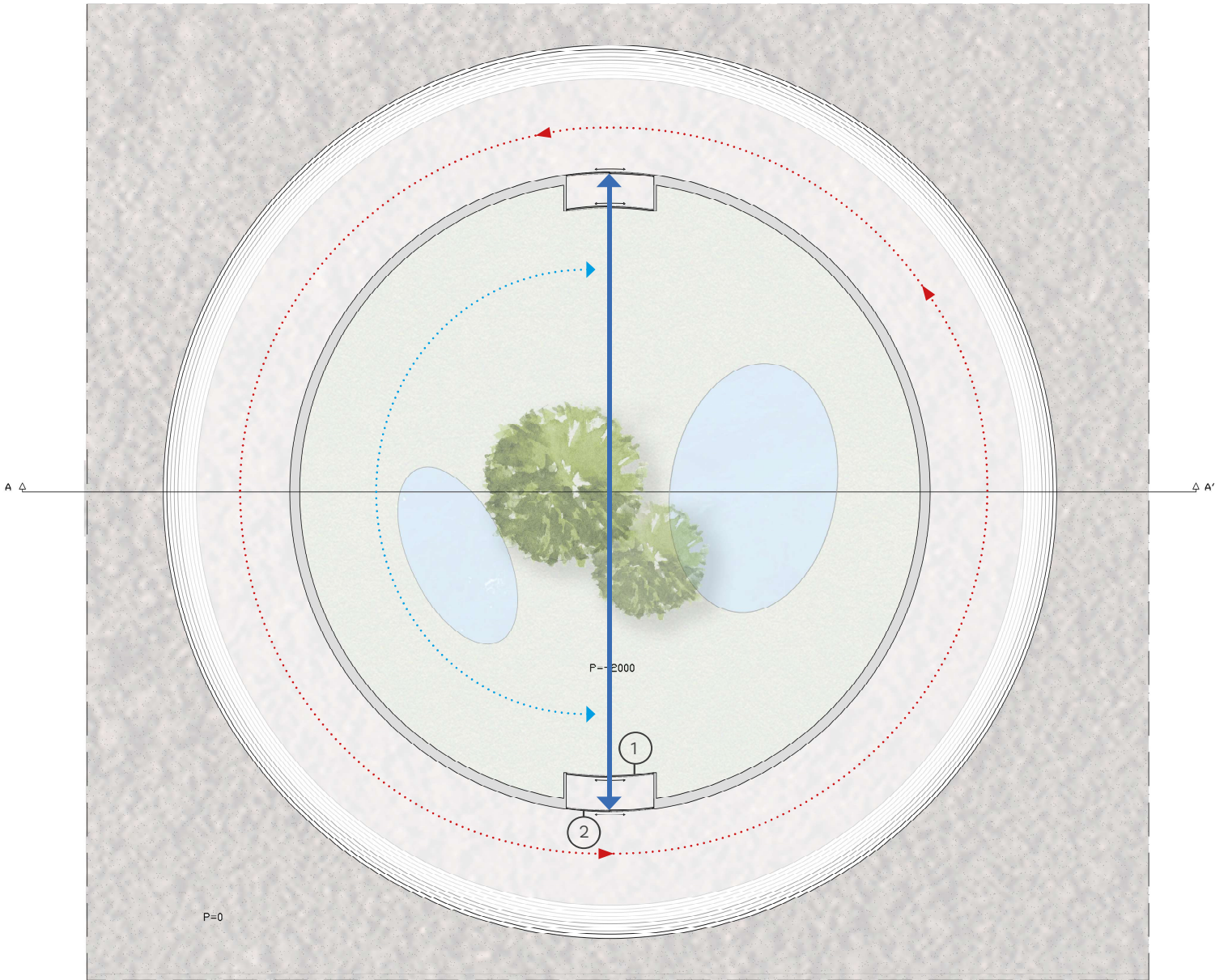


Figure 129. Floor plan of the glass dome, where the red arrows present the continuous route, dark blue arrow presents the 'clear' passage and light blue arrow presents the transition space.

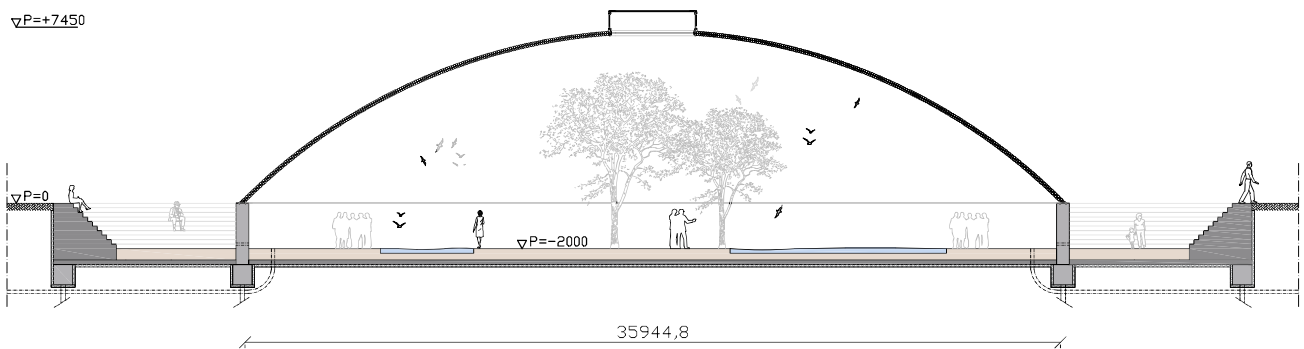


Figure 130. Vertical cross section A-A' of the glass dome

- Glass dome shell out of cast glass components with a transparent TPU interlayer
- Oculus that allows for natural ventilation

And the **interior** elements are:

- Soil layer of 0,5m thick for extensive vegetation
- Two water basins

The oculus needs to allow for natural ventilation to create stack effect. The total surface area of the necessary ventilation opening is calculated and explained in more detail in the next chapter and equals 9,3m². Hence, two designs were made that take in account the total ventilation opening of 9,3m². Both designs include a steel compression ring and **bird net** to prevent the birds from flying out. A **steel compression ring** is required to exert the necessary pressure onto the components, thus to create a sufficient interlock. Because the self-weight of the components is not enough to create a sufficient interlock in both directions.

Design 1 differs from design 2 since the oculus is made from laminated glass panels with small ventilation holes. Design 2 consist of a cylindrical aluminium framed window with laminated glass panels without holes. The **aluminium framed**

window can be opened and is **automatically controlled** for adjustment of the natural ventilation rate during the day and season.

Moreover, **design 2** is preferred above design 1 since the windows can be automatically controlled to allow for an adjustment in the natural ventilation rate. Unlike the small ventilation holes of design 1 that are open the entire day and season.

The interior of the glass dome tries to mimic the natural environment for the Lori parrots. The natural environment for Lori parrots include a green area where extensive vegetation can grow and consist of water basins. The water basins will have a two fold function. First, it will function as drinking basins for the Lori parrots and secondly it can be used as thermal mass. Water is a very efficient thermal mass since it has a high specific heat as explained in the chapter 'thermal performance'. The soil layer has a thickness of 0,5m to allow for extensive vegetation.

The other building components such as glass component and related interlayer require a broader explanation and are explained in the next the chapters

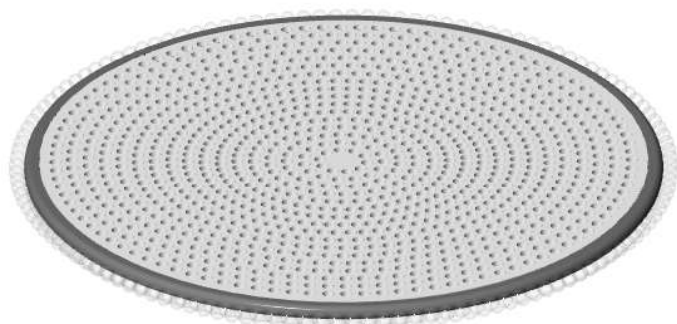


Figure 131. Oculus design 1

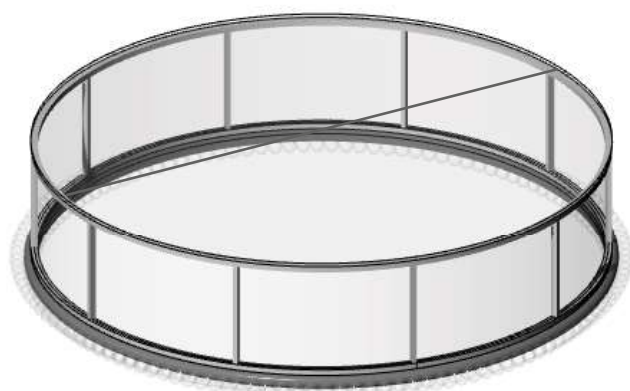
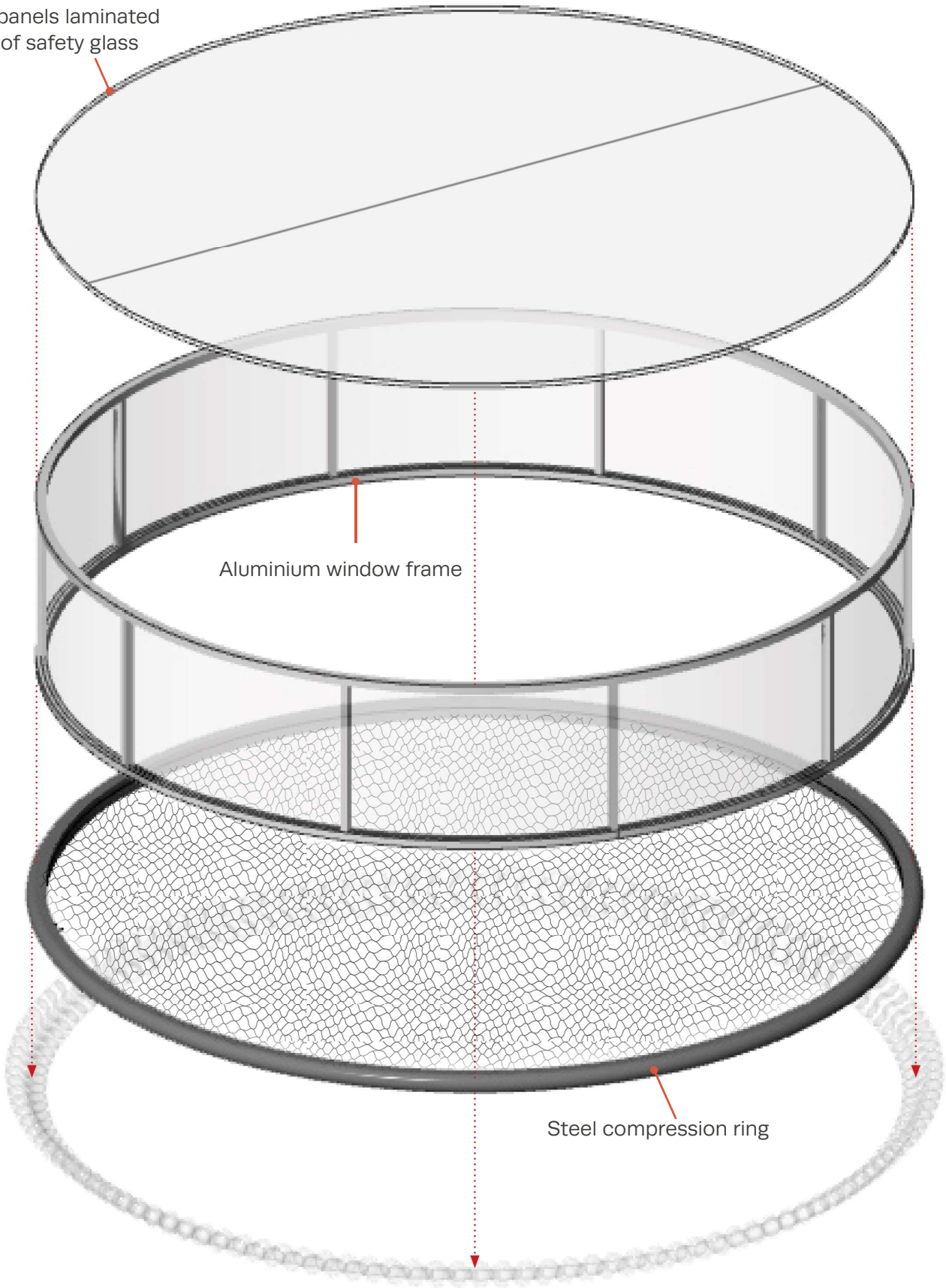


Figure 132. Oculus design 2 (final)

2 panels laminated
of safety glass



Aluminium window frame

Steel compression ring

Figure 133. Exploded view of the final oculus design

3.3 Component design

This chapter presents the general design principles of creating a cast glass structure and new design principles for creating a double curved cast glass structure, i.e. the glass dome. Subsequently, the necessity of a sphere based interlock and component is explained. In addition, the previous glass component attempts and final glass component are explained. Finally, the chapter presents the first mold design.

3.3.1 Design principles

Up to now, only single curved planes or slab were built from cast glass components, such as the Glass bridge and the Crystal House. The requirements of the cast glass components for such structures are shown in figure 134. The dome structure adds complexity to the cast glass component requirements since the dome is a **double curved structure**. Because of the domes double curved surface two requirements were added to the general requirements of the cast glass components and are shown in figure 135. The four general and two new requirements are explained below.

1. Mass <10kg

The first design principle is reducing the mass of the glass component to decrease the annealing time during manufacturing process. As explained in the literature of glass, the annealing process is very important because it prevents the component from residual stresses. High stresses occur during the rapid cooling phase where the surface of the component will cool down faster than its core. This creates a surface compressive zone and core tension zone, this results in shrinkage where high stresses occur. These internal stresses need to slowly remove the component and will determine the annealing time. The amount of internal stresses depends on the temperature difference (surface-core), thermal expansion coefficient and thickness of the section. In simple words, reducing the mass of the component results in a smaller temperature difference between warmer core and cooler surface and this will result in less internal stresses. Finally, this results in a reduced annealing time and related costs.

According to Oikonomopoulou et al. (2017), soda-lime cast glass components of 8,4kg result in an annealing time of 36–38h, while borosilicate cast glass components of 7,2kg result in an annealing time of 20h. Latter can be easily explained due to the fact that borosilicate glass has a lower thermal expansion coefficient which results in a reduced annealing time. In this research it is assumed that

soda-lime cast glass components with a mass of < 3kg result in an acceptable annealing time. Because the glass dome components are rather small.

2. One component

A steel precision mold is needed to produce the cast glass components which construct the dry assembled system of the glass dome. Glass itself may be a durable product however, the production and recycling process of cast glass components is not durable. Glass has a high embodied energy and this is even higher for the included steel molds. Minimization of the amount of different cast glass components minimize the different steel molds. Minimization of the different steel molds is needed to reduce the required production energy and cost for steel molds.

3. Round edges

The contact area of the interlock requires round edges because sharp edges will result in peak stresses with related tensile stresses. Glass is known for its weak tensile strength, thus high tensile stresses need to be avoided. Round edges will contribute to a homogeneous stress distribution with low local tensile stresses and are therefore preferred above sharp edges.

4. Homogeneous mass distribution

It is important to create a homogeneous mass distribution to ensure homogeneous shrinkage during the cooling process. Homogeneous shrinkage is important to reduce the internal stresses. These internal stresses are a consequence of temperature differences, e.g. caused by protrusions. For example, a rectangular shape with one small protrusion, the protrusion cools faster than the larger rectangle resulting in a temperature difference between the protrusion and rectangle. Subsequently this will lead to a crack, most probably around the protrusion where the stresses concentrate. Hence, it is important

to create a homogeneous mass distribution with carefully designed protrusions to avoid stress concentration.

5. Spherical configuration

A dome design has the complexity of having a changing curvature in every horizontal section ($k=1/R$). Straight lines and angles have a fixed direction and cannot accommodate to the changing curvature when using the same component for each ring. Hence, straight lined or single curved components differ for each ring and are not preferred because the amount of different steel molds increases. Unlike spheres, **spheres** are shapes that do not depend on direction, called **"omnidirectional"** shapes. The omnidirectional shape is required in ring and arch direction to create a sufficient interlock as explained in the chapter 'interlocking systems'.

6. Small elements

Smaller elements minimize the tolerances between the glass dome components because the rotation angle between the components reduces when the dimensions of the components become smaller. An additional effect is that the dimensions of the interlayer decrease as well. In the designers world this type of design is defined as "aggrate" design, where elements become infinitely small and allow for complex shapes. It is concluded that small elements are beneficial for a dome design since it will reduce the rotation angle between the components. However it should be noted that the component do need a certain thickness to function as structural component.



(Oikonomopoulou, 2017).



(Smits, 2015).



(Akerboom, 2016).

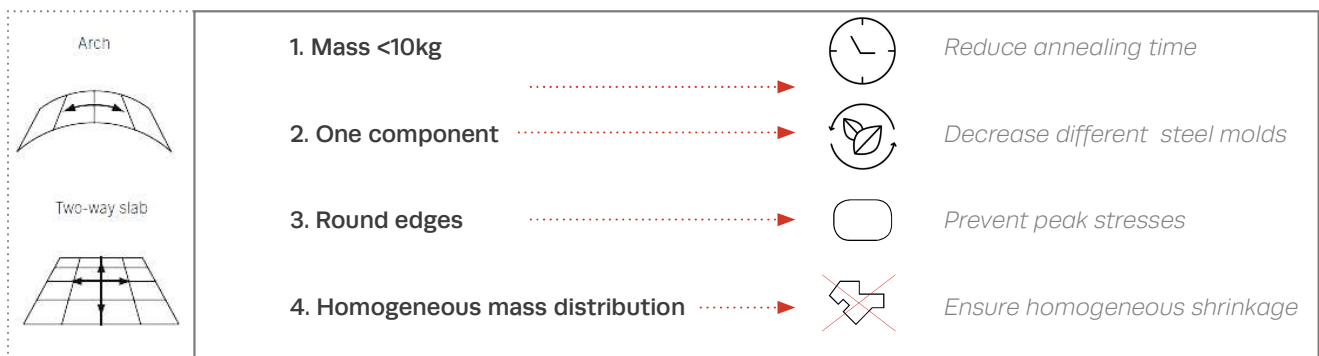


Figure 134. General design principles of cast glass components (curved to non curved structures: arch or wall)



Figure 135. Plus new design principles of cast glass components (double curved structures: domes)

3.3.2 Sphere based design

Why spheres?

Spheres do not depend on direction and are called omnidirectional components. The glass dome requires a sphere interlock in both direction because of two reasons. First, the spheres accommodate to the changing curvature in every horizontal section. Secondly, the arch direction does not show a changing curvature although a spherical arch interlock is required, this is explained below. In general, an arch interlock based on straight lines or one singular curve is possible for constructing one arch because the components are aligned. Applying an arch interlock based on straight lines or one singular curve in a dome structure does not work. This is explained by the fact that the direction of each component for each ring still is different which not enables the arch interlock because to components are not aligned. Different design studies in the software Rhino and Grasshopper were made to gain insight in the consequences of the different shapes and related interlock. All studies showed that constructing one component, to construct the entire dome with, only is created through a spherical interlock in both arch and ring direction.

Why one component?

It should be noted that an adjustable mold could adjust the changing curvature for components based on straight lines or one singular curve. This option is not preferred since this research tries to solve the problem within the shape itself instead of using a high-tech technology. During the design process it was concluded that the question of how to construct a sphere based interlock was already answered by nature. Examples of these sphere based interlock in nature are the wrist and elbow joint or the spine of a human body. These joints clearly show the rotation freedom and interlock between the bones.

Start of the sphere based component design process

The sphere based component design process started by drawing circles or half circles within, above and along other circles, over and over again. Actually, drawing a set of circles and looking for a pattern that interlocks, as shown in sketches in figure 136. It soon became clear that a small inner sphere and a large outer sphere was needed, this to allow for rotation. The same principle is applied for a lamp made out of plastic coffee cups. The smaller cone part is present at the inner-side and the larger cone part is present at the outer-side. The above described start of the sphere based component design process has led to previous attempts, these are explained at next the page.

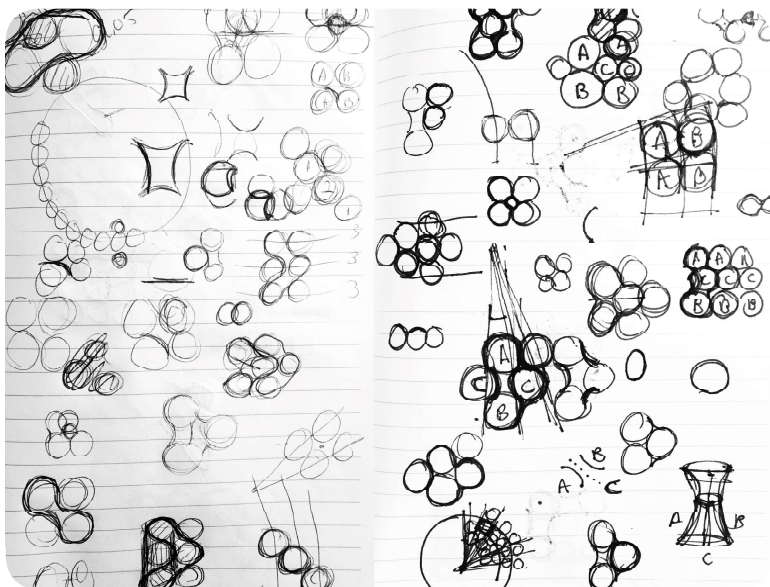


Figure 136. Sketches of the component design process



Figure 137. 'Coffee cup' Lamp (Akkerman, 2017)

3.3.3 Previous attempts

Introduction

The main important previous attempts are presented in this sub-chapter and are based on spheres with a smaller inner-sphere and larger outer-sphere. A brief explanation of design A and B is given below, this explanation gives insight in the pros and cons of both designs.

Design A

The arch interlock of both designs equals a peanut based shape, the two designs differ in the ring interlock.

Design A has a ring interlock located at both centre edges at the inner and outer sphere. The ring interlock consists of spherical protrusions and depressions.

The disadvantage of design A is the created openings between the components, this makes the structure not weather proof.

Design B

Design B consist of two components, where one component equals the shape of design A without the protrusions and depressions. The second component, located at the centre of the first component, ensures a sealed structure.

Moreover, design B results in two complex components. Two complex shapes are not required since it will increase the amount of different steel molds. Finally, this increase in amount of different steel molds will cause higher production costs.

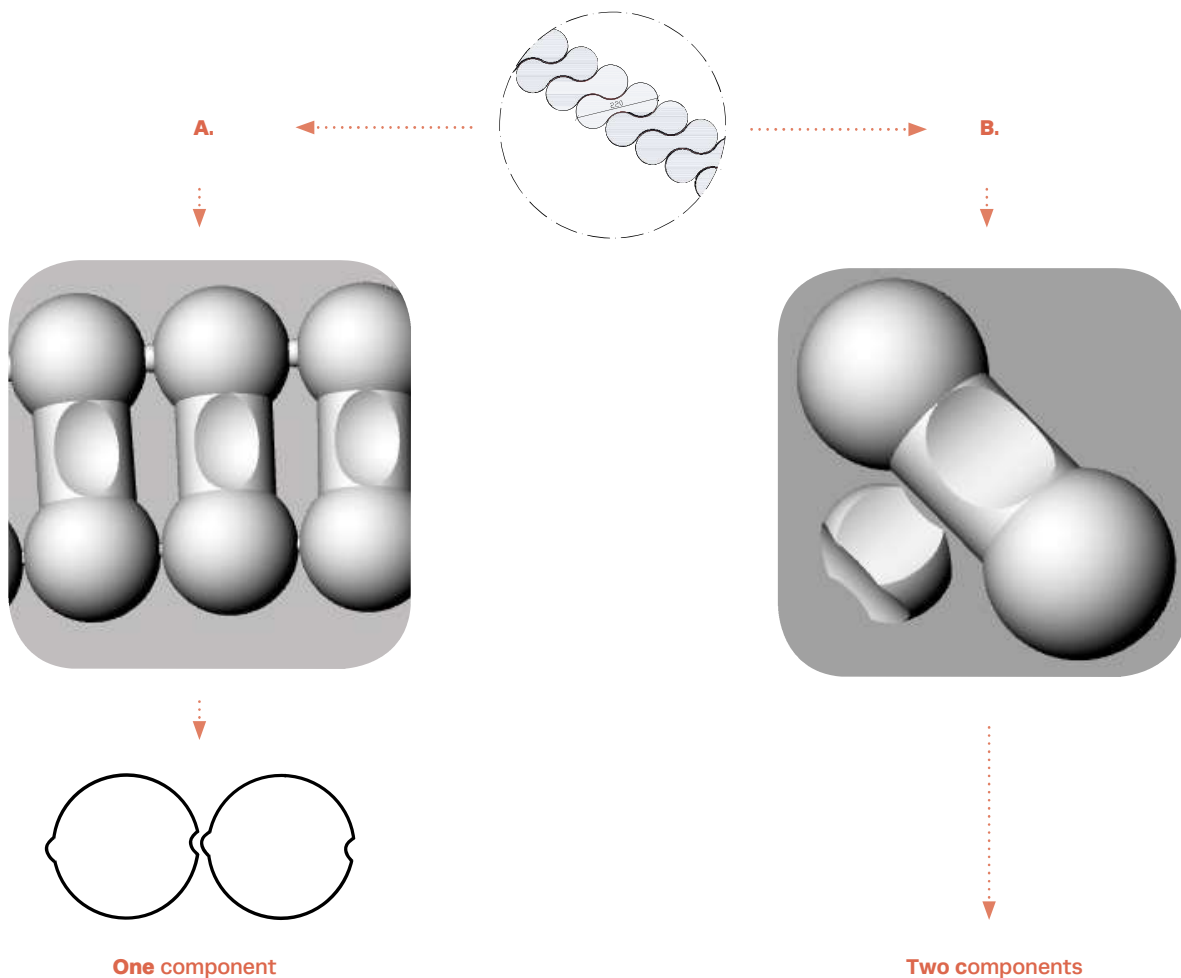


Figure 138. Previous attempts: A and B

3.3.4 Final component

Introduction

The final component is based on several design studies based on spheres. These design studies are obtained from clay studies, 3D prints and from Rhino and Grasshopper models. This chapter presents the final components and explains its related design strategies.

Sphere based design

The final component is constructed out of three different spheres. The inner sphere (A) is smaller than the outer sphere (B). The smallest sphere (C) fits in between the inner and outer sphere (A&B). The dimensions of the three different spheres are given in table 22. Sphere C ensures the ring interlock, as shown in figure 139, and the inner and outer spheres (A&B) will ensure the arch interlock, this principle is shown in figure 140.

The average thickness in the arch direction of the component equals approximately 220 mm and its ring direction equals approximately 45 mm.

The three different spheres are blended together as **one component** and will result in a fully omnidirectional component that can be used in every horizontal and vertical section. The component is smoothed around its edges. However it should be mentioned that this is a very complex 3D modelling process and requires further investigation to avoid peak stresses around its edges. The components are further optimized to reduce the seam thickness between the components in the ring direction, this will be explained in more detail in the next chapter.

Inspiration

The design of the component was inspired by the bone connections of human-beings, most prevailing inspirations:

1. Wrist joint
2. The spine

These two connections are shown in figure 143 and 144, these figures show the **free rotation** possibility of the joints. The wrist joint and spine are used as inspirations for the design of the glass component and the glass component can be seen as a **knuckle** (in Latin: condyle) of a human.

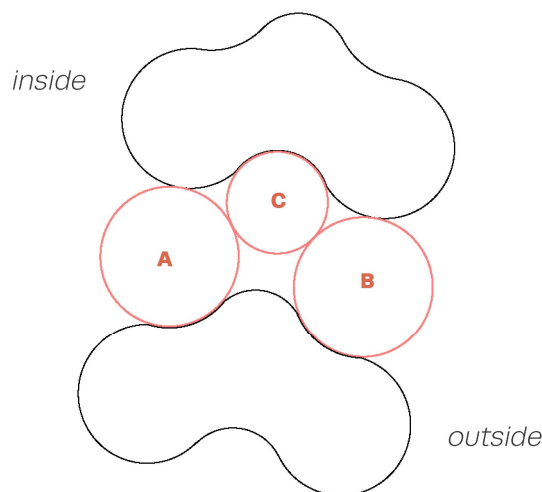


Figure 139. Horizontal section

Sphere	Radius (mm)	Diameter (mm)
A	45,025	92,05
B	46,192	92,19
C	33,460	66,92

Table 22. Dimensions of the spheres

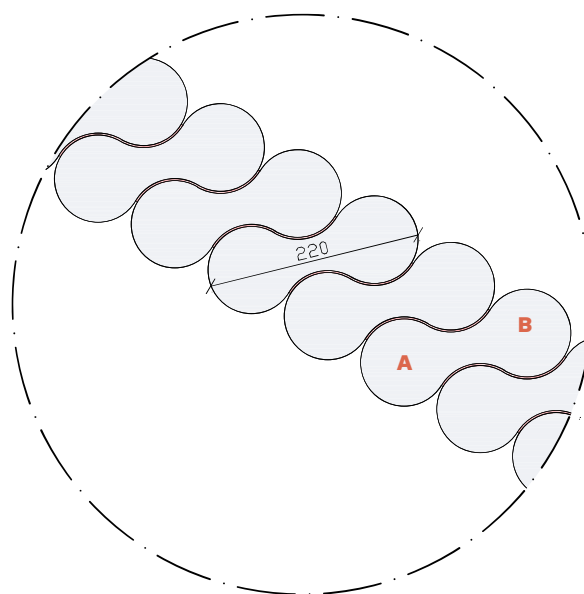


Figure 140. Vertical cross-section

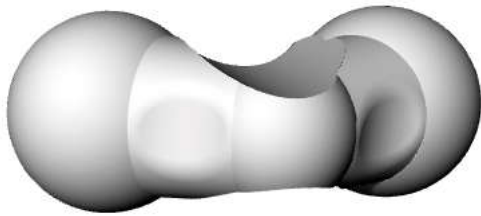


Figure 141. Perspective 1 of the final component

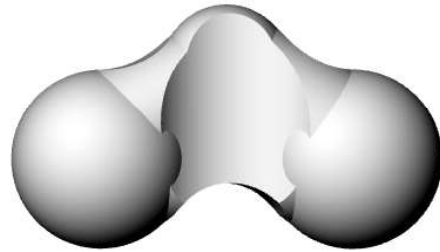


Figure 145. Front view of the final component

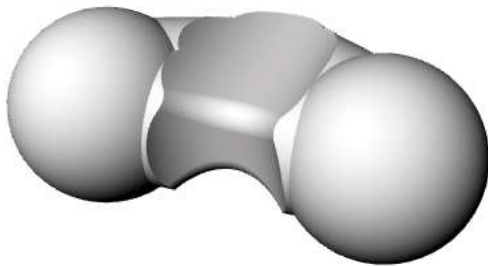


Figure 142. Perspective 2 of the final component

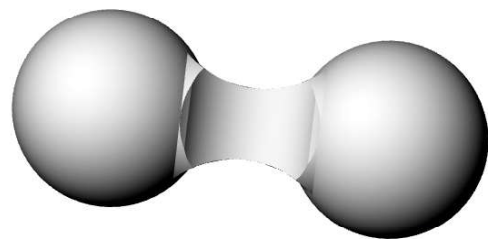


Figure 146. Side view of the final component

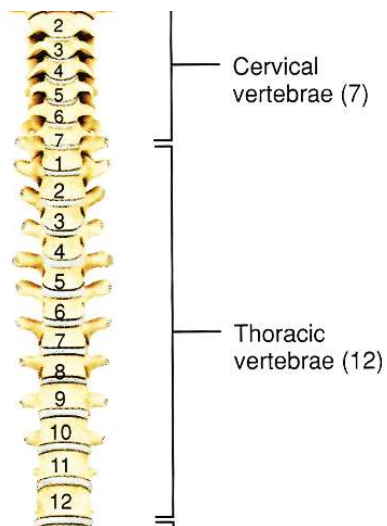
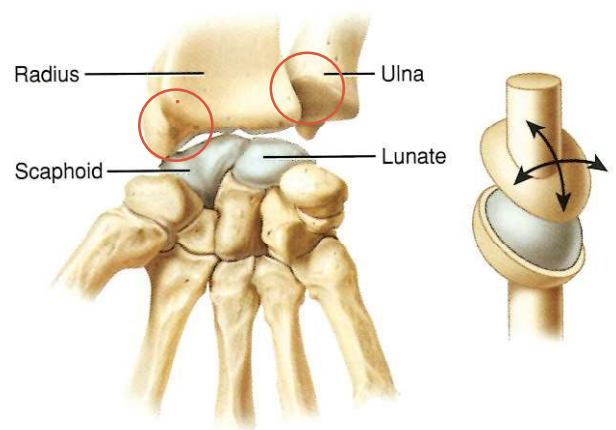


Figure 143. The spine (Tortora and Derrickson, 2009).



(d) Condyloid joint between radius and scaphoid and lunate bones of carpus (wrist)

Figure 144. Wrist joint (Tortora and Derrickson, 2009).

Conclusion

It is concluded that the final component meets the design principles (1-6) because both general and the two new requirements are met.

1. Mass <10kg

The mass of the final component equals approximately 2,5kg <10kg.

2. One component & 5. Spherical configuration

Three spheres are shaped into one component and will reduce the amount of different steel molds. This research proposes the utilization of one steel precision mold, explained in the next chapter.

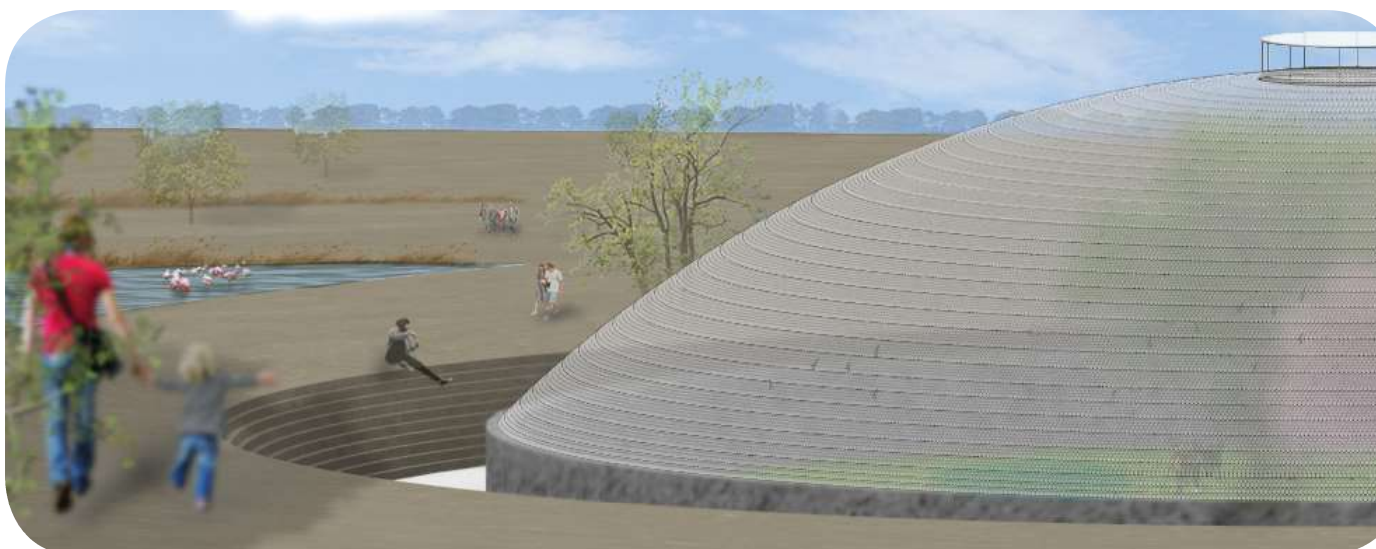


Figure 147. The glass dome during fall season (without white wash paint)

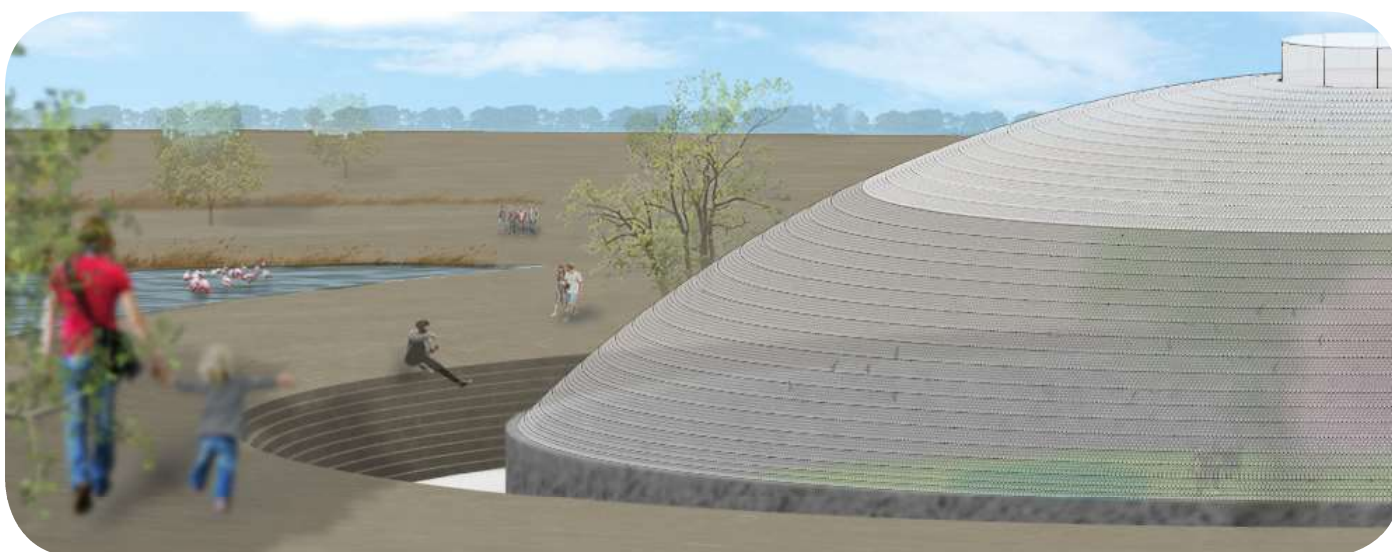


Figure 148. The glass dome during summer season (with white wash paint)

3. Round edges

The majority of the edges of the component are round because the shape is constructed out of three different spheres. It should be noted that some edges require further optimization, this to avoid peak stresses around the edges of the component.

4. Homogeneous mass distribution

The final glass component is not designed with protrusions or depressions where the entire interlock is constructed by the three spheres and will form a homogeneous mass distribution.

6. Small elements

The glass component is rather small: <2,5kg. Although, the glass component does have a significant thickness of 220mm to function as a structural component.

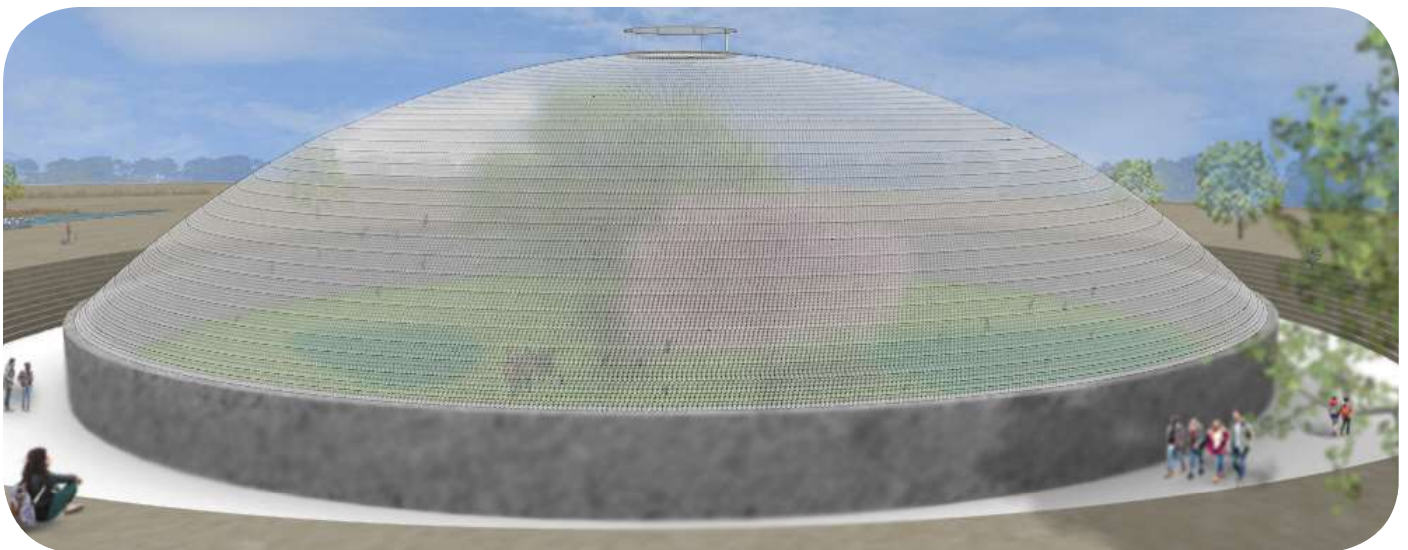


Figure 149. The glass dome during fall season (without white wash paint)

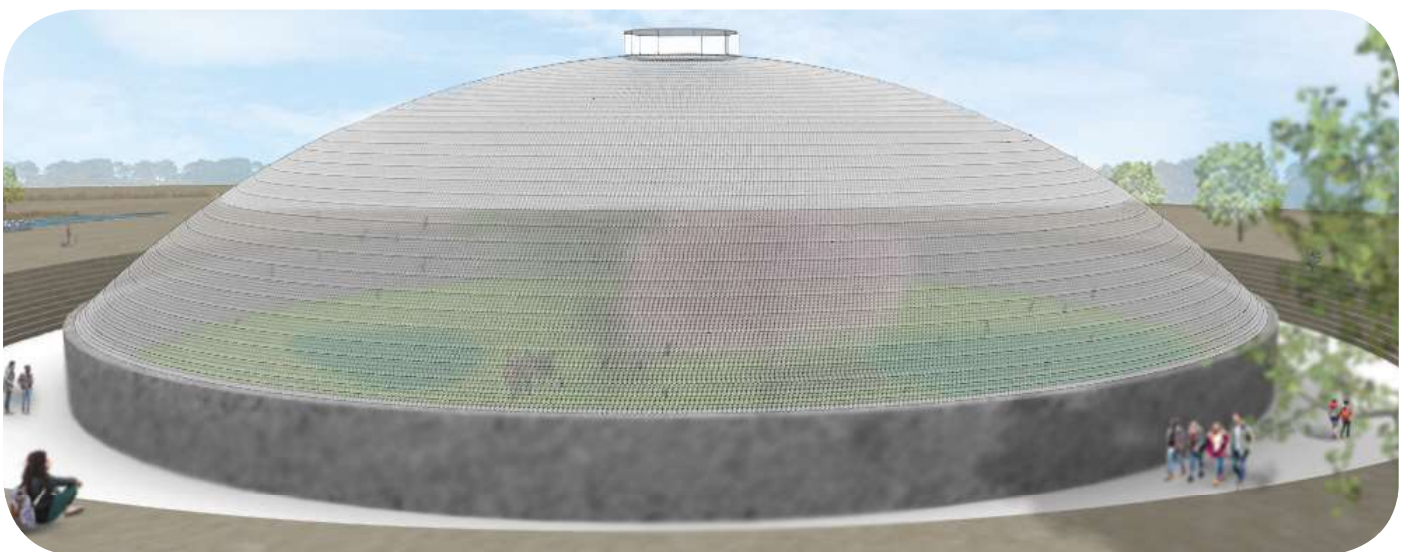


Figure 150. The glass dome during summer season (with white wash paint)

3.3.5 Fabrication

Literature review on cast glass molds distinguishes two different types of steel precision molds: high precision press molds and open precision molds. This research proposes to use a **high precision press mold** to construct accurate glass components. Utilization of a high precision press mold enables to shape the component to its spherical configuration unlike the open precision mold. The post-processing when using a open precision mold include besides polishing the component, removing the funnels created during the casting process. Hence, the preference of a high precision press mold which is less labour intensive, although do need further post processing: polishing the components to **create matt surfaces**. The necessity of creating matt surfaces is explained in more detail in the chapter 'transparency'. Figure 151 presents most important manufacture steps when using a steel high precision press mold.

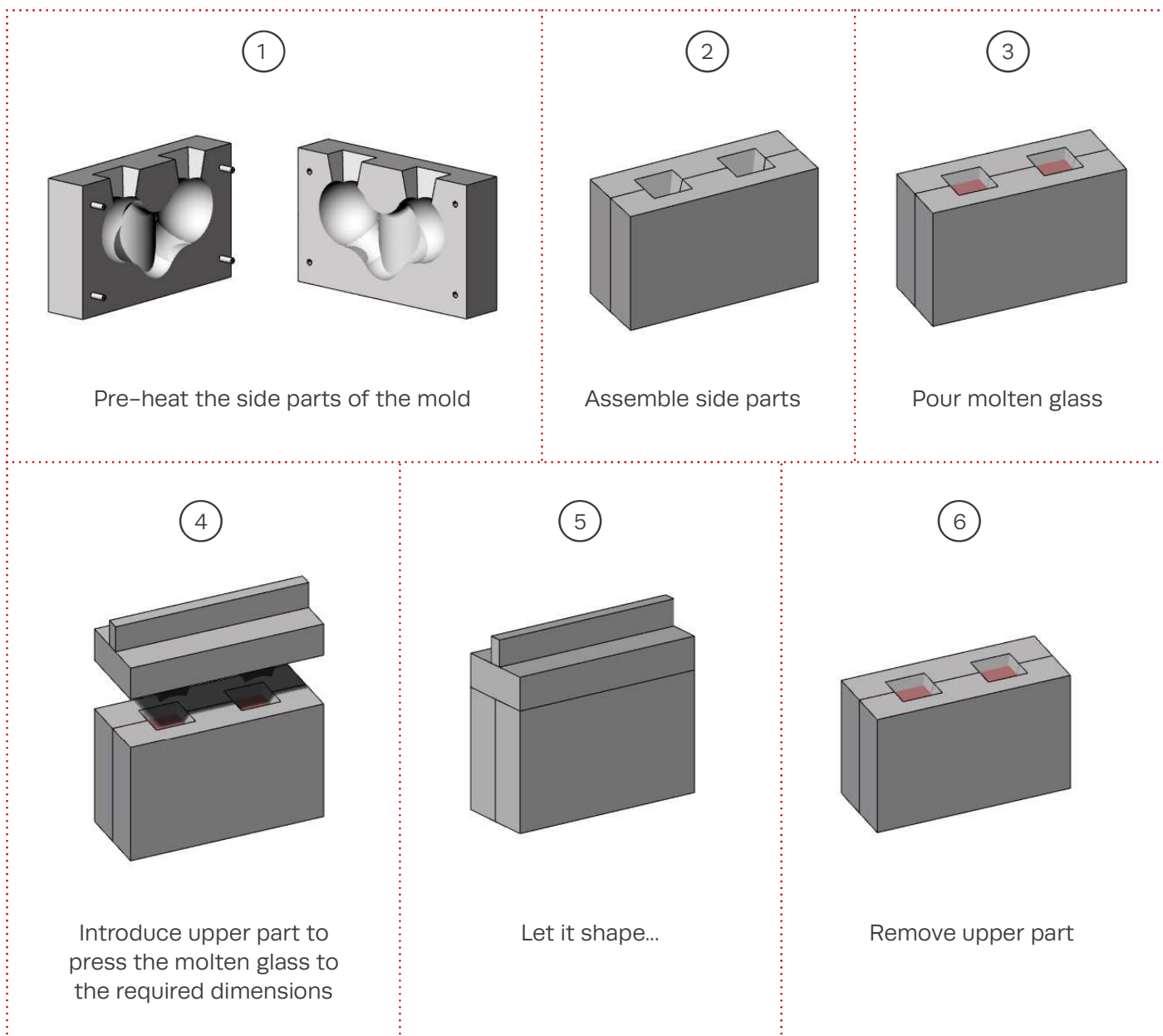
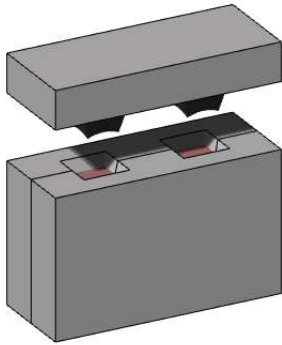


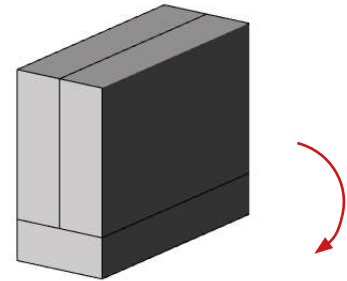
Figure 151. Manufacturing steps of the cast glass components

7



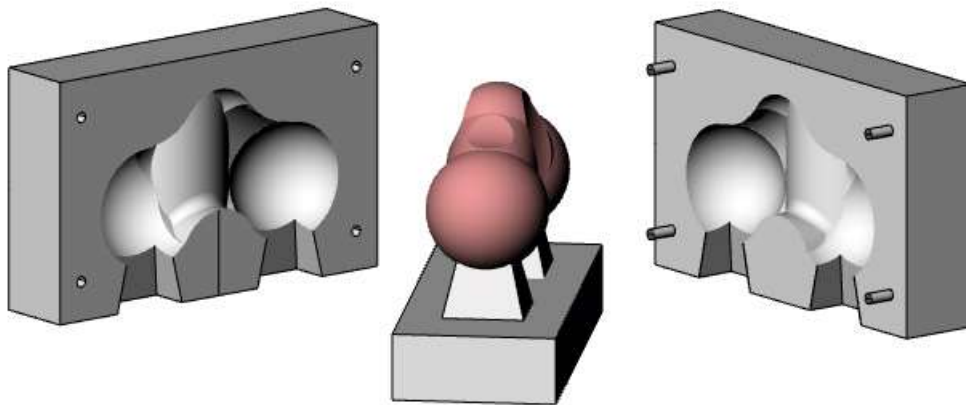
Introduce new flat upper part

8



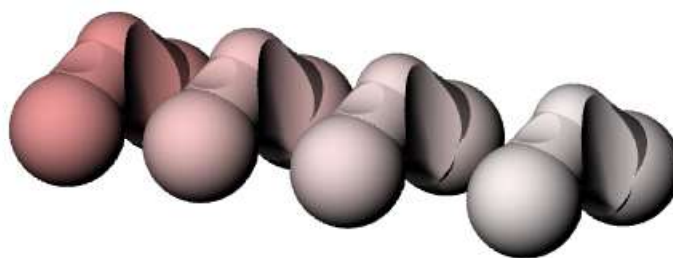
rotate 180°

9



Remove side parts carefully, the component will rest onto the funnels of the mold

10



Slowly cool down the component (annealing phase)

3.4 Interlayer design

Introduction

This chapter addresses the interlayer design of the final component. First, the design principles of the interlayer are explained. Secondly, the chapter presents the interlayer design for both ring and arch direction. The fabrication method and material selection of the interlayer is not included within this chapter and depends on the structural performance of the entire dome system. Hence, the material selection and production method are explained in the chapter 'structural validation'.

3.4.1 Optimization and principles

The interlayer is optimized at its thickness at the centre of the spheres A and B (a1 and a2) with a **maximum thickness of 5mm**. It is assumed that the maximum interlayer thickness of 5mm results in a rigid dome structure. An interlayer thickness that exceeds the 5mm limit is defined as an inefficient interlayer. Mentioned in the previous chapter, the dimensions of the component will determine the dimensions of the interlayer. Large components result in large interlayer dimensions, due to the increased rotation angle between the components for each ring. In addition, large components result in a large opening at the dome top (oculus) because the components will rather reach the thickness limit.

Moreover, scaling the glass components effect the dimensions of the oculus and interlayer thickness, this principle is shown in figure 152.

Latter mentioned figure also gives insight in how the interlayer thickness was determined. The interlayer thickness is determined by using a Grasshopper and Rhino model, where a curve (one lune) is divided into segments. These segments represent the diameter of sphere A or B. The circumference from each ring was obtained at the centre of the segment and represents the horizontal rings of the dome structure. The circumferences of the rings were divided by the dimensions of the segment, i.e. the diameter of sphere A or B. The rounded number led to the exact amount of components for each ring. The thickness of the interlayer, located at a1 or a2, of each ring was then determined by multiplying the not rounded number with the diameter.

The calculations and optimization in Grasshopper and related Rhino model are shown in figure 153.

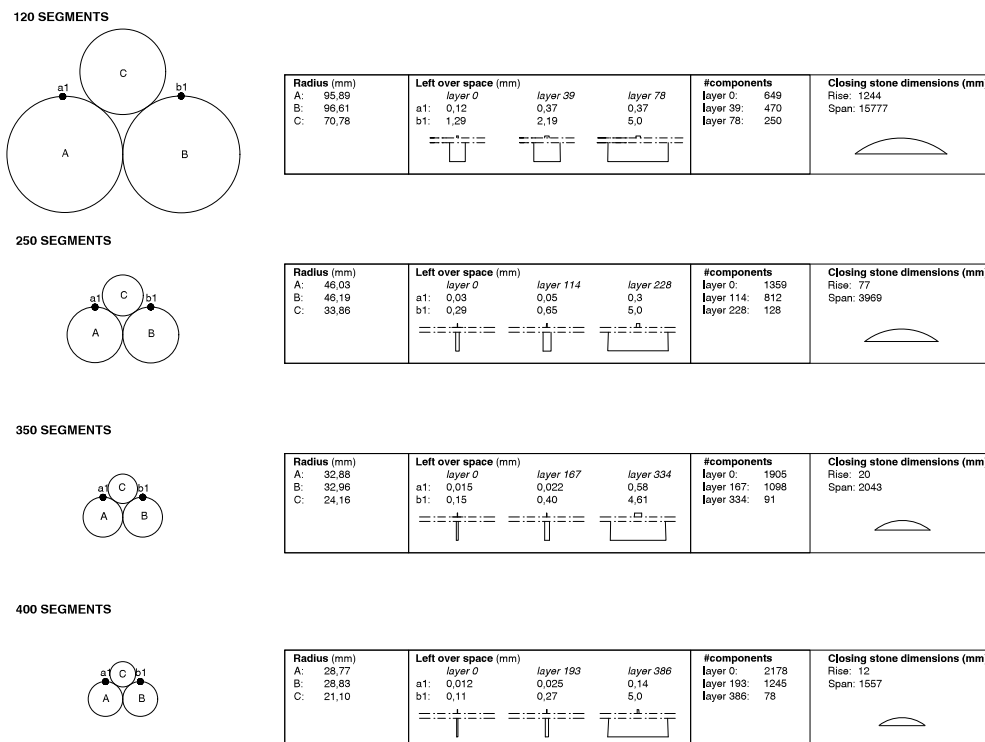


Figure 152. Diagram of the effect of scaling the components

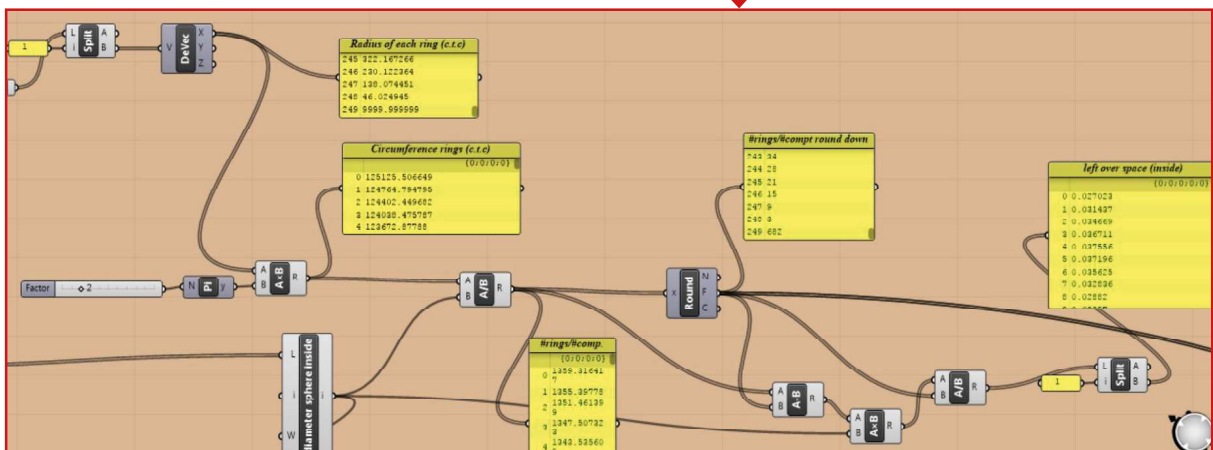
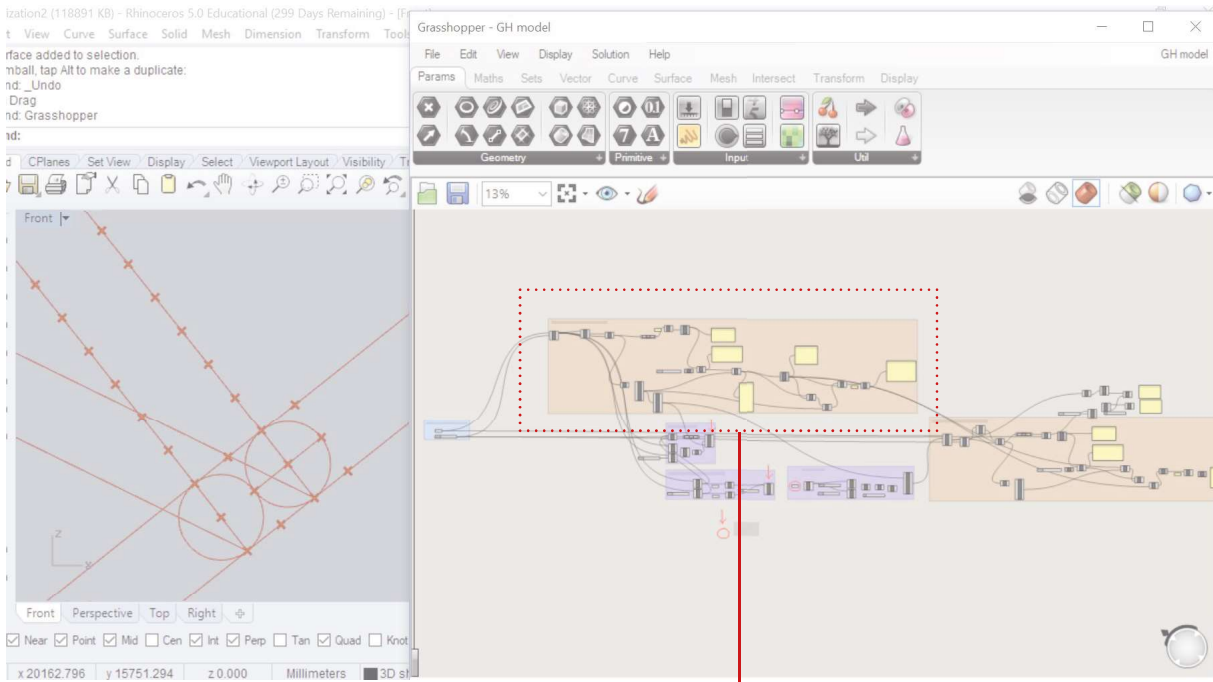


Figure 153. Grasshopper model used for determination of the thickness of the interlayer

3.4.2 Dimensions

The final dimensions of the interlayer are distinguished into ring and arch dimensions. One interlayer geometry in arch direction is utilized due to the fact that the arch direction has one equal curvature at each vertical section. The **arch interlayer** has a **thickness of 2mm** which will ensure the structural performance in the arch direction. The **ring interlayer thickness** is different for each ring and varies in its shape itself, this is a result of the changing ring curvature.

Figure 154 presents the final dimensions of the interlayer in ring and arch direction for three rings: first, middle and last ring. These dimensions are obtained from a Grasshopper and Rhino model. The edge dimensions are measured within the Rhino model and the centre thickness's are

obtained from the Grasshopper model. This figure clearly shows the increase in interlayer thickness while reaching the dome top. This is easily explained since the rotation angle between the components is larger at the dome top caused by the curvature ($k=1/R$).

Figure 154 also presents the amount of components for the three rings: a low amount of components at the dome top and high amount of components at the dome foot.

The **total amount of components** equals **139132** components where **197** components are present **in the arch direction**. Appendix 1 presents the amount of components for each ring.

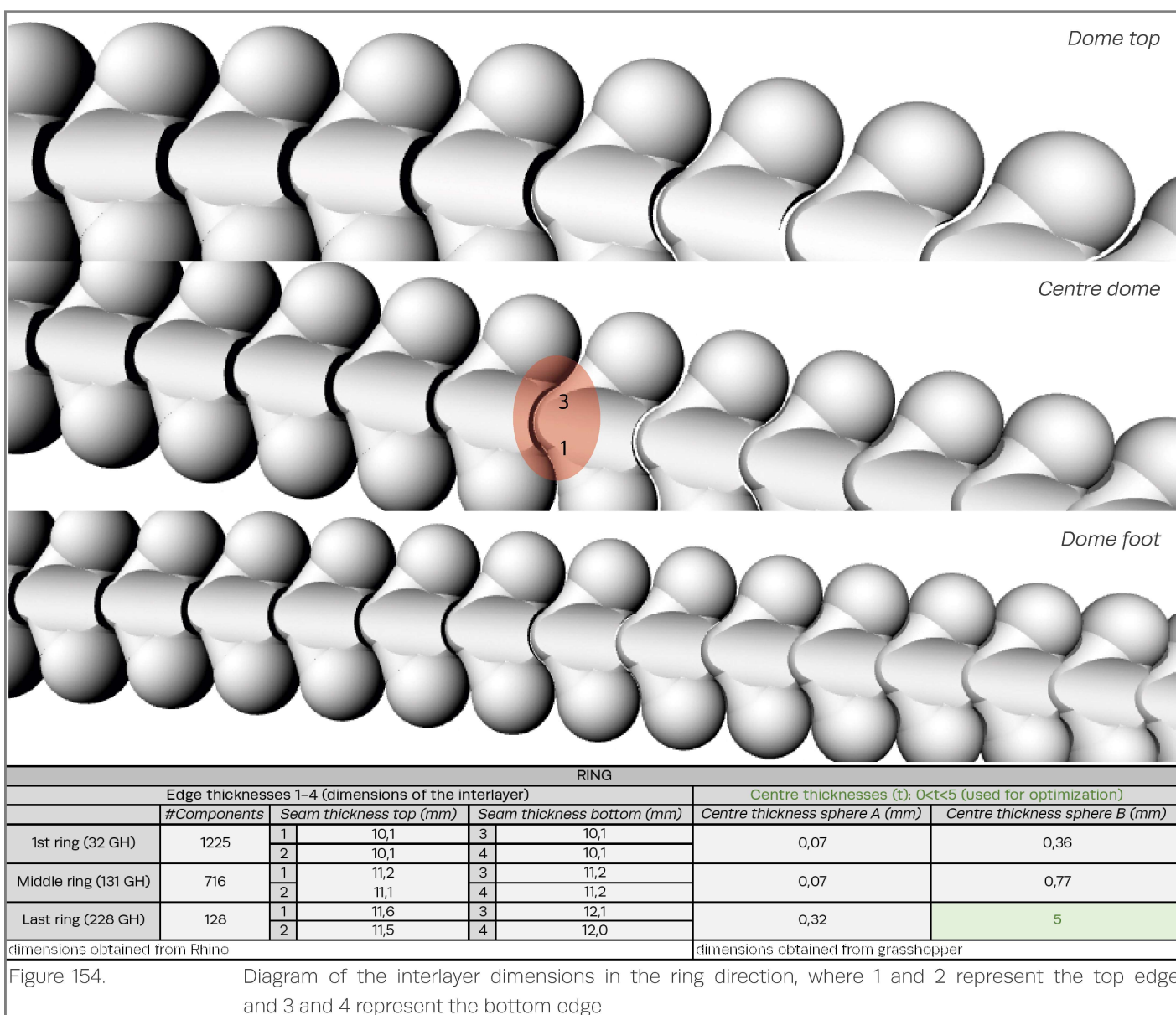


Figure 154.

Diagram of the interlayer dimensions in the ring direction, where 1 and 2 represent the top edge and 3 and 4 represent the bottom edge

Arch direction		
	#Components	Seam thickness (mm)
1 lune / orange slice	197	2

Table 23. Dimensions interlayer arch direction

3.4.3 Geometry

The geometry of the interlayer in ring and arch direction are shown in the figures 155 and 156. The interlayer in arch direction is rather simple due to the equal section thickness and can be compared with a silicon shoe sole for high heels.

On the other hand, the ring interlayer requires a complex geometry to deal with the changing curvature. The ring interlayer thickness is different for each ring and varies in its shape itself. Hence, the ring interlayer geometry is equal for one ring, leading to 197 different ring interlayers.

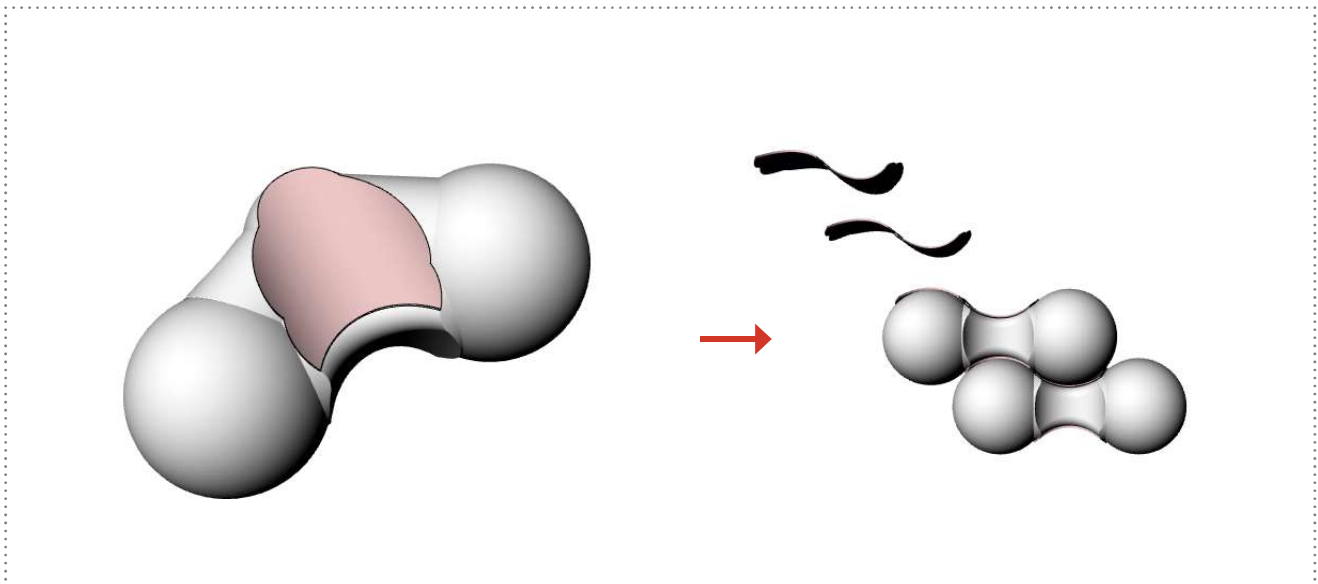


Figure 155. Arch Interlayer geometry

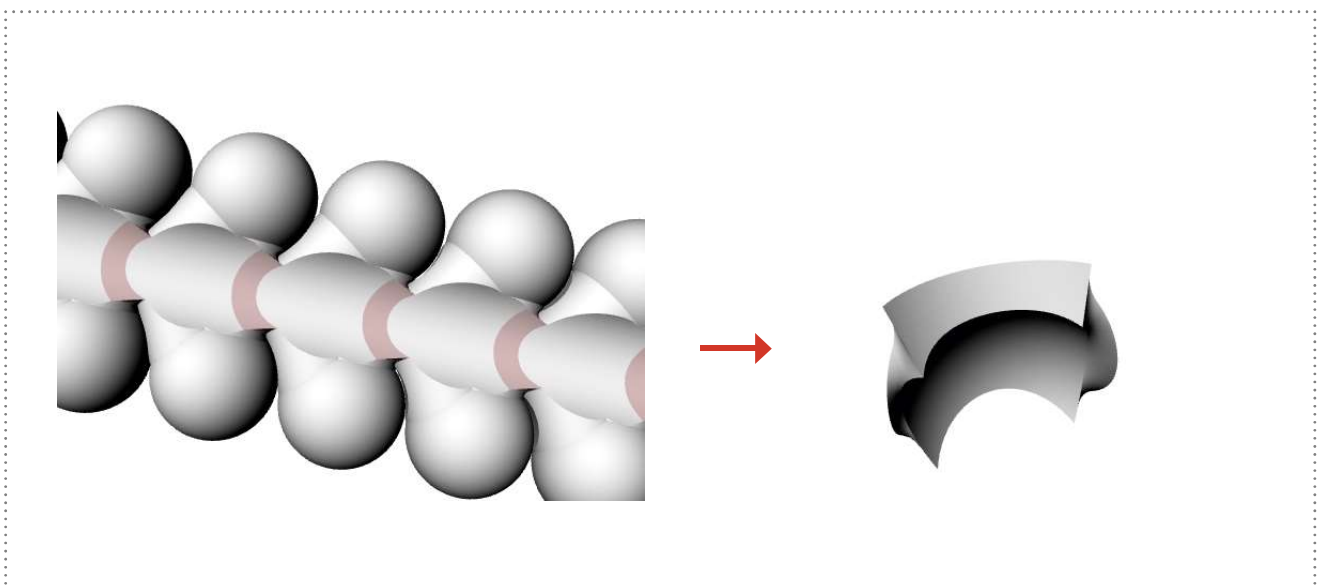


Figure 156. Ring interlayer geometry

3.5 Feasibility

This chapter addresses the feasibility of the glass dome design in terms of construction and maintenance. First, a building proposal is given for constructing the glass dome. Finally, this chapter addresses the maintenance of the glass components to increase the life time.

3.5.1 Construction

The glass dome is constructed from a concrete cylindrical support structure which should be constructed as first. Subsequently, a wooden dome structure may be created which functions as an underlying support structure for the glass components. This wooden structure requires an exact fit and consists of wooden rings and arches. The glass components will rest onto the wooden structure where glass components and interlayers are stacked together from its dome foot till the oculus. The oculus can be placed after finishing the last layer of glass components. Finally, the wooden structure may be removed and the glass dome will function as a rigid dome structure.

The wooden structure should be stored in order to rebuild and maintain the glass dome. It should be noted that small cracks and fog may occur at the surface of the glass components. Fog and small cracks will not effect the structural

performance of the glass components. A glass component should be replaced when larger cracks occur. The effect of bigger cracks in the glass components is beyond the scope of this research but requires further investigation. Investigation on the structural performance of the glass dome, when larger cracks occurs, should be investigated to obtain fundamental knowledge about the redundant structural behaviour. The dome structure should be redundant, in simple words: have a high residual load-bearing capacity and needs to give a warning sign.

The wooden support structure and building steps are presented in figure 158. An example of a wooden support structure is the wooden structure used to construct the Armadillo Vault. In this research it is assumed that the building-workers may use the wooden support structure as scaffolding. However, additional scaffoldings are required to access the wooden structure.



Figure 157. Wooden support structure used for construction of the Armadillo Vault (Arthur, 2017)

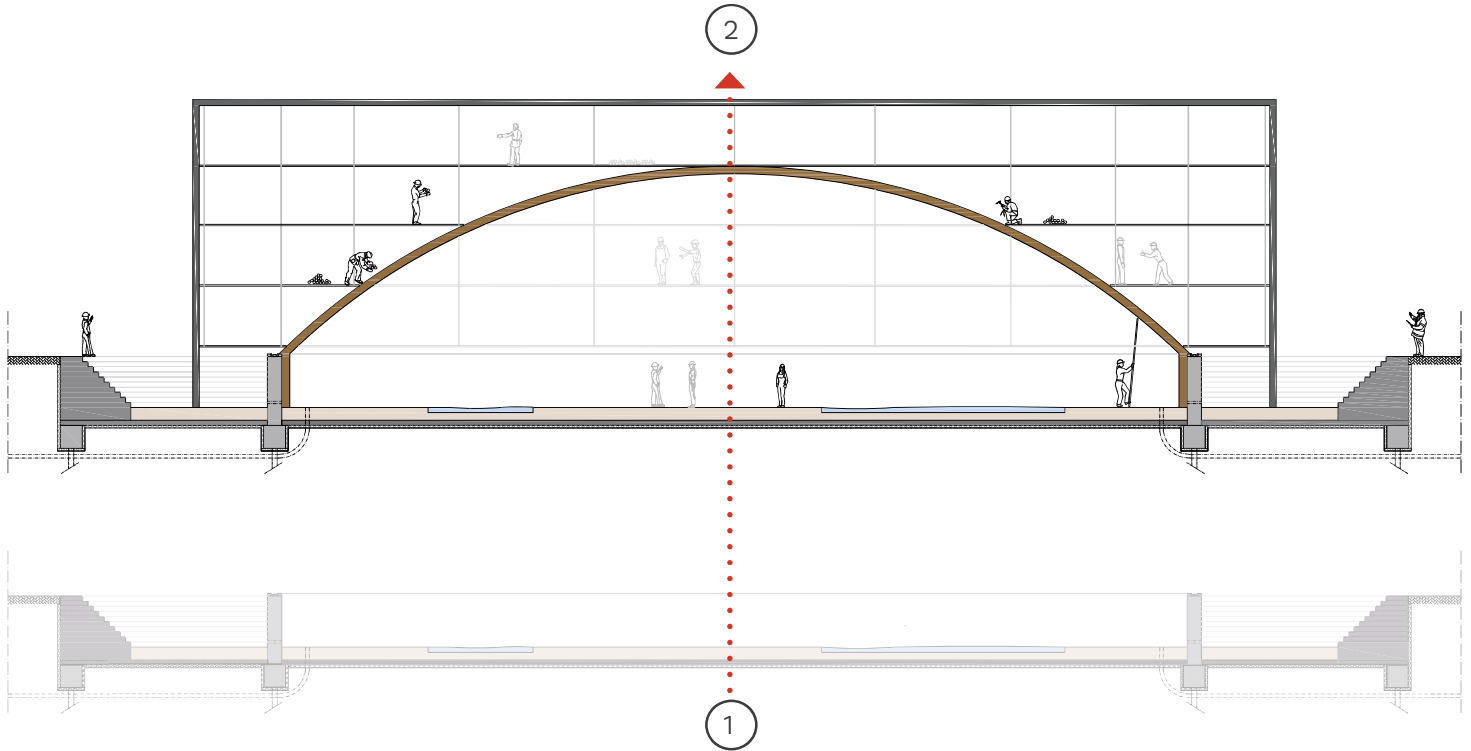


Figure 158. General building steps for constructing the glass dome

3.5.2 Maintenance & Pre-stressing

Maintenance of the dome structure is important to increase its lifespan. In addition, pre-stressing the glass dome system is essential for creating a sufficient interlock in both directions. These two principles, maintenance and pre-stressing, are described by explaining the details A, B(1&2) and C.

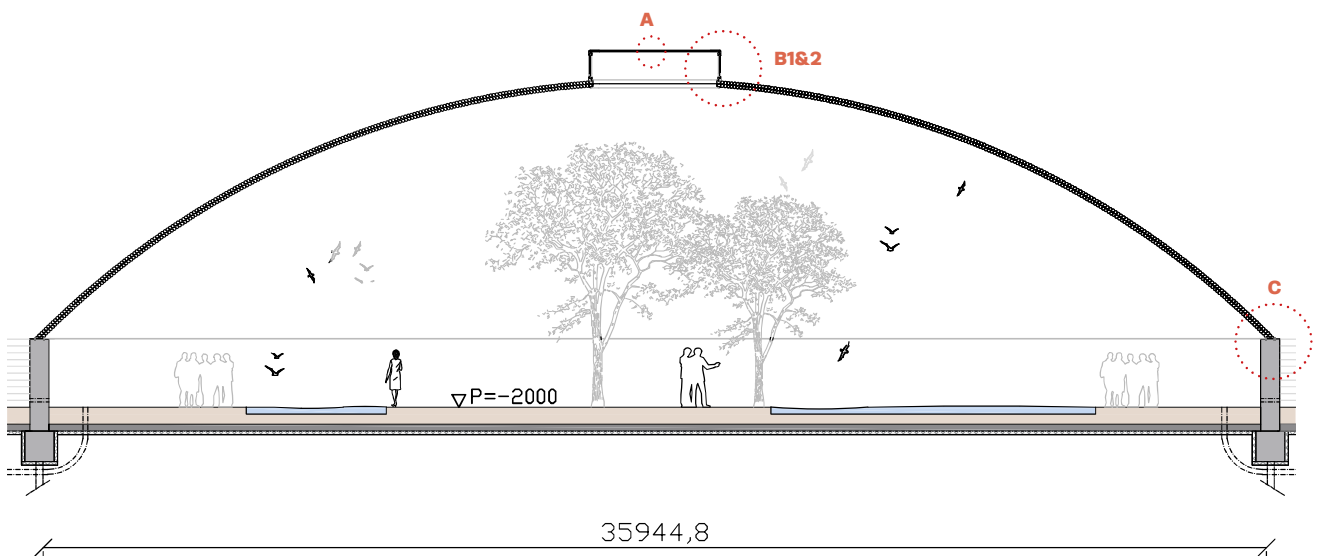


Figure 159. Vertical cross section A-A' and overview of the details

Maintenance

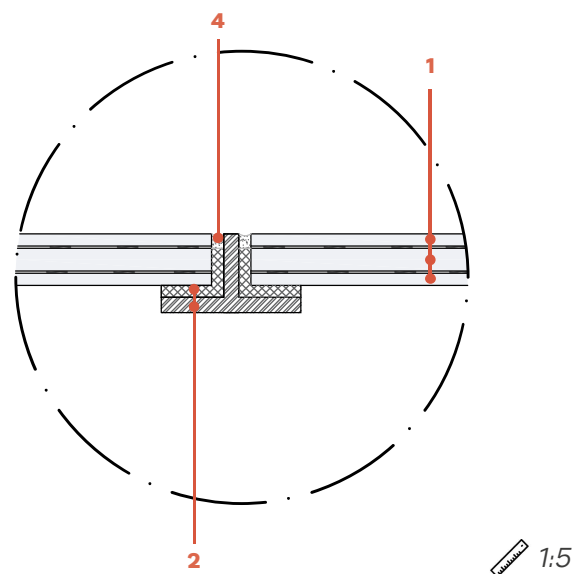
This research proposes to use a **hydrophobic coating** from the company Nanoshell which will prevent the surfaces of the components from fungus, water and pollution. The coating covers the entire component, i.e. interior and exterior surfaces. The interior coating is required as well because the coating will also prevent bird fouling from the Lori parrots^[22].

The dome structure is not completely sealed because the interlayer does not cover the entire component. This will especially cause problems at the dome top because the shallow dome and component geometry allow for collection of rainwater. Hence, this research proposes to fill the **unsealed parts**, that cause rain water problems, with **transparent silicones** (represented in the details by number 4).

It should be noted that further investigation about the sealed performance of the real glass dome is required.

Pre-stressing

As explained in the oculus design chapter, a **stainless steel compression ring** is required to exert the necessary pressure onto the components, thus to create a sufficient interlock. This because the self-weight of the components is not enough to create a sufficient interlock in both directions. The steel compression ring is located at the dome foot. Subsequently tensile stresses always occur due to local protrusions. Hence, a steel tension ring located at the base will prevent the supports from slight yielding. Both steel rings are customized and constructed through a stainless steel investment **casting process**. These customized stainless steel rings are represented in the details by number 6. The details clearly show that the stainless steel rings follow the form of the component, this is necessary to exert a full pressure onto the contact area of the next component. A layer of 5mm **neoprene** was added in between the steel and glass surfaces. Neoprene is a soft rubber and is fundamental to avoid local peak stresses. Moreover, the geometry of the steel rings are different at dome top and foot. This is easily explained since the dome top requires a connection for the aluminium window frame. Unlike the dome foot, where the steel compression ring requires a fixation with the **concrete support structure**.



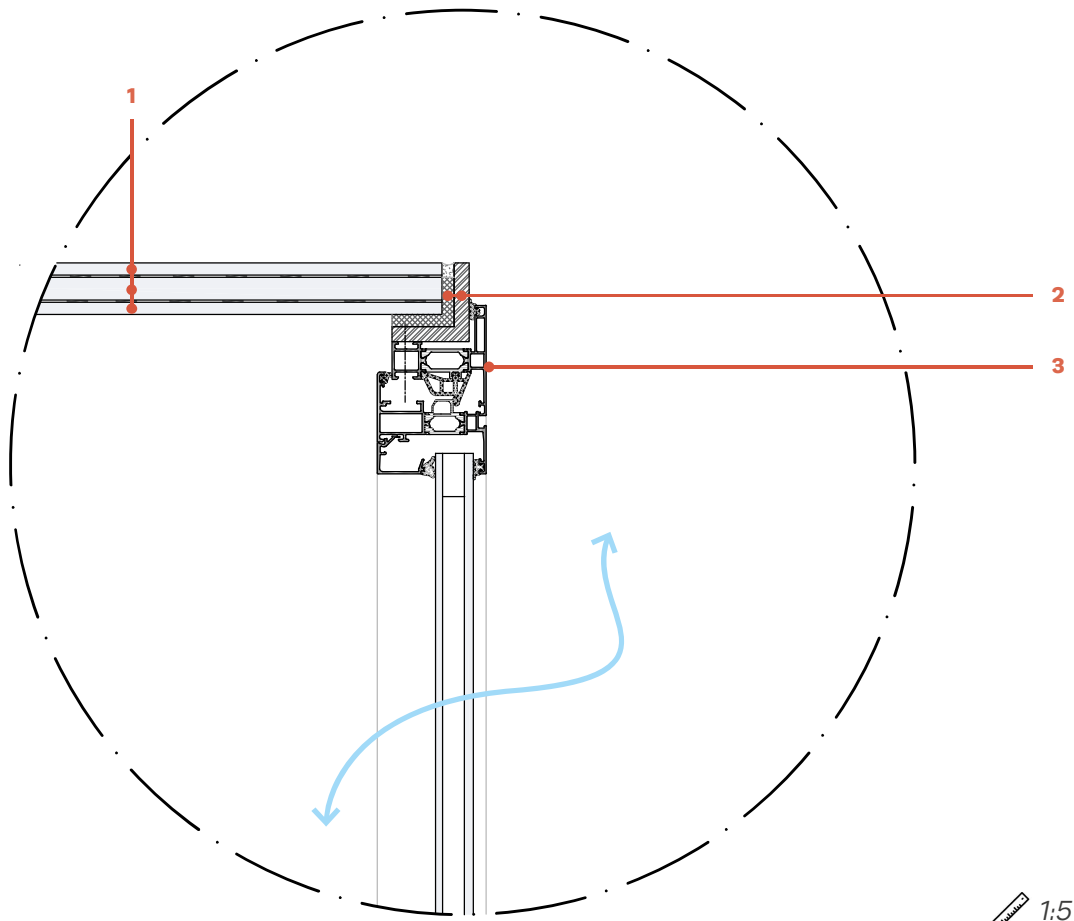
Detail A

Oculus Design

A general explanation of the oculus design is given in the previous chapter. In more detail, the oculus consists of an aluminium window frame which is fixed onto the steel compression ring and laminated safety glass panels by a stainless steel L-profile. Up till now, panels can be laminated up to 3.2x16m. Latter mentioned dimensions are based on the size of the largest glass autoclave for laminating glass panels (Sedak company). Hence, the **laminated safety glass** panels are constructed out of panels from 3.2x16m and include a steel connection in the centre to connect the glass panels, as shown in detail A. Moreover, the safety glass is bonded by a PVB interlayer and has a great load bearing capacity: the remaining glass layers will carry the loads if one of the outer glass layer breaks.

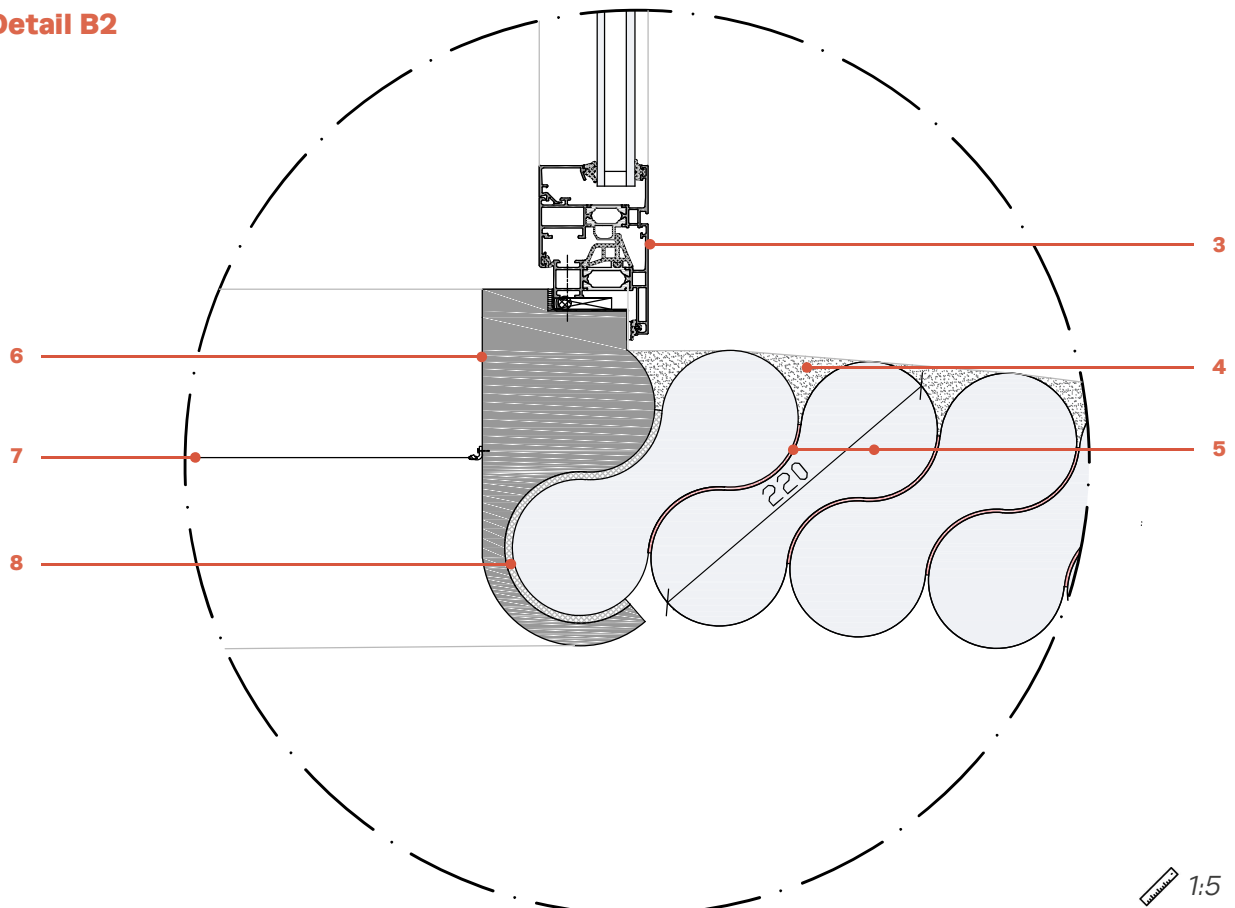
The oculus is designed to allow for natural ventilation where the windows are automatically opened and control the natural ventilation rate. The **automatic openings** solutions could be low tech or high tech. A high tech solution includes a window frame with an integrated operation system. Unlike a low tech solution, such as clamps used for greenhouses that work on temperature differences. These clamps consist of a rod with a liquid that expands at high temperatures, thus slowly pushes the window open^[23].

Detail B1



1:5

Detail B2



1:5

[22] <https://www.nanoshell.co.uk>, [23] <http://www.tuinkassenwinkel.nl>

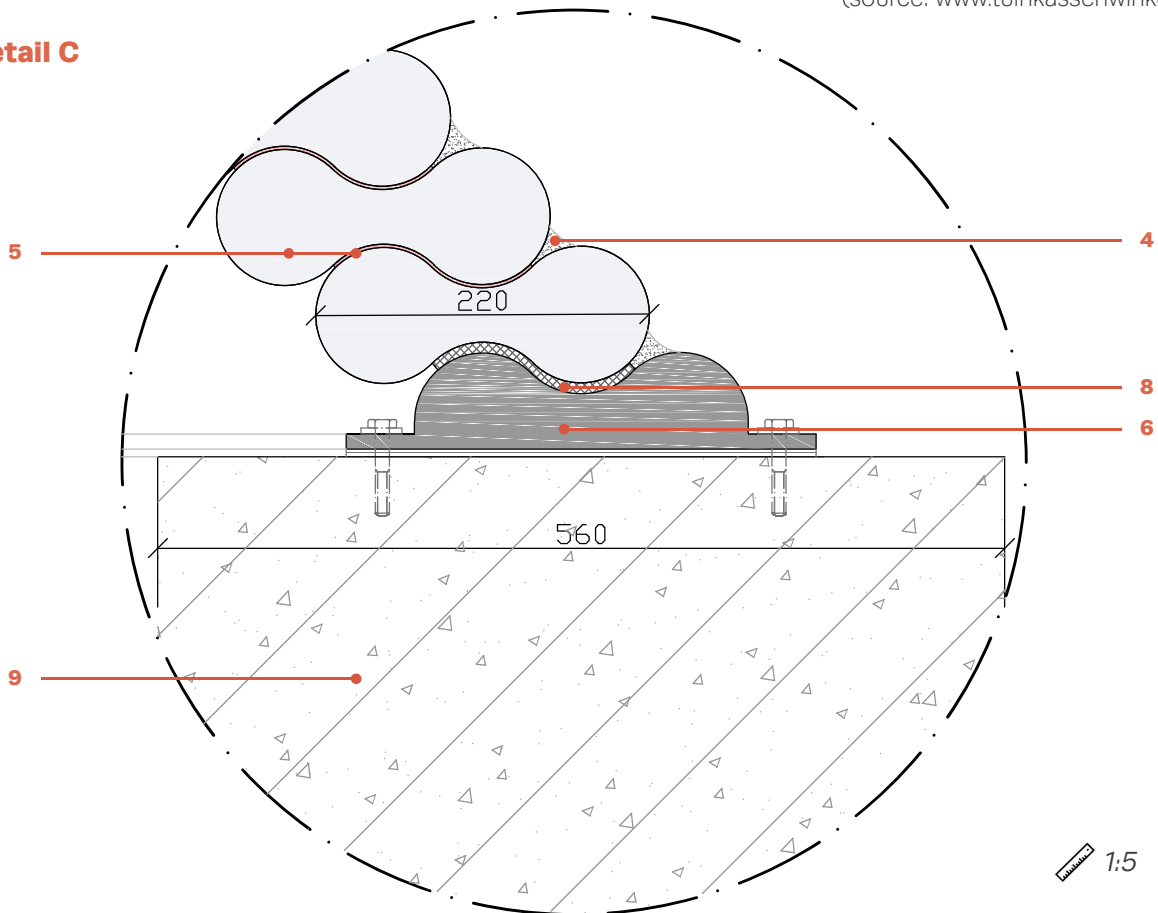
This research aims for low tech solutions such as window clamps that react to temperature differences. This to reduce the building costs of the entire dome design. It should be noted that the opening requirements for using such clamps (e.g. mass limitation per window) require further investigation.

Finally the height of the opening is based on the required opening to ensure natural ventilation. The determination of the surface area of the ventilation opening is explained in the next chapter and equals $9,3\text{m}^2$ (A), which equals $A = 2\pi R_{\text{oculus}} h$. Hence, the required **height** of the opening equals $h = 9,3 / (2 * \pi * 1,9) = 0,8\text{m}$.



Figure160. Window clamps that react to temperature differences (source: www.tuinkassenwinkel.nl)

Detail C



- 1.Safety glass (top to bottom in mm): 8 mm heat strengthened glass, 15 mm tempered glass, 8 mm heat strengthened glass, PVB interlayer
- 2.Embedded stainless steel connection with neoprene interlayer
- 3.Aluminium window frame (Schuco 65)
- 4.Transparent silicone
- 5.Cast glass Soda-lime components and TPU interlayer
- 6.Customized casted stainless steel compression (top) and tension (base) ring
- 7.Bird-net
- 8.Neoprene (soft rubber)
- 9.Concrete support structure

Introduction

Five cast glass components were developed in 1:2 scale in order to validate the component design and further develop the final mold design. The prototypes were made to gain insight in the casting process and allocate the residual stresses. The production technique is different from the final production technique since the final design method proposes to use a high steel precision press mold, as explained in the previous chapter. The production technique for the prototypes requires a cheap and fast method. Hence, the prototypes are made from cheap and disposable molds. Note that the cheap disposable molds are based on the design of the high precision molds, as shown in figure 161. The difference between the disposable and steel mold is the open surface of the disposable mold. The open surface of the disposable molds will allow for air circulation and creates funnels which need to be removed.

The following subjects are addresses in this chapter:

- The construction of the molds
- Selected type of glass and key temperatures
- Firing process
- Post-processing and results
- Analysis of the residual stresses
- Conclusion and final mold design

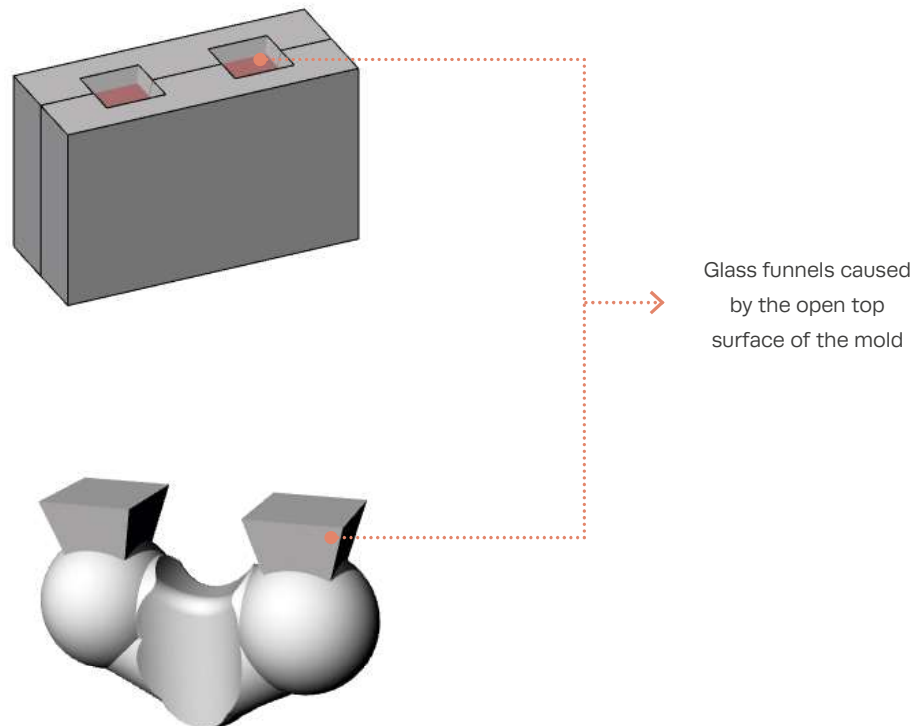


Figure 161. Disposable mold design of the prototypes

3.6.1 Construction of the molds

Five molds were constructed at the TU Delft Glass Lab. According to Bristogianni et al. (2017) the used production technique is called "lost-wax investment casting". The mold and model are disposable till the end of the process. The steps that need to be taken to create these molds are explained below.

① 3D model in Rhinoceros

The first step that needs to be taken is to create a 3D model of the glass component in Rhinoceros with funnels. The 3D model with funnels is needed for creating a 3D print from PLA. The 3D print is the positive volume of the component and is needed for creating the negative volume, i.e. creating the counter mold. The funnels are essential because the funnels create gaps for pouring since the entire mold is further enclosed.

Two options of the 3D model with funnels were drawn in Rhinoceros and are shown in figure 163. The 3D model with two funnels was chosen because this will allow for circulation of air during the pouring process. Circulation of air is required to prevent the components from trapped air bubbles.

Finally, the 3D model with two funnels was send to the 3D PLA printer. The PLA component is shown in figure 162.

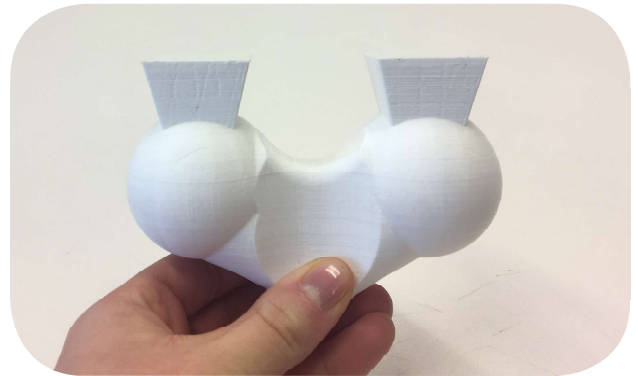
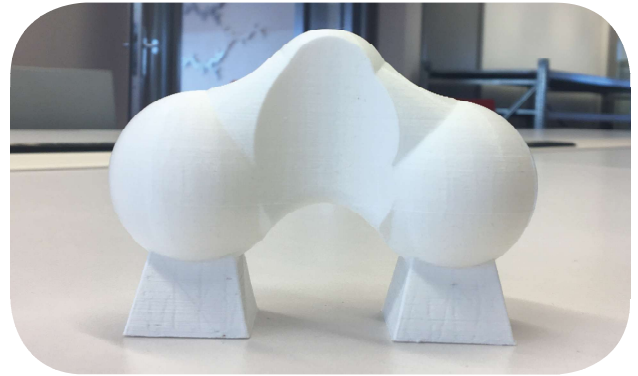


Figure 162. PLA 3D print of the component

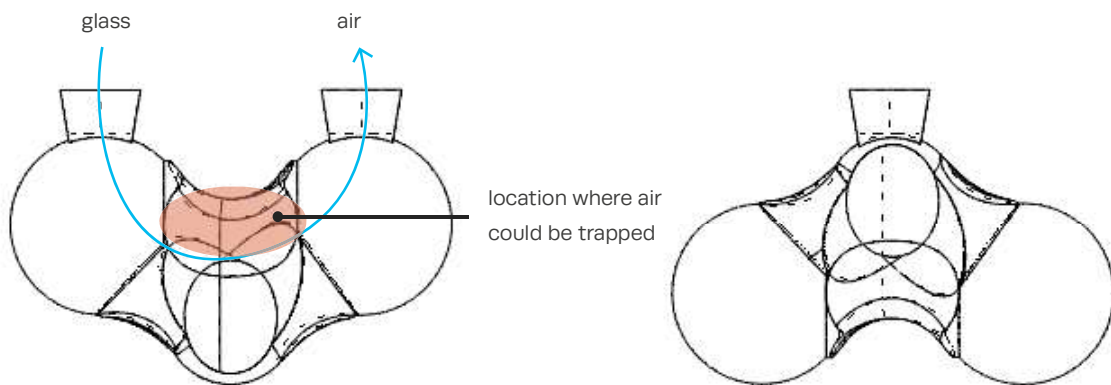


Figure 163. (left) 3D model with two funnels which allows for air circulation, (right) 3D model with one funnel

2 Silicon mold

The counter mold is created by taken three steps. The first step is creating the silicon mold, where the silicon mold will function as a counter mold for shaping the 3D models made from wax.

The silicon counter mold is constructed from Mold Max™ Silicones which include two compounds: part A and B. It is important to weigh the different compounds and use a ratio of 1(B):10(A). The ratio of 1:10 will ensure the right composition for creating an accurate silicone model. The ratio of the compounds for this research equals: 1120 grams of part A and 112 grams of part B.

Subsequently, the PLA 3D print was fixed with clay on a flat table around the edges of the funnels and was treated with soap water. The clay fixation is needed to prevent up-lifting of the 3D model during pouring and soap water was used to detach the clay easily afterwards. A wooden box around the 3D model was created by using clamps and clay to prevent leakages. Then, the silicone composition was poured from one side and was cured for 16 hours.



Figure 164. (left) weigh the part A and B, (right) wooden box and clay fixation



Figure 165. (left) pouring the silicones, (right) silicone mold after curing

3 Wax 3D models

Five wax 3D models were created to construct the final molds from crystal cast. This because wax is a soft material and can be easily removed by using steam. The wax was heated in a fryer to approximately 70°C. Then, the wax was poured from one side (in one funnel) to allow for air circulation. The wax models were cured for 3–4 hours.

After 3–4 hours of curing, the wax models were carefully removed from the silicone mold. The wax model is shown in figure 166. All wax models showed air bubbles located at the top of the wax component. This effect is easily explained since air was trapped underneath the silicone mold. These air bubbles were treated with a soft red wax from the Dutch 'Gouda' cheese. This red wax is important for creating an accurate final mold because it fills the occurred holes caused by the air bubbles.

Moreover, the wax models did not show shrinkage due to the almost symmetrical geometry and even mass distribution.

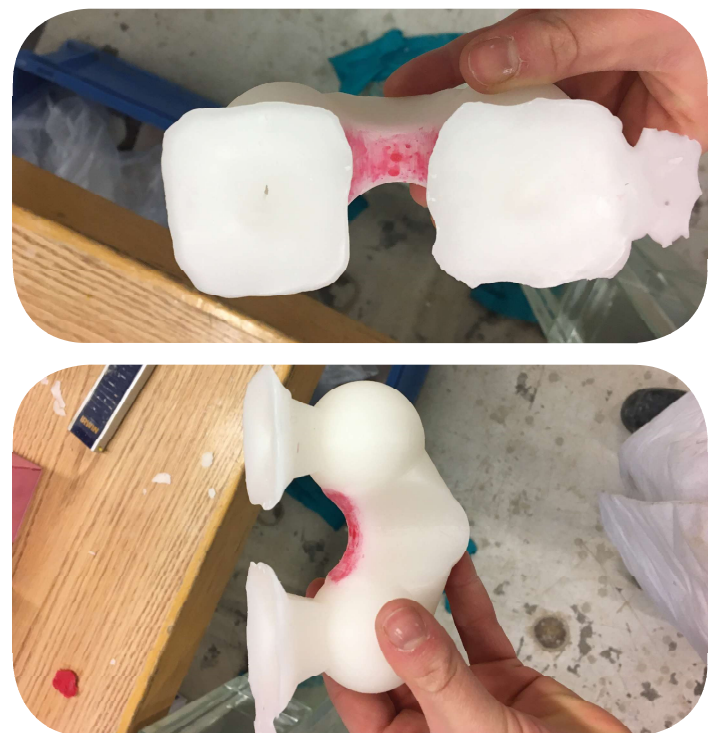


Figure 166. Wax models, treated with red 'Gouda' wax to fill the occurred air bubbles

④ Final Crystal cast mold

Finally, five disposable molds were created from the powder "Crystal Cast M248". The Crystal Cast M248 is a plaster-bonded powder which can withstand temperatures up to 900°C^[24]. Two different mold designs were made, distinguished in A and B. Three A molds were constructed where the funnels were not connected. Secondly, two B molds were constructed where the funnels were connected. These two different mold designs were made to obtain knowledge about their different or non different casting results.

The steps that need to be taken to construct the A and B molds are explained below. The wax models were placed on a flat surface and fixed with clay and treated with soap water. The wax models for the B molds were connected with one thick clay layer. And the wax models for the A molds were fixed at the table through two layers of clay. Subsequently, bounding boxes from wooden plates and clamps were made around the wax models. The bounding boxes require an offset range of 1,5–2 cm, this to ensure a sufficient wall thickness of the mold (to prevent the mold from cracks). The dimensions of the molds are: A = 10 x 15 x 12 cm and B = 13 x 20 x 15 cm. Again, the wooden box was sealed with clay. Next, the powder was mixed with water in the following ratio 2,75:1 (9350 ml powder and 3400 ml water) and poured into the molds from one side when a homogeneous mixture was reached.

The Crystal cast molds were cured for 1 hour. The bounding box and clay residues were removed after the curing process. Then, the wax models were dewaxed from the crystal cast molds. The crystal cast molds were placed upside down (the wax is facing down) above a water bath with a boiler. The water was heated through the boiler and the entire bath was covered by plastic bags to produce steam. The wax models melt through the produced steam. Finally, the molds were cleaned with water to remove any wax residues.

It should be noted that further post-processing of the mold was not possible, such as removing bumps. The post-processing of the molds it not possible because the molds do not have a large surface opening and are further enclosed.

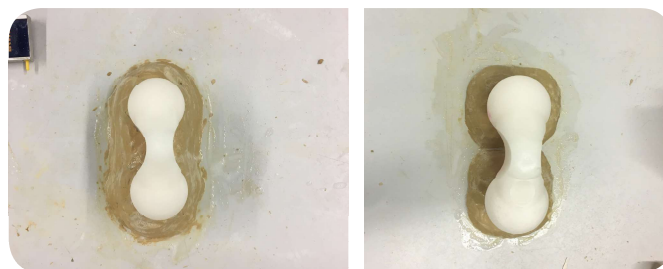


Figure 167. (left) one clay layer of mold B, (right) two clay layer of mold A



Figure 168. (left) bounding box of mold A, (right) the Crystal Cast M248 powder



Figure 169. (left) Crystal cast mold with wax model A, (right) water bath with boiler and plastic bags.



Figure 170. Final Crystal cast molds: (left) B molds, (right) A molds.

[24] <http://www.goldstarpowders.com>

3.6.2 Glass type and key temperatures

The raw material for producing the cast glass models is B 270® i Ultra-White Glass. This type of glass has a high visible transmittance and is defined as crown glass. According to Knight Optical, B 270® i Ultra-White Glass is an **optical glass** type (modified soda-lime glass) and has the following general properties: density of 2,55gr/cm³ and luminance transmittance for a 2mm thick material of 91,7%.

According to Knight Optical the **key temperatures** of B270 glass are:

- Strain point: 511°C
- Annealing point: 541°C
- Softening point: 724°C
- Forming temperature: 827°C
- Forming temperature: 915°C
- Forming temperature: 1033°C

The associated viscosities of these above mentioned key temperatures are presented in figure 171. According to Shelby (2005), the viscous range of 10⁵-10³ Pa-s is the range where B270 glass forms a viscous melt. The viscous melt corresponds to a temperature range of 827-1033°C. The softening point occurs below the 827°C at 724°C and 10^{6.6} Pa-s, where the glass B270 deforms under its self-weight. The critical temperature range is 780-660°C where crystallization can take place. Rapid cooling is necessary to avoid formation of crystals which could result in cloudy glass. Concerning Bristogianni et al. (2017), the temperature range between the annealing and strain-point (541-511°C and 10¹²-10^{13.5} Pa-s) requires controllable and slow cooling. The slow and controllable cooling is very important because residual stresses caused by the rapid cooling need to be released. As mentioned in the literature, these internal stresses occur due to uneven shrinkage caused by cooling and could increase the amount of cracks under mechanical or thermal shocks. Hence, it is important to held the glass for a sufficient time within the temperature range of 541-511°C. Because at this temperature range the glass is still viscous enough to keep its shape and molecular rearrangement can take place (to release the internal stresses).

The above described key temperatures were kept in mind for the firing schedules.

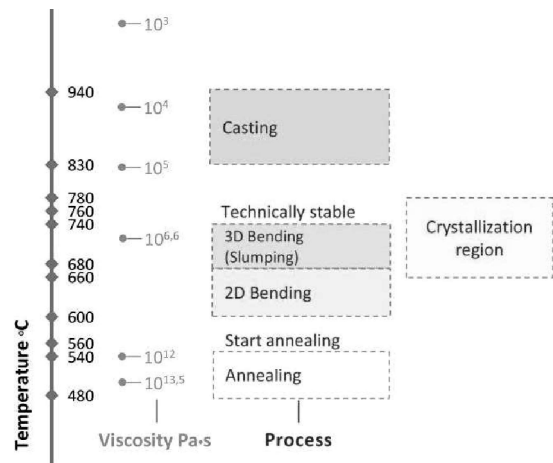


Figure 171. Temperature dependence of viscosity, and corresponding workability for B270 glass (Bristogianni et al., 2017)

3.6.3 Firing process

The glass models were made by using the **“flowerpot”** production technique. The steps that need to be taken before firing the glass models in the kiln and firing schedules are explained below.

① Volume measurement

The first step that needs to be taken is measuring the volume in order to determine the amount of glass. The amount of glass was calculated by multiplying the volume of the model (with funnels) with the mass density of the B270 glass (2,55gr/cm³). In addition, 4% of the mass was added to the final mass quantity, which takes in account the attached glass at the surface of the flowerpots. Note that, the percentage is rather small since the components are small and require small flowerpots. Appendix three presents the exact values of the glass masses for each mold. Finally, the molds were engraved with the numbers E1-E5 to refer to the amount of glass and to remember which glass model corresponds with which mold.



Figure 172. Measuring the volume through water

2 Flowerpot treatment

Two small and three medium flowerpots made from terracotta were used for pouring the glass. The flowerpots were well cleaned with water and dried with paper. Appendix three presents an overview of the dimensions of the diameter of each flowerpot and shows the location of the flowerpots with associated molds.

3 Glass treatment

Next, the glass masses were measured for each mold, since the glass was already cleaned and smashed into smaller pieces by other students. Subsequently, the glass pieces were placed into the associated flowerpots.

4 Firing

The molds were placed in the kiln and the flowerpots were placed on top of the spacers. The height of the spacers and position is shown in appendix three. The spacers and thus flowerpots were placed on top of the opening of one funnel, as shown in figure 163. The presence and location of the spacers allow for air circulation, causing less air bubbles within the glass model.

The kiln was programmed according the key temperatures and sufficient annealing time for reducing the internal stresses as explained in the previous chapter. The maximum kiln temperature was set on 950°C which corresponds to the temperature of the kiln environment. The Crystal cast mold can withstand temperatures up to 900°C. Hence, it is assumed that the temperature within the mold is lower than 950°C and will not cause a damaged mold.

One firing schedule was made to create the five models, the models were placed in the kiln with other models as shown in the figures. The firing schedule is shown in figure 178. In short, the temperature steps were:

- at 130°C the molds and flowerpots were dried
- at 750°C the glass deforms from gravity
- at 850°C the glass flows
- at 950 °C the glass flows easily
- Between 950–560 °C the glass was rapidly



Figure 173. Flowerpots filled with B270 glass pieces



Figure 174. Flowerpots on top of the spacers



Figure 175. Glowing glass within the molds during firing



Figure 176. Results after firing (left) mold B where the glass is connected, (right) A molds where the glass is not connected

cooled: "quenching" the glass to avoid formation of crystals

- Between 560–540°C the glass was soaked, i.e. at 560°C the glass can still deform and at 540°C the molecules cannot move enough to accommodate stress
- Between 540–510°C the glass was slowly and controllable cooled, this to release the internal stresses
- Between 480–25°C the glass was cooled faster but still slow enough to avoid thermal shocks.



Figure 177. Glowing flowerpots during firing

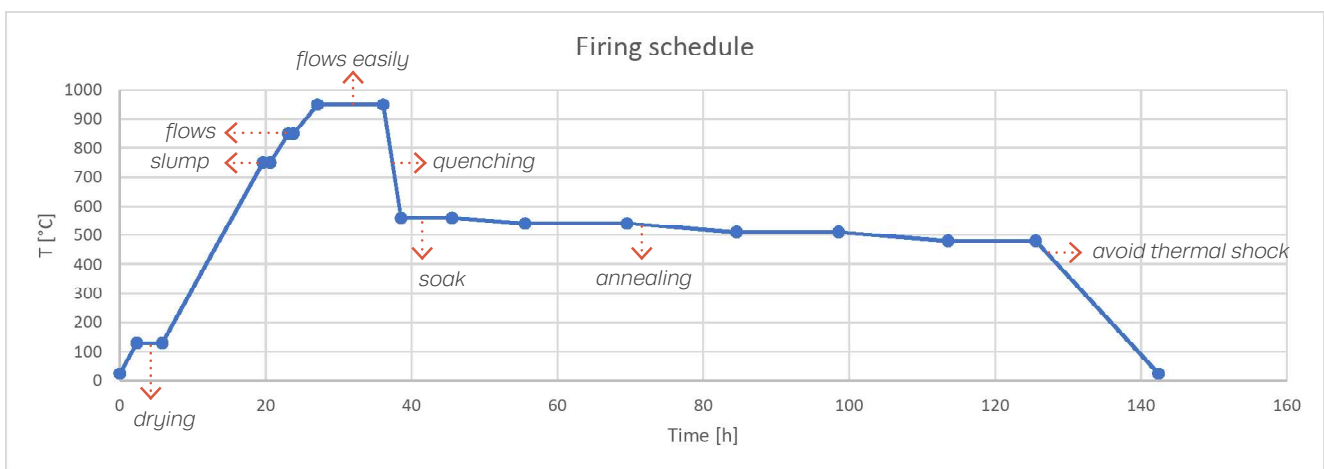


Figure 178. Firing schedule of the kiln for production of the five models

3.6.4 Post-processing and results

The molds were removed from the kiln when the kiln reaches room temperature, at this point the post-processing begins. The post-processing is distinguished into two processes: 1. releasing the molds and 2. post-processing the glass models to its final shape.

1 Releasing the molds & results

The Crystal cast molds dissolve through water in approximately 15–20 minutes. Hence, the molds were placed in a bucket filled with water and after 15–20 minutes the molds were easily removed from the glass model. The observations of the remaining five glass models are summarized in appendix three, the main conclusions of the observations are given at the next page.

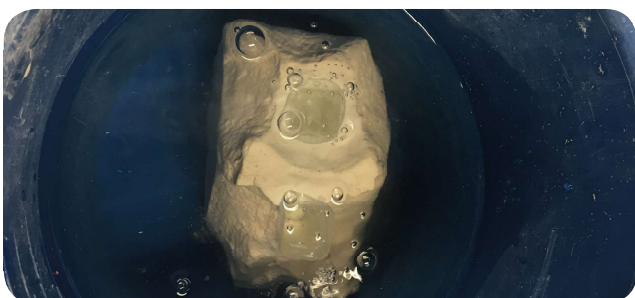


Figure 179. Dissolving the Crystal Cast mold



Figure 180. The remaining glass model after the Crystal Cast mold was dissolved

Conclusion of the observations

The most important conclusion of the observations of the five glass models is that all glass models showed large air bubbles at the sphere surfaces. In addition, small air bubbles at all models were located on top of surfaces of the funnels. It is concluded that glass models obtained from mold B (where the funnels were connected) showed respectively less air bubbles. Moreover, it is concluded that the firing process resulted in transparent components where almost no crystallization took place. Because the glass surfaces were not opaque (milky glass). Finally, the presence of the air bubbles is caused by trapped air bubbles within the mold during the casting process and need to be avoid next time.

2 Post processing the glass models

First, the largest parts of the funnels were removed by using a saw with water. Next, the funnels were shaped to a sphere by using a polishing machine. The polishing machine needs to allow for manual control. This manual controllability is required to create a spherical configuration.

Secondly, small bumps were removed by using dental tools. In addition the gaps from the air bubbles were treated to remove the sharp edges. The bumps are a result from the manual production technique and are unavoidable. The gaps caused from the trapped air bubbles are avoidable, this is explained at the end of this chapter.

Finally, the spheres of all components were polished to matt surfaces. This treatment was required to equalize the polished area of the funnels with the entire spheres. In addition, the surfaces of the glass component were not completely smooth which is a consequence of the rough surface of the Crystal Cast molds.

Six different polishing discs grades were used to polish the glass models. The sic different polishing discs grades are presented in figure 181. The glass components and discs grades were treated with water during the entire process. Usage of water is essential during the polishing process in order to cool down the glass surface. Subsequently, the cooled glass surface prevents the glass from cracks during the polishing process.

POLISHING DISC GRADES						
DISC COLOUR	YELLOW (SMALL DOTS)	BLACK	RED	YELLOW (LARGE DOTS)	WHITE	BLUE
GRADE	METAL 400 GRIT	RESIN 120 GRIT	RESIN 200 GRIT	RESIN 400 GRIT	RESIN 800 GRIT	RESIN 1800 GRIT

Figure 181. The six different polishing disc grades (source: www.warm-glass.co.uk)



Figure 184. Removing the largest part of the funnels



Figure 183. Shaping the funnels to a spherical configuration



Figure 182. Final polishing of the glass components with the six polishing disc grades.

3.6.5 Analysis of the residual stresses

Stress birefringence

A laptop screen is a polarized white light source and is together with a crossed polarized film used to perform a qualitative analysis of the residual stress regions.

According to McKenzie (2011), a crossed polarized film blocks the light transmittance. Stress free glass is defined as an optical isotropic material and when placed between the polarized light and crossed polarized film observed as equally bright glass. The opposite, glass subjected to stress becomes an optical anisotropy material, i.e. occurrence of birefringence. The birefringence correlate with two refractive indices. Thus, when the polarized white light from the laptop passes the glass model it divides into two polarized components. The two polarized components have a different speed caused by the different refraction indices thus form a phase difference between the two components. The phase difference results in the change in the net polarisation and are seen as different colours through the crossed polarized film. The different colours are called 'isochromatic fringes'. Dark areas are called 'isoclinic fringes' and locate the areas with the same principal stress. 'Isoclinic fringes' are not dependent of the stress quantity in comparison with the 'isochromatic fringes'.

Results and conclusion

It was concluded from the results of the qualitative analysis of the residual stress regions that the models showed few stresses. The low stresses are represented by the polarisation film as light blue colours or 'isochromatic fringes'. The remarkable stresses are shown in figure 185 and 186. Figure 185 shows a divided stress zone at the top edge of the component. Latter mentioned stress region is hard to declare but could be a consequence of an uneven shrinkage pattern during the casting process. Figure 186 clearly shows the stresses at the top edge of the model which are caused by the flow pattern of the glass during the casting process. The flow pattern is presented as a 'fish-bone' stress pattern in the figure. Finally, it should be noted that the air bubbles could have influence the path of the refracted light which makes the polarization test less accurate.



Figure 185. Light-blue isochromatic fringes located at the left top edge



Figure 186. Light-blue isochromatic fringes showing the glass flow of the casting process



Figure 187. Little to no light-blue isochromatic fringes



Figure 188. Little to no light-blue isochromatic fringes



Figure 190. Glass prototypes in arch configuration



Figure 189. Glass prototypes in ring configuration

3.6.6 Conclusion & final mold

The prototypes were made by using the flower-pot production technique and were obtained from a mold designed with two funnels located at the top edges of the spheres. The results from the casting process have shown that the rapid cooling caused high transparent models because crystallization was avoided. However, the glass models were textured caused by the rough surfaces of the Crystal Cast molds. In addition, the glass models show few stresses which is a consequence of the sufficient annealing process. Note that the used polarization test for addressing these stress regions is a qualitative analysis and does not give quantitative results.

Moreover, all the models showed large air bubbles located at the front sphere surfaces or side sphere surfaces. These air bubbles most often occurred at the non-pouring side, thus the side where the air left the other funnel. The glass models obtained from the B mold (where the funnels were connected) showed

less air bubbles. It is concluded from these results that next time the air bubbles need to be avoided by using vents. These vents are made from wax and are attached at the wax model, as shown in the example of creating a flower model in figure 192. Because of the mentioned reasons above the final mold design is shown in figure 191 where two vents are located at the sphere side (where most bubbles occurred). The final mold is constructed with one funnel where the poured glass follows gravity since most mass is located at the spheres. It is assumed that one funnel at the top ensures a equally distributed mass during the entire casting process.

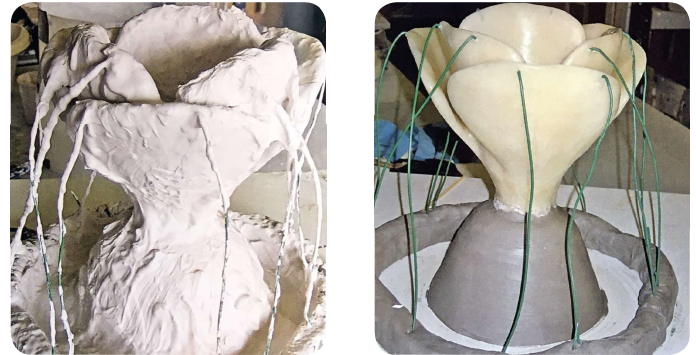


Figure 192. Flower model where green wax threads were used to create vents (Thwaites, 2011)

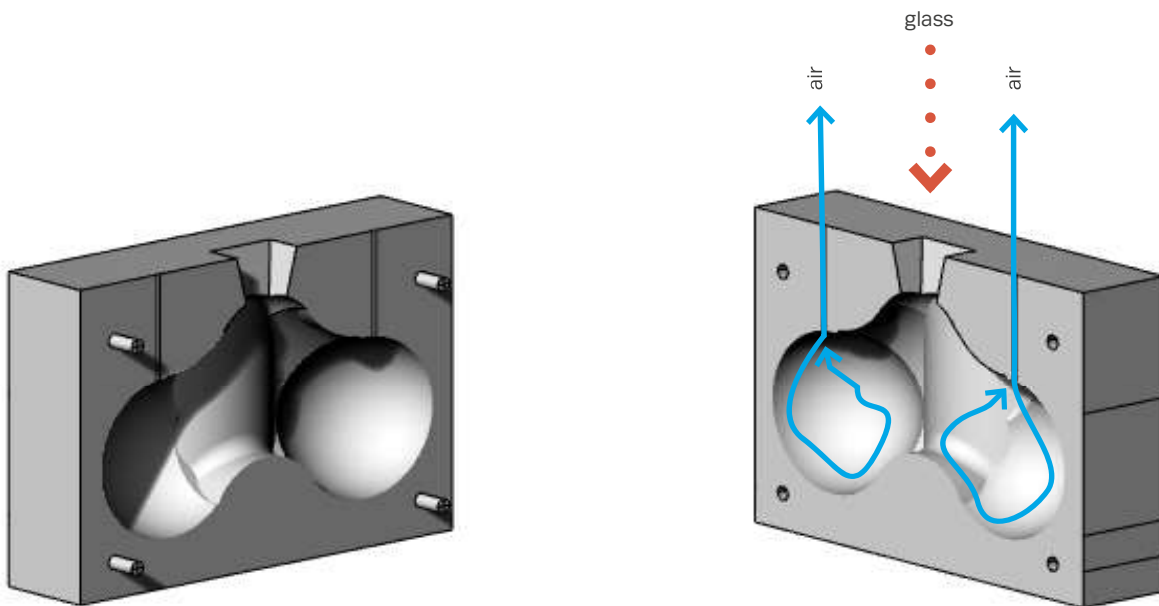


Figure 191. New proposed mold design with two vents and one funnel at the top of the mold

3.7 Transparency

New definition of transparency

The material glass itself is a transparent material however not always observed by the human eye as transparent. In physics the definition of transparent is: "a synonym for transmission and specifies the wavelengths for which a material is permeable, and to which extent" (Weller et al., 2009, p. 34). For example, the cast glass blocks of the Crystal House have a visible transmittance of approximately 0.8 and a smooth surface resulting in a high transparency for visible light. The visible light transmittance of the glass dome should be lower in order to notice the presence of the glass dome structure by the Lori parrots. Hence, the glass dome components should be polished to a **slightly matt** surface area while still **transmitting the colours** of the environment. The colours of the environment, such as trees, the sky or flowers, need to be transmitted through the glass components in order to mimic the colours of a natural habitat for the Lori parrots on the glass dome surface.

Transparency is not only about having a colour through transmission, **reflections** and **distortions** also contribute to it. Distortions are perceived by the human (or birds) eye as a consequence of refracted light beams. The direction of the refracted light beams depend on the thickness of the component and geometry, thus determines how the distortion is observed. The inner-side of the glass components will work as a **hollow lens** where the light beams diverge. It is assumed that the majority of the light beams pass the spheres which form a positive lens because the components are stacked on top of each-other. In addition, the positive lens will work as a **converging lens**. The light beams are falling onto the glass component and are refracted and converge to its focal point, observed by the human eye as a real image or colour scheme. Subsequently, behind the focal point the light beams will form an **inverted image** caused by the converge refraction^[25].

The above described converging effect was tested by subjecting the prototype to daylight. First the component was placed in front of a tulip where the camera was placed in front of the component, resulting in a **real colour scheme**. Secondly, the component was placed in front of a building with a clear blue sky where the camera was placed from a distance (stretched arm), resulting in an **inverted colour scheme**. From these tests is concluded that the spheres will work as a very **strong converging lens** because the focal point lies almost against the component. Finally, the effect of the positive and negative lens of the component will also happen in the real dome design. Although the real dome design will have more distortions as a result of the interaction between the components. It should be noted that the perceived distortions only are determined and validated through a real physical model of the glass dome design and require further research.

Finally, a new meaning of transparency formulated which relates to the glass dome design, which is: **a synonym for reflecting, transmitting and distorting colours of the environment in the interest of designing a noticeable dome structure for Lori parrots.**

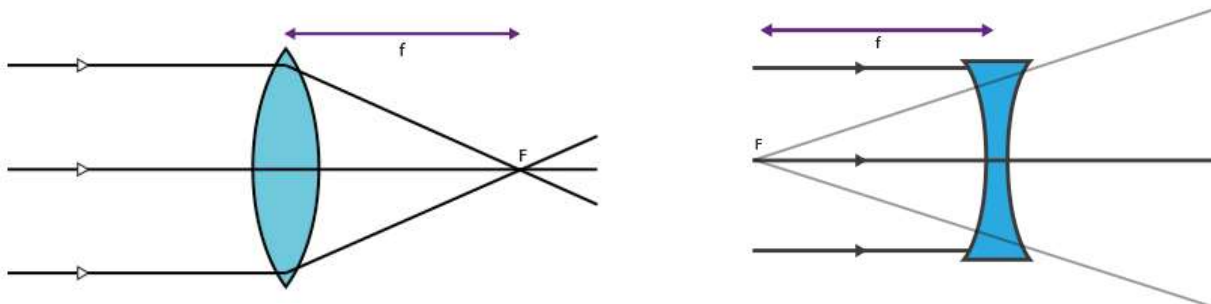


Figure 193. (left) positive lens, light beams converge (right) negative lens, light beams diverge
(source: www.denatuurkundefabriek.nl)

[25] <http://denatuurkundefabriek.nl>



Figure 195. (left) image, (right) Real colour scheme of the image, where the camera was placed in front of the focal point.



Figure 194. (left) image, (right) Inverted colour scheme of the image, where the camera was placed behind the focal point.

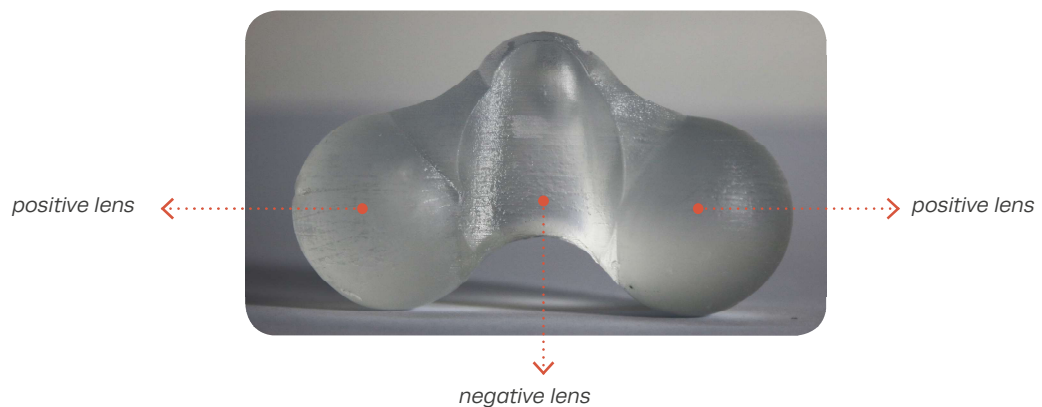


Figure 196. Overview of the component and lens types



4. Validation

4.1 Structural validation

4.1.1 Introduction

This chapter addresses the structural validation of the glass dome, derived from analytical, numerical and experimental analyses. An experimental qualitative analysis is performed at arch level. This analysis gives fundamental insight of the structural behaviour of the dry assembled system of the glass dome. For both analytical and numerical analyses simplifications of the real dome design are made in order to validate the structural performance. Because the omnidirectional components require complex simulations and it is predicted that even these complex simulations will not lead to accurate results, it is assumed that only real physical experiments will validate the structural performance of the glass dome.

4.1.2 Analytical analysis

1. Introduction

The membrane theory of masonry domes is used to define the analytical stress analysis of the glass dome. This chapter provides fundamental knowledge about the critical stress and membrane stresses within the glass dome under symmetrical loading, i.e. only subjected to its self-weight. Secondly, this chapter provides an interlayer material selection. And at the end of this chapter an approximation of the support reactions and related wall thickness of the support structure is given.

2. Stresses in the glass dome

Membrane stresses & critical stress

Stresses in dome structures are generally low, this is explained in the chapter 'forces in domes'. The membrane theory is used to determine the hoop and meridian stress resultants subjected to its self-weight. Self-weight is the most prevailing load case, explained in more detail in sub-chapter 'global effect'. Table 24 presents the input data for the equations and graphs which include: weight per unit area, radius of the sphere, knock down factor and Young's modulus of Soda-lime glass. The hoop, meridian and buckling stresses were derived from this and are shown in table 25. This table shows that the critical buckling stress is very high and therefore local buckling will not occur. The glass dome is in no danger of local buckling because the glass dome has a reasonable thickness and the external loads will be less than its self-weight. The hoop and meridian resultants are plotted in figures 197 and 198. Figure 197 presents the stress resultants for the glass dome. It is concluded from these figures that the hoop and meridian resultants are compressive

when Φ lies within $0-51,82^\circ$, after this the hoop resultant becomes a tensile stress.

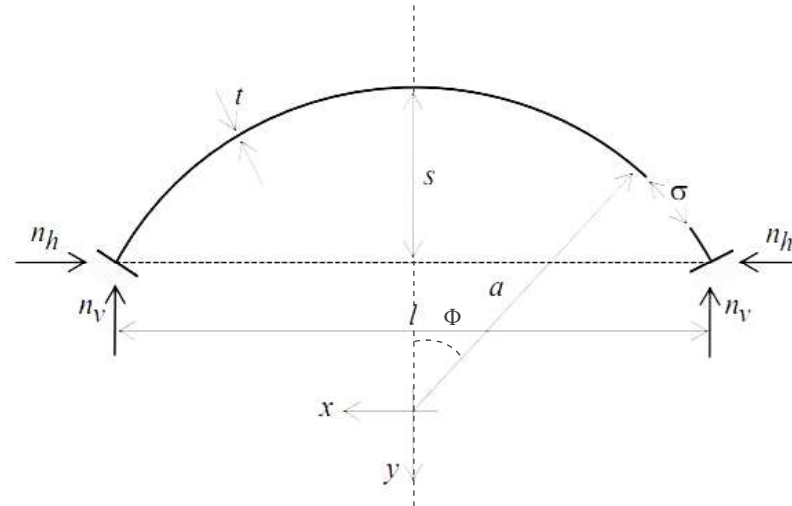
The main dimensions of the glass dome are based on the **compressive shell boundaries** where **phi lies within $0-45^\circ$** . Note that a compressive force system is performed till phi reaches $51,82^\circ$. Using the minimum phi of $51,82^\circ$ is not preferred because when a tensile stress does occur the stress will increase rapidly, as shown in figure 198. Hence, the compressive shell boundaries of the glass dome are: $0 < \Phi < 45^\circ$ because of the reasons mentioned above.

Tensile stresses

Tensile stresses occur due to global or local effect. The local effect is caused by the imperfect flat surface area of glass as explained in the literature review of interlocking systems. Tensile stresses due to global effect are caused by asymmetrical loading (wind and snow), where asymmetrical loading results in eccentricity of the line of thrust.

The glass dome has a reasonable thickness which is equal to approximately 220 mm. The glass dome is constructed from cast glass components out of Soda-lime glass. Soda-lime (0080) has a density of $2,49 \times 10^3 \text{ kg/m}^3$ * which is equal to a weight per unit area of $2,49 \text{ kN/m}^2$. Typical snow load according the literature of Heyman (1995) might be $1,5 \text{ kN/m}^2$ and the expected wind stresses are even smaller: 1 kN/m^2 . External loads from wind and snow are less than its self-weight. Hence it is assumed that stresses from snow or wind are from the same order as the stresses resulting from the self-weight of the glass dome.

*obtained from the CES EduPack 2016



based on (Hoogenboom, 2017)

CALCULATION INPUT				
index	description	value	unit	used formula
a	radius sphere	25,44	m	
r	radius at dome foot	17,99	m	
l	span at dome foot	35,98	m	
s	sagitta dome	7,45	m	
t	thickness	2,2E-01	m	
A	surface area dome	842,15	m ²	$2\pi rs$
g	gravitational acceleration	9,81	m/s ²	
d	density*	2,5E+03	kg/m ³	
w	self-weight	5395,5	N/m ²	dtg
E	young's modulus*	6,97E+10	N/m ²	
k	knock down factor**	0,25		
*obtained from CES EduPack 2016 for Soda-lime glass (0080)				
**(Heyman,1995)				

Table 24. Input data of the analytical calculations

STRESSES (subjected to its self weight)				
index	description	value	unit	used formula
Stress resultants				
NΦt	meridional stress at top	-6,86E+04	N/m	$N\Phi = -(wa)/(1+\cos(\Phi))$
NΦb	meridional stress at base	-8,04E+04	N/m	$N\Phi = -(wa)/(1+\cos(\Phi))$
NΘt	hoop stress at top	-6,86E+04	N/m	$N\Theta = (-wac\cos(\Phi)) - N\Phi$
NΘb	hoop stress at base	-1,67E+04	N/m	$N\Theta = (-wac\cos(\Phi)) - N\Phi$
Values of the stress resultants in the glass dome from the top ($\Phi=0$) to the base ($\Phi=45$)				
Critical buckling stress				
σ_{cr}	critical buckling stress	2,13E+08	N/m ²	$\sigma_{cr} = kE(t/r)$

Table 25. Stress resultants and critical buckling stress

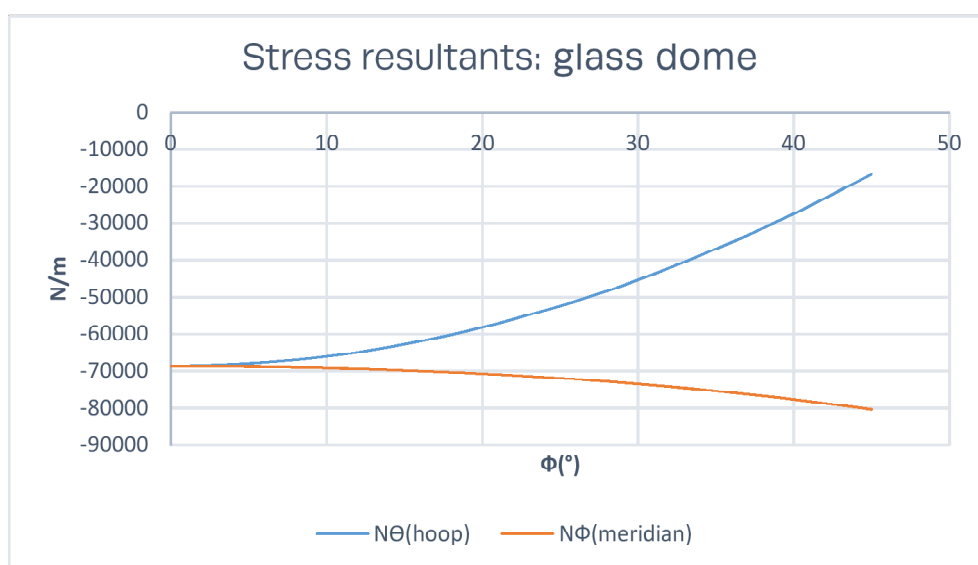


Figure 197. Stress resultants of the glass dome

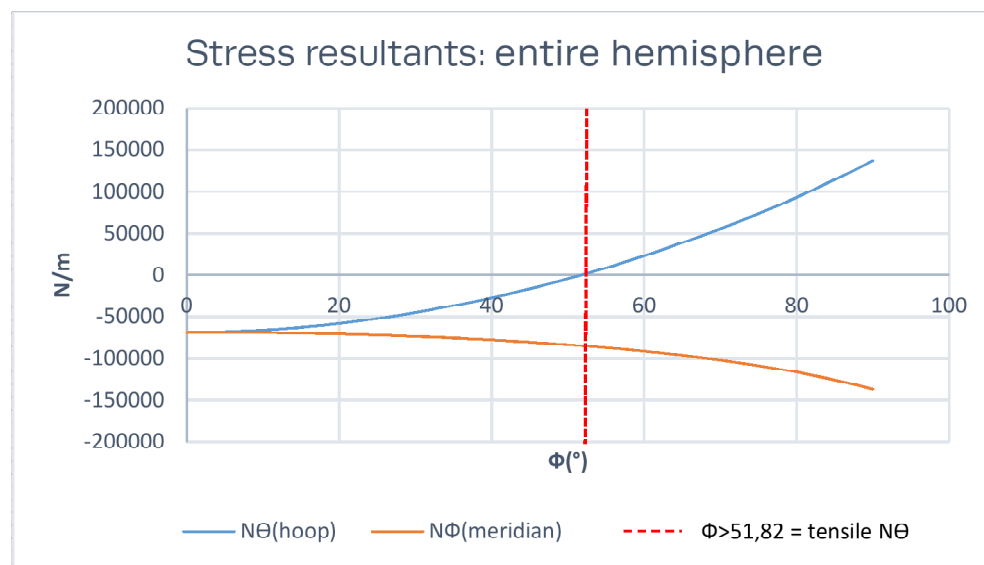


Figure 198. Stress resultants of the entire hemisphere

3. Interlayer

Introduction

This research proposes interlayers that accommodate for local protrusions of the glass dome components. These interlayers are applied between two glass surfaces and are located in the ring and arch direction. According to Oikonomopoulou et al. (2014), a solely glass system with dry assembled cast glass bricks fail at an average compressive stress of 20–30MPa. Based on this research the assumption is made that glass dome components will fail at around its compressive strength of 20–30MPa when no interlayer is applied. The contact area of the interlayer with the component therefore should maintain the requirement presented in equation 1:

$$\sigma_{\text{contact}} \leq 20 \text{ MPa} \tag{1}$$

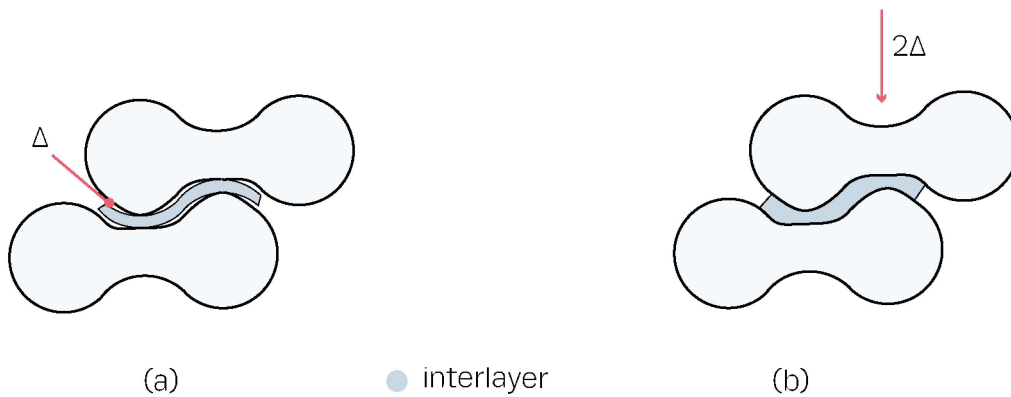


Figure 199. (a) contact area before subjected to stress, (b) full contact area subjected to the maximum stress

Hooke’s law is used to determine the interlayer stiffness interval and is shown in equation 2. The maximum stress (20 MPa) ensures a full contact area where the deviation (2Δ) is the only variable. The deviation (Δ) is multiplied with a factor 2 because both sides show a deformation, this principle is shown in figure 199. According to Aurik (2017) a glass component requires full contact between all surfaces, which equals 2 surfaces, after a displacement of 2Δ . For the glass dome this equals 2 surfaces in the ring direction and 2 surfaces in the arch direction.

It is assumed that the stiffness of glass is much stiffer than the interlayer stiffness. In this research an assumption is made for the maximum displacement of 2Δ , where according to Aurik (2017) $2\Delta \leq 2 \cdot 0,25 \text{ mm}$. This assumption is based on the cast glass bridge design with dry assembled system, because this research will not provide structural simulations of the glass dome components and interlayers. The maximum interlayer stiffness is obtained from equation (1), equation (2) and fact that $2\Delta \leq 2 \cdot 0,25 \text{ mm}$ and is shown in equation (3):

$$\sigma_{\text{contac}} = E_{\text{int}} \cdot 2\Delta / t_{\text{int}} \tag{2}$$

$$E_{\text{int}} / t_{\text{int}} \leq 20 / (2 \cdot 0,25) \leq 40 \text{ N/mm}^3 \tag{3}$$

Interlayer material selection

Interlayer thickness

The analysis from this chapter and literature review of interlayers make it possible to formulate a stiffness interval for suitable interlayers. It is assumed that the force system of the glass dome is based on compression and therefore only the local effect is taken in account for determination of the interlayer stiffness interval. The 'real' global effect is not within the scope and based on the glass bridge design. According to Aurik (2017), the maximum interlayer stiffness equals:

$$E_{int}/t_{int} \leq 20/(2 \cdot 0,25) \leq 40 \text{ N/mm}^3.$$

The interlayer thickness plays an important role because it determines the stiffness of the entire glass dome system. A thicker interlayer absorbs more stresses resulting in a lower stiffness of the entire system.

The interlayer thickness of the glass dome design does not change in the arch direction and is equal to 2mm. The opposite, the interlayer in the ring direction does change due to the changing curvature and varies from 10 mm till 12 mm, at its edges, from dome foot till dome top. In addition, the interlayer stiffness decreases when the interlayer thickness increases. It is concluded that the minimum interlayer stiffness occurs at the dome top, where the interlayer thickness is maximal.

The interlayer stiffness range is determined by using the interlayer thickness of 2mm in arch direction and maximum interlayer thickness of 12mm in ring direction (located at the dome top). The maximum thickness's are used for both ring and arch direction because this results in the minimum interlayer stiffness and thus maximum stresses occur at this thickness. Note that the maximum arch interlayer thickness is equal to the minimum arch interlayer thickness because this thickness does not change due to the equal curvature.

The minimal interlayer stiffness equals:

$$E_{int} = (20/(2 \cdot 0,25)) \cdot 2 = 80 \text{ N/mm}^2$$

The maximum interlayer stiffness equals:

$$E_{int} = (20/(2 \cdot 0,25)) \cdot 12 = 480 \text{ N/mm}^2$$

Resulting in an interlayer stiffness range of:

$$0,08 \text{ GPa} \leq E_{int} \leq 0,48 \text{ GPa}$$

Interlayer requirements

To create full contact of all surfaces, with the interlayer and component, a ratio of $E_{int}/t_{int} \leq 40$ is N/mm^3 is required. The stiffness interval is determined by using the latter required ratio, where $E_{int} \geq 0,08 \text{ GPa}$ with a thickness of 2 mm and $E_{int} \leq 0,48 \text{ GPa}$ with a thickness of 12 mm. According to Aurik (2017) a stiffness of 0,03 GPa is equal to the minimum stiffness of the interlayer while creating a stable arch structure. This research assumes a minimum stiffness of 0,03 GPa since the arch direction is the most crucial direction. Hence, **the stiffness interval** for the interlayer of the glass dome is :

0,03 GPa \leq E_{int} \leq 0,48 GPa

Additional requirements are given below and are used as input data for the CES EduPack 2017 software. The results from CES EduPack 2017 present the suitable interlayer materials and are shown in table 26. The interlayer requirements are divided in two aspects: general interlayer requirements and manufacturing requirements. Table 27 presents the suitable interlayer materials based on the manufacturing requirements.

General Interlayer requirements:

- Mechanical: $0,03 \text{ GPa} \leq E_{int} \leq 0,48 \text{ GPa}$
- Transparency: Optical quality, transparent, translucent.
- Durability UV-light: Fair, good, excellent.
- Compressive strength: $\geq 25 \text{ MPa}$.
- Maximum service temperature $\geq 50^\circ\text{C}$.

Manufacturing requirements:

- Thickness range: 2–12 mm
- Solid 3D complex shapes

Results CES EduPack

The additional requirements such as durability, optical properties, service, strength have result in suitable materials and production techniques. The suitable materials are: PVDC, TPU, PEBA and PVC. The manufacturing requirements have resulted in three suitable production techniques which are: rotational molding, polymer forging

and compression molding. Compression molding is preferred above the other production techniques because it has large thickness range. It should be noted though that the compression molding production technique is very labour intensive. However figure 200 shows that the relative cost of the production technique compressions molding depends on the batch size. It is concluded that the costs of the glass dome interlayers are relatively low because the batch size is larger than 1000 interlayers. The material PEBA and TPU and compression molding production technique were selected for constructing the interlayers of the glass dome. These materials and production technique allow for a large thickness range, durable complex shaped interlayer and ensure transparency and strength. Heat shrink plastics were eliminated during the material selection process due to the limited section thickness of the thermal molding process: 0,25–6mm. The section thickness range of the interlayer of the glass dome is 2–12 mm and heat shrinks plastics cannot be used.

Results: general requirements				
	$\sigma_{comp.}$ (MPa)	Transparency	UV-resistance	Young's modulus (GPa)
PVDC	38,6–42,6	Translucent	Fair	0,11–0,17
TPU	61,1–71,2	Optical quality	Fair	0,247–0,253
PEBA	40,6–43,4	Transparent	Fair	0,0721–0,0739
PVC	38,6–42,6	Translucent	Fair	0,11–0,17

Table 26. Results general interlayer requirements (obtained from CES EduPack, 2017).

Results: manufacturing requirements			
material	production technique	section thickness(mm)	shape
PVC	Rotational molding	2,5–6	3D solid
PVDC			
PVDC	Polymer forging	6,25–25	3D solid
PEBA	Compression molding	1,5–25	3D solid
TPU			

Table 27. Results manufacturing interlayer requirements (obtained from CES EduPack, 2017).

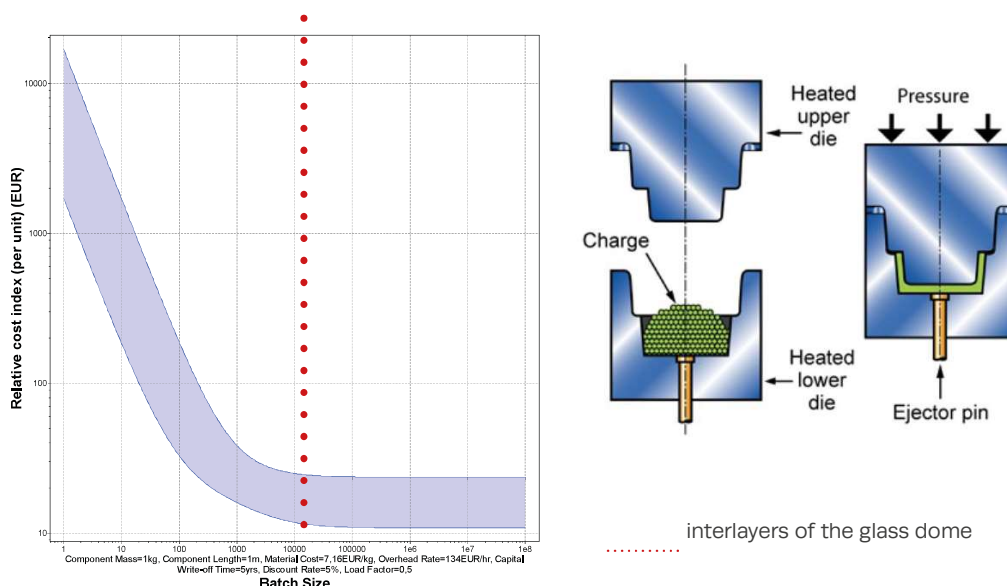


Figure 200. (Left)Relation cost and batch size, (right) schematic process of the compression molding production technique (obtained from CES EduPack, 2017).

Interlayer material and stiffness entire system

Finally, **TPU** is chosen as most promising interlayer material since it has a higher compressive strength in comparison with PEBA. Most common example of a TPU application know a days is transparent cover to protect your iphone, as shown in figure 202.

The stiffness of the entire dome system is derived from the **weighted mean** of the interlayer thickness (t1) and young modulus (E1) and glass component thickness(t2) and Young-modulus(E2), where the interlayer thickness (t1) is defined as the maximum interlayer thickness and equals 12mm. The **maximum interlayer thickness** is used because this results in the minimal stiffness, or the so called worst case scenario where most stresses are absorbed by the interlayer.

The **stiffness** of the **entire dome system** equals: $(t1/(t1+t2) * E1) + (t2/(t1+t2)*E2) = (12/(12+45)*0,253) + (45/(45+12)*69,7) = 55,1 \text{ GPa}$. It should be noted that the stiffness of the real entire dome system is higher than the calculated previous value, because the maximum interlayer thickness is used for the calculation of the weighted mean. In reality, the interlayer thickness varies in every horizontal section and is equal to 2mm in the arch direction. This research focusses on the worst case scenario and uses the maximum interlayer thickness because of the complexity of the ring interlayer. The ring interlayer is complex because it does not only change in every horizontal direction but the thickness also changes in its geometry. The changing thickness of the ring interlayer in its geometry is shown in figure 201.

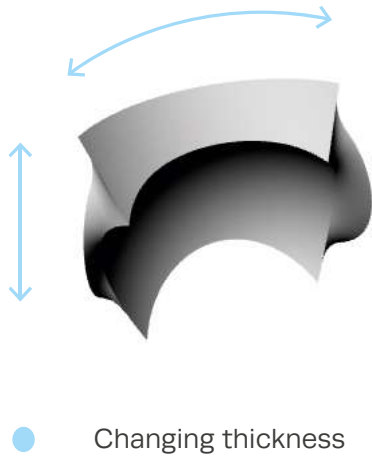


Figure 201. Changing thickness in geometry of the ring interlayer



Figure 202. TPU case of an iphone (soure: www.nl.aliexpress.com)

4. Support reactions and thickness

According to Heyman (1995) the orange slice-technique can be used to determine the reaction forces for a hemispherical dome, where two lunes form a quasi-two-dimensional arch. The collapse mechanism of an 'orange-slice' arch with a minimum thickness for a hemispherical dome is shown in figure 203. This Figure shows that the upper part descends vertically and does not deform while the adjacent lunes move apart from P till the base of the dome. The forces on one orange slice of last mentioned figure are presented in figure 204.

The collapse mechanism of the glass dome, assuming a minimum thickness, is based on figure 204 however the adjacent lunes will show less till almost no displacement. The collapse mechanism of the glass dome, assuming a minimum thickness, will therefore result in a 3 hinge collapse mechanism instead of a 5 hinge collapse mechanism, this principle is shown in figure 205.

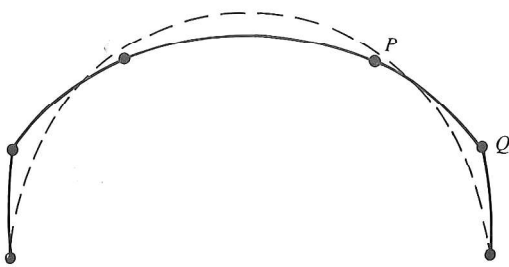


Figure 203. Collapse mechanism of the arch of minimum thickness (Heyman, 1995)

The forces necessary to create equilibrium of the glass dome are shown in figure 206. The distributed self-weight is replaced through force W , located at $(\pi/4)r$ which is equal to $1/4$ length of the entire arch with length: πr . Simple statics of equilibrium result in the equation $H = (W \cdot (r - (\pi/4)r)) / s$, which is further explained in the figure.

The glass dome spans 36m and weighs 4500kN, this requires a horizontal support force of 2350kN. The horizontal support force is uniformly disturbed around the base which results in a distributed force of 20,8kN/m. The related thickness of the supported wall underneath the dome structure is equal to **560mm**, the explanation of the calculated thickness is given in table 28. This table also presents an overview of the support reactions and thickness of the supported wall underneath the glass dome.

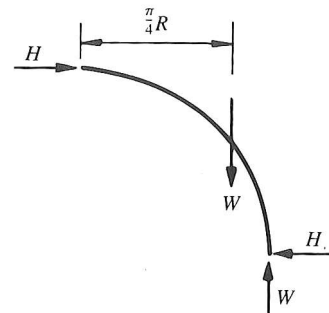


Figure 204. Forces on segment of a hemispherical dome (Heyman, 1995)

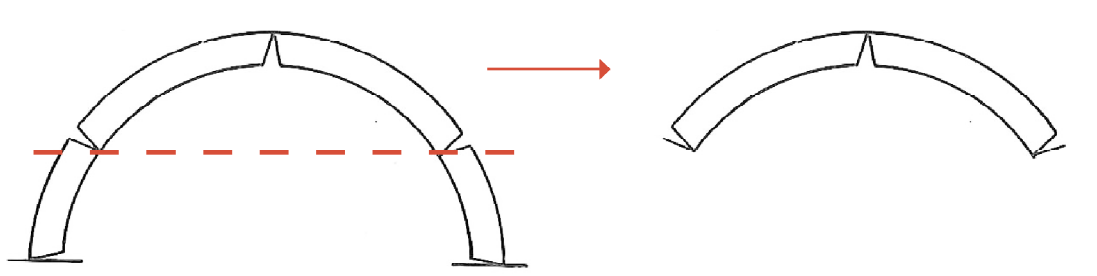


Figure 205. (left) 5 hinge collapse mechanism for a hemispherical dome, (right) 3 hinge collapse mechanism for the glass dome based on (Heyman, 1995)

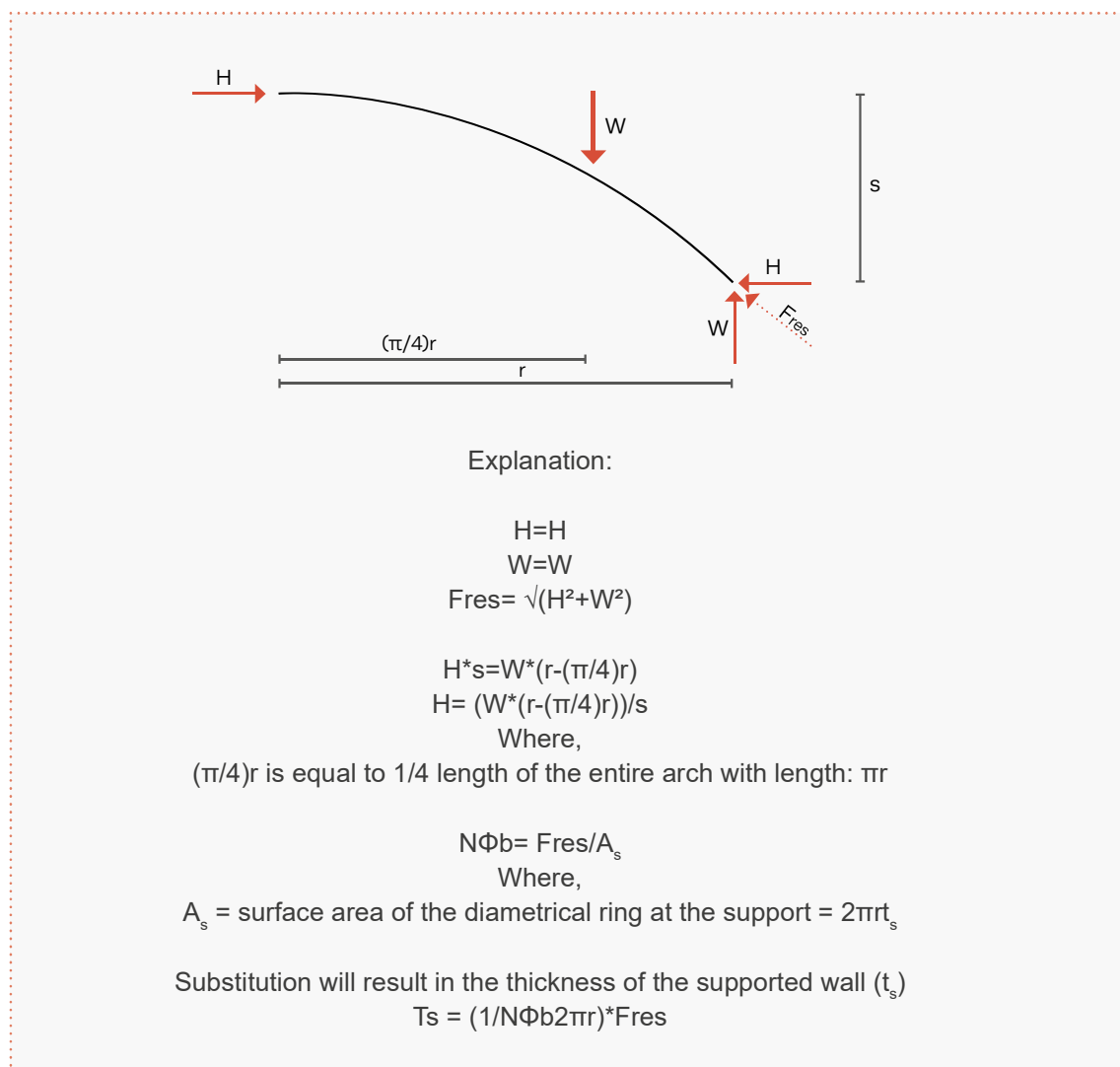


Figure 206. Forces on segment of the glass dome and explanation

SUPPORT				
Support reactions				
<i>index</i>	<i>discription</i>	<i>value</i>	<i>unit</i>	<i>used formula</i>
W	selfweight	4,54E+06	N	A_w
H	horizontal support	2,35E+06	N	$W(r-(\pi/4)r)/s$
H*	horizontal support	2,08E+04	N/m	$H/2\pi r$
Fres	resultant force	5,12E+06	N	$\sqrt{H^2+W^2}$
Thickness supported wall				
NΦb	meridional stress at base	-3,65E+05	N/m ²	$N\Phi = -(w_a)/(1+\cos(\Phi))$
Ts	wall thickness	0,56	m	$(1/N\Phi b * 2\pi r) * F_{res}$

Table 28. Overview of the calculations of the support thickness

5. Conclusion

The glass dome has a purely compressive force system (the membrane stresses, i.e. arch and ring stresses, are in compression) with a finite thickness. Because of these reasons the supports will give away slightly. It is assumed from this chapter and the chapter 'design' that the supports of the glass dome are encircled by a steel ring and will resist the minimum occurred tensile stresses, this will prevent the supports from yielding. It should be noted that a fully compressive force system is never reached because tensile stresses will always occur, because local tensile stresses at the component are caused by the local protrusions as read in the chapter 'interlayer'.

However, numerical analysis needs to validate the assumptions made in this chapter which includes the validation of the purely compressive system under its self-weight and asymmetrical loading. This to validate that the external loads from wind and snow are less than its self-weight, thus are from the same order as the stresses resulting from its self-weight of the glass dome. The numerical analysis is presented in next sub-chapter.

4.1.3 Numerical analysis

Introduction

The numerical analysis was performed in the Diana software. This software is specialized in structural analyses and utilizes the Finite Element Method. In simple words, the dome structure is drawn in small elements which will form a mesh for which structural calculations can be performed. This chapter will validate three main assumptions made in the chapter 'analytical analysis', which are:

- The dome structure will form a pure compressive structure under its self-weight.
- External loads, such as wind and snow, are from the same order as the stresses resulting from the self-weight.
- Local stresses at the base on one component are in compression for both load cases and will not exceed the maximum strength of the component and interlayer.

This chapter explains the input data for the Diana model, presents the results and finally discusses the results to conclude if the above described assumptions are validated.

Input data

The input data for the Diana model is described below and include aspects 1-5:

1. Geometry

As explained at the beginning of this chapter, a simplification of the real dome design is required and constructs the Diana-model. The Diana model consists of a clear shallow dome structure with a uniform thickness of 0,22m. The Diana model was drawn in Rhinoceros and imported in the Diana software. The dome model in Rhinoceros was constructed from sixteen surfaces by dividing the arch in four segments and subsequently using the sweep rail tool to create equal surfaces. Using the function in Rhino 'sweep rail' is essential for creating a uniform dome shell. The dome surface was divided in sixteen surfaces to construct a symmetrical mesh in the Diana software.

2. Material properties

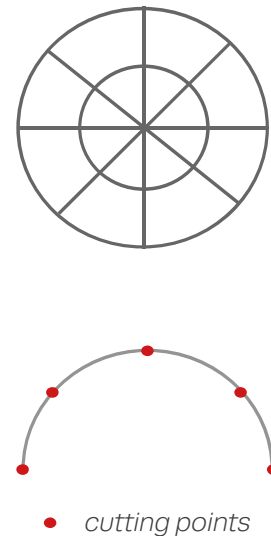


Figure 208. (top), top view dome with sixteen surfaces, (bottom) arch divided in four segments

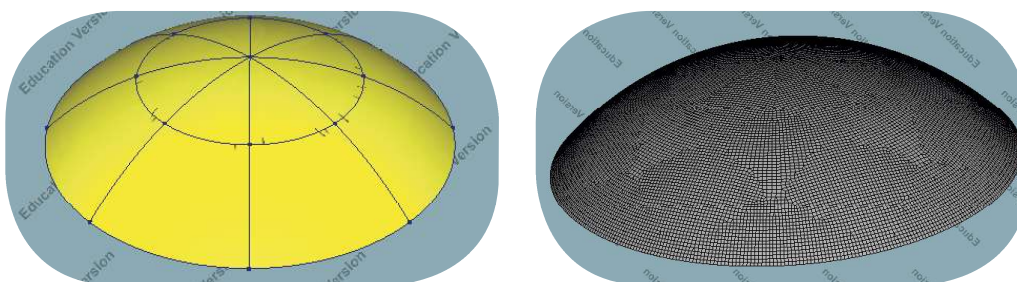


Figure 207. (left) Geometry of the Diana-model, (right) mesh of the Diana-model

The glass dome structure is assessed on its elastic performance where the following aspects were used as direct input: Young's modulus, mass density and Poissons ratio. The density and Poissons ratio were obtained from the material properties of Soda-lime glass. The Young's modulus was obtained from the previous chapter, where the Young's modulus presents the elasticity of the entire system, i.e. interlayer + glass components. The related values are shown in figure 209. Note that the thermal expansion coefficient and compressive strength also were added but will not influence the output of the linear static analysis.

3. Support structure

The glass dome is supported around its base with a steel fixation which will prevent rotation and displacement in x,y and z direction.

4. Local element axis.

It should be noted that the local element axis was set on the x-axis. In addition, the results should be read from the x-axis because of the set local element axis.

5. Loads

The analysis was performed for two load cases which are:

- Self-weight (symmetrical loading)
- Self-weight + Wind load on one side of 1kN/m² (asymmetrical loading)

Direct input	
Young's modulus	5.51e+10 N/m ²
Young's modulus at 28 days	N/m ²
Poisson's ratio	0.22
Thermal expansion coefficient	9.16 1/K
Mass density	2500 kg/m ³
Charateristic strength at 28 days	N/m ²
Mean compressive strength at 28 days	3.42e+08 N/m ²

Figure 209. Direct input data of the Diana model

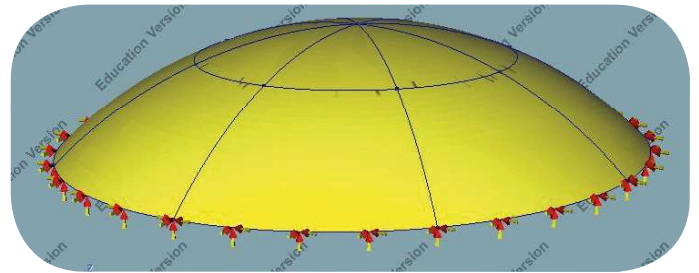


Figure 210. Boundary conditions of the Diana model

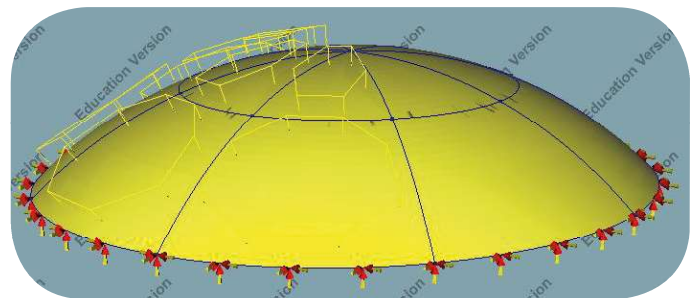


Figure 211. Asymmetrical load-case (yellow lines present the wind load)

Simulations

As described at the previous page, the simulations are performed for two load-cases: symmetrical and asymmetrical load case. The results from the linear static analyses present the stress resultants for the ring and arch direction, total displacement in the z-direction and principle stresses. The output data obtained from the Diana software is presented in the overview in figure 212 and a summary is given in table 29.

The results show that the largest stress resultant, for both load cases, occurs at the base in the arch direction. This is simply explained, since the arch direction is most crucial direction where most stress transfer will take place and the base will absorb all the stresses from its self-weight and additional loads. The lowest stress resultant occurs, for both load cases, at the dome base in ring direction. The difference of the stress resultants between the two load-cases is small because the self-weight is the dominant load-case.

However, the asymmetrical load-case will cause a difference in the line of thrust because the location of the stress resultants will change. The different located stress resultants result in

a different deformation scheme, where the maximum displacement at the dome top slightly increases.

The stress resultants and displacement in z-direction for both load cases are not from the same order, in terms of size. Latter mentioned difference is neglected because the difference between the stress resultants and displacement in z-direction between the two load cases is rather small.

Finally it is concluded that the principle stresses at the base are in compression and do not exceed the compressive strength of the interlayer, because all principle stresses are smaller than and $61,6e^6 \text{ N/m}^2$ (compressive strength of the TPU interlayer). Note that in the real dome design the principle stresses probably would be higher since the components do not have a full contact area. Based on latter mentioned reason a safety factor of 2 is used which is multiplied with the largest principle stress: $2 * 6,44e^5 = 12,8e^5 \text{ N/m}^2$. Resulting in a new principle stress of $12,8e^5 \text{ N/m}^2$ which is still smaller than $61,6e^6 \text{ N/m}^2$.

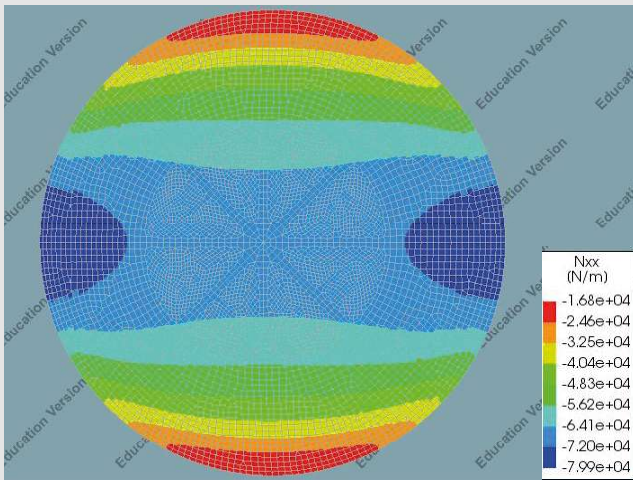
Stress resultants (N/m *e^4)			
direction		LC 1 (Sym)	LC2 (Asym)
Ring	top	-6,41	-7,12
	base	-1,68	-1,72
Arch	top	-6,41	-7,12
	base	-7,99	-8,92

Displacement z-direction (m *e^-4)		
direction	LC 1 (Sym)	LC2 (Asym)
Top	-2	-2,32
Base	0	0

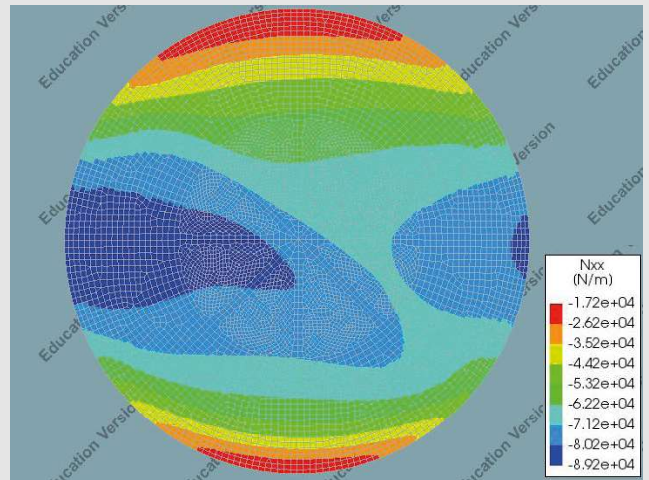
Principle stresses at base (N/m2)		
	LC 1 (Sym)	LC2 (Asym)
S2 (min)	-8,86E+04	-7,98E+04
S3 (max)	-4,76E+05	-6,44E+05

Table 29. Summary results from Diana model

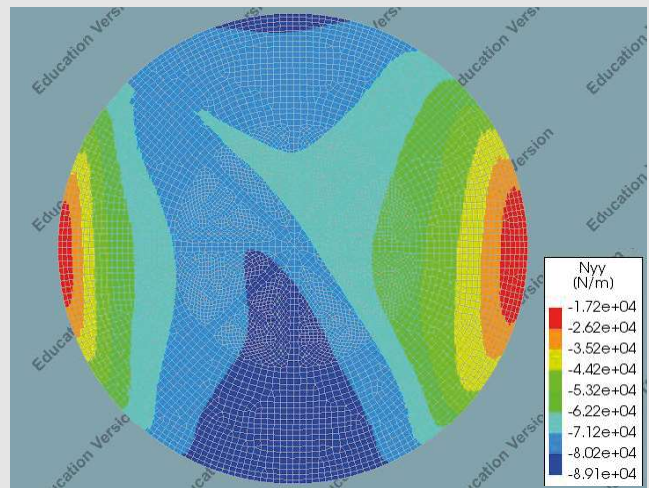
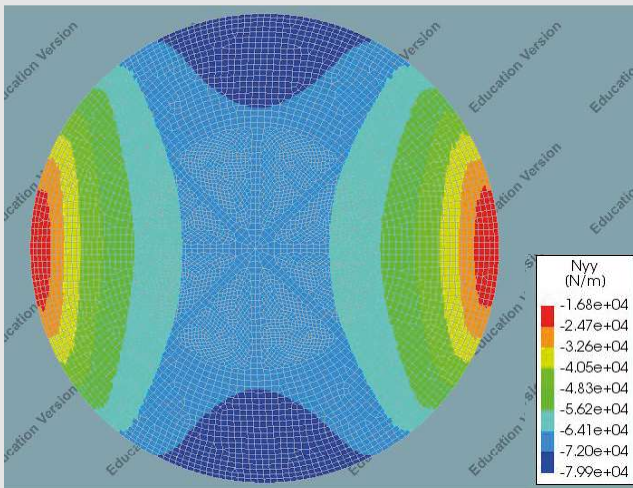
LOAD-CASE 1: SELF-WEIGHT
(symmetrical)



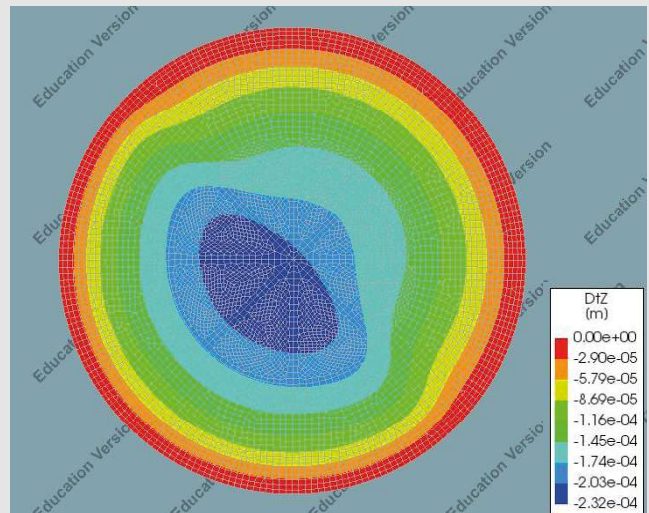
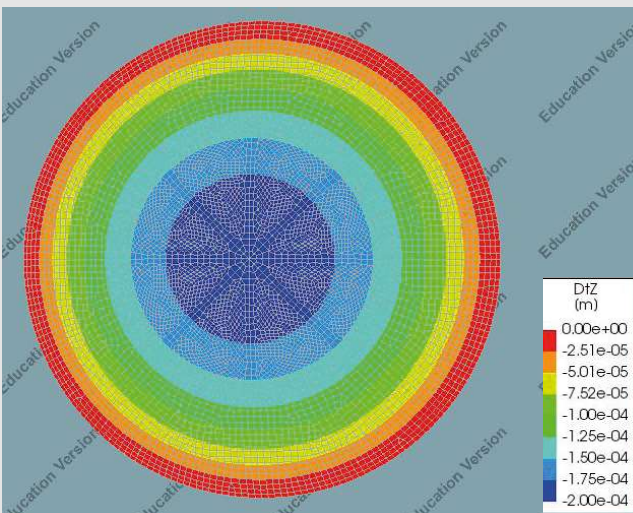
LOAD-CASE 2: SELF-WEIGHT+WIND
(asymmetrical)



Stress resultants arch direction (Nxx)

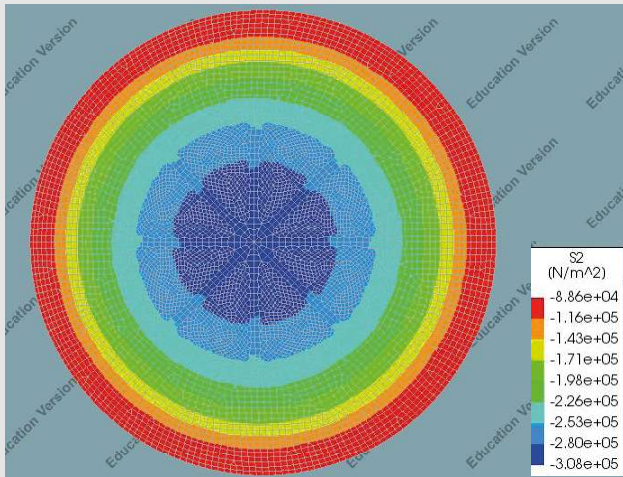


Stress resultants ring direction (Nyy)

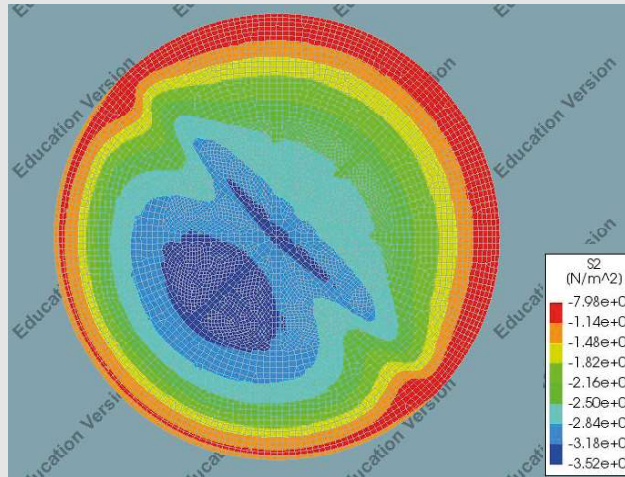


Displacement in z-direction

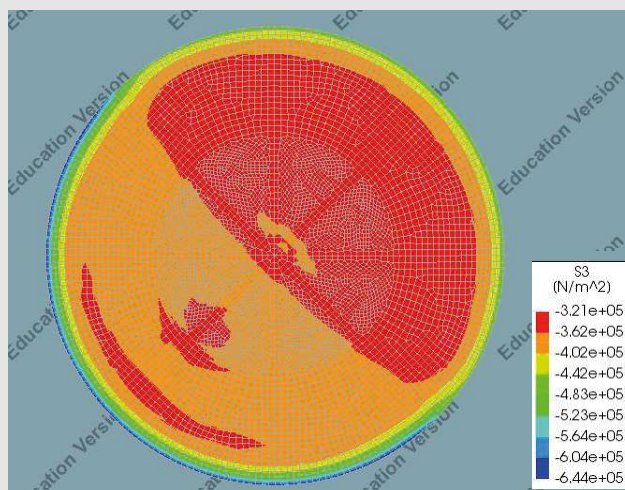
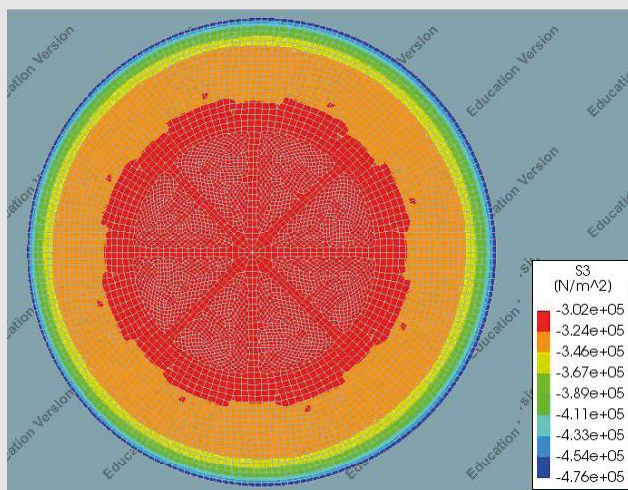
LOAD-CASE 1: SELF-WEIGHT
(symmetrical)



LOAD-CASE 2: SELF-WEIGHT+WIND
(asymmetrical)



Minimum principle stress S2



Maximum principle stress S3

Figure 212. Results of the Diana model

Conclusion

This chapter focussed on the validation of the following assumptions made in the chapter 'analytical stress analysis':

- The dome structure will form a pure compressive structure under its self-weight.
- External loads, such as wind and snow, are from the same order as the stresses resulting from the self-weight.
- Local stresses at the base on one component are in compression for both load cases and will not exceed the maximum strength of the component and interlayer.

First, the simplified Diana model of the glass dome proved that the glass dome structure ensures a **pure compressive structure** when subjected to its self-weight or asymmetrical loads, such as wind. This is because the membrane forces are in compression for both load cases, which is a result the shallow dome design.

Secondly, external loads from wind will lead to stress resultants and displacements in z-direction that may be described as results that are from the same order as load case 1: self-weight. This is because the difference between the stress resultants and displacement in z-direction between the two load cases is rather small.

Thirdly, the maximum local stress on one component is a compressive stress and does not exceed the compressive strength of the glass interlayer. It should be noted that in the real dome design the principle stresses probably would be higher since the components do not have a full contact area. It is concluded that even when the maximum principle stress is multiplied with a safety factor of 2, the local compressive stress does not exceeds the compressive strength of the interlayer.

Finally it is concluded that the Diana model validates the analytical analysis, as shown in table 30. The stress resultants shown in the table show slight difference between the Diana and Hand calculations. The slight difference is easily explained since the hand calculations will not take in account all material properties, such as Poissons ratio and Young's modulus. Because of these reasons mentioned above it is assumed that the assumptions made in the chapter analytical analysis are validated.

Stress resultants (N/m *e^4)				
direction		Diana	Hand	Diana
		LC 1 (Sym)	LC 1 (Sym)	LC2 (Asym)
Ring	top	-6,41	-6,86	-7,12
	base	-1,68	-1,67	-1,72
Arch	top	-6,41	-6,86	-7,12
	base	-7,99	-8,04	-8,92

Table 30. Stress resultants obtained from both analytical and numerical analyses

4.1.4 Experimental analysis

Introduction

The aim of the experimental analysis is to gain fundamental insight in the structural behaviour of the interlock system in most crucial direction, which is the arch direction. Because of this above mentioned aim the experimental analysis focuses on a physical arch test with a qualitative research. The arch model is a scale model of the real dome and has a scale of approximately 1:60. The glass components made from gypsum have a scale of 1:4 and do not contain the ring interlock since the test will focus on the arch interlock. It should be noted that the inner sphere of the real component is scaled to 1:4, however the scale of the arch equals 1:60 which will lead to a different size of outer sphere. Hence, latter mentioned scale difference will in general result in larger components with a bigger rotation angle due to the increased curvature.

This chapter explains the test set-up, results and observations. Finally, this chapter ends with a conclusion about the interlock in the arch direction.

Test set-up

The test set-up is shown in figure 213 and include the following building elements:

1. Gypsum components

The glass components for the physical arch test are made from gypsum 3D prints. A 3D printer was utilized to create accurate components with a precise contact area. The material gypsum was chosen as test material due to its brittle behaviour which equals glass. Note that in reality the gypsum prints will behave slightly different regarding their structural performance. This is easily explained because gypsum has a lower tensile and compressive strength. The different characteristics of the gypsum components will result in a smaller overall structural performance in comparison with glass.

2. Interlayer

An interlayer of 1 mm PU was chosen as a suitable material for the physical arch test. The interlayer was roughly cut in small pieces and extended the contact area in ring direction during the test. The extended interlayer in ring direction is not a problem since interlock of the arch direction was tested.

3. PLA 3D prints

PLA 3D prints were used and functioned as support structures to fix the gypsum components.

4. MDF structure

The MDF structure consists of two parts, as shown in figure 213. The first part consists of 4 MDF arches, where two arches will fix the inner spheres and the other two will fix the outer spheres. These wooden arches functioned as ring forces, in the real dome design the components in ring direction will ensure a rigid structure. It should be noted that since the MDF structure was hand made the structure did not perfectly fit. However, during the test it was opted that this was not a problem since the arch was stable under its self-weight and the applied point load, which is a result of the sufficient arch interlock.

The second MDF structure functions as a base support and prevents the system from lateral forces and displacements. The second MDF structure was constructed from glue and nails.

Appendix 2 provides photos of the construction process of the physical arch.

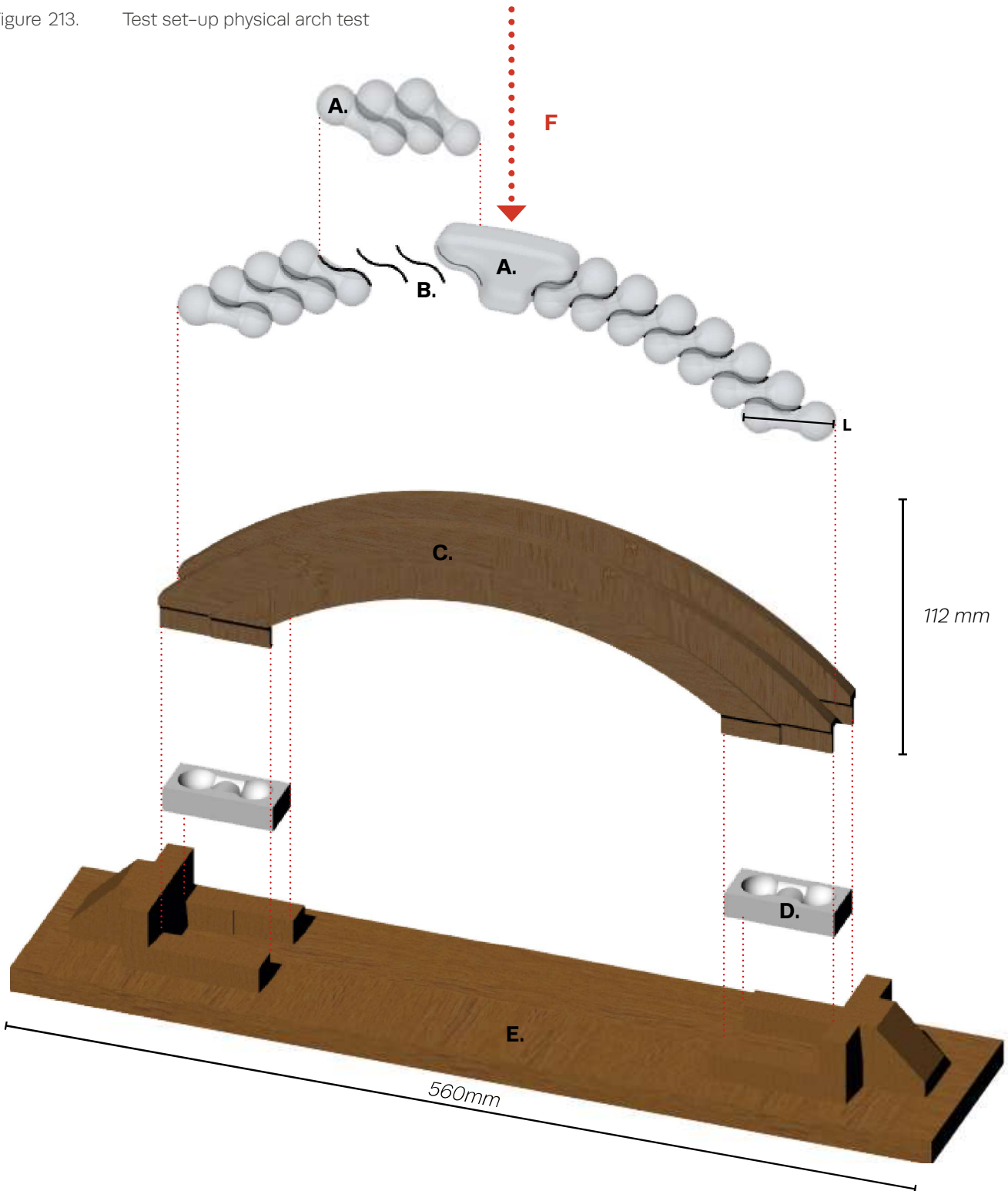
Load and equipment

The test was performed at the Material Science faculty under guidance of Fred Veer. A high precision pressure bench of 100 ton was used to control the strength during the test, where a point load was applied at the top of the oculus during the test. It should be noted that an asymmetrical load-case would have been more interesting. This research focused on a rather simple test set-up, since an asymmetrical load case requires a more complex test and model.

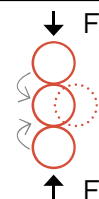
PHYSICAL MODEL: VALIDATION ARCH INTERLOCK

Goal: test structural performance of the arch interlock

Figure 213. Test set-up physical arch test



- A. Gypsum 3D prints, length (L) of ~ 57 mm.
- B. Interlayer of 1 mm PU
- C. MDF support structure, ensure the ring forces. →
- D. PLA 3D prints.
- E. MDF, base support structure against lateral forces and displacements.



Test observations

The figures 214–217 present the observations during the test and an explanation is given below:

- The maximum standard force carried by the arch equals 53N = 5,3kg.
- The first deformation drop (red dot in figure 218) was observed during the test as an audible crack, the components 3 and 12 move upwards and caused the deformation. The deformations followed were caused again by the upward movement of the components 3 and 12.
- The interlayer located on top of component 2 was moved sideways, this effect is caused by component 3, because the stresses onto interlayer 2 increase during the test due to the upward movement of component 3.

OBSERVATIONS DURING THE PHYSICAL ARCH TEST

1

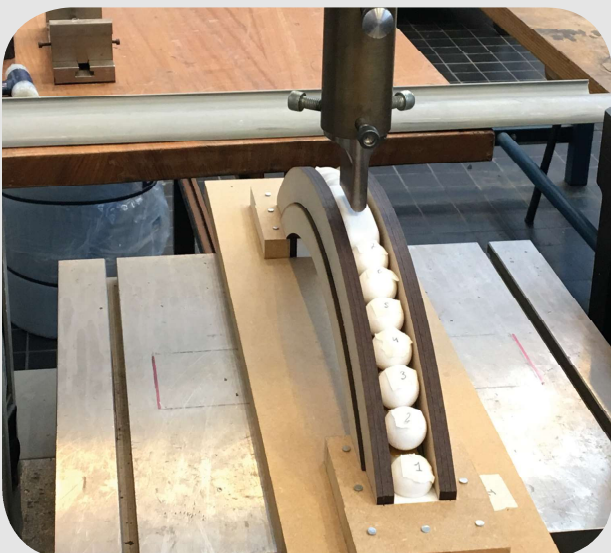
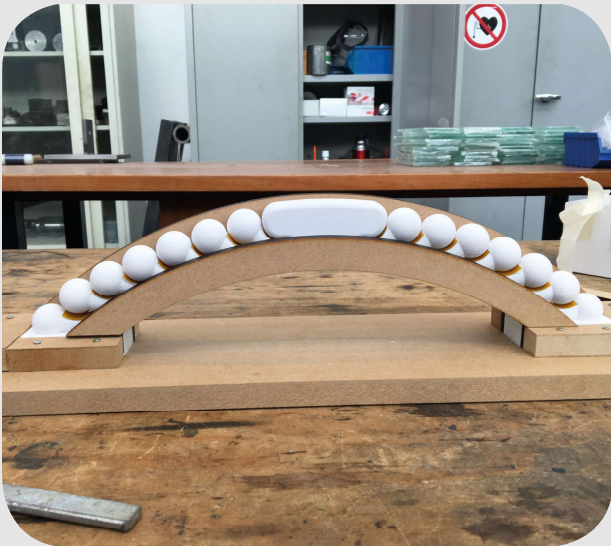
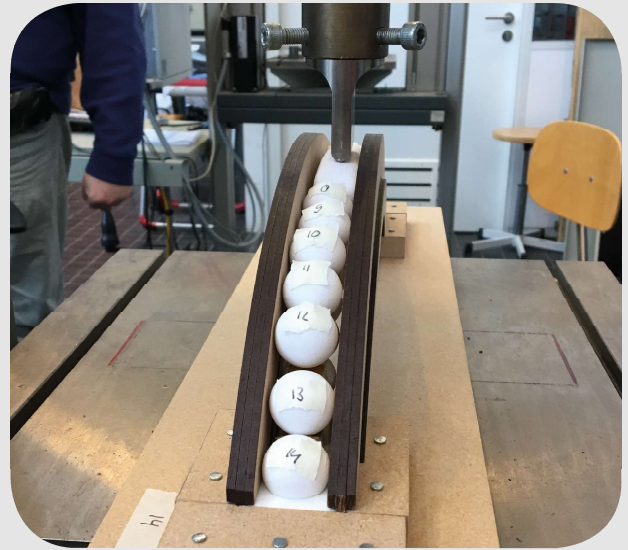


Figure 214. Test set-up physical arch test



② Figure 215. Component 3 and 12 are pushed upwards, this effect increases during the test



③ Figure 216. Increment of the upward movement at components 3 and 12



④ Figure 217. Observation of displacement during the test (audible cracks).

Final results and conclusion

The figures 218 and 219 show the final results of the test. The first conclusion was made before execution of the physical arch test. During the building process of the physical arch it was concluded that the dome requires a **compressive ring** at the oculus of the glass dome. The self-weight of the components does not create the required compression onto the next components, hence does not cause a full interlock. This effect, of not using a compression ring, was shown in the physical arch model at the components 3 and 12. The components 3 and 12 already had an upward movement before the physical arch test was performed.

Secondly, the physical arch model is a simplification of the entire dome design and constructed by hand, this caused two imperfections. The first imperfection is the distance between component 1 and 14 which is not precise enough to construct the perfect arch and related interlock. Secondly, the components of the entire dome design are held together by the action of membrane forces: hoop and meridional forces. However, the physical arch model focuses on the most crucial direction, which is the meridional (arch) direction. The physical arch is not inclined by real hoop forces and will result in a reduced overall strength. The components of the physical arch are made from 3D gypsum prints. Gypsum is chosen to mimic the main characteristic of glass: brittle material. However, gypsum has a lower density of 2,3 g/cm³, in comparison with glass (2,5 g/cm³) and therefore it is assumed that the gypsum components are pushed upwards way earlier than the real glass components.

Finally, the physical arch test was performed to gain insight in the structural behaviour of the interlock of the glass components in most crucial direction: meridional/ arch direction. It is concluded that the interlock in the arch direction is sufficient for an arch which is subjected to a centre point load of <53N. The physical arch test has proved that the arch interlock causes a **redundant system** because when the maximum load is applied the components will give a warning sign before the entire structure collapse. The warning sign equals a deformed arch with coherent connection, which is caused by the sufficient arch interlock. It is very important that the arch interlock will create a redundant system because the visitors and Lori parrots need to leave the glass dome safely. In addition, the warning sign gives the opportunity to minimize the damage because actions can be taken to repair the structure.

The interlayer could have caused unbroken components since a resilient interlayer (PU) was used which absorbs peak stresses and provides distributed stresses onto the next component.

Note that further investigation and experiments are required to gain fundamental knowledge about the structural behaviour of the real glass dome components.

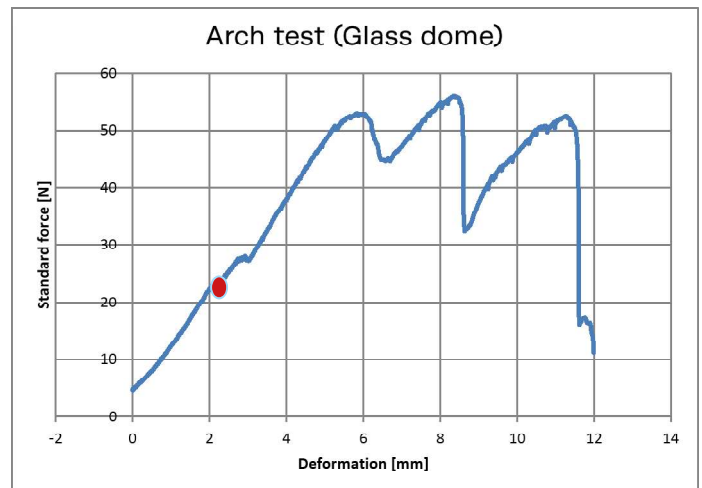
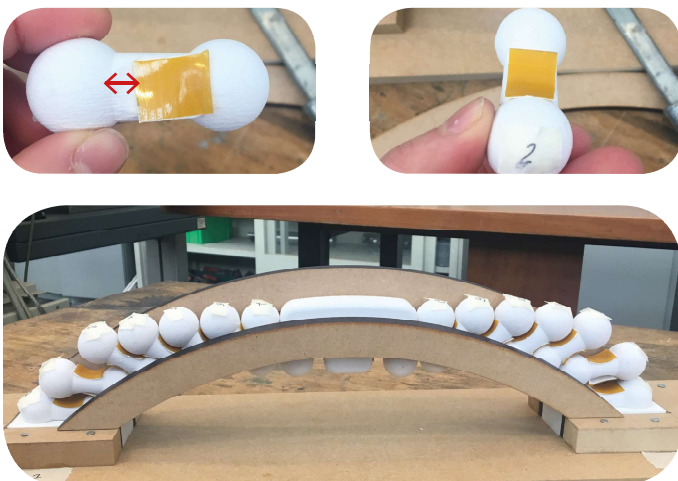


Figure 219. (top) displacement of interlayer, (bottom) total displacement showing the redundant system

Figure 218. Graph of the applied force and associated displacement

4.1.5 Conclusion

Mentioned in the introduction of this chapter, the structural validation is based on a simplified glass dome design, where for both numerical and analytical analyses a shallow dome with uniform thickness model was created. Experimental analysis was performed to obtain insight in the structural performance of the arch interlock in the most crucial direction. Hence, a simplified component without the ring interlock was designed and used as a component of the physical arch test. These above mentioned simplifications were required because the real glass dome is constructed from omnidirectional components with a complex geometry. It is assumed that even complex simulations will not result in accurate results. In order to validate the real dome design 'real' experiments should be performed, i.e. a scale model of the glass dome design with the cast glass components.

This chapter defined the stress resultants for the glass dome for both analytical and numerical analyses. From these analyses is concluded that the simplified **glass dome design is in pure compression** for both load-cases: self-weight (symmetrical) and self-weight + wind load (asymmetrical). It is concluded that the self-weight load case is dominant and external loads will be in the same order of magnitude. This was concluded from the small differences of the numerical and analytical analyses for both load cases. Note that the locations of the stress resultants is different for both load-cases, which is caused by the different line of thrust. And it is concluded that the maximum local compressive principle stress (located at the base) does not exceed the compressive strength of the glass component or interlayer, even when this principle stress is multiplied with a safety factor of 2.

The stiffness of the entire system (glass components+interlayers) equals: **55,1Gpa**. The stiffness is derived from the maximum interlayer thickness (t_1) and young modulus (E_1) and glass component thickness(t_2) and young-modulus(E_2). It should be noted that the stiffness of the real entire dome system is higher than the calculated previous value. The maximum interlayer thickness of 12mm is used for the calculation of the weighted mean because this results in the minimal stiffness, or the so called worst case scenario where most stresses are absorbed by the interlayer. In reality, the interlayer thickness varies in every horizontal section and is equal to 2mm in the arch direction.

From the performed **interlayer** selection is concluded that **TPU** could function as a suitable interlayer. The selection is based on material and manufacturing requirements where most important requirement equals the interlayer stiffness/thickness ratio:

$$E_{int}/t_{int} \leq 20/(2*0,25) \leq 40 \text{ N/mm}^3,$$

Resulting in an interlayer stiffness range of:

$$0,03 \text{ GPa} \leq E_{int} \leq 0,48 \text{ GPa}$$

This above mentioned requirement is set to ensure homogeneous loading and to prevent peak stresses from local protrusions. It should be noted that the temperature dependent behaviour, time dependent behaviour and effect of the interlayer thickness on elasticity modulus of the real dome design is not calculated. Hence, the stiffness interval is based on the literature of the Glass bridge.

The experimental analysis has shown that the **arch interlock is sufficient** for an arch which is subjected to a point load of <53N. The arch interlock caused a **redundant system** because the components gave warning sign before the entire structure collapsed. The interlayer could have cause unbroken components since a resilient interlayer (PU) was utilized.

Finally, the structural validation has proved that the simplified glass dome design has a **pure compressive redundant system**, where an interlayer of **TPU** deals with the local protrusions and ensures homogeneous loading.

4.2 Thermal validation

4.2.1 Introduction

The Design Builder energy software was used to perform accurate thermal calculations. Within this software a Design Builder model was created which is a simplification of the real dome design. The Design Builder model is simple and consists of a glass dome shell with uniform thickness and concrete basement. Creating thermal comfort in the interior of the glass dome is not simple because the glass dome and warm environment of Villars Les Dombes will increase overheating risk in the interior during summer. Hand calculations were performed before thermal simulations were run. These hand calculations predict and determine the natural ventilation rate and are presented in the first chapter. Secondly, the input and output data of the thermal calculations are addressed and analysed. The analysis of the thermal calculations will present the effectiveness of the passive strategies.

4.2.2 Natural ventilation rate

Stack ventilation is used to ensure an air flow in the interior of the glass dome. The earth ducts cause stack effect because a large temperature difference will occur between the inlet and outlet opening due to heat exchange with soil. Stack effect is further enhanced by the large height difference between the two openings, which equals 9,5m. This chapter provides an estimation of the ventilation rate (n) caused by stack ventilation. These estimations are based on hand calculations where formulas 8–11 were used:

$$n=Q/V \quad (8)^{[26]}$$

The air flow through an orifice can be calculated from equation 9:

$$Q = Cd \cdot A_{eff} \cdot \sqrt{(2\Delta P/\rho)} \quad (9)^{[26]}$$

$$\Delta P = gh \cdot (P/R) \cdot (1/T_{out} - 1/T_{in}) \quad (10)^{[26]}$$

The atmosphere pressure above sea level can be calculated from equation 11:

$$P = P_0 \cdot (1 - 2,25577 \cdot 10^{-5} \cdot h)^{5,25588} \quad (11)^{[27]}$$

The incoming fresh air is pre-heated or pre-cooled by **six earth ducts** located underneath the base structure of the glass dome. Concerning Yoshida, Zheng and Pan (n.d.) it is important to consider the temperature difference between the inlet and outlet temperature of the earth duct to assess the ventilation of large enclosures. Many simulations models were developed to determine this temperature difference, e.g. studies from Mei (1991), Benkert (1997), Mihalakakou (1994) and Yoon (2006)^[28]. These simulations are complex and the including dimensions of the earth tube

are beyond the scope of this research. In reality the outlet temperature of the earth ducts should be calculated from the calculation of ATEHE (air-to heat exchanger). According to Yoon (2006), the outlet air temperature of the earth duct during summer decreases 4°C and rises 2°C during winter and these values are used for this research. Latter assumption is made because the literature of Yoon (2009) is based on a design method for earth-to-air heat exchanger systems which consist of multiple pipes with a close arrangement, which is similar to the earth ducts for the glass dome design.

Extreme temperatures and assumptions were used for estimation of the natural ventilation rate. The extreme summer temperature equals 35°C and the extreme winter temperature equals -5°C. Other used assumptions are:

- The incoming fresh summer air, obtained from the outlet of the earth tube, increases as it reaches the oculus. It is assumed that an outdoor temperature of 35°C leaves the oculus with a temperature of 40°C. The temperature difference between the inlet and outlet temperature equals then 40–31 = 9°C. This principle is shown in figure 220.
- The coldest day in winter is used for determination of the natural ventilation rate in winter situation. The coldest day in winter has a temperature of -5°C. Natural ventilation is needed during the occupancy hours and non-occupancy hours because the glass dome functions as an aviary. During the occupancy hours an interior temperature of 19°C is required while during the non-occupancy hours an interior temperature of 18°C is required.

- It is assumed that Lori parrots are comfortable within equal environments as humans.
- The ventilation rate is assessed by the maximum designed surface area of the opening which is obtained from CAD and Rhino drawings. The maximum surface area is equal to the dimensions of the oculus because the glass components should stay intact. The total surface area is equal to 10,6m², obtained from the radius of the oculus (Ro), where $A_{max} = \pi R_o^2$.

The assumptions and formulas mentioned above are used as input data for an estimation of the natural ventilation rate and are given in table 31. Hand calculations were performed and are distinguished into two parts: the summer and winter situation. These hand calculations are shown on next page.

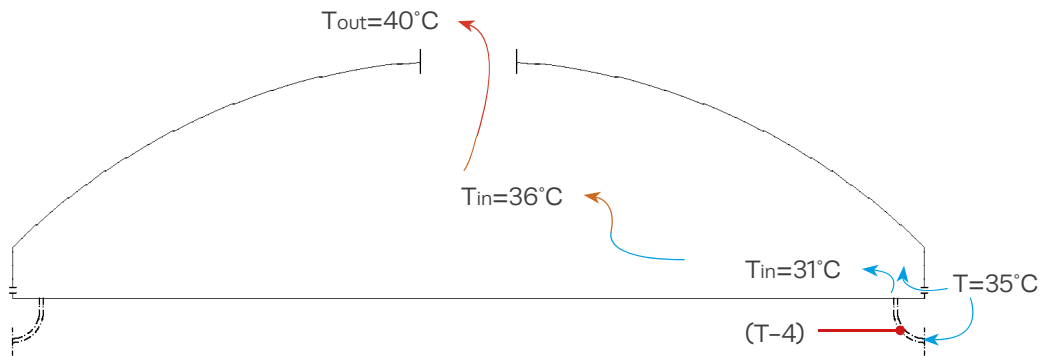


Figure 220. Schematic principle of pre-heated inlet air and increased outlet temperature.

Constants				
Index	What	Value	Unit	
Cd	coefficient of discharge	0,6	/	
p	density air	1,2	kg/m ³	
g	gravitational acceleration	9,81	m/s ²	
R	gas constant air	287	J/kgK	
P	atmospheric pressure above sea level	101325	Pa	
a	altitude Parc des Oiseaux	278	m	
Dimensions dome				
Index	What	Value	Unit	
A	area of openings	10,6	m ²	
h	height difference between openings	9,5	m ²	
V	Entire volume glass dome design	6037	m ³	
Temperature				
When	Outdoor (°C)	Indoor (°C)	Inlet/outlet earth duct (°C)	Outlet (°C)
summer*	35	30	31	40
winLer**	-5	19	-3	19
winter***	-5	18	-3	18
* during occupancy & non-occupancy hours				
** during occupancy hours				
** during non-occupancy hours				

Table 31. Input data for estimation of the natural ventilation rate

[26] Bokel, 2017

[27] <https://www.engineeringtoolbox.com>

[28] "Mei (1991) proposed a simulation model based on heat transfer balance at the earth tube, taking into account changes in the soil temperature, physical properties of the soil, tube material, fluid nature and time. By analysing the transmission model of various heat mediums, Benkert (1997) proposed the GATE model in which air temperature in the length direction along the tubes can be calculated with a high level of accuracy. Mihalakakou (1994) proposed a model by which length, radius, air wind speed and depth of the tube underground could be considered at the same time, and proposed a total performance calculation of ATEHE (air-to-earth heat exchanger). Yoon (2006) developed the simulation model of heat and moisture movement between tube and soil and verified it with measurements" (Yoshida, n.d., p.4).

Analytical analysis ventilation rate

Summer situation

The natural ventilation rate during summer for the **(non)occupancy** is:

$$P = 101325 * (1 - 2,25577 * 10^{-5} * 278)^{5,2588} = \mathbf{98028 \text{ Pa}}$$

$$\Delta P = 9,81 * 9,5 * \left(\frac{98028}{287}\right) * \left(\frac{1}{313} - \frac{1}{304}\right) = \mathbf{-3,0 \text{ Pa}}$$

$$Q_s = 0,6 * 10,6 * \sqrt{\frac{2 * 3}{1,2}} * 3600 = \mathbf{51197 \frac{m^3}{h}}$$

$$n_s = \frac{51197}{6037} = \mathbf{8,5 \text{ h}^{-1}}$$

Winter situation

The natural ventilation rate during winter for the **occupancy hours** is:

$$\Delta P = 9,81 * 9,5 * \left(\frac{98028}{287}\right) * \left(\frac{1}{292} - \frac{1}{270}\right) = \mathbf{-8,9 \text{ Pa}}$$

$$Q_{w,o} = 0,6 * 10,6 * \sqrt{\frac{2 * 8,9}{1,2}} * 3600 = \mathbf{88182 \frac{m^3}{h}}$$

$$n_{w,o} = \frac{88182}{6037} = \mathbf{14,6 \text{ h}^{-1}}$$

The natural ventilation rate during winter for the **non-occupancy hours** is:

$$\Delta P = 9,81 * 9,5 * \left(\frac{98028}{287}\right) * \left(\frac{1}{291} - \frac{1}{270}\right) = \mathbf{-8,5 \text{ Pa}}$$

$$Q_{w,n} = 0,6 * 10,6 * \sqrt{\frac{2 * 8,5}{1,2}} * 3600 = \mathbf{86177 \frac{m^3}{h}}$$

$$n_{w,o} = \frac{86177}{6037} = \mathbf{14,2 \text{ h}^{-1}}$$

Optimization ventilation rate

The analytical analysis of the ventilation rate shows high ventilation rates for summer and winter situation. This sub-chapter proves that these high ventilation rates exceed the minimum and maximum ventilation rate and presents the new dimensions of the ventilation opening. The old dimensions of the opening is reduced till the required ventilation rate is reached.

The minimum ventilation rate depends on the occupancy rate and required airflow rate per person. The required airflow rate per Lori parrot is not taken in account because of the made assumption that Lori parrots are comfortable in equal environments as humans. In this research it is assumed that the occupancy rate of the glass dome equals 100 people, where 1 person requires an airflow rate of 35 m³/h. The maximum ventilation rate depends on the required air velocity, where the required air velocity is equal to ≤ 0,5 m/s. This is due to the fact that air velocities of ≤ 0,5 m/s are indicated by humans as pleasant till unnoticed air velocities.

The **minimum ventilation rate** equals:

$$Q = 100 * 35 = 3500 \frac{m^3}{h}$$

$$n = \frac{3500}{6037} = 0,6 \text{ h}^{-1}$$

Conclusion

From both sub-chapters: 'analytical analysis of the ventilation rate' and 'optimization ventilation rate', is concluded that the calculated natural ventilation rates exceed the minimum and maximum ventilation rate: 8,5;14,2;14,6 > 0,6;2 h⁻¹. The area of the ventilation opening is reduced to reach the minimum and maximum ventilation rate. This research proposes **adjustable openings**, with a maximum area of **9,3m²**, and **earth duct dampers** to control the natural ventilation rate during the day (occupancy and non-occupancy hours) and season. A controlled natural ventilation rate is required to respond to the number of visitors and different natural ventilation rate during summer and winter. The natural ventilation rate has the following range: **0,6–2h⁻¹** and is explained in more detail in the next chapter.

The minimum temperature difference and maximum ventilation rate are used to determine the area of the opening. This is shown in equation 12, where a small temperature difference and a large ventilation rate require a large opening. It is beneficial to create a higher air velocity during summer, with a higher ventilation rate in order to create a slight breeze. This research proposes to use a **maximum ventilation rate** of **2 h⁻¹** which will cause a slight breeze. Note that the air velocity cannot exceed 0,5 m/s because this will create discomfort as shown in equation 13.

$$A = \frac{n \cdot V}{C_d \cdot 3600} * \sqrt{\frac{p}{2 \Delta p}} = m^2 \quad (12)$$

$$v = \frac{n \cdot V}{A \cdot 3600} \leq 0,5 \text{ m/s} \quad (13)$$

It is assumed that the minimum temperature difference occurs when the outdoor temperature is equal to 25°C and the indoor thermal comfort temperature equals 25,6°C, resulting in a temperature difference of 0,6°C. Using equation 12 this results in an opening area of:

$$\Delta P = 9,81 * 9,5 * \left(\frac{98028}{287}\right) * \left(\frac{1}{299} - \frac{1}{298}\right) = -0,21 \text{ Pa}$$

$$A = \frac{2 * 6037}{0,6 * 3600} * \sqrt{\frac{1,2}{2 * 0,21}} = 9,3 \text{ m}^2$$

And an air velocity of:

$$v = \frac{2 * 6037}{9,3 * 3600} = 0,4 \text{ m/s} \leq 0,5 \text{ m/s}$$

4.2.3 Input data Design Builder

Introduction

This chapter defines the input data of the Design Builder model for executing thermal simulations. The input data include the following aspects: **opening hours** of 'Parc des Oiseaux', **geometry**, **ventilation rate**, **materialization**, **thermal mass** and **weather file**. These aspects are explained in more detail below. The desired indoor temperatures are also part of the input data and can be found in the chapter: 'thermal performance'.

1. Opening hours

The zoological garden 'Parc des Oiseaux' closes during winter and is open from the 8th of April till the 12th of November. The Lori parrots are housed inside during winter and are not held in the aviary. The simulations will focus on providing thermal comfort from the **8th of April** till the **12th of November**^[29] because of last mentioned reason.

2. Geometry

The geometry of the Design Builder model is a simplification of the entire dome design and includes a dome with a uniform thickness of 0,22m and support structure with a wall thickness of 0,56m. The support structure is located below ground level: 2m-P. The thickness of the glass dome is obtained from the thickness of the glass components and the thickness of the support structure is obtained from structural analysis, as mentioned in the previous chapters.

Two **adjustable openings** of **9,3m²** are inserted in the geometry: one encircled at the base and one at the oculus. The adjustable openings and **six earth ducts** will ensure natural ventilation and are shown in figure 221.

3. Ventilation rate

The defined natural ventilation range equals **0,6–2 h⁻¹**. The minimum ventilation rate equals 0,6 h⁻¹ and during hot summer days a ventilation rate 2 h⁻¹ is preferred. Table 32 presents the scheduled ventilation scheme according the visiting and non-visiting hours during summer and fall season. The park closes during the winter and the glass dome remains sealed while the glass dome absorbs maximum solar energy.

The maximum ventilation rate of 2h⁻¹ is set for the summer and warmer fall days. This maximum ventilation rate is required during day and night time because of two reasons. During the day the ventilation rate causes a slight breeze which is beneficial for the visitors and Lori parrots. Secondly, the natural maximum ventilation rate enhances the effect of eliminating the stored solar energy by creating a larger convective stream during the night. Moreover a maximum ventilation rate during summer and warm fall days is required to create acceptable operative temperatures in the interior of the glass dome.

During the colder fall days a scheduled ventilation scheme is set which follows the occupancy rate

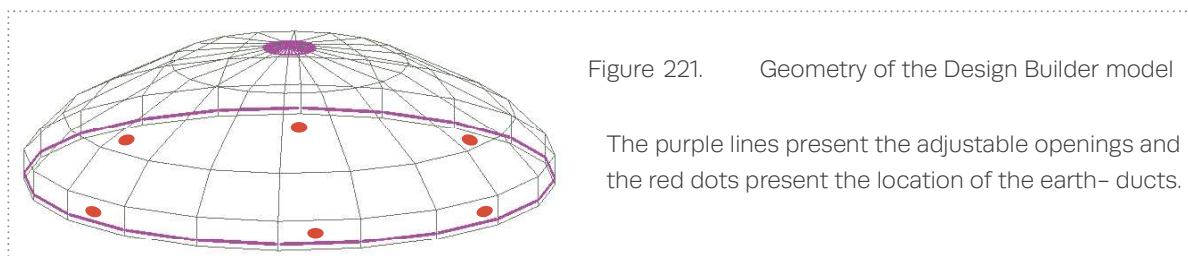


Figure 221. Geometry of the Design Builder model

The purple lines present the adjustable openings and the red dots present the location of the earth- ducts.

Schedule of the natural ventilation rate									
day-month	Time								
	07:00	08:00	09:00	12:00	14:00	17:00	18:00	19:00	0:00
08/04-30-09	2	2	2	2	2	2	2	2	2
01/10-12/11	0,6	0,95	1,3	1,65	2	1,65	1,3	0,95	0,6

Table 32. Scheduled ventilation rate scheme for the (non)-visiting hours during summer.

[29] <http://www.parcdesoiseaux.com>

and solar radiation during the day. The minimum ventilation rate is set during the morning to keep higher operative temperatures. The natural ventilation rate increases till 2 o'clock, at the time when most visitors are present and the solar radiation is maximal.

It should be noted that the ventilation schemes for the visiting and non-visiting hours are identical because of the made assumption that Lori parrots are comfortable under the same conditions as humans.

4. Materialization

The Design Builder model is materialized into two different models. The first model consists of a glass dome constructed from **soda-lime glass** with equal properties and a concrete basement with lost form-work insulation. The lost form-work insulation is translated in the Design Builder model as a layer of 100 mm of XPS. The second model differs from the first model because approximately **50%** of the glass surface is covered with a **white wash paint** as explained in the chapter 'thermal performance'. The surface properties of the different models are shown in table 33. The white wash paint is translated in the Design Builder model as a reduction of the visible and solar transmittance. This because white glass reflects short wavelengths, such as UV and visible light and does not absorb short and long wavelengths of the solar spectrum. The U-value is calculated from the material properties of soda-lime glass obtained from Ces EduPack (2017) and thickness of the glass dome.

A chalk based white wash paint (Eclipse F4 from Sudlac) is proposed which is biodegradable and will not harm nature^[30]. The **white wash paint** is applied each **summer** and is washed out through precipitation. Because of this latter mentioned reason it is assumed that the white wash paint is washed out at the beginning of October. This washed out effect through precipitation is beneficial because during the colder fall days a reduction in solar and visible transmittance is not required. A reduced solar and light transmittance will reduce the operative temperature while during colder fall days an increased operative temperature is preferred.

The glass surfaces which are not covered by a white wash paint have transmission factors which are based on the values of the Crystal house cast glass bricks. This latter mentioned assumption needs to be taken because a cast glass double curved structure has not been built before. The transmission values of the Crystal house cast glass bricks are shown in figure 222.

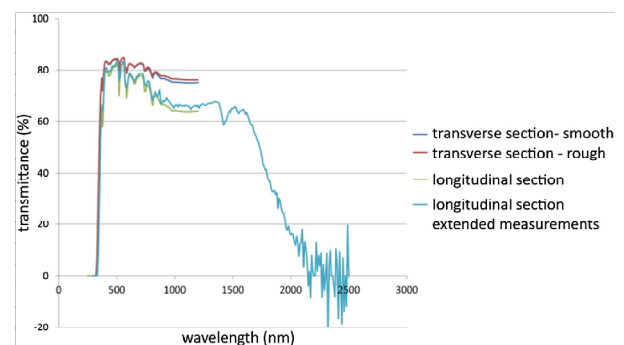


Figure 222. Optical transmittance data of the standard Poesia brick (Tijssen, 2014).

$$R = \frac{d}{\lambda} = \frac{0,22}{0,7} = 0,31 \frac{m^2 K}{W}$$

$$U = \frac{1}{R} = \frac{1}{0,31} = 3,2 \frac{W}{m^2 K}$$

Glass properties			
Type	Solar transmittance (SHGC)	Light transmittance	U-value
Model 1: 8th of April- 12th of November			
Soda-lime glass	0,75	0,8	3,2
Model 2a: 8th of April- 30th of September			
Soda-lime glass	0,75	0,8	3,2
White glass	0,1	0,15	3,2
Model 2a: 30th of September- 12th of November			
Soda-lime glass	0,75	0,8	3,2

Table 33. Properties of Soda-lime glass and white painted glass.

[30] <http://www.hortidaily.com>

5. Thermal mass

The internal thermal masses include **earth** (intensive vegetation) and **water** (drinking basins for the Lori parrots) and are inserted in the Design Builder model. These internal thermal masses are very useful during summer and reduce the high interior temperatures, because, especially for water, a high amount of solar energy can be stored within these internal masses.

An earth layer of 0,5m thick and water layer of 0,03m thick was inserted in the Design Builder model with a corresponding surface area of $\pi R_{dome}^2=1016m^2$, which equals the total surface area of the ground floor. The earth layer of 0,5m thick allows for intensive vegetation. In the real dome design, the water basins cover a surface area of 47m² and 107m² with a corresponding thickness of 0,2m. Figure 223 presents the floor plan with the location of the water basins. The exact location and thickness of the water basins could not be inserted in Design Builder because the Design Builder software uses one internal thermal mass input which is layer based.

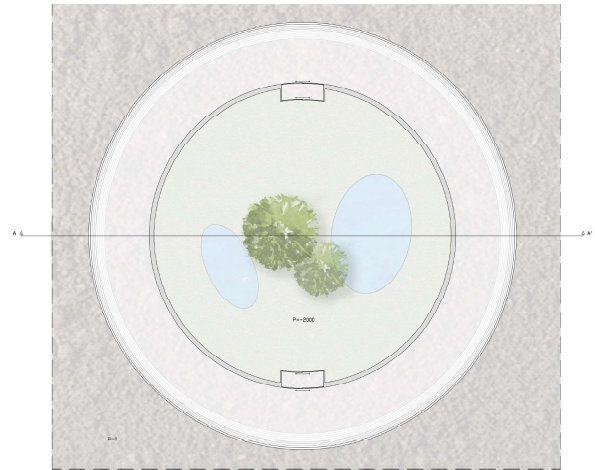


Figure 223. Floor plan of the glass dome with water basins (blue).

6. Weather file

The weather data from **Lyon Bron** was used to perform hourly weather simulations. Weather data from Villars Les Dombes could not be used due to the limited availability of the weather files within the Design Builder software. It is assumed that the weather data from Lyon Bron and Villars Les Dombes are similar because these two locations have almost the same longitude and latitude and the distance between these two locations is rather small: <40km. However, it should be noted that a different altitude results in a different air pressure, as shown in equation: $P = P_0 * (1 - 2,25577 * 10^{-5} * h)^{5,25588}$. The altitude of Villars Les Dombes was inserted in the Design Builder model to take in account the air pressure difference and equals 279,2m, this results in a height difference of $279,2 - 201,8 = 77,4m$.

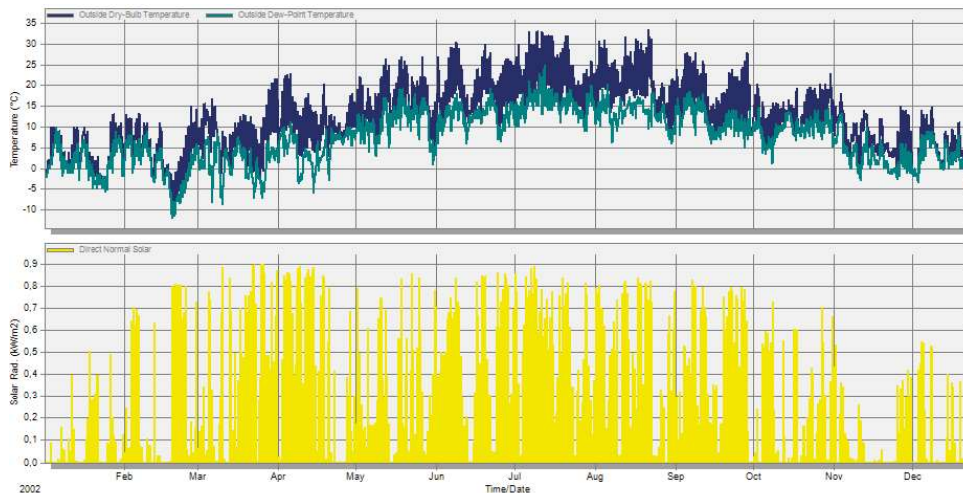


Figure 224. Site data of Lyn Bron: (top) outside dry bulb–temperature and outside dew–point temperature, (bottom) solar radiation.

4.2.4 Thermal simulation: passive design

Annual graphs

Two thermal simulations were performed to assess the efficiency of a solely passive design where no temperature margins were set. The difference between these two simulations expresses itself in materialization. The first one consists of model with a solely Soda-lime glass dome and the second simulation consists of a model where approximately 50% of the dome surface is covered by a white wash paint.

From annual graphs of the operative temperature in hourly interval was concluded that model 2 performs best in terms of creating an operative temperature range of 18–30°C (non-occupancy hours) and 19–30°C (occupancy hours). This is easily explained since the white wash paint reduces the solar and visible light absorption during summer, which results in a lower operative temperature. Secondly, the white wash paint is washed out at the beginning of October, which results in an increased operative temperature during the

colder fall days. From figure 226, annual graph of the operative temperature in hourly interval of model 2 with white wash paint, is concluded that the glass dome reaches its maximum operative temperature at 42,2°C, when the air temperature is 39,4°C and the radiant temperature equals 45,1°C. Secondly, it is concluded that the glass dome reaches its minimum operative temperature at 4,0°C, when the air temperature is 3,2°C and the radiant temperature equals 4,6°C.

Moreover, it can be concluded that the passive strategy of using white wash paint is very efficient since it drastically reduces the operative temperature during summer time and increases the operative temperature during colder fall days. When the white wash paint is not applied operative temperatures of above the 60°C could occur. Secondly the operative temperature never drops below 0°C and will not cause ice formation in the interior of the glass dome during the opening hours of 'Parc des Oiseaux': 8th of April till 12th of November. Finally, an active system, for both heating and cooling, is required to obtain the required operative temperature range.

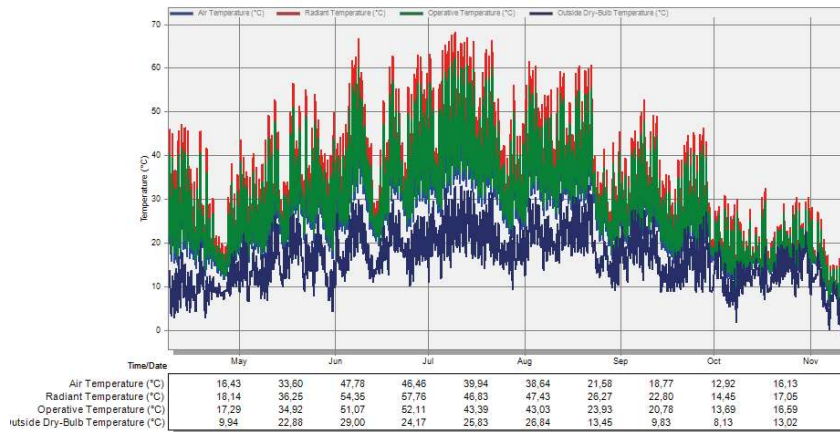


Figure 225. Annual graph of the operative temperature (green) in hourly intervals model 1 (without white wash)

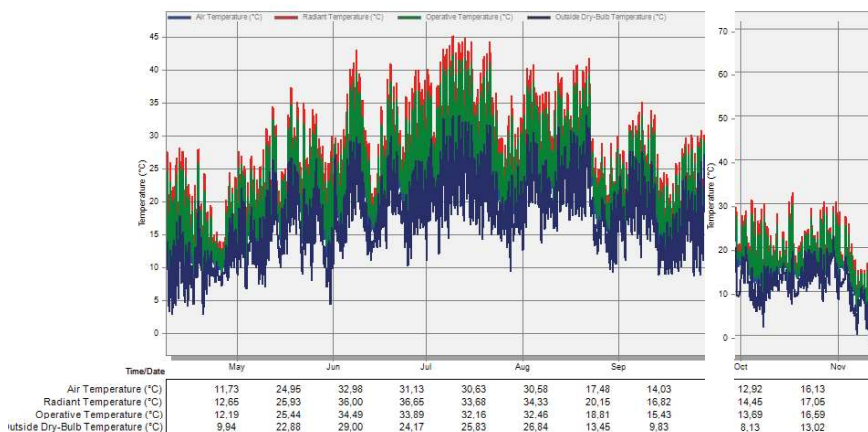


Figure 226. Annual graph of the operative temperature (green) in hourly intervals model 2 (with white wash)

Thermal simulations of model 2 of three days in July and three days in November are performed to gain fundamental knowledge about the operative temperature fluctuations during warm and cold days during the opening hours and are presented in figures 227–232.

Figure 227. Operative temperature (green) at 06/07

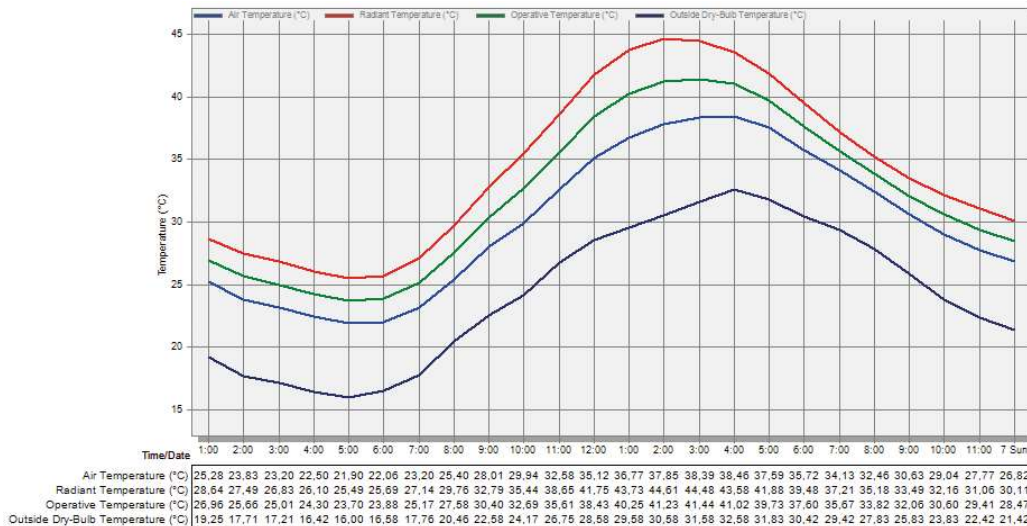


Figure 228. Operative temperature (green) at 07/07

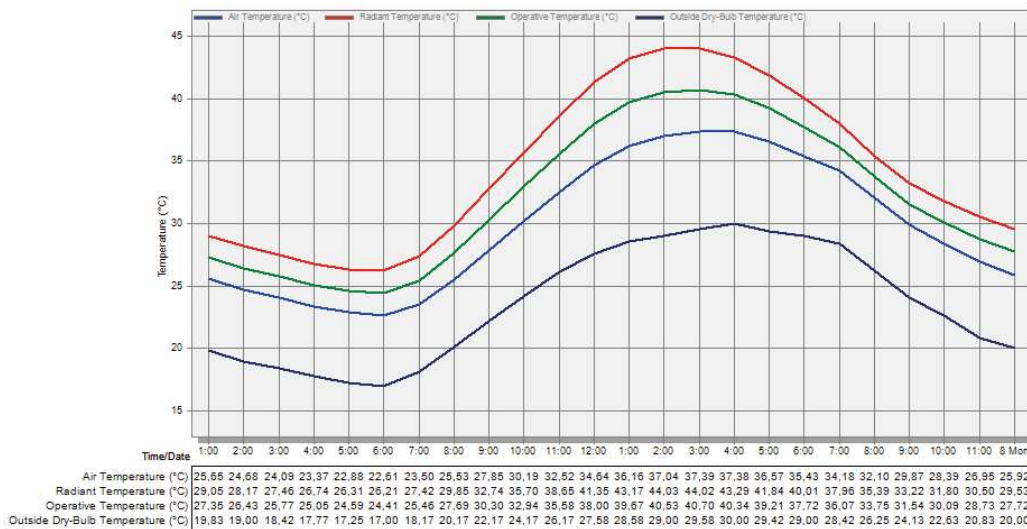


Figure 229. Operative temperature (green) at 08/07



Figure 230. Operative temperature (green) at 10/11

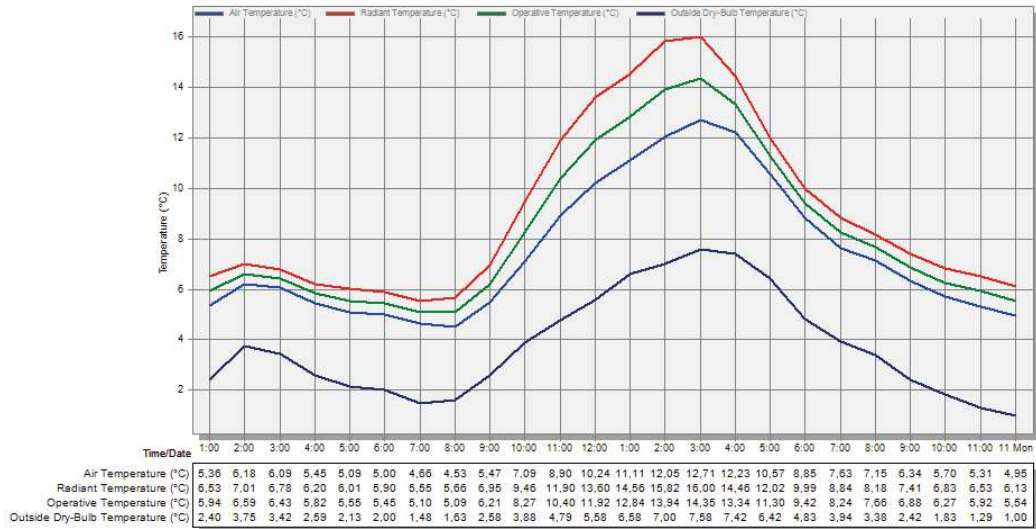


Figure 231. Operative temperature (green) at 11/11

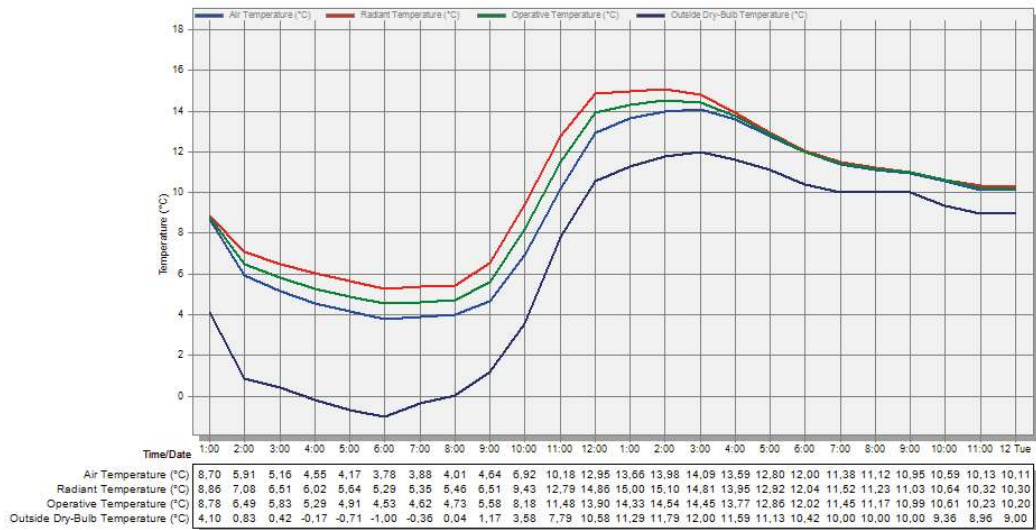
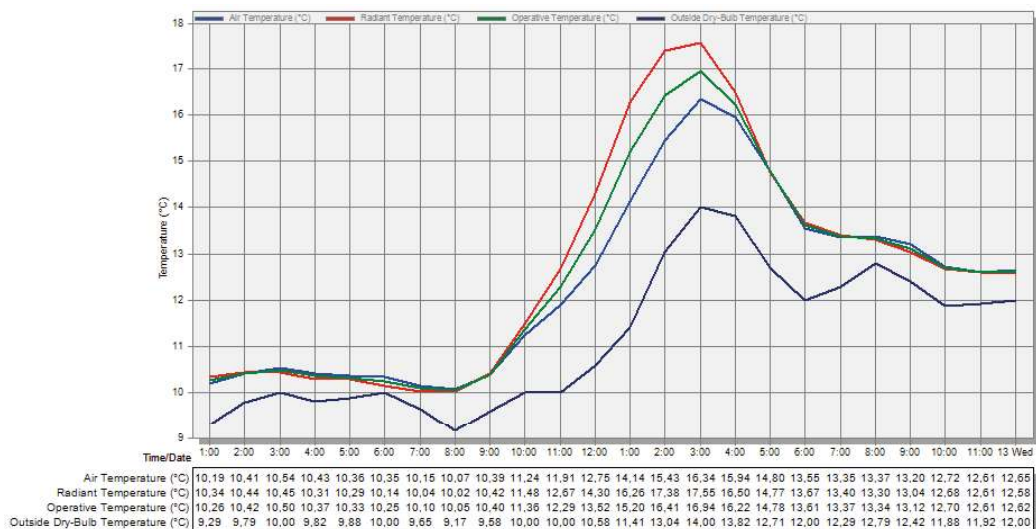


Figure 232. Operative temperature (green) at 12/11



Daily graphs

From the daily graphs of the operative temperature during three warm summer and three colder fall days it is concluded that the operative temperature is always warmer than the outside dry-bulb temperature.

The operative temperature is approximately 10°C higher than the outside dry-bulb temperature during summer.

The operative temperature has relative high values during the colder fall season at daytime which is caused by the high solar and light transmittance of the glass surface (because the white wash paint is washed out). The relative high operative temperatures during the colder fall season at night-time are caused by the effectiveness of the internal thermal masses. The internal thermal masses release the stored solar energy during the night which will result in increased operative temperatures.

Conclusion

From this sub-chapter it is concluded that the natural ventilation, internal thermal masses and white wash paint are efficient passive systems for reducing the overheating risk during hot summers days while absorbing solar energy during colder fall days.

However, the passive systems do not ensure full comfort because the entire operative temperature range does not lie in the range of 18–30°C (non-occupancy hours) and 19–30°C (occupancy hours). The temperature zones that do not lie within the last mentioned required range are shown in grey in figure 233. Additional active heating and cooling systems are required to achieve full thermal comfort in the interior of the glass dome. The active system acts as a heating system when operative temperature is < 18/19°C and acts as a cooling system when the operative temperature is > 30°C. Next chapter addresses the size of the additional mechanical heating/cooling unit.

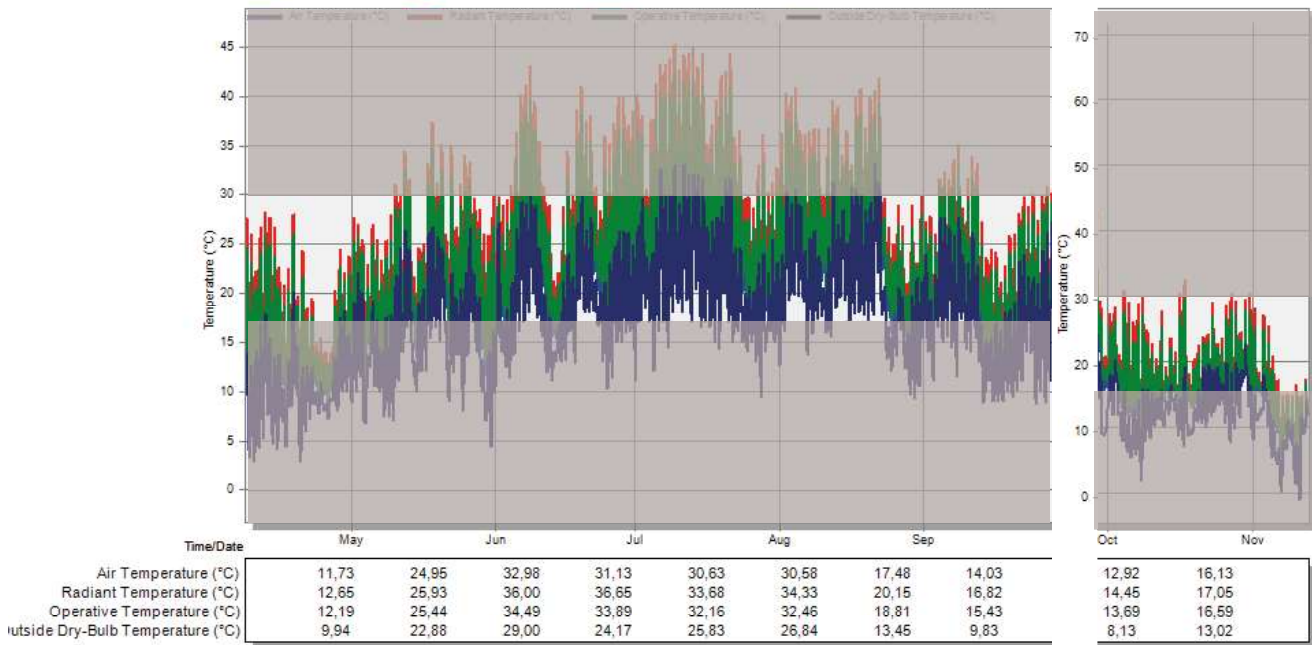


Figure 233. Annual graph of the operative temperature (green) in hourly intervals of the Soda-lime glass dome where white wash paint is applied from the 8th of April to 30th of September and white wash paint is washed out from the 1st of October to 12th of November. The grey parts present the temperatures <18/19°C where additional active heating or cooling systems are required.

4.2.5 Heating/cooling unit

Introduction

This chapter addresses the additional heating/cooling unit and provides thermal simulations to determine the size of the heating/cooling unit. This research proposes utilization of an air-to-water heat pump in combination with ventilation convectors, the so called fan coils. Other systems such as: heated floors or solar collectors are not preferred because heated floors cannot be utilized due to the soil upper layer and solar collectors will obstruct the view within the zoological garden 'Parc des Oiseaux'.

Air to water heat pump & fan coils

The air-to-water heat pump and fan coils function both as a heating and cooling system.

An air-to-water heat pump extracts energy from outside air and compresses the air to a higher temperature during the colder fall days. This heated air exchanges its heat with an enclosed water circuit through condensation, which ensures the distribution of hot water. This warm water pipe is located underneath the support structure of the glass dome where heat exchange takes place through air by utilization of fan coils. The fan coils will provide warm air to the interior of the glass dome where the operative temperature can be controlled by using a thermostat. This principle is shown in figure 234.

The above described process of the air-to-water heat pump and fan coils work reversed during warm summer days when it cool the interior of the glass dome. The outside air is expanded instead of compressed which causing a reduction in temperature.

Next, heat is absorbed (evaporator) instead of dissipated (condenser) causing a decreased temperature of the enclosed water circuit. Subsequently, the fan coils will provide colder air to the interior of the glass dome^[30].

The coefficient of performance (CoP) and cooling efficiency (EER) of the air to water heat pump depend on the temperature difference between the condenser and evaporator. Small temperature differences result in a high efficiency. The weather data of Design Builder and literature showed that Lyon Bron has a moderate climate resulting in an efficient air to water heat pump. This research assumes that the CoP is equal to 3,6 and the EER equals 2,6. Note that the real CoP and EER fluctuate during the day and season depend on other factors such as the type of air to water heat pump.

Finally, the air-to-water heat pump and fan coils can be included in the basement and will not obstruct the view within the zoological garden 'Parc des Oiseaux'.

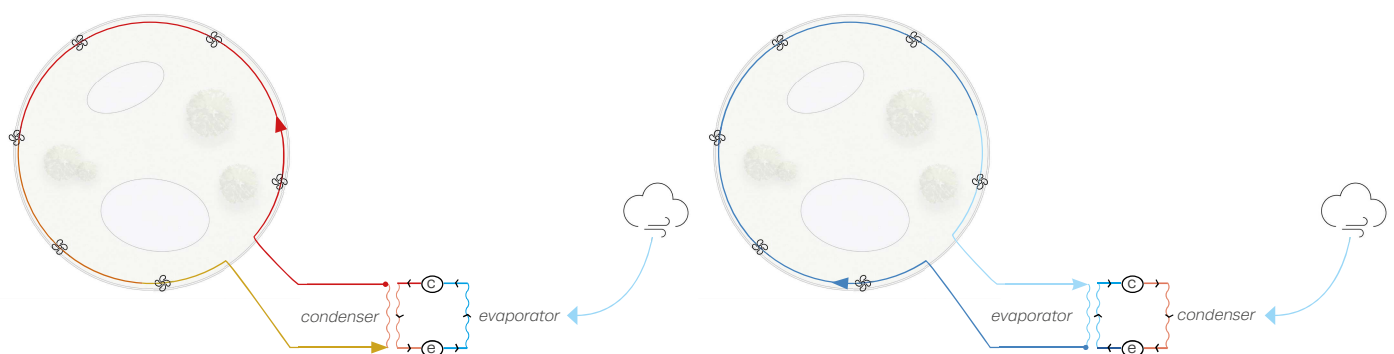


Figure 234. Scheme of the additional heating /cooling system: air to water heat pump and fan coils during summer (right) and fall season (left).

[30] <https://www.warmtepomp-info.nl>

Size of the heating unit

Temperature margins and heating and cooling setback temperatures were set for determination of the size of the mechanical heating/cooling unit. These temperature margins and heating and cooling setback temperatures are shown in table 34. The temperature margins are based on the required minimum and maximum comfort temperatures during occupancy hours. And the setback temperatures are based on the non-occupancy hour to create thermal comfort to the

Lori parrots when the 'Parc des Oiseaux' closes. Other input data for the Design Builder model includes the previous defined CoP value of 3,6 of the air-to-water heat pump unit with fan coils.

Temperature margins and setback temperatures		
	Margin	Setback
min	19°C	18°C
max	30°C	30°C

Table 34. Temperature margins and setback temperatures

Annual power demand graph

Figure 235 and 236 present the power demand of the air-to-water heat pump and fan coils during the non-visiting and visiting hours. The active system ensures a comfort range of 18–30°C (non-visiting hours) and 19–30°C (visiting hours). From these two graphs is concluded that the power demand for cooling is primary. The mechanical unit requires a maximum power demand for cooling of 171 kW and maximum power demand for heating of 135 kW. Moreover, the resulting power demand of the mechanical unit is calculated from the maximum power demand, CoP and EER and equals **171/2,6= 65,7kW for cooling** and **135/3,6=37,5kW for heating**.

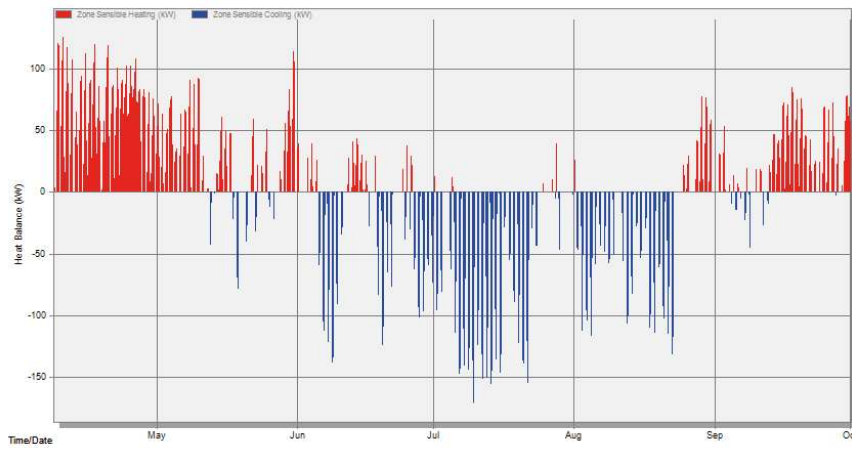


Figure 235. Sensible zone heating /cooling (kW) from the 8th of April to the 30th of September

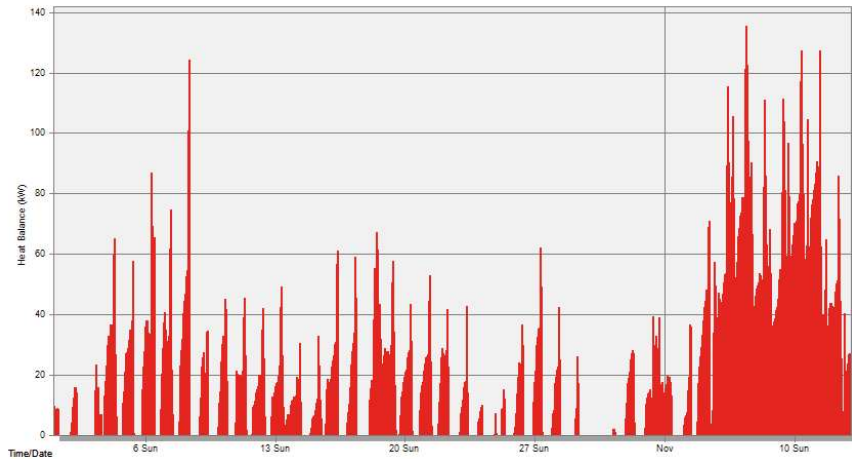


Figure 236. Sensible zone heating (kW) from the 1st of October to the 12th of November

4.2.6 Conclusion

From this chapter it is concluded that an efficient passive design for the glass dome consists of the following passive systems: adjustable openings, earth ducts ,internal thermal masses (water basins and soil) and glass surfaces which are covered with a white wash paint. The passive systems meet the main aim of this research because overheating risk during the majority of hot summer days is reduced and solar absorption is maximized during the colder fall days. The solar absorption is maximized during the colder fall days because it is assumed that the white wash paint is washed out at the beginning of October through precipitation.

Moreover, to obtain thermal comfort, the comfort zone should lie in between the 18–30°C during the non visiting hours and 19–30°C during the visiting hours. However, it was obtained from the thermal simulations that an additional active heating / cooling system is required to achieve this full comfort zone during the opening hours of 'Parc des Oiseaux'. This research proposes to perform an **air-to-water heat pump with fan coils** to achieve a **full comfort zone** during the opening hours of 'Parc des Oiseaux. The air-to-water heat pump requires a maximum power demand of **65,7kW for cooling** and **37,5kW for heating**. The output data of the simulations were analysed in Excel and from this analysis it was concluded that a full comfort zone is created through **passive systems (61,1%)** and an **active system (38,9%)**. The new optimized annual operative temperature graphs are presented in figure 237 and 238. Finally, it is concluded that a combined strategy, including an active system and passive systems, will ensure a full comfortable interior of the glass dome for Lori parrots, visitors and caregivers.

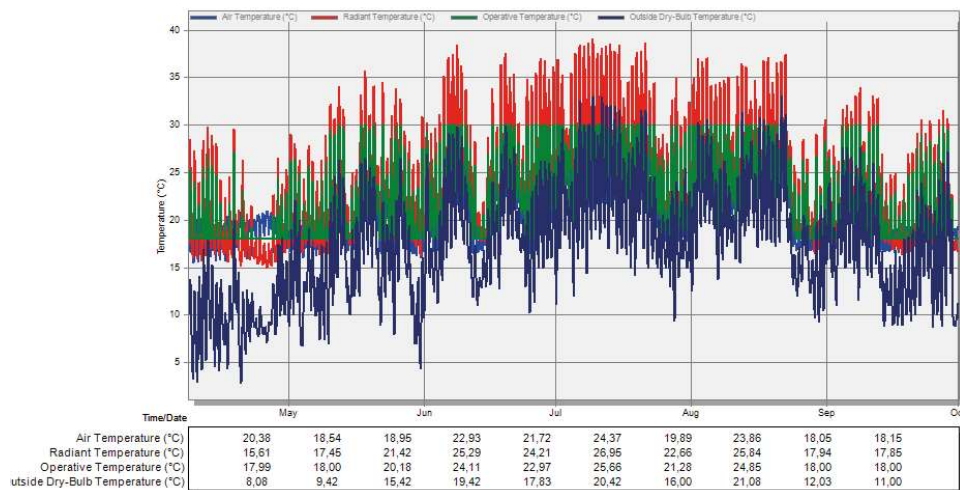


Figure 237. Annual graph of the optimized operative temperature (green) in hourly intervals from the 8th of April to the 30th of September

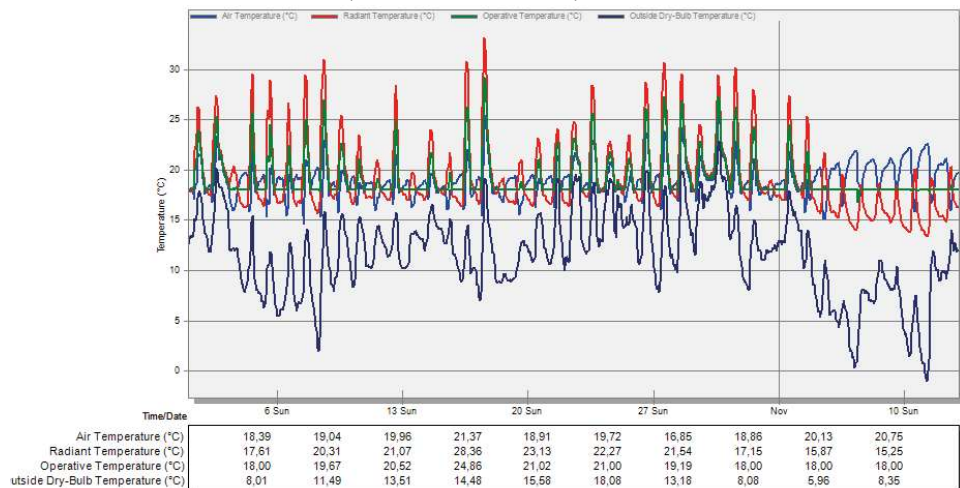
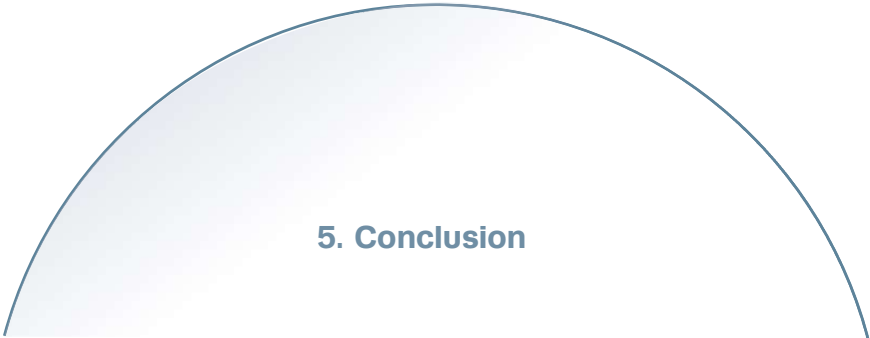


Figure 238. Annual graph of the optimized operative temperature (green) in hourly intervals from the 1st of October to the 12th of November



5. Conclusion

5.1 Conclusion

In general, the main goal of this research is to develop a **solely glass dome** from **structural assembled cast glass components** while providing **thermal comfort for Lori parrots** and being **minimum invasive** for the local environment: 'Parc des Oiseaux'. Sub research goals were made in order to achieve the main research goal and are divided into structural and durability sub research goals. In retrospect,

The structural goals are:

- Create a structural scheme based on compression.
- Design an optimal shape for one type of component.
- Minimize the visible steel connections.

The durability goals are:

- Minimize the number of different required molds.
- Design a dry assembled construction method.
- Perform passive climate strategies for thermal comfort

The conclusion discusses the above described goals and how these goals are met and validated. This explanation relates to the general glass dome design, dry assembled system method, prototype, transparency and structural and thermal validations. In addition, the challenges that this research has encountered are addressed. Finally, recommendations are provided that require further research.



The general dome design aims for an increased flying height for Lori parrots while maintaining a pure compressive force system and providing thermal comfort to the Lori parrots and visitors. An increased flying height is required to ensure a spacious liveable environment for the Lori parrots. The first two aspects are achieved by a shallow cast glass dome design and lowered cylindrical concrete support structure. The **shallow dome** is based on the shell boundaries for **compressive** shells, where Φ equals $0^\circ \leq \Phi \leq 45^\circ$. The concrete support structure will increase the rise of the dome with 2m which results in a new dome **rise of 9.5m** and increased flying height for the Lori parrots. Note that this increase in flying height cannot be obtained from the dome shell because this will not create a fully compressive structure, because increasing the dome rise results in an increase of angle Φ , where membrane tensile stresses can occur.

Concerning the third aim, providing thermal comfort to the Lori parrots and visitors, two adjustable openings of 9.3m² are inserted in the geometry: one encircled at the base and one at the oculus. The oculus is not constructed from cast glass because natural ventilation and reduction of the amount of different steel molds for producing cast glass components are required. The oculus is constructed from an cylindrical aluminium window frame that is fixed onto the steel compressive ring and laminated glass panels. The window is automatically openable in order to provide the glass dome from natural ventilation. Concerning the interior of the glass dome, the interior functions as an aviary for Lori parrots and includes a green area with extensive vegetation and water basins. The function of the water basins is two folded. First, it will function as drinking basins for the Lori parrots. Secondly both water basins and soil can be used as efficient thermal mass. It is concluded that an efficient **passive design** for the glass dome consists of the following passive systems: **adjustable openings**, six **earth ducts**, internal **thermal masses** and utilization of a **white wash paint** on 50% of the glass dome surface. The six earth ducts and large difference between the inlet and outlet height of 9.5m will enhance stack ventilation. Regarding the white wash paint, a chalk based white wash paint (Eclipse F4 from Sudlac) is proposed which is biodegradable and will not harm the local environment. The white paint is removed at the beginning of the colder fall days through precipitation, resulting in a high solar and visible transmission and higher comfort temperature. Unlike the hot summer days, the white wash paint reduces the solar and visible light transmittance to avoid overheating in the interior of the glass dome. To obtain thermal comfort, the **comfort zone** should lie in between the **18–30°C** during the non visiting hours and **19–30°C** during the visiting hours. This because the main function of the aviary is a passage and is defined as a **semi-outdoor environment**. Resulting in a broad temperature range, where Lori parrots are almost comfortable in equal environments as humans.

Assembled system



The dry and assembled system of the glass dome is constructed from **omnidirectional** cast glass components that are equal in geometry. Hence, only **one steel precision mold** is needed to produce the cast glass components and thus will reduce the production costs. The interlayer out of **TPU** between the glass components differs in geometry for each ring due to the changing curvature. Unlike the interlayers located in the arch direction that do not differ in geometry and have an equal thickness. The omnidirectional component is constructed from **three different spheres** that are blended together as one component. Resulting in fully omnidirectional components that form the interlock in the arch and ring direction and handle the changing curvature. The component design and interlock was inspired by the bone connections of the human body, such as **the spine**, that can adjust the changing curvature without changing the component geometry. This research was encouraged by designing **one component** that **adapts the changing curvature** rather than using a high-tech method, such as an adaptable mold, that is complex and expensive. Moreover, the component design can be seen as a knuckle (in Latin: condyle) of a human.

The glass dome components will fail without using an interlayer due to **local protrusions**. These local protrusions result in hard-to-hard material contact with local (tensile) peak stresses and cause failure. The TPU interlayer functions as a **resilient interlayer** which will absorb the occurred tensile stresses and ensures homogeneous load-transfer onto the next glass components.

Constructing the entire glass dome is realised by a **wooden structure** and subsequently applying a **pre-stress** onto the glass components. First, this wooden structure is located underneath the glass dome shell and is carried and fixed onto the constructed foundation and concrete cylindrical walls. Next, the glass components will rest onto the wooden structure where the glass components and interlayers are stacked together by building-workers from its dome foot to the oculus. Finally, when the last ring layer is placed, a **customized compressive steel ring** is fixed. This steel compression ring and steel tension ring form a sufficient interlock between the components. It should be noted that although the force system of the glass dome is in compression, tensile stresses always occur due to local protrusions. Resulting in a **steel customized tension ring** located at the base that will prevent the supports from slight yielding.

Prototype



Five cast glass components were developed in 1:2 scale in order to validate the component design and further develop the final mold design. The prototypes were obtained from a mold with two funnels that were located at the top of the spheres, where the glass was poured from one side. Moreover, the prototypes give insight in the casting process and allocate the residual stresses. All prototypes showed **large air bubbles** located at the front sphere surfaces or side sphere surfaces. These air bubbles most often occurred at the non-pouring side, thus the side where the air left the other funnel. The glass models obtained from the B mold (where the funnels were connected) showed less air bubbles. It is concluded from these results that next time the air bubbles need to be avoided by creating vents within the mold. Finally, this research proposes to use a **high precision steel press mold** with **one funnel** and **small vents** located at the spheres where the air was trapped. Moreover, utilization of a high precision press mold enables to shape the component to its spherical configuration and thus allows for less post-processing.

It is concluded from the results of the qualitative analysis of the residual stress regions that the models showed acceptable stresses. The located stresses are represented by the polarisation film as light blue colours or 'isochromatic fringes' and do not represent the quantity.

Transparency



The visible light transmittance of the glass dome should be lowered in order to notice the presence of the glass dome structure by the Lori parrots. The glass dome components are polished to a slightly **matt surface area** while still **transmitting the colours** of the environment, in order to mimic the colours of a



Figure 239. Glass prototypes in stacked dome configuration

natural habitat for the Lori parrots onto the glass dome surface. Transparency is not only about observing a colour through transmission, **reflections and distortions** also contribute to it. Distortions are perceived by the human (or birds) eye as a consequence of refracted light beams. The direction of the refracted light beams depend on the thickness of the component and geometry, determining how the distortion is observed. The inner-side of the glass components will work as a **hollow lens** where the light beams diverge. Unlike the outer-sphere that work as a **positive lens** and form the majority of the structure because the components are stacked on top of each-other. In summary, the light beams are propagating through the glass spheres and are refracted and converge to its focal point, observed by the human eye as **a real image** or colour scheme. Subsequently, behind the focal point the light beams will form an **inverted image** caused by the converge refraction. This research presents a new meaning to **transparency** which relates to the glass dome design and is: **“a synonym for reflecting, transmitting and distorting colours of the environment in the interest of designing a noticeable dome structure for Lori parrots”**.



Structural validation was derived from analytical, numerical and experimental analyses. Experimental qualitative analyses were performed at arch- and component level. The structural validation was based on a **simplified glass dome** design because the omnidirectional components require complex simulations. These analyses give fundamental insights about the structural behaviour of the dry assembled system of the glass dome. It is concluded from both analytical and numerical analyses that the simplified glass dome design is in **pure compression** for both load-cases: self-weight (symmetrical) and self-weight + wind load (asymmetrical). It is concluded that the self-weight load case is dominant and external loads will be in the same order of magnitude. This is concluded from the small differences of the numerical and analytical analyses for both load cases.

The experimental analysis show that the arch interlock is sufficient for an arch which is subjected to a point load of <53N. The physical arch test proved that the arch interlock causes a **redundant system** because when the maximum load is applied the components will give a **warning sign** before the entire structure collapse. The warning sign equals a deformed arch with coherent connection, which is caused by the sufficient arch interlock. Regarding the real dome design, this means that the interlock will form a redundant structure. Note that the deformation of the real dome design will be much smaller as a result of the action of the ring forces.

Apart from these structural validations, analytical and numerical thermal simulations have been performed to validate the thermal performance in the interior of the glass dome. In order to validate the thermal performance both analytical and numerical simplifications of the real dome design have been made. The output data of the simulations is analysed in Excel and from this analysis it is concluded that a full comfort zone is created through **passive systems (61%)** and **active system (38,9%)**. The passive systems meet the main aim of this research because overheating risk during hot summer days is reduced and solar absorption is maximized during the cold fall days. This research proposes to perform an **air-to-water heat pump with fan coils** to achieve a full comfort zone during the opening hours of 'Parc des Oiseaux. The air-to-water heat pump requires a maximum power demand of **65,7kW for cooling** and **37,5kW for heating**.



*Finally It may be concluded that the glass dome design meets the main aim of this research: develop a solely glass dome from structural dry assembled cast glass components while providing thermal comfort to Lori parrots and being minimum invasive for the local environment, the reason is two folded. First, **omnidirectional components** that are equal in geometry create a **solely glass dome** from structural **dry assembled** cast glass components. This results in a new meaning of transparency that relates to what is best for the birds. Secondly, the majority of systems, that establish **thermal comfort** in the interior of the glass dome, cover **passive systems***

5.2 Recommendations

The validations of both structural and thermal performance are based on a simplified glass dome design. These above mentioned simplifications were required because the real glass dome is constructed from omnidirectional components that have a **complex geometry**. It is assumed that even complex simulations will not result in accurate results. In order to validate the real dome design **physical experiments** should be performed, i.e. building a scale model of the glass dome design with the cast glass components and associated interlayers. It should be noted though that complex simulations do give a better approximation of the structural behaviour of the glass dome design than the simplified glass dome design. Due to the time-frame and difficulty of mandatory accuracy of the simulations these simulations were not performed. Additional real physical experiments and simulations are distinguished in structural and thermal performance and explained below.

Structural performance

The structural performance of the real glass dome system should be analysed by utilization of simulations and **physical experiments**. The model is constructed from the omnidirectional cast glass components and interlayers of TPU, in both ring and arch direction. The simulations and experiments should **investigate both load cases**: the symmetrical and asymmetrical load-case. This to obtain fundamental insight in the structural behaviour of the entire system, regarding their compressive performance and deformation.

Secondly, the stiffness of the entire glass dome system is calculated for the worst case scenario: i.e. using the maximum interlayer thickness located at dome top, interlayer Young's modulus, thickness of the glass component and Young's modulus of glass. Subsequently, the interlayer stiffness interval is obtained from Hooke's law and maximum displacement of 2Δ . According to Aurik (2017) a glass component requires full contact between all surfaces, which equals 2 surfaces, after a displacement of 2Δ . The deviation (Δ) is based on the Glass Bridge design since the structural simulations of the glass dome do not include calculations of the interlayer and thus require further research. Moreover, values of the Glass Bridge design were used because it is a curved cast glass structure which could form two lunes of a dome structure. Secondly, there are no existing cast glass structures in curved or double curved configuration. Experiments and simulations should be performed to determine the **elastic behaviour** of the **different interlayers** within the glass dome system, i.e. varying interlayer thickness in its geometry and in each ring. Other factors that influence the elasticity and were beyond the scope of this research are: time dependent behaviour (creep), temperature dependent behaviour and friction. Friction occurs between the component and interlayer which is a result of the contact area of the interlayer with the component. Further investigation in temperature dependent, time dependent behaviour, interlayer geometry and friction is required.

Thermal performance

The thermal performance of the interior of the real glass dome should be analysed as well by utilization of simulations and real physical experiments. The model is again constructed from the omnidirectional cast glass components and interlayers of TPU in both ring and arch direction. The model should investigate the **sealed performance** of entire dome structure designed from the glass components and interlayers. This results in the real thermal comfort performance of the interior glass dome, assessed on **infiltration**. Secondly, experimental research, i.e. constructing a set of components constructed from steel precisions

molds, should investigate the light transmittance, reflectance and distortions through the stacked omnidirectional cast glass components and associated interlayers. Because physical experiments can determine the visualization, thus validate if the matt components form a **noticeable structure** to the Lori parrots and if the transmitted, reflected and distorted colours really **mimic a natural environment** onto the glass dome surface.

Finally, the thermal simulations showed that a full thermal comfort zone is created through passive systems and active systems. Although, the thermal simulations did not take in account local heating or cooling elements during the non-visiting hours. **Local active systems** could be useful beyond the openings-hours to obtain thermal comfort to the Lori parrots while reducing the overall power demand of the active system. Because Lori parrots can house themselves around these active systems, e.g. local heating tubes where birds can sit on. The effect of local cooling or heating units onto the overall power demand is beyond the scope of this research and requires further research.

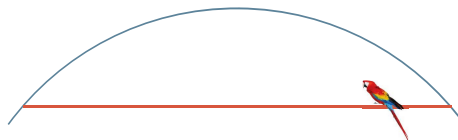


Figure 240. Solution for a local heating system

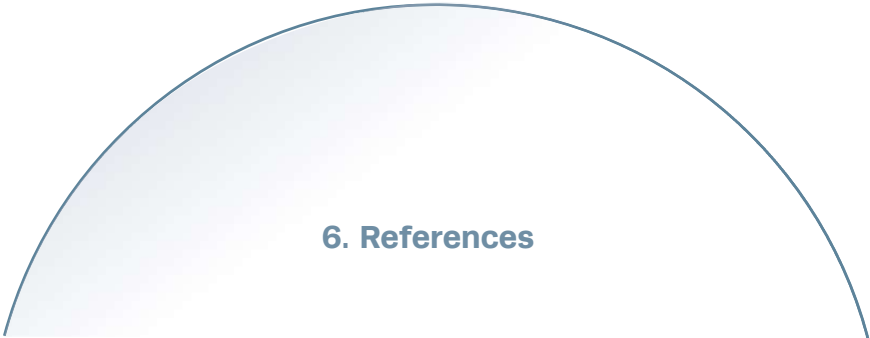
VISION

Just like the quote of Richard Rogers mentioned below, the glass dome design process is measured against the past, built for the present and tries to encourage the possibilities of future configurations in cast glass.

“Architecture is measured against the past, you build in the present, and try to imagine the future”

(Richard Rogers)

The glass dome research measured the pros and the cons from old masonry domes till glass domes that use steel main structures. This research is made to build in the present resulting in a large dome structure where the majority is constructed from a solely glass system. This has led to an innovative design for domes that tries to create an **new way of thinking**. This new way of thinking includes using cast glass as a structural component and using omnidirectional geometries that interlock. **Omnidirectional cast glass interlocking components** are useful in the future because theoretically they can be used to design **every form** while serving as **structural components**.

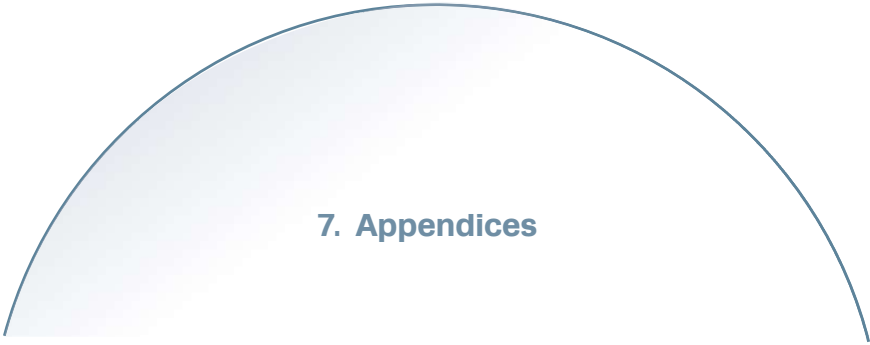


6. References

References

- ASHRAE Standards Committee. (2004). *Thermal Environmental Conditions for Human Occupancy*. Retrieved from http://www.almashvac.ir/fh/download/ASHRAE_Thermal_Comfort_Standard.pdf
- Augustynowicz, E., Block, P., C Barentin, C., Frick, U., Echenagucia, M., Popescu, M., & Van Mele, T. (n.d.). *The Armadillo Vault*. Retrieved from http://block.arch.ethz.ch/brg/files/RIPPMANN_AAG2016_armadillo-vault_1472480994.pdf
- Aurik, M. (2017). *Structural Aspects of an Arched Glass Masonry Bridge*. Retrieved from <https://repository.tudelft.nl>
- Barou, L. (2016). *Transparent restoration*. Retrieved from <https://repository.tudelft.nl>
- Bokel, R. (2017). *Natural ventilation*. Retrieved from – https://blackboard.tudelft.nl/bbcswebdav/pid-2755697-dt-content-rid-9443128_2/courses/38639-161704/Building%20Physics_2014_2015_Q4_Lecture%205.pdf
- Borgart, A. (2017). *Lecture 1: Structural Shell Geometry*. Delft, The Netherlands: TU Delft.
- Bristogianni, T., A Veer, F., Nijse, R., & A Oikonomopoulou, F. (2017). *Design & production of a structural a structural cast glass element for a transparent dome*. Delft, The Netherlands: TU Delft.
- Burgess, J. (n.d.). *Low emissivity of glass*. Retrieved from <https://www.buildmagazine.org.nz/assets/PDF/Build123-58-Low-Emissivity-Glass.pdf>
- Doukari, K. (2013). *The Transparent Facade of the Future*. Retrieved from <https://repository.tudelft.nl>
- Estrin, Y., Dyskin, A. V., & Pasternak, E. (2011). *Topological interlocking as a material design concept*. Retrieved from <http://www.sciencedirect.com/science/article/pii/S0928493110002882>
- Göppert, K., Paech, C., Arbós, F., & Teixidor, C. (2007). *Glass Monument in Remembrance of the Terrorist Attacks in Madrid of March 11, 2004*. Retrieved from <http://www.bellapart.com/uploads/files/entradas/glass-monument-in-remembrance-of-the-terrorist-atta.pdf>
- Granta material intelligence. (2016). *CES EduPack (2016) [Software]*. Retrieved from <https://software.tudelft.nl/86/>
- Heyman, J. (1995). *The Stone Skeleton*. Cambridge, USA: Press Syndicate of the University of Cambridge.
- H.M.E. Janssen, F., & R.W.G. Houben, H. (2013). *Reinforced ice structures*. Eindhoven, The Netherlands: Tu Eindhoven.
- Kintingu, S. H. (2009). *Design of interlocking bricks for enhanced wall construction flexibility, alignment accuracy and load bearing*. Retrieved from <http://go.warwick.ac.uk/wrap/2768>
- KNIGHT OPTICAL. *Technical /Sheet Glasses TSG-B270 [Online]*. <http://www.knightoptical.com/technicallibrary/sheet-and-technical-glasses/>.
- Lee, J. (n.d.). *An Analysis of the Effect of the Building Envelope on Thermal Comfort Using the EnergyPlus Program*. Retrieved from <http://apps.acsa-arch.org/resources/proceedings/uploads/streamfile.aspx?path=ACSA.Tech.2001.18.pdf>
- Louter, C. (2016). *Laminated connections for structural glass components: a full scale experimental study*. Retrieved from <https://repository.tudelft.nl>
- MCKENZIE, H. W., & HAND, R.J.(2011). *Basic Optical Stress Measurement in Glass*, Sheffield, UK, Society of Glass Technology.
- Museum Florence. (n.d.). *Dome*. Retrieved from <https://www.museumflorence.com/monuments/2-dome>

- Nakano, J. (2003). *Evaluation of thermal comfort in semi outdoor environments*. Retrieved from <http://www.wul.waseda.ac.jp/gakui/honbun/3534/3534.pdf>
- Nicol, F., & Roaf, S. (2007). *Progress on Passive cooling: adaptive thermal comfort and passive architecture*. Retrieved from <https://books.google.nl>
- Nicol, F., Humphreys, M., & Road, S. (2012). *Adaptive Thermal Comfort*. London, United Kingdom: Routledge
- Nijssse, R. (2003). *Glass in structures*. New York, United States: Princeton Architectural Press.
- Nijssse, R. (2015). *The Future of all glass structures*. Retrieved from <https://repository.tudelft.nl/>
- Oikonomopoulou, F., Veer, F., Nijssse, R., & Baardolf, K. (2014). *A completely transparent, adhesively bonded soda-lime glass block masonry system*. Retrieved from <http://journals.library.tudelft.nl>
- Oikonomopoulou, F., A Veer, F., Bristogianni, T., & Nijssse, R. (2017). *The construction of the Crystal Houses façade: challenges and innovations*. Retrieved from <https://repository.tudelft.nl>
- Pan, S., Zheng, M., & Yoshida, H. (n.d.). *Commissioning of a Coupled Earth Tube and Natural Ventilation System at the Design Phase*. Retrieved from <http://oaktrust.library.tamu.edu/bitstream/handle/1969.1/6240/ESL-IC-07-11-39.pdf?sequence=1>
- Prenis, J. (1973). *The Dome Builders Handbook*. Philadelphia, Pennsylvania, United States: Runnign press.
- Regnier, C. (2012). *Guide to Setting Thermal Comfort Criteria and Minimizing Energy Use in Delivering Thermal Comfort*. Retrieved from <https://www.osti.gov/scitech/servlets/purl/1169480>
- Rodriguez-Ubinas, E., Montreo, C., Porteros, M., Vega, S., Navarro, I., Castillo-cagigal, M., . . . Gutiérrez, A. (2014). *Energy and Buildings*. Retrieved from <http://sciencedirect.com>
- Roeder, E. (n.d.). *Extrusion of glass*. Retrieved from <http://www.extra.research.philips.com>
- Santamouris, M. (2006). *Adaptive thermal comfort and buildings*. Retrieved from <http://www.aivc.org>
- Schittich, C., Staib, G., Balkow, D., Schuler, M., & Sobek, W. (2007). *Glass Construction Manual* (2nd ed.). Basel, Switzerland: Birkhäuser.
- Schueller, W. (1996). *The design of building structures*. Upper Saddle River, New Jersey: Prentice Hall, Inc
- SHELBY, J. E. (2005). *Introduction to Glass Science and Technology*, Cambridge, UK, The Royal Society of Chemistry.
- Vereyken, K. (2007, December 08). Les spirales en Spina Pesce [arêtes de poisson], Le calibrage des briques. Retrieved from <http://www.solidariteetprogres.org/documents-de-fond-7/culture/les-secrets-du-dome-de-florence>
- Weller, B., Härth, K., Tasche, S., & Unnewehr, S. (2009). *Glass in Building*. Basel, Switzerland: Birkhäuser.
- Wurm, J. (2007). *Glass Structures*. Basel, Switzerland: Birkhäuser.
- Ye, G., Yang, C., Chen, Y., & Li, Y. (2003). *A new approach for measuring predicted mean vote (PMV) and standard effective temperature (SET)*. Retrieved from <http://www.sciencedirect.com>
- Yoon, G., Tanaka, H., & Okumiya, M. (2009). *Study on the design procedure for a multi-cool/heat tube system*. Retrieved from <https://www.sciencedirect.com/science/article/pii/S0038092X09000619>



7. Appendices

7.1 Amount of components

ring	#comp
1	1225
2	1220
3	1216
4	1211
5	1207
6	1202
7	1198
8	1193
9	1189
10	1184
11	1180
12	1175
13	1170
14	1166
15	1161
16	1156
17	1152
18	1147
19	1142
20	1137
21	1133
22	1128
23	1123
24	1118
25	1114
26	1109
27	1104
28	1099
29	1094
30	1089
31	1084
32	1079
33	1075
34	1070
35	1065
36	1060
37	1055
38	1050
39	1045
40	1040
41	1035
42	1030
43	1025
44	1019
45	1014
46	1009
47	1004
48	999
49	994
50	989

51	984
52	978
53	973
54	968
55	963
56	957
57	952
58	947
59	942
60	936
61	931
62	926
63	920
64	915
65	910
66	904
67	899
68	894
69	888
70	883
71	877
72	872
73	867
74	861
75	856
76	850
77	845
78	839
79	834
80	828
81	823
82	817
83	812
84	806
85	800
86	795
87	789
88	784
89	778
90	772
91	767
92	761
93	756
94	750
95	744
96	739
97	733
98	727
99	721

100	716
101	710
102	704
103	699
104	693
105	687
106	681
107	675
108	670
109	664
110	658
111	652
112	646
113	641
114	635
115	629
116	623
117	617
118	611
119	605
120	599
121	594
122	588
123	582
124	576
125	570
126	564
127	558
128	552
129	546
130	540
131	534
132	528
133	522
134	516
135	510
136	504
137	498
138	492
139	486
140	480
141	474
142	468
143	462
144	456
145	450
146	444
147	438
148	432

149	426
150	419
151	413
152	407
153	401
154	395
155	389
156	383
157	377
158	370
159	364
160	358
161	352
162	346
163	340
164	334
165	327
166	321
167	315
168	309
169	303
170	296
171	290
172	284
173	278
174	272
175	265
176	259
177	253
178	247
179	241
180	234
181	228
182	222
183	216
184	209
185	203
186	197
187	191
188	185
189	178
190	172
191	166
192	159
193	153
194	147
195	141
196	134
197	128



Figure 241. Impregnation of the components

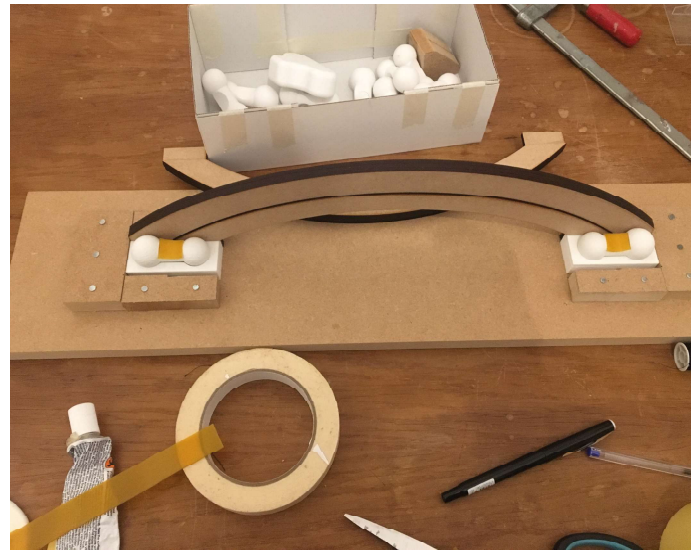


Figure 242. Construction process of the physical arch

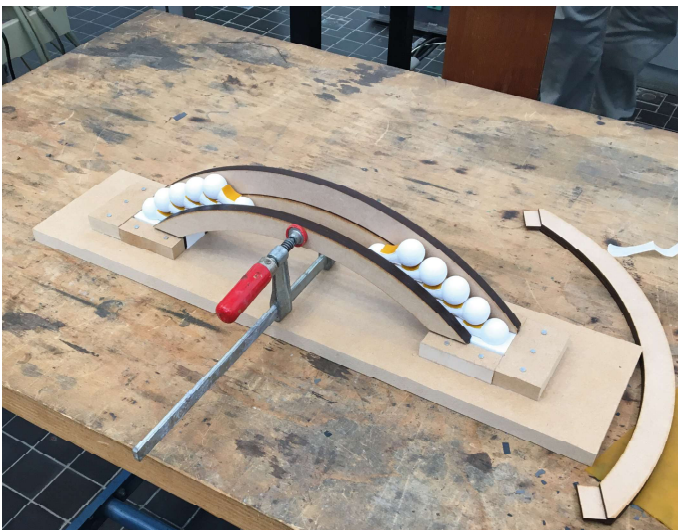


Figure 243. Construction process of the physical arch



Figure 244. Detail of the physical arch



Figure 245. Construction process of the physical arch

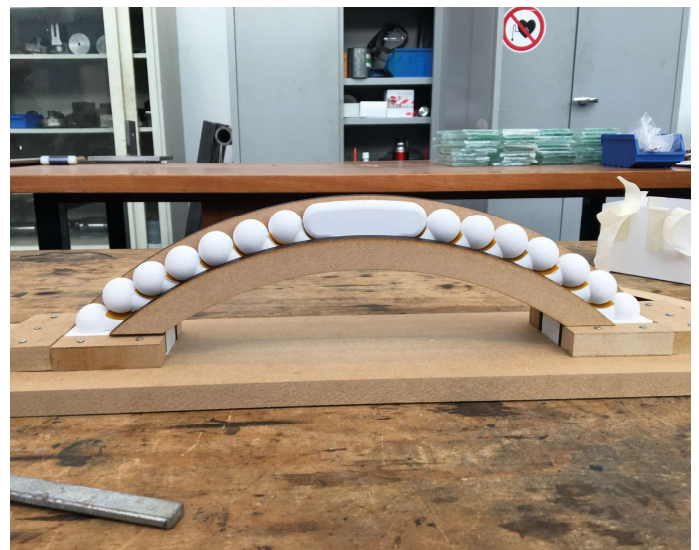


Figure 246. The final physical arch

WEIGHT OF THE GLASS COMPONENTS

Weight of glass components			
Component	Water(g)	Glass(g)	Component(g)
E1	135	358	369
E2	195	517	526
E3	140	371	376
E4	195	517	523
E5	140	371	384
<i>water(g)*2,55(g)*1,04 = component weight</i>			

Table 35. Overview of the weight of each component

GENERAL OVERVIEW OF THE KILN

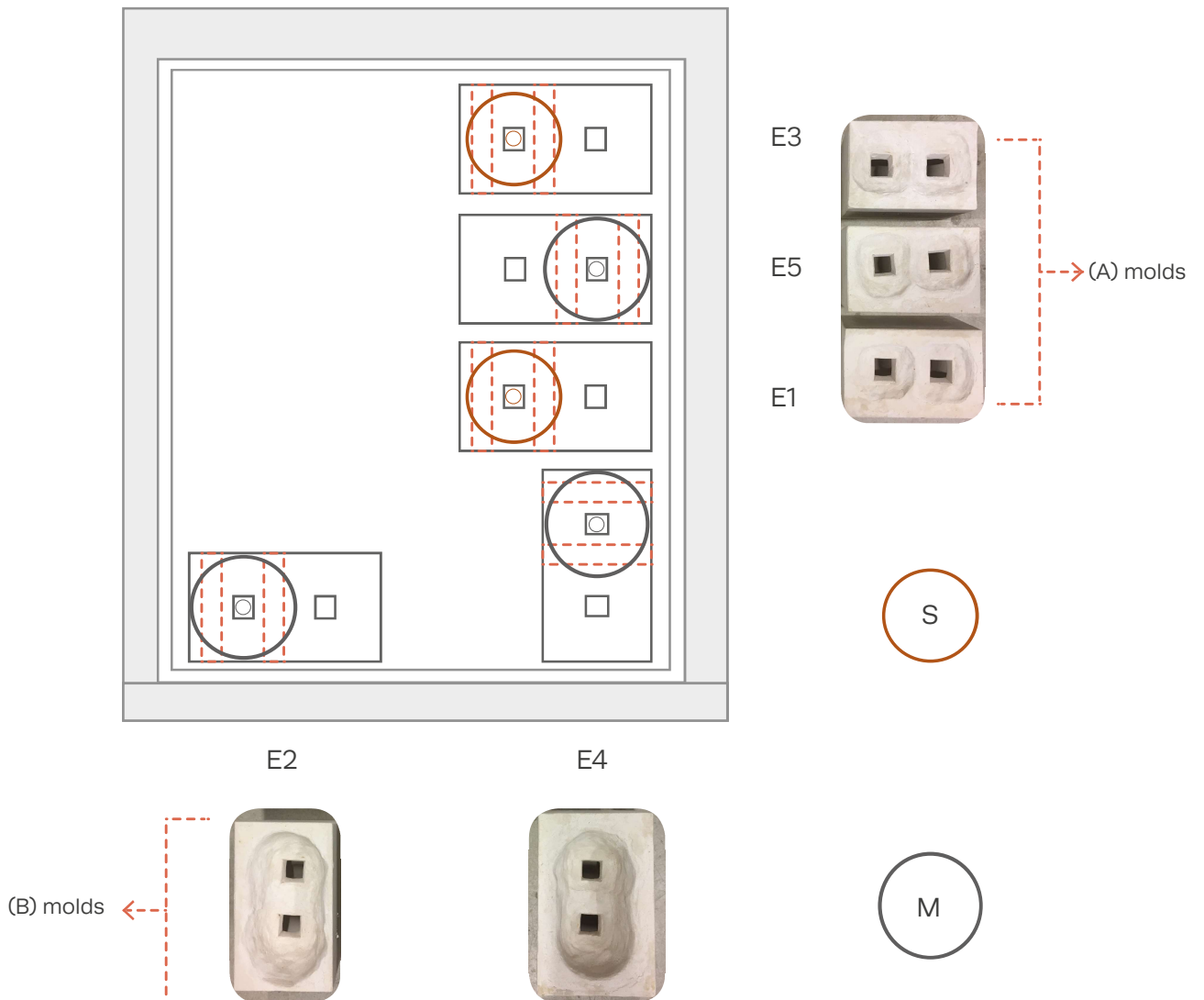
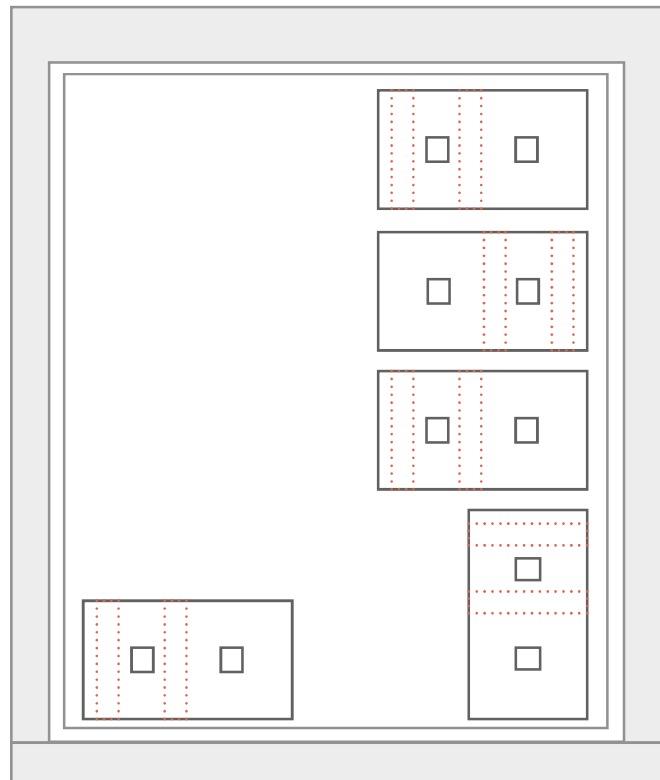


Figure 247. Overview of the mold location and name

HEIGHT OF THE SPACERS



$h=1,5\text{cm}$

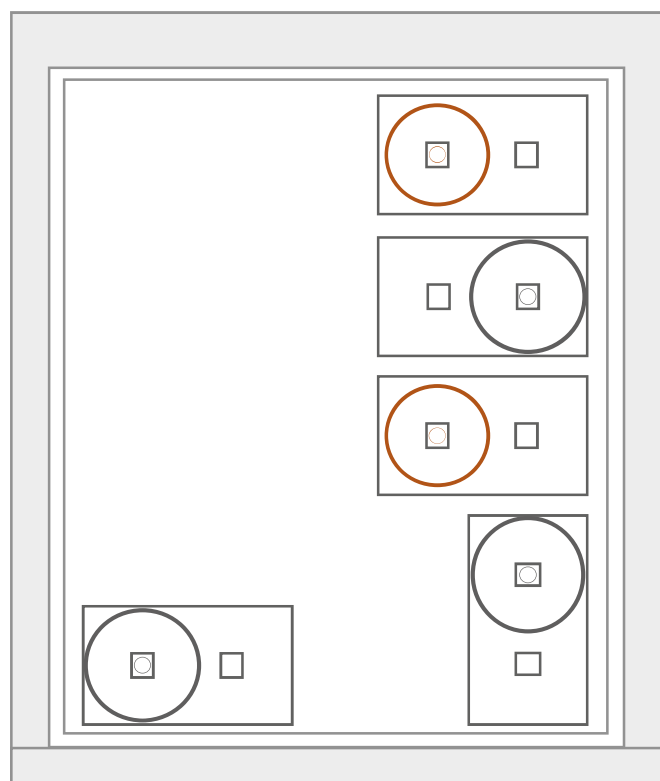
$h=3\text{cm}$

$h=2,5\text{cm}$

$h=1,5\text{cm}$

$h=2,5\text{cm}$

DIAMETER FLOWERPOTS



$d=1,6\text{cm}$

$d=1,6\text{cm}$

$d=1,6\text{cm}$

$d=1,6\text{cm}$

$d=1,5\text{cm}$

OBSERVATIONS MODELS FROM (A) MOLDS

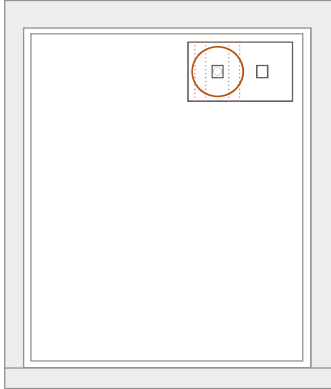


Location in the kiln

Observation

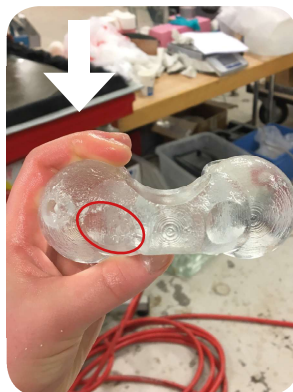
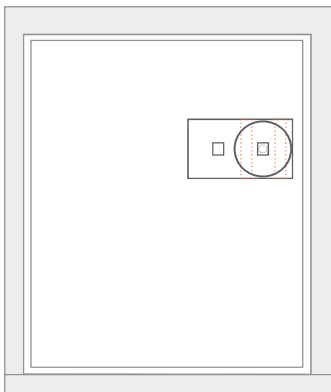
Explanation

E3



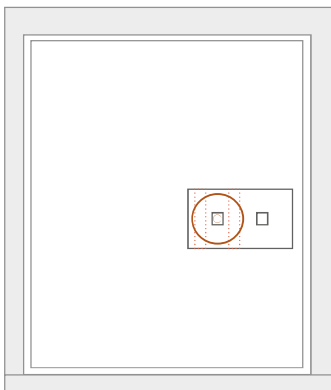
- One big air bubble at the front side with small air bubbles at the side. The air bubbles are located at the non-pouring side
- one big bump is located at the centre of the component

E5



- One large air bubble is located at the side where the glass was poured.
- A part (red circle) of left top surface is pushed inwards.

E1



- One big air bubble at the front side. The air bubble is located at the non-pouring side
- Small air bubbles located at both top surfaces of the funnels

OBSERVATIONS MODELS FROM (B) MOLDS

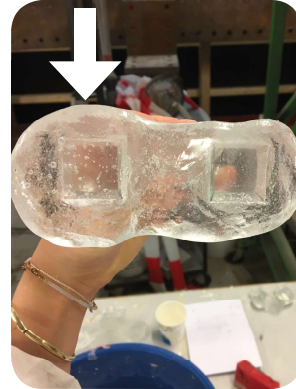
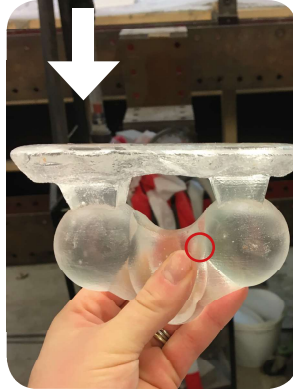
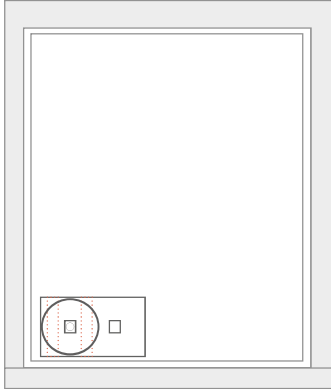


Location in the kiln

Observation

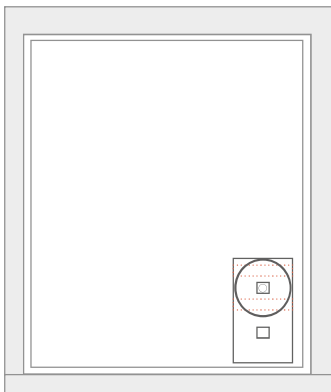
Explanation

E2



- One large air bubble located at the inner sphere at the non-pouring side (red circle)
- Left funnel (pouring side) shows small air bubbles
- Very smooth surface

E4



- One big air bubble at the front side. The air bubble is located at the non-pouring side
- Left funnel (pouring side) shows small air bubbles



white arrow represents the pouring side

